Publishers' page

Publishers' page

Publishers' page

Publishers' page

Contents

Preface

Main progress in fracture mechanics was attained in the middle of 20$^{\text{th}}$ century following formulation of well-known Griffith-Irwine fracture criterion. At the second part of the 20$^{\text{th}}$ century all basic problems of static fracture mechanics were solved. A substantial contribution to this development was made by Russian scholars (N. A. Zlatin, B. V. Kostrov, E. M. Morozov, L. V. Nikitin, V. S. Nikiphorovski, V. Z. Parton, L. I. Slepjan, V. E. Fortov, G. P. Cherepanov, G. I. Barenblatt, E. I. Shemyakin, V. M. Titov, L. A. Merzhievsky, V. F. Kuropatenko, G. I. Kanel and others) and by foreign scientists (J. D. Achenbach, W. T. Ang, K. B. Broberg, J. W. Dally, J. D. Eshelby, L. B. Freund, J. F. Kalthoff, W. G. Knauss, K. Ravi-Chandar, D. A. Shockey, A. Shukla, A. J. Rosakis, M. L. Williams and others). To a great extent, the progress in the field is due the achievements of the St. Petersburg—Leningrad Scientific School of Mechanics by G. V. Kolosov, V. V. Novozhilov and L. M. Kachanov. Contributions of this institute include the establishment of the fundamental principles of fracture analysis as a process, occurring at different scale levels.

However, despite such a progress in the development of the science of fracture, many important problems remain. One of the most challenging of these is dynamic fracture. This is usually regarded as a rupture of material under intense hi-rate loading taking place within relatively short time period.

In this book a new phenomenological approach in studies of brittle fracture initiation, development and arrest under shock pulses is presented. The approach was developed in the late 1990's and the beginning of 2000's and is based on invariant parameters independent of the mode and history of fracture. Demand for a new approach in fracture dynamics was imposed by impossibility to explain and predict experimentally observed peculiarities of dynamic fracture utilizing classical approaches in fracture. New approach provides an opportunity to predict fracture of both 'intact' media and media having macrodefects such as cracks and sharp notches. A qualitative explanation is thus obtained for a number of principally important effects of high-speed dynamic fracture that can not be clarified within the framework of previous approaches. We show that it is possible to apply this new strategy to solve the problems of dynamic rupture, erosion, crater formation, crack extension and arrest, etc. By extending well-known classical principles of Linear Elastic Fracture Mechanics, the suggested approach conserves the intrinsic 'industrial' character of the analysis and can be considered as a basis for new testing methods and for certification of dynamic strength characteristics of structural materials.

The method is very convenient to be embedded into numerical computational schemes in order to predict dynamic fracture development and arrest.

Moreover, the approach turned out to be very useful in other areas in order to simulate and predict fast transient processes. Examples included in the book cover dynamic yielding, electric breakdown, cavitation in liquids, detonation of gaseous media.

Specialists can use the methods described in this book to determine critical characteristics of dynamic strength and optimal effective fracture conditions for rigid bodies. This book can also be used as a special educational course for guidance on the deformation of materials and constructions, and fracture dynamics.

We, the authors, are grateful to Prof. A. A. Utkin, Dr. A. V. Kashtanov, Prof. R. V. Goldstain, Prof. P. Ståhle, Dr. A. Zhivkov, Prof. A. M. Bragov, Prof. V. I. Smirnov, Prof. S. A. Atroshenko, Dr. A. A. Gruzdkov, Ms. E. Sitnikova, Mr. G. A. Volkov, Mr. L. M. Isakov and all our colleagues for support, advice and valuable discussions we had while preparing this book. We are specially thankful to Ms. Natalia Bratova for inestimable help while editing the book.

Chapter 1

Basic principles of quasistatic fracture mechanics

Introduction to quasistatic fracture mechanics. Brittle fracture. Surface energy. Classical criteria for brittle fracture. Griffith—Irwine approach

1.1 Griffith approach

Studies in fracture date back to the ancient times. In this connection one can mention giant constructions of Tan dynasty in Ancient China, the legendary Semiramida's gardens (the first example of hanging structures) or the Egyptian Pyramids. Obviously people were aware of the secrets of strength even at these early times. The experiments of Galilei (Galilei, 1683) and Leonardo da Vinci (da Vinci, unknown) raised the problem of how defects can influence strength of a structure. Later investigations by famous scientists (E. Mariotte (Mariotte, 1686) in the 17th century, C. Coulomb (Coulomb, 1776) in the 18th and O. Mohr (Mohr, 1906) in the 19th century) contributed to development of the strength theory. Finally, the basis of modern fracture was formed in fundamental works of A. Griffith (Griffith, 1920) in 1920 and J. Irwin (Irwin, 1948) in 1948.

In (Griffith, 1920) A. Griffith introduced a new concept into fracture theory — surface energy of a fracture process. This energy is proportional to the surface appearing as a result of a fracture process with proportionality constant being the property of the fractured material. This idea makes it possible to use energy balance as a critical condition for crack propagation.

Consider the simplest example: elastic plane with a central crack with length $2a$ (Fig. 1.1) is uniformly stretched in direction perpendicular to the crack direction. Following Griffith one can construct critical condition for

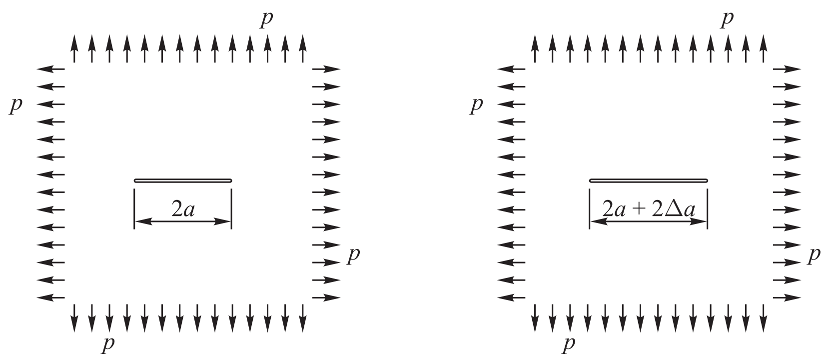

Fig. 1.1.

crack advancement.

	a	$a + \Delta a$
Elastic energy	U	$U + \Delta U$
Applied forces work	A	$A + \Delta A$
Surface energy	Π	$\Pi + \Delta\Pi$

In compliance with Griffith's idea:

$$\Delta\Pi = \gamma\Delta\Sigma,$$

where $\Delta\Sigma$ is the new surface formed as a result of the crack advancement and γ is the specific surface energy that is constant for a given material.

Following Griffith one can formulate condition for crack advancement: *if the functional $U - A + \Pi$ is minimized for initial geometry then the crack does not propagate.* Obviously this occurs when

$$\Delta U - \Delta A = -\Delta\Pi. \tag{1.1}$$

Therefore, one can determine the critical situation and find the critical load p, leading to crack extension from the following condition:

$$\Delta U + \Delta\Pi = \Delta A. \tag{1.2}$$

Griffith (Griffith, 1920) conducted his proof for two confocal ellipses, with inner ellipse representing the crack and the outer one representing loaded external boundary. Having the energy balance derived, the semiaxes of the outer ellipse were extended to infinity.

Here a modified proof invented by S. Nazarov (see ex. Morozov, 1984) is presented.

Consider a convex domain Ω^0 having a smooth boundary. Ω^0_D stands for its homothetic dilatation.

$$\Omega^0_D = \left\{ x, y \in R^2; \frac{x}{\chi_1(D)}, \frac{y}{\chi_2(D)} \in \Omega^0 \right\},$$
$$\chi_i(D) = D + O(1), \quad D \to +\infty,$$
$$M = \{x, y \in R^2; |x| \le a, y = 0\}.$$

Let D be large enough to hold $M \in \Omega^0_D$ and $\Omega_D = \Omega^0_D \backslash M$. Finally

$$\overrightarrow{\sigma^{(n)}}\Big|_{\partial\Omega^0_D} = p\vec{n} \tag{1.3}$$

and

$$\sigma_{yy}\big|_M = \sigma_{xy}\big|_M = 0.$$

Plain strain conditions are supposed. $\vec{u}_D$ denotes the solution of Lame's equations within Ω_D and satisfying boundary conditions (1.3). This solution can be presented as a sum:

$$\overrightarrow{u_D} = \vec{v}(x, y) + \vec{w}(x, y) + \vec{v}_D(x, y), \tag{1.4}$$

where $\vec{v}(x, y)$ corresponds to dilatation of Ω^0_D (domain without a crack):

$$\vec{v} = p\frac{(1 - 2\nu)(1 + \nu)}{E}(x, y), \tag{1.5}$$

$$\sigma_{xx}(\vec{v}) = \sigma_{yy}(\vec{v}) = p; \quad \sigma_{xy}(\vec{v}) = 0,$$
$$e_{xx}(\vec{v}) = e_{yy}(\vec{v}) = p\frac{(1 - 2\nu)(1 + \nu)}{E}; \quad e_{xy}(\vec{v}) = 0.$$

Then, $\vec{w}(x, y)$ is the solution of Lame's equations in $R^2\backslash M$ with boundary conditions

$$\sigma_{yy}(\vec{w})\big|_M = -p; \quad \sigma_{xy}(\vec{w})\big|_M = 0;$$
$$\sigma_{ij}(\vec{w}) = O(r^{-2}), \quad r \to +\infty, \quad r = \sqrt{x^2 + y^2}.$$

Finally, the third summand in (1.4) can be estimated (see V. Mazja and B. Plamenevsky (Mazja, Plamenevsky, 1978) by:

$$|\sigma_{ij}(\vec{v}_D)| \le \frac{C}{D}\left\{\frac{1}{D} + \frac{\max[1, ((|x| - a)^2 + y^2)^{-1/4}]}{(r + 1)^2}\right\}. \tag{1.6}$$

Therefore:

$$\int_{\Omega_D^0} \sigma_{ij}(\vec{v}_D) e_{ij}(\vec{w}) d\Omega_D^0 \leq$$

$$\leq \frac{C}{D} \int_{\Omega_D^0} \frac{1}{(r+1)^2} \left(\frac{1}{D} + \frac{\max[1, ((|x|-a)^2 + y^2)^{-1/4}]}{(r+1)^2} \right) dxdy = O\left(\frac{1}{D}\right). \tag{1.7}$$

Denoting

$$\begin{gathered} U^0 = \frac{1}{2} \int_{\Omega_D^0} \sigma_{ij}(\vec{v}) e_{ij}(\vec{v}) d\Omega_D^0, \\ A^0 = p \int_{\partial\Omega_D^0} \vec{n}\vec{v} d\partial\Omega_D^0, \\ A^a = p \int_{\partial\Omega_D^0} \vec{n}\vec{v} d\partial\Omega_D^0 + p \int_{\partial\Omega_D^0} \vec{n}\vec{w} d\partial\Omega_D^0 + p \int_{\partial\Omega_D^0} \vec{n}\vec{v}_D d\partial\Omega_D^0, \\ A^0 = A^a = 0, \quad \text{when} \quad x, y \in M \end{gathered} \tag{1.8}$$

one can receive:

$$\begin{aligned} U^a = \frac{1}{2} \int_{\Omega_D} \sigma_{ij}(\vec{u}_D) e_{ij}(\vec{u}_D) d\Omega_D = U^0 + \frac{1}{2} \int_{\Omega_D} \sigma_{ij}(\vec{v}_D) e_{ij}(\vec{v}_D) d\Omega_D + \\ + \frac{1}{2} \int_{\Omega_D} \sigma_{ij}(\vec{w}) e_{ij}(\vec{w}) d\Omega_D + \frac{1}{2} \int_{\Omega_D} \underline{\sigma_{ij}(\vec{v}) e_{ij}(\vec{w} + \vec{v}_D) d\Omega_D} + \\ + \frac{1}{2} \int_{\Omega_D} \underline{\sigma_{ij}(\vec{w}) e_{ij}(\vec{v}) d\Omega_D} + \frac{1}{2} \int_{\Omega_D} \underline{\underline{\sigma_{ij}(\vec{w}) e_{ij}(\vec{v}_D) d\Omega_D}} + \\ + \frac{1}{2} \int_{\Omega_D} \underline{\sigma_{ij}(\vec{v}_D) e_{ij}(\vec{v}) d\Omega_D} + \frac{1}{2} \int_{\Omega_D} \underline{\underline{\sigma_{ij}(\vec{v}_D) e_{ij}(\vec{w}) d\Omega_D}} = \\ = U^0 + \frac{1}{2} \int_{\Omega_D} \sigma_{ij}(\vec{v}_D) e_{ij}(\vec{v}_D) d\Omega_D + \frac{1}{2} \int_{\Omega_D} \sigma_{ij}(\vec{v}) e_{ij}(\vec{w} + \vec{v}_D) d\Omega_D + \\ + \frac{1}{2} \int_{\Omega_D} \sigma_{ij}(\vec{w}) e_{ij}(\vec{w}) d\Omega_D + \frac{1}{2} \int_{\Omega_D} \sigma_{ij}(\vec{v}_D) e_{ij}(\vec{w}) d\Omega_D. \end{aligned}$$

Here the summands were merged using the Betti's formula. Recollecting

(1.6) and (1.7) one can obtain:

$$U^a = U^0 + \frac{1}{2}\int\limits_{\Omega_D} \sigma_{ij}(\vec{w})e_{ij}(\vec{w})d\Omega_D + \frac{1}{2}\int\limits_{\Omega_D} \sigma_{ij}(\vec{v})e_{ij}(\vec{w}+\vec{v}_D)d\Omega_D + O\left(\frac{1}{D}\right). \tag{1.9}$$

Using the Green's formula one can write:

$$\int\limits_{\Omega_D} \sigma_{ij}(\vec{v})e_{ij}(\vec{w}-\vec{v}_D)d\Omega_D = \int\limits_{\Omega_D^0} \overrightarrow{\sigma^{(n)}}(\vec{v})(\vec{w}+\vec{v}_D)d\partial\Omega_D^0 - 2\int\limits_{-a}^{a} \overrightarrow{\sigma^{(n)}}(\vec{v})(\vec{w}+\vec{v}_D)dx.$$

Besides that

$$A^a - A^0 = p\int\limits_{\partial\Omega_D^0} \vec{n}\vec{w}d\partial\Omega_D^0 + p\int\limits_{\partial\Omega_D^0} \vec{n}\vec{v}_D d\partial\Omega_D^0 = \int\limits_{\partial\Omega_D^0} \overrightarrow{\sigma^{(n)}}(\vec{v})(\vec{w}+\vec{v}_D)d\partial\Omega_D^0,$$

$$\overrightarrow{\sigma^{(n)}}(\vec{v}) + \overrightarrow{\sigma^{(n)}}(\vec{w})\Big|_{|x|\le 0, y=0} = 0, \qquad \int\limits_{-a}^{a} \overrightarrow{\sigma^{(n)}}(\vec{v}_D)dx = O\left(\frac{1}{D}\right).$$

Summarizing one can obtain:

$$U^a = U^0 + \frac{1}{2}\int\limits_{\Omega_D} \sigma_{ij}(\vec{w})e_{ij}(\vec{w})d\Omega_D + A^a - A^0 - 2p\int\limits_{-a}^{a} w_y dx + O\left(\frac{1}{D}\right). \tag{1.10}$$

And finally:

$$\begin{aligned}\frac{1}{2}\int\limits_{\Omega_D} \sigma_{ij}(\vec{w})e_{ij}(\vec{w})d\Omega_D &= \int\limits_{\partial\Omega_D^0} \overrightarrow{\sigma^{(n)}}(\vec{w})\vec{w}d\partial\Omega_D^0 - \int\limits_{-a}^{a} \overrightarrow{\sigma^{(n)}}(\vec{w})\vec{w}dx = \\ &= p\int\limits_{-a}^{a} pw_y dx + O\left(\frac{1}{D}\right),\end{aligned} \tag{1.11}$$

$$\overrightarrow{\sigma^{(n)}}(\vec{w})\Big|_M = -p\vec{j}.$$

It should be noted that when $D \to +\infty$

$$\frac{1}{2}\int\limits_{R^2\setminus M} \sigma_{ij}(\vec{w})e_{ij}(\vec{w})d\Omega = p\int\limits_{-a}^{a} w_y(x,y)dx. \tag{1.11$'$}$$

Joining (1.11) and (1.10) whilst $D \to +\infty$ one can obtain:

$$(U^a - U^0) - (A^a - A^0) = -p \int\limits_{-a}^{a} w_y(x, y) dx. \tag{1.12}$$

The function $\vec{w}(x, y)$ is the solution of the first basic problem of the crack theory. It reads:

$$2\mu w_y \Big|_{|x| \leq 0, y=0} = 2(1-\nu) p \sqrt{a^2 - x^2}.$$

This solution will be received later.

Using the solution one can rewrite (1.12) to obtain the expression to calculate the critical load to be applied in order to advance the crack:

$$(U^a - U^0) - (A^a - A^0) = -\frac{(1-v^2)p^2 a^2 \pi}{E}. \tag{1.13}$$

The energy balance condition reads:

$$\Delta U - \Delta A + \Delta \Pi = 0 \quad \text{or} \quad \frac{dA}{da} - \frac{dU}{da} = \frac{d\Pi}{da}.$$

Besides that:

$$\Delta \Pi = 4\gamma \Delta a. \tag{1.14}$$

Then

$$\frac{(1-v^2)p^2 2a\pi}{E} = 4\gamma \tag{1.15}$$

or

$$p_{cr}^2 = \frac{2\gamma E}{\pi a (1-v^2)}. \tag{1.16}$$

1.2 The first basic problem of the crack theory

Consider a plane strain problem for an elastic plane weakened by a crack $\{|x| \leq a, y = 0\}$ loaded on its faces by uniformly distributed pressure p. Using Kolosov's formulas (see, e.g., Muskhelishvili, 1966) one can write:

$$\begin{gathered} \sigma_{xx} + \sigma_{yy} = 4Re\varphi', \\ \sigma_{yy} - \sigma_{xx} + 2i\sigma_{xy} = 2(\bar{z}\varphi'' + \psi'). \end{gathered} \tag{1.17}$$

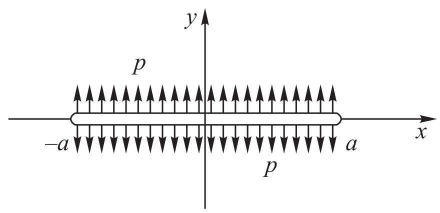

Fig. 1.2.

Due to the symmetry of the problem the simplified Westergaard method (Westergaard, 1939) can be used. Assuming

$$\varphi'(z) = \frac{1}{2} Z_{\mathrm{I}}(z), \quad \psi'(z) = -\frac{1}{2} z Z_{\mathrm{I}}'(z), \tag{1.18}$$

one will obtain:

$$\begin{aligned} \sigma_{xx} &= Re Z_{\mathrm{I}} - y Im Z_{\mathrm{I}}', \\ \sigma_{yy} &= Re Z_{\mathrm{I}} + y Im Z_{\mathrm{I}}', \\ \sigma_{xy} &= -y Re Z_{\mathrm{I}}', \\ 2\mu w_x &= (1-2v) Re Z_0 - y Im Z_{\mathrm{I}}, \\ 2\mu w_y &= (1-2v) Im Z_0 - y Re Z_{\mathrm{I}}, \\ \frac{dZ_0}{dz} &= Z_{\mathrm{I}}. \end{aligned} \tag{1.19}$$

Now the problem (1.5) is reduced to finding the analytical function $Z_{\mathrm{I}}(z)$ that fulfills the following boundary condition:

$$Re Z_{\mathrm{I}}\big|_{|x|\le a, y=\pm 0} = -p \tag{1.20}$$

and decreases at infinity as:

$$|Z_{\mathrm{I}}(z)| \sim O(|z|^{-2}). \tag{1.20$'$}$$

The problem is solved by:

$$Z_{\mathrm{I}} = -\frac{1}{\pi\sqrt{z^2-a^2}} \int\limits_{-a}^{a} \frac{p\sqrt{a^2-\zeta^2}d\zeta}{\zeta - z} +$$

$$+\frac{1}{\sqrt{z^2-a^2}} \sum_{k=0}^{\infty} \left[\frac{a_k'}{(z-a)^{k+1}} + \frac{a_k''}{(z+a)^{k+1}} \right],$$

where a_k', a_k'' are arbitrary real constants. Taking into account that deformation energy concentrated in the vicinity of the crack tips V_1, V_2 should be finite:

$$\int\limits_{V_{1,2}} \sigma_{ij}\varepsilon_{ij}dv < \infty,$$

we can conclude that $a_k' = a_k'' = 0\ \forall k$. Thus the solution of our problem is given by well-known Keldish—Sedov's formula (Keldish, Sedov, 1937):

$$Z_{\mathrm{I}} = -\frac{1}{\pi\sqrt{z^2 - a^2}} \int\limits_{-a}^{a} \frac{p\sqrt{a^2 - \zeta^2}d\zeta}{z - \zeta}. \tag{1.21}$$

Polar coordinate system (r, θ) with the origin at the crack tip $(x = a)$ is introduced. Old coordinates are coupled with the new ones by:

$$z = a + re^{i\theta}.$$

Finally, one will obtain the following expressions for displacements and stresses in the vicinity of right crack tip:

$$\begin{aligned}
\sigma_{xx} &= \frac{K_{\mathrm{I}}}{\sqrt{2\pi r}} \cos\frac{\theta}{2}\left(1 - \sin\frac{\theta}{2}\sin\frac{3\theta}{2}\right) + \ldots, \\
\sigma_{yy} &= \frac{K_{\mathrm{I}}}{\sqrt{2\pi r}} \cos\frac{\theta}{2}\left(1 + \sin\frac{\theta}{2}\sin\frac{3\theta}{2}\right) + \ldots, \\
\sigma_{xy} &= \frac{K_{\mathrm{I}}}{\sqrt{2\pi r}} \cos\frac{\theta}{2}\sin\frac{\theta}{2}\cos\frac{3\theta}{2} + \ldots, \\
w_x &= \frac{K_{\mathrm{I}}}{\mu}\sqrt{\frac{r}{2\pi}} \cos\frac{\theta}{2}\left(1 - 2v + \sin^2\frac{\theta}{2}\right) + \ldots, \\
w_y &= \frac{K_{\mathrm{I}}}{\mu}\sqrt{\frac{r}{2\pi}} \sin\frac{\theta}{2}\left(2 - 2v - \cos^2\frac{\theta}{2}\right) + \ldots, \\
K_{\mathrm{I}} &= \lim_{z\to a}\sqrt{2\pi(z-a)}Z_{\mathrm{I}} = \frac{1}{\sqrt{2\pi a}} \int\limits_{-a}^{a} p(\zeta)\frac{a+\zeta}{a-\zeta}d\zeta.
\end{aligned} \tag{1.22}$$

If $p = p_0 = \text{const}$ then:

$$\begin{aligned} Z_{\mathrm{I}} &= \frac{p_0}{\pi\sqrt{z^2-a^2}} \int\limits_{-a}^{a} p(\zeta) \frac{a^2-\zeta^2}{z-\zeta} d\zeta = p_0 \left(\frac{z}{\sqrt{z^2-a^2}} - 1 \right), \\ K_{\mathrm{I}} &= p_0\sqrt{\pi a}, \\ Z_0 &= p_0 \left(\sqrt{z^2-a^2} - z \right) + C, \\ 2\mu w_y\big|_{y=0} &= 2(1-v) Im Z_0 = 2(1-v) p_0 \sqrt{a^2-z^2}. \end{aligned}$$

Now expressions (1.12)–(1.15) can be checked. One should also note that expressions (1.22) are identical to the well-known Sneddon formulas (Sneddon, 1946). They were also obtained by M. Williams (Wiliams, 1957) and G. Irwin (Irwin, 1957).

1.3 Irwin's criterion

Following reasoning of Morozov (Morozov, 1984), approach based on the energy balance is applied to the problem of fracture surface propagation in three-dimensional space. The surface of the body after fracture process (in the accepted terms) can be presented as: $\partial\Omega \cup M^+ \cup M^- \cup \Delta\Sigma^+ \cup \Delta\Sigma^-$. Accounting the boundary conditions

$$\Delta\overrightarrow{\sigma^{(n)}}\Big|_{\partial\Omega} = 0 \quad \text{and} \quad \left[\overrightarrow{\sigma^{(n)}} + \Delta\overrightarrow{\sigma^{(n)}}\right]\Big|_{M\cup\Delta\Sigma} = 0,$$

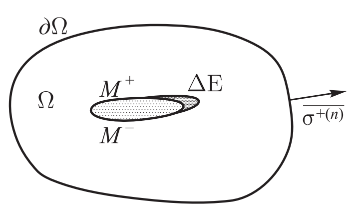

Fig. 1.3.

one can write:

$$\Delta A = \int_{\partial\Omega} \overrightarrow{\sigma^{(n)}} \Delta\vec{u} d\partial\Omega = \int_{\partial\Omega} \left(\overrightarrow{\sigma^{(n)}} + \Delta\overrightarrow{\sigma^{(n)}}\right) \Delta\vec{u} d\partial\Omega =$$

$$= \int_{\partial\Omega\cup M\cup\Delta\Sigma} \left(\overrightarrow{\sigma^{(n)}} + \Delta\overrightarrow{\sigma^{(n)}}\right) \Delta\vec{u} d\partial S = \int_{\Omega} (\sigma_{ij} + \Delta\sigma_{ij})\Delta e_{ij} d\Omega.$$

Besides that:

$$\Delta U = \frac{1}{2}\int_{\Omega} (\sigma_{ij} + \Delta\sigma_{ij})(e_{ij} + \Delta e_{ij}) d\Omega - \frac{1}{2}\int_{\Omega} \sigma_{ij} e_{ij} d\Omega.$$

Therefore:

$$\Delta U - \Delta A = -\frac{1}{2}\int_{\Omega} \Delta\sigma_{ij}\Delta e_{ij} d\Omega = -\frac{1}{2}\int_{\partial\Omega\cup M\cup\Delta\Sigma} \Delta\overrightarrow{\sigma^{(n)}}\Delta\vec{u} dS =$$

$$= -\frac{1}{2}\int_{\Delta\Sigma} \Delta\overrightarrow{\sigma^{(n)}}\Delta\vec{u} dS = \frac{1}{2}\int_{\Delta\Sigma} \Delta\overrightarrow{\sigma^{(n)}}\Delta\vec{u} dS = \frac{1}{2}\int_{\Delta\Sigma^+} \Delta\overrightarrow{\sigma^{(n)}}\Delta\vec{u}^+ dS +$$

$$+ \frac{1}{2}\int_{\Delta\Sigma^-} \Delta\overrightarrow{\sigma^{(n)}}\Delta\vec{u}^- dS = \frac{1}{2}\int_{\Delta\Sigma^+} \Delta\overrightarrow{\sigma^{(n)}}(\Delta\vec{u}^+ - \Delta\vec{u}^-) dS =$$

$$= \frac{1}{2}\int_{\Delta\Sigma^+} \Delta\overrightarrow{\sigma^{(n)}}[\Delta\vec{u}] dS. \tag{1.23}$$

Here the following conditions were used:

$$\overrightarrow{\sigma^{(n)}}\big|_{\Delta\Sigma^+} = -\overrightarrow{\sigma^{(n)}}\big|_{\Delta\Sigma^-}, \quad \overrightarrow{\sigma^{(n)}} + \Delta\overrightarrow{\sigma^{(n)}}\big|_{\Delta\Sigma} = 0 \quad \text{and} \quad [\Delta\vec{u}] = \Delta\vec{u}^+ - \Delta\vec{u}^-.$$

Applying (1.23) to the first basic problem of the crack theory (the case of plane strain) and accounting that in this case $\overrightarrow{\sigma^{(n)}}\big|_{\Delta\Sigma^+} = -\overrightarrow{\sigma^{(y)}}\big|_{\Delta\Sigma^+}$ and $\Delta\vec{u} = \vec{u}^+ - \vec{u}^-$ one can obtain:

$$\Delta U - \Delta A = \frac{1}{2}\int_{0}^{a} (\sigma_{yy}(u_y^+ - u_y^-) + \sigma_{xy}(u_x^+ - u_x^-)) dx.$$

Now, using expressions (1.22) at the crack surface ($y = 0$), one can receive:

$$\sigma_{yy} = \frac{K_{\mathrm{I}}}{\sqrt{2\pi x}} + \dots, \quad \sigma_{xy} = 0;$$

$$u_y^+ = u_y^- = \frac{K_{\mathrm{I}}}{\mu}(2 - 2v)\sqrt{\frac{\Delta a - x}{2\pi}} + \dots$$

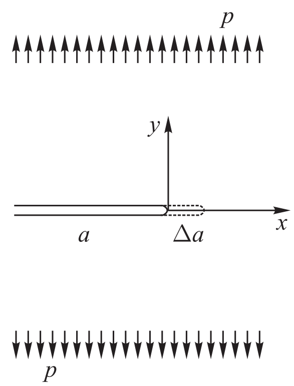

Fig. 1.4.

and then:

$$\Delta U - \Delta A = \frac{1}{2}\int_0^a \frac{K_{\mathrm{I}}^2(2-2v)}{2\pi\mu}\sqrt{\frac{\Delta a - x}{x}}dx = -\frac{K_{\mathrm{I}}^2(1-v)}{2\mu}\Delta a.$$

Taking into account the expression for the surface energy change $\Delta\Pi = 2\gamma\Delta a$ one can finally rewrite the Griffith energy balance to the following form:

$$K_{\mathrm{I}} < K_{IC} = \sqrt{\frac{2\gamma E}{1-v^2}}. \tag{1.24}$$

The relation obtained is usually called Irwin's criterion for fracture or the critical stress intensity factor criterion: if the stress intensity factor in the tip of the crack is less than the critical value, typical of the material fractured, then the crack does not propagate.

In the particular case when $p = p_0 = \mathrm{const}$ one gets $K_{\mathrm{I}} = p_0\sqrt{\pi a}$ and critical amplitude of the load can be determined as (see (1.16)):

$$p_{cr}^2 = \frac{2\gamma E}{\pi a(1-v^2)}.$$

References

Coulomb, C., 1776, Sur une Application des Regles de Maximus et Minimis a Quelques Problems. Memoires de Mathematique et de Physique Academic Rogaldes Sciences per divera Savane Anne, Paris.

Galilei, G., 1683, Discorsie Demonstrazioni Matenatiche Sopra dua Nuove Scienze, Leiden: Elsevier Science.

Griffith, A., 1920, The phenomena of rupture and flow in solids, Phil. Trans. Roy. Soc. Ser. A. V. 221. P. 163–198.

Irwin, G., 1948, Fracture dynamics. Fracturing of metals, Cleveland: ASM, P. 147–166.

Irwin, G., 1957, Analysis of the stress and strain near the end of the crack, J. Appl. Mech. V. 24. N 3. P. 361–364.

Keldish, M., Sedov, L., 1937, Effective solution of some boundary problems for harmonic functions, Doklady Physics, V. 16. N. 1. P. 7–10.

Mariotte, E., 1686, Traite de Mouvement des Eaux, Paris.

Mazya, V., Plamenevsky, B., 1978, Estimations in L_p and in Gelder classes, Math. Nachrichten. V. 81. P. 25–82.

Mohr, O., 1906, Abbandlungen Aus Dem Gebiete der Technischen Mechanic, Berlin: Wilhelm Ernst & Sohn.

Morozov, N. F., 1984, Mathematical aspects of crack theory, Moscow: Nauka.

Muskhelishvilli, N. I., 1966, Some basic problems of mathematical theory of elasticity, Moscow: Nauka.

Sneddon, I., 1946, The distribution of stress in neighborhood of a crack, Proc. Roy. Soc. Ser. A. V. 187. P. 229–260.

da Vinci, Leonardo, date unknown, Codice Atlantico, Folio 82 rect — B.

Westergaard, H. M. J., 1939, Bearing pressures and cracks, Appl. Mech. V. 6. P. 49–53.

Williams, M. L., 1957, On the stress distribution at the base of a stationary crack, J. Appl. Mech. V. 34. N 1. P. 109–114.

Chapter 2

Fractals and fracture*

Fractals. Application of fractal approach to fracture problems. Fracture initiated from an angular notch

2.1 Introduction

It is obvious that propagation of fracture surface is a much more complicated process as comparing to simple extension of a rectilinear crack with smooth edges, as it is treated in the linear fracture mechanics. In reality fracture process results in creation of surface with a big number of irregularities of different sizes (Fig. 2.1). Nature of these irregularities is mainly defined by the structure of material and the geometry of the specimen (see, e.g., Ravi-Chandar & Knauss, 1984). In this chapter fractal approach will be applied to fracture connected problems. Obviously, peculiar macroscopic parameters of irregularities of a fracture surface are mainly defined by the process of fracture surface appearance.

It is natural that the simulation of such a complicated object as an ideal mathematical crack ignores its interior structure. This approximation is quite suitable in many cases but there is a wide class of problems where accounting of the geometrical structure of fracture surface plays the principal role. These are problems that include energy consuming processes where one is forced to use specific energy parameters per unit of length, square or volume. But if the boundary of the investigated fracture zone is strongly uneven and can be poorly approximated by a smooth surface then the actual length of edge, the actual square or volume of the whole

*Authors acknowledge Dr. A. Kashtanov for his significant contribution to this chapter.

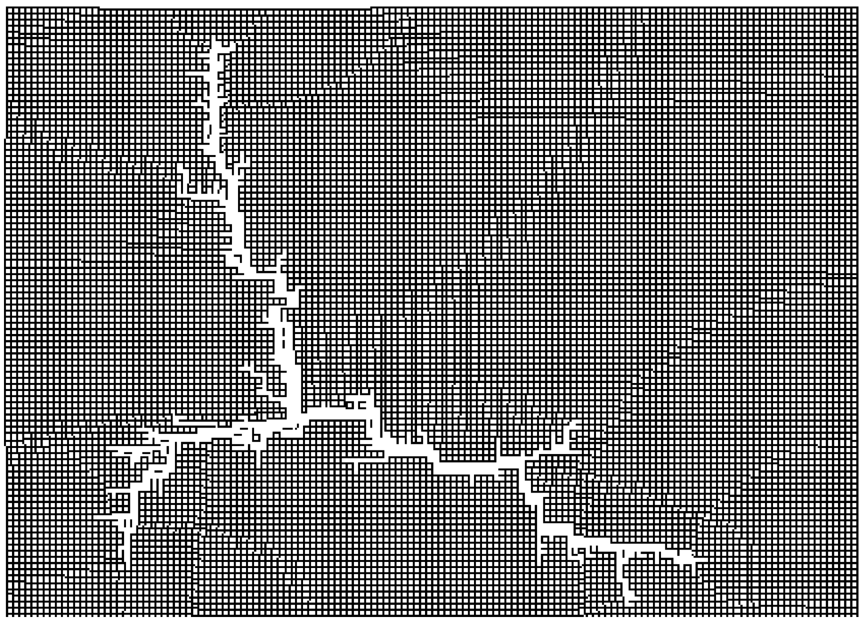

Fig. 2.1. Typical fracture surface.

object are vastly differing from what the traditional theory is working with. Incidentally, a number of experimental effects contradicting Griffith's approach is known. In order to solve this problem a modification of Griffith's criterion is needed.

In some cases Neuber—Novozhilov's (see chapter 4 or Morozov and Petrov, 2000) approach is helpful while trying to account for structure of a fracture surface. This approach is coupling some structural size to microfracture features. Another approach was proposed and experimentally tested by B.Mandelbrot (Mandelbrot, 1983). He supposed a statistical self-similarity of fracture surfaces and suggested a fractal model of quasibrittle crack. This approach gave a possibility to construct a more precise connection between micro singularities of fracture and its macroscopic parameters. On the one hand, it stimulated translation of the classical theory of brittle quasistatic fracture to another language (the most sequential statement one can find in the works of Mosolov (Mosolov, 1991) and Goldstein & Mosolov (Goldstein, Mosolov 1993). It has also caused attempts to classify fracture scale levels (Goldstein, Mosolov 1992). At the same time introduction of fractal correction for calculation of specific properties allows one to take into consideration surface roughness and to receive a more precise model of fracture process. In this chapter fractal approach is used to solve problems of crack mechanics, which do not have an adequate solution within the framework of traditional fracture theory. Successful attempts to apply fractals to brittle fracture were published by Kashtanov and Petrov (Kashtanov, Petrov, 1998, Kastanov, Petrov, 2001). These results are extensively used in this chapter.

2.2 Fractals in nature

2.2.1 *The fractal concepts and their physical interpretations*

The concept of fractal is known for a long time but attitude to it was rather ambiguous since the time when the first fractal curves were constructed. Actually, the appearance of Cantor's set and Peano's curve gave rise to a split among mathematicians of the nineteenth century. While the majority of scientists considered them as some pathological entities, their founders regarded the results as a hymn to abstract mathematics. They were admired by the fact that pure science has managed to step over the limitations of its natural origin (Mandelbrot, 1983).

However, it was impossible to explain the origin and nature of these curves staying within the framework of classical theories based on Euclid's geometry and Newton's mechanics. All this resulted in a crisis of naturalism which began in the end of the 19th century and was lasting almost a half of the century. During this period the main principles of modern science were formed. Fractal geometry, being one of the newest branches of mathematics had raised as a result of work of such scientists as Poincare, Cantor, Peano, Hausdorff, Sierpinski and Mandelbrot.

A concept that offers a possibility of giving a strict definition of fractal set is the concept of fractional metric dimension. It was introduced by F. Hausdorff while he was studying various sets with non-integer dimensions. Let $N(\varepsilon)$ be the minimal number of m-dimensional solid spheres with radius ε, needed to cover some limited set $X \subset R^m$. This set has metric dimension D, $0 \le D \le m$, if at $\varepsilon \to 0$ the number of spheres $N(\varepsilon)$ grows as $C\varepsilon^{-D}$ where $C \ge 0$, that is $\lim_{\varepsilon\to 0} N(\varepsilon)\varepsilon^D = C$. Set X is called fractal if its Hausdorff dimension D is not an integer.

For example, if we have ordinary two-dimensional region then $N(\varepsilon) \approx \Omega^{-2}$ or $\lim_{\varepsilon\to 0} N(\varepsilon)\varepsilon^2 = \Omega$, where Ω is the area of the considered region.

For the ordinary curve one will have $N(\varepsilon) \approx L\varepsilon^{-1}$, $\lim_{\varepsilon\to 0} N(\varepsilon)\varepsilon = L$. Here L is the curve length.

Thus, for any set:

$$D = -\lim_{\varepsilon\to 0} \frac{\ln N(\varepsilon)}{\ln \varepsilon} \tag{2.1}$$

because of:

$$-\lim_{\varepsilon\to 0} \frac{\ln N(\varepsilon)}{\ln \varepsilon} = -\lim_{\varepsilon\to 0} \frac{-D\ln\varepsilon + \ln C}{\ln \varepsilon} = D. \tag{2.2}$$

Now one can calculate the length of a plane fractal curve. For this purpose it can be approximated by a broken line constructed of identical segments with length ε. Then, using the definition of Hausdorff, under assumption that ε is small enough one will get:

$$L(\varepsilon) = N(\varepsilon)\varepsilon = C\varepsilon^{1-D} = C_0(l/\varepsilon)^D\varepsilon. \tag{2.3}$$

Here a constant C is represented as $C = C_0 l^D$, L is the fractal length of the considered curve, l is the macroscopic length of this curve and C_0 is some dimensionless constant. It is obvious that fractal and macroscopic lengths of the considered curve should be coincided, so $L = l|_{D=1} \Leftrightarrow C_0 = 1$. Hence, the metric length of the curve is related to its topological length by a relation:

$$L(\varepsilon) = (l/\varepsilon)^D\varepsilon. \tag{2.4}$$

Well-known examples of fractal sets include Cantor set ($D = \ln 2/\ln 3$ — Fig. 2.2a) and von Koch curve ($D = \ln 4/\ln 3$ — Fig. 2.2b).

The property of self-similarity is held for these objects as well as for other regular fractals: they can be divided into indefinitely small parts in such a way that each part will appear as a small copy of the whole object. In other words, if one will look at a regular fractal with or without microscope he will see exactly the same picture.

Let's examine von Koch figure in details. The polygonal line obtained at k'th step consists of 4^k segments of length $1/3^k$ and has an overall length equal to $(4/3)^k$. Thus, the length of the limiting polygonal line when $k \to \infty$ (that is the length of von Koch curve) is increasing infinitely and its Hausdorff dimension is:

$$D = \lim_{k\to\infty} \frac{\ln 4^k}{\ln 3^k} = \frac{\ln 4}{\ln 3} > 1.$$

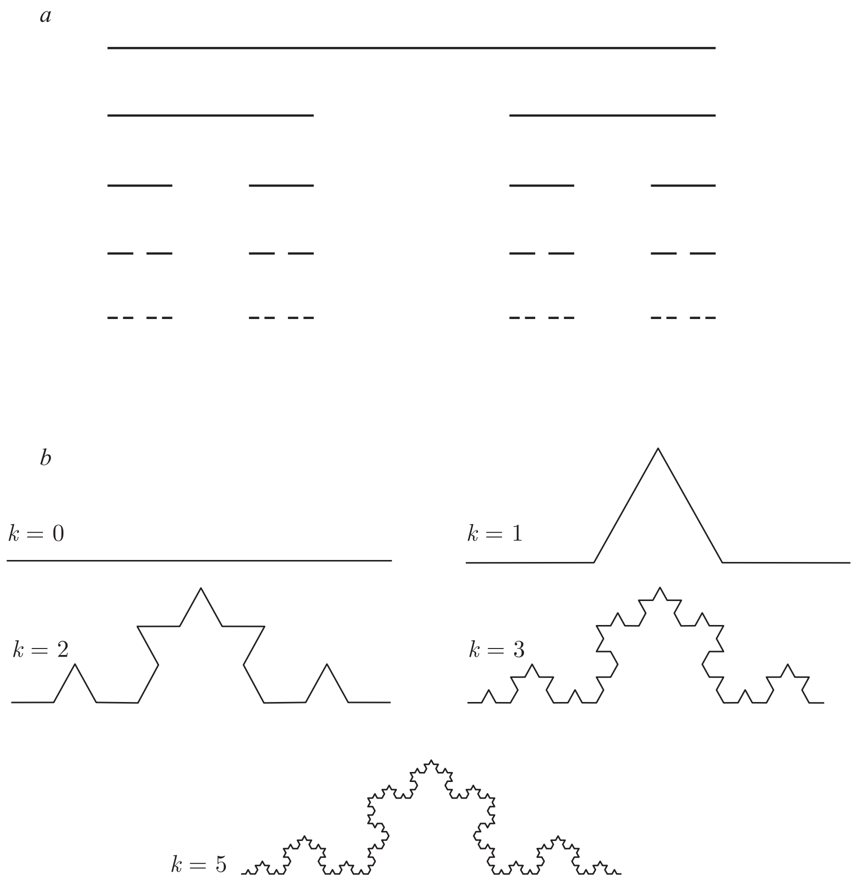

Fig. 2.2. *a* — Cantor set, *b* — Von Koch curve.

Besides that, von Koch curve consists of four identical parts similar to the whole curve with the ratio of similarity equal to 1/3. Further, each part can be again divided into four identical parts and so on. Therefore, the length of any piece of this curve is infinite.

In the same manner the dimension of any other regular fractal set can be calculated. For example, the dimension of Cantor set is:

$$D = \lim_{k\to\infty} \frac{\ln 2^k}{\ln 3^k} = \frac{\ln 2}{\ln 3} < 1$$

and its length equals zero:

$$L = \lim_{k\to\infty} \frac{2^k}{3^k} = 0.$$

In spite of the fact that the definition of fractal dimension was formulated by F. Hausdorff in 1919, fractal geometry remained a subject of abstract mathematics for quite a long time. Scientists came across natural objects having fractal properties only in the second half of the twentieth century. In 1961 L. Richardson tried to measure the length of Great Britain's coastal line and ended up with an interesting effect. He took a map of the UK and followed the UK coastal line with some preset spread of a pair of compasses. He made this in such a manner that every new step of compasses began at the point where the previous one ended. Then the length of coast should be approximately equal to the number of steps multiplied by the magnitude of the compasses spread. He iterated the procedure with smaller and smaller spread and expected that the measured length would quickly approach some defined value — the true length of coastal line. Surprisingly the behaviour of the length measured was opposite to the expected: it increased infinitely with reduction of compasses spread. Nevertheless such a behavior can easily be explained. Reducing the spread of the pair of compasses he took into account smaller and smaller capes and bays. And while using a map of a greater scale, new irregularities of coastal line, not visible at the previous map, were appearing. Obviously these new irregularities were making contribution to measured length. As a result he found that the coast is so uneven that it is not possible to precisely approximate it with a polygonal line.

However, fractal properties of a coastal line, so evidently exhibited in the previous paragraph do not allow considering it as a fractal. By definition the fractal set is a set with fractional metric dimension. Procedure of measurement of dimension assumes reduction of the measurement step to zero. Obviously this condition cannot be satisfied for a natural object: one cannot choose a step smaller than some size related to the microstructure of an object investigated. In 1967 B. Mandelbrot (Mandelbrot, 1983) formulated a revolutionary concept allowing usage of fractals to model natural processes and phenomena. He defined fractal as a structure consisting of parts that are similar to the whole structure. According to this definition various objects, which were characterized as “strange”, “confusing”, branched, wrinkled, porous etc., could now be studied using strict quantitative terms of fractal dimension. Here it is necessary to mention that though fractal models for natural objects allow giving a more precise description of structure of these objects, all the models are only approximations of actual objects in some restricted range of scale levels. Nature normally provides much more complicated structures than a human can construct. Nevertheless, in some cases fractal approximation is much more precise and convenient than the linear one.

Even so, using this approach one faces a very serious problem. The definition of physical fractal structure given by Mandelbrot does not supply a definition of "physical" fractal dimension. This dimension has to be evaluated from some experimental procedure or numerical method. There are different approaches to determination of dimension of natural objects but all of them are applicable only in some limited range of scales.

Dimension of cluster can be considered as the first example. Let cluster $X \subset R^m$ consist of elementary particles of size $\varepsilon_{\min}$. To define fractal dimension one can operate with sizes within the range $\varepsilon_{\min} \leq \varepsilon \leq \varepsilon_{\max}$, where $\varepsilon_{\max}$ is a scale comparable to geometrical size of the considered object. The cluster can be divided into cubes with size ε. Let $N(\varepsilon)$ be the smallest possible number of such m-dimensional cubes needed to cover the whole cluster. It is usually stated that the cluster is having fractal dimension D if for all scales from a considered range the following relation is fulfilled:

$$N(\varepsilon) \sim (\varepsilon/\varepsilon_{\min})^D, \quad \varepsilon_{\min} \leq \varepsilon \leq \varepsilon_{\max}. \tag{2.5}$$

The magnitude D is determined as a slope of linear dependency $\ln N(\varepsilon)$ as a function of $\ln \varepsilon$.

Another widely spread definition of dimension of a physical fractal for a plane curve is based on the Richardson's method. Suppose one intends to measure the length of some plane curve using a pair of compasses. If for any spread of compasses within the range $\varepsilon_{\min} < \varepsilon < \varepsilon_{\max}$ the relation

$$N(\varepsilon) \sim \varepsilon^{-D}, \quad \varepsilon_{\min} < \varepsilon < \varepsilon_{\max} \tag{2.6}$$

is fulfilled, then the considered curve is a fractal with dimension D. This dimension is called the fractal dimension of Richardson. It is easy to see that within the considered range the length of a fractal curve can be expressed as:

$$L = (l/\varepsilon)^D \varepsilon, \quad \varepsilon_{\min} < \varepsilon < \varepsilon_{\max}. \tag{2.7}$$

This definition of physical dimension is very close to the one of Hausdorff.

Another definition of dimension of a curve dimension is known as "box dimension". Suppose, one covers the considered curve using squares (boxes) with side ε_i. At the next step each box is divided into four smaller boxes with sides $\varepsilon_{i+1} = \varepsilon_i/2$ and the number of squares containing at least one point of the curve is calculated. If relation (2.6) is fulfilled within some range of sizes then the considered curve is a fractal.

Unfortunately it is proven only for mathematical definition of Hausdorff dimension that the magnitude of the fractal dimension is not depending on coverage (see, e.g., Falconer, 1990). For physical fractals different procedures of approximated definition of fractal dimension give different values. Therefore even for similar natural objects it is impossible to consider fractal dimension as a typical property of these objects without a reference to the procedure of how the dimension was measured.

2.3 Measurement of fractal dimension

There exists a big number of approaches, based on different definitions of fractal dimension, to how one should measure fractal dimension of an object. Here some methods applicable to measurements of dimension of quasi-brittle fracture surfaces are presented. These are metallographic methods, widely used as direct methods of fractal analysis.

The slit islands analysis (SIA) is the first of them. A specimen containing a crack is coated with nickel (or, in some cases, silver) and then polished in a plane parallel to the crack surface until many small "islands" become visible on the crack surface. These "islands" are the specimen material surrounded by "lakes" of the covering material (i.e. nickel or silver). This procedure provides transition from complicated three-dimensional structure of fracture surface to plane structures of "coastal lines of islands". Individual "islands" are photographed with high resolution registration techniques and their square S and perimeter P are measured. The values obtained are plotted in full logarithmic coordinates $\log S$ versus $\log P$ and approximated by a straight line. Then the fractal dimension of the fracture surface is defined as: $D = \alpha + 1$ where α is a fractal dimension of "coastal lines" determined using relation $P \sim S^{\alpha/2}$. Thus α is defined directly by the slope of the constructed plot.

Another widely spread metallographic method to determine fractal dimension is the method of vertical sections. It differs from the slit islands method by alignment of the polished plane. In this method the vertical sections of crack surface are produced. Then the magnitude α is determined by the relation between the length of the surface profile L and the scale of measurements ε: $L(\varepsilon) \sim \varepsilon^{1-\alpha}$. For reliability the magnitude α is calculated as the average value of magnitudes obtained on cuts with different alignment with respect to overall direction of crack propagation.

Another frequently used metallographic method is the profile Fourier analysis. It implies the calculation of power spectrum (the sum of squared amplitudes) of crack surface profile. For regular fractals and statistically self-similar structures in the interval of self-similarity the power spectrum $s(k)$ can be approximated by $s(k) \sim k^{-B}$, where k is the wave vector and index B is the exponent coupled with fractal dimension D by the following relation: $B = 2(3 - D)$.

The apparent shortage of metallographic methods is the dependency of measured result on a specific approach and chosen measurement scale. In other words values of dimension obtained using one or another method do not coincide. At the same time these values do correlate between each other and do reflect singularities of the fracture surface investigated.

Many other methods are used to measure fractal dimension [see e.g. Falconer, 1990 or Borodich and Onishchenko, 1999], but it is necessary to note that any of these methods is rather inaccurate. One has to carry out measurements on a big number of scale levels. However, natural objects display only 3–4 levels of statistical self-similarity. This does not allow for evaluation of fractal dimension with high accuracy. Besides that, there are no homogeneous fractal aggregates in nature. Any natural fractal represents a multifractal object: it consists of parts with different fractal dimensions. That the character of crack surface irregularities varies vastly is especially visible in experiments on brittle materials. For fast running cracks three zones with different degree of roughness are usually distinguished: the mirror zone (adjacent to the crack initiation point), misty and hackle zone (appearing as the crack propagates). Different zones and transitions between them are characterized by different values of fractal dimension. In this sense it would be more correct to speak about dimension of some area of the fracture surface, rather than about the dimension of the whole crack.

The conclusion is unfortunately not very promising: only if measured fractal dimensions of two cracks differ really alot one can state that two cracks really have different fractal dimensions. For this reason it is a doubtful way to modify existing classical fracture theories introducing some "fractal corrections" obtained experimentally. A much more fruitful approach is the simulation of crack as a fractal with dimension determined at some fixed scale level from some theoretical reasoning. Then, solving a specific problem for a crack, described by an introduced fractal, it is possible to determine some physical magnitudes. Values for these magnitudes can be easily received experimentally, for example, the value of the critical load or the critical stress. In particular, it is offered to evaluate the fractal dimension so that it satisfies the energy balance equation.

2.3.1 *Fractals in brittle fracture mechanics*

For a long time it is known that the dislocation structure of metals is changing as the load is increased. This modification is displaying transition from homogeneous to cellular dislocation structure accompanying plastic deformation process (this result was published by Zolotuhin (Zolotuhin, 1998), see also Ivanova et. al, 1994). In fig. 2.3 scheme for transition from homogeneous to cellular dislocation structure under plastic deformation process is presented.

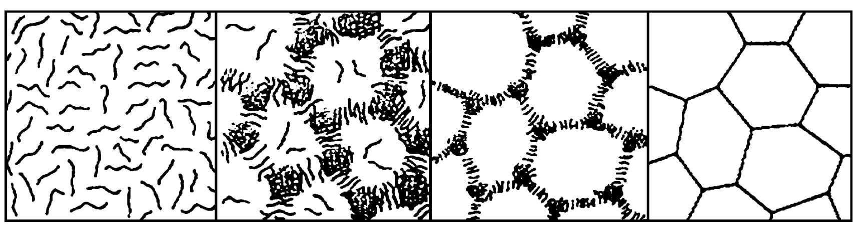

Fig. 2.3. Scheme for transition from homogeneous to cellular dislocation structure under plastic deformation process.

At the initial stage of plastic deformation there are a lot of dislocations uniformly distributed in a material volume. As the strains increase, dislocations are accumulated into tangles. Further, these tangles are shaped into a precisely arranged cellular structure. Tangles aggregated into the cell walls are fractals with dimensions varying continuously from $D = 1$ (random distribution of dislocations) via $1 < D < 2$ (flabby tangles) to $D = 2$ (precise geometrical walls of cells).

Fractal model of brittle fracture allows considering it in the same manner: the fracture process can be represented as a process of gradual increase of fractal dimension of the appearing crack. In ideal material prior to application of the load, fractal dimension of the fracture surface is $D = 0$ and the crack does not exist. As the load is increased the precrack zone is formed as a result of appearance of numerous microcracks. In the plane case this process can be simulated by some kind of lacunar fractal (ex. Cantor set, Fig. 2.2) with dimension less than 1. The dimension of this fractal is gradually increasing to $D = 1$, corresponding to appearance of an evident macrocrack. On this stage quasistatic fracture is usually studied in a classical solid mechanics formulation. The further growth of fractal dimension results in increase of roughness of the crack surface and this can be modeled by some invasive fractal with dimension $D > 1$ (such as von Koch curve, Fig. 2.2b). When the fractal dimension is close to 2 branching begins since the crack cannot increase its roughness anymore and tries to release the excess of accumulated energy in such a way. This effect is observed in experiments on fast running cracks.

In the majority of static problems it is sufficient to consider the process of fracture only on the stage when the crack can be simulated by a single line segment (fractal dimension of the crack is close to 1). At the same time consideration of fracture process as a process of growth and interaction of microcracks gives solutions to problems unsolvable within the framework of classical fracture mechanics. This process can also be related to the first lacunar stage of macrocrack extension as well as to the third stage when fracture surface is developing and changing.

While constructing the fractal model it is important to remember that the fractal length has no additive property: consider two fractal curves having the same dimension D but having different macroscopic lengths l_1 and l_2. According to (2.4) the fractal lengths of these curves measured using step ε are equal to:

$$L_1 = (l_1/\varepsilon)^D \varepsilon, \quad L_2 = (l_2/\varepsilon)^D \varepsilon. \tag{2.8}$$

Now consider a curve with the same dimension and macroscopic length equal to $l_1 + l_2$. Its fractal length is:

$$L = \left(\frac{l_1 + l_2}{\varepsilon}\right)^D \varepsilon. \tag{2.9}$$

Evidently, if $D > 1$ then

$$L_1 + L_2 < L. \tag{2.10}$$

Besides that it is necessary to note that any self-similar fractal curve, such as von Koch figure, with fractality arising from locally transverse disturbances of a line, cannot be a model for brittle crack. In contrast to a coastal line the crack surface should be kinematically admissible: the faces

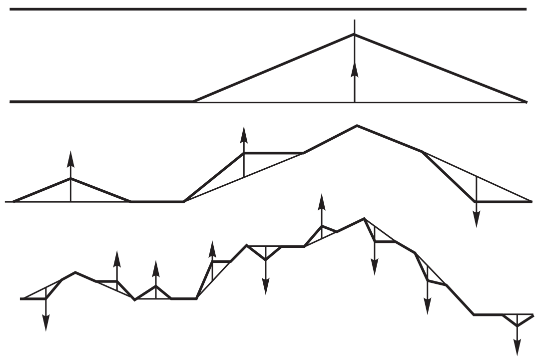

Fig. 2.4. An example of self-affine fractal curve.

of the crack should have a possibility to slide apart as two rigid bodies. Self-similar fractal curve (ex. von Koch figure) has recessive segments receding backwards, against the common direction of crack propagation (Fig. 2.2b). In this case, the separation of crack faces is impossible without additional fracture, but then the evolution of fracture surface cannot be represented as a growth of a simple fractal crack. For this reason self-similar (or locally disturbed) fractals are not convenient to use while simulating fracture surfaces. Instead, it is better to consider the self-affine fractals obtained from a line by disturbances normal to crack direction (Fig. 2.4).

2.4 The plane problem for angular stress concentrator

2.4.1 *The plane problem for angular stress concentrator*

As discussed in the previous chapter, the plane problem for angular stress concentrator is one of the most important problems in crack mechanics, and it cannot be solved utilizing the classical equation of energy balance. Consider an elastic plane with an angular notch with an angle $2\pi - 2\omega$. Suppose the plane is loaded by a uniform load p applied at infinity in direction given by y-axis (Fig. 2.5).

It is necessary to find the solution of Lame equation with boundary conditions $\sigma^n = 0$, $\sigma^{ns} = 0$ at the notch faces and $\sigma_{xy} = 0$, $\sigma_y = p$ at infinity. In accordance with Griffith's concept of energy balance equation the linear crack is generated in the angular vertex when the load has reached the critical value p_*. To generate a crack of some predefined length l it is necessary to commit the work ΔW. It will result in a change of surface energy of the system by $\Delta\Pi$ proportional to the length l of the crack generated.

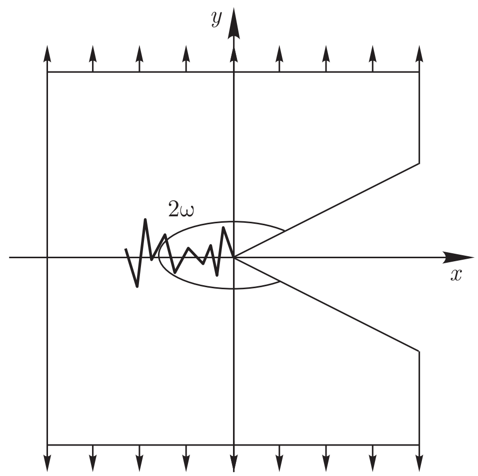

Fig. 2.5. Plane containing an angular notch.

Following Griffith's hypothesis in the case of brittle fracture all the work committed is spent exclusively on generation of a new surface. Thus, at the moment of crack initiation the equation of energy balance takes the form:

$$\Delta W = \Delta\Pi. \tag{2.11}$$

As shown above, at the moment of crack initiation $\Delta W \sim l^{2\mu}$ where μ is the least positive root of the following equation (Fig. 2.6):

$$\mu \sin(2\omega) + \sin(2\mu\omega) = 0. \tag{2.12}$$

So, $\Delta W \sim l^{2\mu}$, but at the same time $\Delta\Pi \sim l$. Hence, magnitudes of different orders are appearing in the left and right-hand side of the energy balance (2.11). This means that the critical load level is impossible to define.

It will be demonstrated that the mentioned problem can be avoided assuming crack fractality. Suppose a crack is generated in the vertex of a notch and is propagating "in average" along the x-axis. This crack can be represented as a fractal with some dimension D. The crack is occupying the region $[0, l]$ along the x-axis and $[0, l_1]$ along the y-axis. Thus $l_1 \ll l$. Therefore the "true" length of the crack L is related to its linear length l by the fractal law (4.7). Now if at any fixed scale ε one will consider that the crack length L is proportional to $l^{2\mu}$ then $\Delta\Pi \sim L$ and $\Delta W \sim l^{2\mu} \sim L$. Thus, eliminating L it is possible to write the Griffith criterion for the

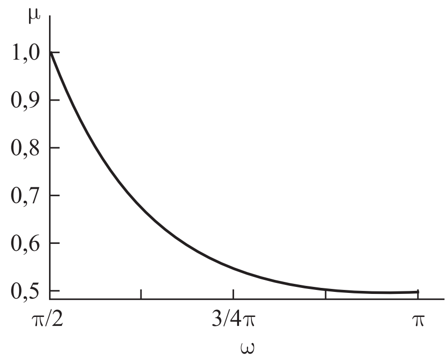

Fig. 2.6. μ as a function of ω.

stated problem. If $L \sim l^{2\mu}$ then in accordance with (2.7) one will get:

$$D = 2\mu. \tag{2.13}$$

It should be noted that if $\omega \in [\pi/2, \pi]$ then $D \in [1, 2]$ and the magnitude of D can be used as a value for Hausdorff dimension of the fractal curve.

Thus, the equation of Griffith's energy balance allows natural generalization to the case of fracture developing from the vertex of an angular notch. The basic technique of such a generalization is the introduction of crack fractality. Then the crack dimension can be uniquely determined by the angle of the notch.

2.4.2 *Hypotheses of fractal generalization of the Griffith energy balance*

Consideration of brittle crack as a fractal makes it possible to construct an equation of energy balance and to determine the critical load in problems with angular stress concentrators. In order to make this the following assumptions are made:

- Griffith's hypothesis is correct. Thus, all the work spent on the system is consumed for generation of a new fracture surface.
- Developing crack can be simulated by a fractal with undefined dimension D.
- The work of the crack opening ΔW is the integral parameter of the stated problem and is determined at the macroscopic scale level.
- The surface energy of a crack $\Delta\Pi$ is calculated using the crack

fractal length to take into account the microstructure of the crack surface.

- The fractal dimension D of the simulated crack can be found from request on correctness of energy balance (2.11) at the macroscopic scale.

In crack mechanics there exists a basic parameter describing the elementary fracture cell at each scale level $d = \frac{2}{\pi} \frac{K_{\mathrm{I}C}^2}{\sigma_C^2}$ (structural approach to fracture is presented in every detail in chapter 4 or in works of Morozov (Morozov, 1984) and Petrov (Petrov, 1996). Here σ_C is the ultimate strength of material and $K_{\mathrm{I}C}$ is the quasistatic fracture toughness. For rectilinear crack $\omega = \pi$ having length $2a$ the quasistatic fracture toughness can be determined at the macroscopic scale by $K_{\mathrm{I}C} = p_*(\pi)\sqrt{\pi a}$. Naturally at another scale level the "true" crack length is changing in accordance to (2.7) and the value of static fracture toughness is also changed. In other words each spatial scale can be described by its own characteristic scale d of a fracture process. Generally speaking, this fracture scale is not related to real geometrical structure of material. At each scale level the fractal law (2.7) has the form:

$$L = (l/d)^D d. \tag{2.14}$$

It was discussed above that only one scale level is used. Thus d can be considered as a value defined experimentally at the macroscopic scale.

2.5 The problem of symmetric hole

As an application of principles stated above, consider an important particular case of angular notch problem, namely, the problem of symmetric hole (Fig. 2.7).

Consider an elastic plane weakened by a hole formed by circular arcs. This problem can be investigated using the method of bipolar coordinates (see Ufland, 1950). Let

$$z = x + iy; \quad \zeta = \alpha + i\beta.$$

Then

$$z = ai \coth \frac{\zeta}{2}; \quad 0 \le \alpha < \infty, -\pi \le \beta \le \pi \tag{2.15}$$

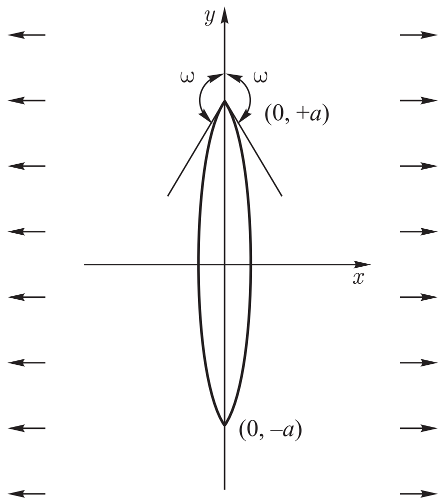

Fig. 2.7. Plane with a symmetric hole.

and

$$\frac{x}{a} = \frac{\sin\beta}{\mathrm{ch}\alpha - \cos\beta}, \quad \frac{y}{a} = \frac{\mathrm{sh}\alpha}{\mathrm{ch}\alpha - \cos\beta}, \tag{2.16}$$

One could note that the line $\alpha = \text{const}$ is a circle $x^2 + (y - a\coth\alpha)^2 = a^2/\mathrm{sh}^2\alpha$ having its center at the point with coordinates $(0, a\coth\alpha)$ and radius $a/|\mathrm{sh}\alpha|$; and the line $\beta = \text{const}$ is a circle $(x - a\cot\beta)^2 + y^2 = a^2/\sin^2\beta$ having the center in the point with coordinates $(a\cot\beta, 0)$ and radius $a/|\sin\beta|$. By the way, the lines $\beta = \text{const}$ coincide with the hole surface.

Introducing:

$$h = \frac{a}{\mathrm{ch}\alpha - \cos\beta}; \quad g^2 = \left(\frac{d\zeta}{dz}\right)^2 = h^{-2} \tag{2.17}$$

and following the considerations of the previous chapter one can obtain (see Morozov, 1986):

$$\begin{aligned}
a\sigma_{\alpha\alpha} &= \left[(\mathrm{ch}\alpha - \cos\beta)\frac{\partial^2}{\partial\beta^2} - \mathrm{sh}\alpha\frac{\partial}{\partial\alpha} - \sin\beta\frac{\partial}{\partial\beta} + \mathrm{ch}\alpha\right]\frac{\Phi}{h},\\
a\sigma_{\beta\beta} &= \left[(\mathrm{ch}\alpha - \cos\beta)\frac{\partial^2}{\partial\alpha^2} - \mathrm{sh}\alpha\frac{\partial}{\partial\alpha} - \sin\beta\frac{\partial}{\partial\beta} + \cos\beta\right]\frac{\Phi}{h},\\
a\sigma_{\alpha\beta} &= -(\mathrm{ch}\alpha - \cos\beta)\frac{\partial^2}{\partial\alpha\partial\beta}\frac{\Phi}{h}.
\end{aligned} \tag{2.18}$$

Here Φ gives a solution of biharmonic equation having the form (in bipolar coordinates):

$$\left[\frac{\partial^4}{\partial\alpha^4} + 2\frac{\partial^4}{\partial\alpha^2\partial\beta^2} + \frac{\partial^4}{\partial\beta^4} - 2\frac{\partial^2}{\partial\alpha^2} + 2\frac{\partial^2}{\partial\beta^2} + 1\right]\frac{\Phi}{h} = 0 \qquad (2.19)$$

and the common solution of considered problem is:

$$\Phi = \Phi_1 + \Phi_2, \qquad (2.20)$$

where Φ_1 defines the uniaxial tension along x-axis and equals to:

$$\Phi_1 = pah\frac{\mathrm{sh}^2\alpha - (\mathrm{ch}\alpha - \cos\beta)^2}{2(\mathrm{ch}\alpha - \cos\beta)}, \qquad (2.21)$$

$$\begin{aligned}\Phi_2 = pah\Bigg\{&(2K_1 - 1)\cos\beta + K_1(\mathrm{ch}\alpha - \cos\beta)\ln\frac{\mathrm{ch}\alpha - \cos\beta}{\mathrm{ch}\alpha + \cos\beta} + \\ &+ \frac{1}{\sqrt{2\pi}}\int\limits_{-\infty}^{\infty}(A\cos\alpha\,\mathrm{ch}(\lambda\beta) + B\sin\beta\,\mathrm{sh}(\lambda\beta))e^{-i\lambda\alpha}d\lambda\Bigg\},\end{aligned} \qquad (2.22)$$

where

$$K_{\mathrm{I}} = \frac{1 - 2\sin^2\omega\int_0^\infty \frac{\lambda d\lambda}{\mathrm{sh}(2\lambda\omega) + \lambda\sin(2\omega)}}{4\int_0^\infty \frac{\mathrm{sh}^2(\lambda\omega) - \lambda^2\sin^2\omega}{\lambda(\lambda^2+1)(\mathrm{sh}(2\lambda\omega) + \lambda\sin(2\omega))}d\lambda}. \qquad (2.23)$$

The asymptotic expression for stresses in the initial problem and for displacement field in the problem of the same hole with cuts of length $l \ll a$ are (Morozov, 1986):

$$\sigma_{yy}(0,y)|_{y\to\pm a} = pc_1(\omega)\left(\frac{r}{2a}\right)^{\mu(\omega)-1} + \ldots, \qquad (2.24)$$

$$u_y(0,y)|_{y\to\pm a+l} = 6pK_{\mathrm{I}}(\omega)l^{\mu-1/2}\frac{\sqrt{|r-l|}}{(2a)^\mu} + \ldots. \qquad (2.25)$$

Here $r = |y-a|$, μ is determined by equation (2.12), $c_1(\omega)$ is a defined coefficient ($c_1(\pi) = 1/2$ and $c_1(\pi/2) = 3$) and $K_{\mathrm{I}}(\omega)$ is defined by (2.23). The work of the crack opening is:

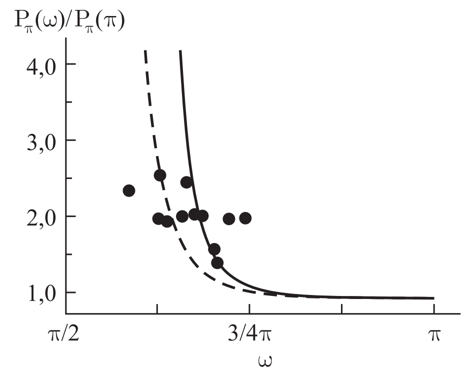

Fig. 2.8. Critical load amplitude as a function of the hole length.

$$\Delta W = -\int_0^l \sigma_{yy} u_y dr \bigg|_{x=0} = -6\sqrt{\pi}(2a)^{1-2\mu} p^2 \frac{\Gamma(\mu)}{\Gamma(\mu+3/2)} K_{\mathrm{I}}(\omega) c_1(\omega) l^{2\mu}, \tag{2.26}$$

where $\Gamma(z) = \int_0^\infty t^{z-1} e^{-t} dt$ is the Euler Gamma-function.

The surface energy of the growing crack can be calculated using its "true" fractal length to account the microstructure of fracture process. Because of (2.14) change of the surface energy can be presented as:

$$\Delta\Pi = -4\gamma (l/d)^D d, \tag{2.27}$$

where γ is the surface energy density.

To determine the critical load from the balance equation (2.11) in terms of (2.26) and (2.27) one has to demand coincidence of exponents of l in the left and right-hand side of the energy equation. Condition (2.13) has to be valid in the considered problem. Now the value for the critical load p_* can be expressed in the following way (solid line in Fig. 2.8 corresponds to the length of a hole $2a$ equal to 1):

$$p_*^2 = \frac{2\gamma \Gamma(\mu+3/2)}{3\sqrt{\pi}\Gamma(\mu) K_{\mathrm{I}}(\omega) c_1(\omega)} \left(\frac{2a}{d}\right)^{D-1}. \tag{2.28}$$

Thus, simulation of a crack as a fractal with dimension determined by the value of an angle of the angular notch made the problem solvable: energy balance equation is satisfied and the load needed to initiate fracture process is found. The asymptotic solution for stress and displacement fields are obtained: $\sigma \sim r^{D/2-1}$, $u \sim r^{D/2}$ (where r is the distance from the hole vertex) which coincide with asymptotic solution given by Goldstein & Mosolov (Goldstein, Mosolov, 1993). It should also be mentioned that it was assumed that the attention should be paid to microstructure of the crack only at the stage when its surface energy is calculated. At the same time the work spent on crack opening was determined at the macroscopic scale level.

References

Borodich F. M., Onishchenko D. A., 1999, // Int. J. Solids Struct. 1999. V. 36. P. 2585–2612.

Falconer, K. J., 1990, Fractal geometry: mathematical foundations and applications, Chichester: John Wiley.

Goldstein R. V., Mosolov A. B., 1992, Appl. Math. Mech., V. 56. P. 663–671.

Goldstein R. V., Mosolov A. B, 1993, Proc. Russian Academy of Sciences, V. 329. P. 429–432.

Ivanova, V. S., Balankin, A. S., Bunin, I. Zh., Osksogoev, A. A, 1994, Synergethics and fractals in material science, Moscow: Nauka.

Kashtanov, A. V., Petrov, Yu. V., 1998, Energy balance in the problem of the fracture of an elastic plane with an angular notch, Vestn. St.-Peterb. Gos. Univ. Ser. 1: Mat. Mekh. Astron., Issue 4, No. 22, 102–104.

Kashtanov, A. V., Petrov, Yu. V., 2001, Fractal Fracture of an Elastic Plane Weakned by a Lunate notch, Journal of Mathematical Sciences, Vol. 103, No. 2.

Mandelbrot, B. B., 1983, The Fractal Geometry of Nature, NY: Freeman.

Morozov, N. F., 1984, Mathematical aspects of crack theory, Moscow: Nauka.

Morozov, N., Petrov, Y., 2000, Dynamics of Fracture. Springer-Verlag, Berlin-Hidelberg-New York

Mosolov, A. B., 1991, Journal of Technical Physics, V. 61. N 7. P. 57–60.

Petrov, Y. V., 1996, “Quantum” macromechanics of dynamic fracture of solids, St.-Petersburg: IPME RAS, Preprint N 139.

Ravi-Chandar, K., Knauss, W. G., 1984, International Journal of Fracture, V. 25–29.

Ufland, Ia. S., 1950, Bipolar coordinates in theory of elasticity, Moscow: Gostechizdat.

Zolotuhin, I. V., 1998, Soros Educational Journal, V. 7. P. 108–113.

Chapter 3

High rate fracture

High rate fracture. Experimental results on high speed and pulsed loading. Inapplicability of classical strength criteria in problems of dynamic fracture

3.1 High rate fracture

Studies in dynamic fracture date back to the first half of the 20^{th} century when the first experimental results on fracture, coursed by intensively applied loads (Hopkinson, 1901, Wallner, 1938, Schardin and Struth, 1939, Wells and Post, 1958) and the first analytical solutions for cracks moving with speeds comparable to that of a Reyleigh wave appeared (Yoffe, 1951, Broberg, 1960, Atkinson and Eshelby, 1968). Later, in the 70's and the early 80's dynamics of fracture became a special area of interest for experimentalists and it was then that the main effects characterizing fracture under high loading rates were experimentally observed (Bradley and Kobayashi, 1970, Kobayashi et al., 1974, Dally, 1979, Ravi-Chandar and Knauss, 1984a, b, c, d, Dally and Shukla, 1980, Kalthoff, 1986, Dally and Barker, 1988, Rosakis and Zehnder, 1985). Along with this, the majority of analytical solutions, classical for the modern dynamic fracture, were published (Freund, 1972a,b,c, Kostrov, 1966, Kostrov and Nikitin, 1970, Achenbach, 1974, Willis, 1975, Freund, 1990, Broberg, 1989). The 80's and the early 90's were the time when modern approaches to fracture dynamics have been formed.

3.2 Experimental fracture dynamics. Overview

Among the experimental methods of research on dynamic crack-growth resistance and fast fracture, the methods of dynamic photoelasticity and caustics are the most effective. These methods have been developed in the last three decades. The most important feature of these methods is the ability of direct tracking of quantitative characteristics of the material stress state during the ongoing fracture process. This is possible using a combination of classical methods of optical image processing with high-speed photography techniques. In this chapter principles and peculiarities of both methods, being applied to fast-start and crack-propagation problems in brittle solids, will be examined.

3.3 Methods of dynamic photoelasticity

The basis of the dynamic photoelasticity method is the ability of different vitreous polymers to perform the photoelastic phenomenon. The effect is stipulated by the fact that mechanical stresses, being applied to optically transparent materials, result in appearance of optical anisotropy. This leads to appearance of birefringence; a linearly polarized light wave passing through a tensile plane decomposes into two orthogonally polarized rays, each of which propagating at its own speed.

Afterwards both rays are brought together into a common polarization plane and an interference pattern appears. This pattern can be analyzed using well-known methods. The difference in optical distance (phase difference), following mechano-optical rheological laws, corresponds to the local plane strain in the point. This provides a possibility to define quantitative characteristics of the in-plane deflection mode at each point of the sample.

With this type of modeling, vitreous polymers with clearly expressed elastic-brittle and photoelastic properties are usually used. In particular, Homalite-100 and modified epoxy KTE are such materials (see, e.g., Kobayashi and Dally, 1977). Homalite-100 is a transparent vitreous polymer with birefringence. Owing to its processability, it is intensively used in studies by the photoelastic method. It can be obtained as large sheets with optical-quality polished surfaces. An important characteristic of this material is its ability to preserve its properties under sustained loading. It was demonstrated by A. B. Clark and R. J. Sanford (Clark and Sanford, 1956) that this material's optical constant does not depend on the rate of loading. The study of Homalite-100 dynamic behavior revealed (Kobayashi et al., 1973) that this material is suitable for analyses of crack propagation using the photoelastic method. Nowadays it is widely used by American and European researchers as one of the most brittle birefringent materials available.

Other materials, also often used in photoelasticity experiments, are compounds based on an epoxide resin. The KTE epoxide (see, e.g., Kobayashi and Dally, 1977) is obtained by polymerisation of resin Epon 828. Polymerisation is achieved with the help of a vulcanising ingredient, polyxypropylenamine.

Plates, made of KTE epoxide, have a strong birefringence and are effectively used in dynamic investigations using the photoelastic method. The epoxide compounds in comparison to Homalite-100 are more viscous and at the same time more sensitive to the loading rate.

Principal mechano-optical values of Homalite-100 and KTE epoxide are given in Table 3.1 (Kobayashi and Dally, 1977).

Parameter	Homalite-100	KTE epoxy
$c_1 \quad (m/s)$	2150	1970
$c_2 \quad (m/s)$	1230	1130
E_d *(GPa)*	4.82	3.86
μ_d *(GPa)*	1.84	1.47
ν_d	0.31	0.34
ρ *(Ns^2/m^4)*	122	117
K_{IC} *(MN/m$^{3/2}$)*	0.45	1.18
$C_{\sigma d}$ *(MN/mm)*	0.45	1.18

Table 3.1

HereE_d and μ_d are the dynamic Young's modulus and the shear modulus respectively; ν_d is the Poisson's ratio; K_{IC} is the static fracture toughness (critical stress intensity factor in quasistatic conditions); $C_{\sigma d}$ is the material optical constant under dynamic loading; and ρ is the mass density.

Elastic constants under dynamic loading are determined by measurement of the longitudinal $c_1$and the transverse c_2 wave velocities. These measurements are carried out by observations, of the stress-wave propagation in a half-plane loaded dynamically, for example by a charge of an explosive substance using the photoelastic method.

The material optical constant $C_{\sigma d}$ is a parameter linking the optical characteristic isochromat sequential number N to the main stresses by means of the optical rheological law:

$$2\tau = \sigma_1 - \sigma_2 = \frac{NC_{\sigma d}}{h}, \tag{3.1}$$

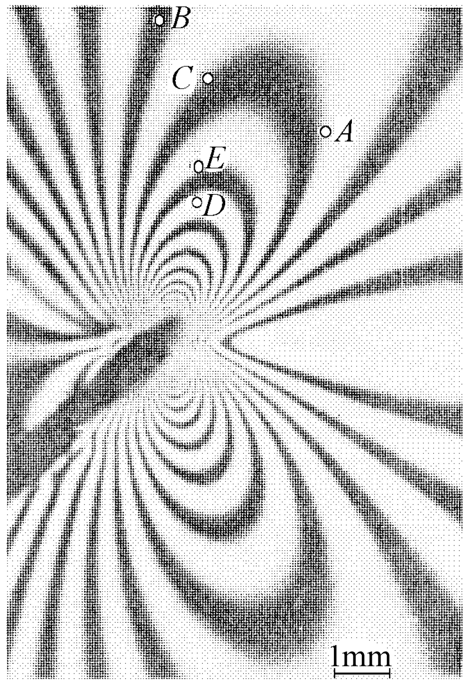

Fig. 3.1.

where τ is the peak shear stress in the plate; σ_1- σ_2 is the difference of principal stresses and h is the thickness of the specimen. Measurement of $C_{\sigma d}$ under dynamic loading can be performed on the basis of simultaneous measurement of axial deformation and the number of fringes in the specimen, loaded by uni-axial impact (Clark and Sanford, 1956).

A stress state in the crack-tip vicinity is determined by means of temporal scanning of isochromats. The pattern is obtained with the help of high-speed photography. Different systems of high-speed photography are used. Examples of usable cameras are the Kranz-Shardin multi-spark camera (33,000–85,0000 frames/s) and a streak camera of SPR-1(2) type (1–2 million frames/s). Dimensions and forms of isochromats recorded on the photographs reflect fairly accurately the instantaneous value of the stress intensity factor. Again, the ability to determine the crack-tip position in the process of its propagation allows measurement of its length as a function of time. A typical pattern of behavior of isochromats in the crack-tip vicinity is shown in Fig. 3.1.

To determine the instantaneous values of the parameters of the stress intensity factor $K(t)$, the dimensions and forms of the isochromats are measured and characterised. The characteristics of the stress-field intensity are acquired on the basis of analytical and experimental test results. Analytical calculations of isochromat forms are carried out with the help of the Vestergaard function of stresses:

$$Z(z) = \frac{K}{\sqrt{2\pi z}}\left[1 + \beta\left(\frac{z}{a}\right)\right] + \alpha,$$

where $z{=}re^{i\theta}$. The expression $\frac{K}{\sqrt{2\pi z}}$ gives the singular part of the stress field surrounding the tip of a crack with the length $2a$, located in the center of a plane plate. Parameters α and β permit to take a more precise account of the boundary influence and the applied loads. Furthermore, the domain adjacent to the crack tip, where the described isochromat analysis is used, expands alittle. The parameters K, α and β determine the characteristic form of isochromat loop near this domain. Expressions for τ and for the difference $\sigma_1 - \sigma_2$ from (3.1), calculated according to the Vestergaard function, make it possible to compute the stress intensity factor from the measured geometrical characteristics of isochromats near the crack tip.

3.4 The method of caustics

Stress intensity factors for stationary and expanding cracks can be determined experimentally using schlieren optical methods. P. Manogg (Manogg, 1964) has worked out a method of schlieren figures, which later became well — known in fracture mechanics as the method of caustics (Theocaris and Gdoutos, 1972).

Let us consider the fundamental principles of the method of caustics (see, e.g., Kalthoff et al., 1977, Rosakis et al., 1988). Let the notched specimen from the transparent material, illuminated by exterior forces, be lightened by a parallel optical beam. The cross-section of the specimen cut by a plane passing through the zone around the crack tip is shown in Fig. 3.3.

An increase of the intensity of the stresses in the zone closer to the crack tip leads to decrease in the plate thickness and changes the material's, index of refraction. Hence, as the first approximation, the region of the crack tip is acting as a divergent lens, deflecting the light from the axis of the beam. This causes appearance of a schlieren figure, limited by an intense light edge (caustic), that can be observed on a screen beyond the specimen (Fig. 3.3).

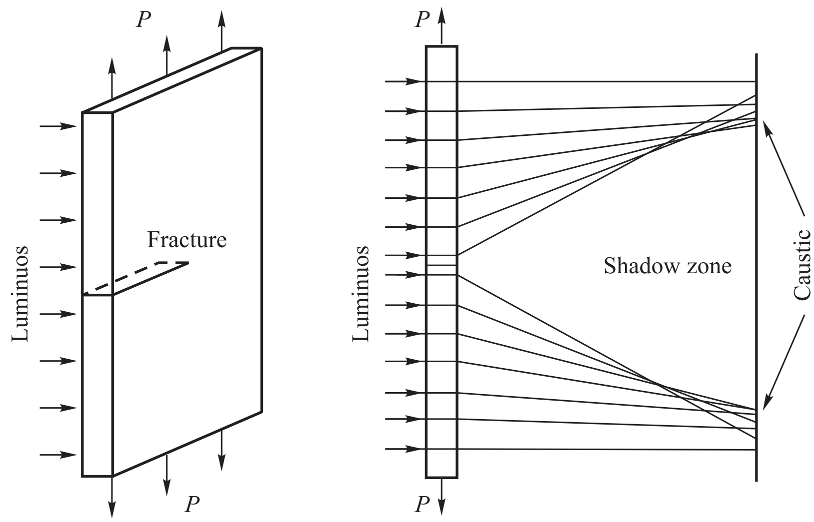

Fig. 3.2.

The boundary between light and shadow for the given figure is determined by the annular domain surrounding the crack tip, the radius of which depends on the distance between the screen and the specimen. Appearance of one caustic is typical for isotropic materials, and appearance of two caustics for anisotropic ones. For transparent materials this method can be used in transmitted light, and for non-transparent materials in reflected light.

P. Manogg (Manogg, 1964) computed the form of schlieren figures for a tensile crack supposing that the stress distribution near the crack tip is described by Sneddon's formula. Following his course of reasoning:

Let x_1 and x_2 be the screen coordinates of a ray being transmitted through a non-deformed plate and X_1 and X_2 be the same coordinates after deformation of the plate. Let us consider the deformed specimen surface in the crack tip ('lens') given by the equation:

$$x_3 + f(x_1, x_2) = 0.$$

Regarding distance from the specimen to the screen z_0 as much greater than its thickness ($z_0 \gg f$), one can get:

$$(X_1, X_2) = (x_1, x_2) - 2z_0 \nabla f.$$

The caustic is an envelope of beams. Its equation is written by assignment

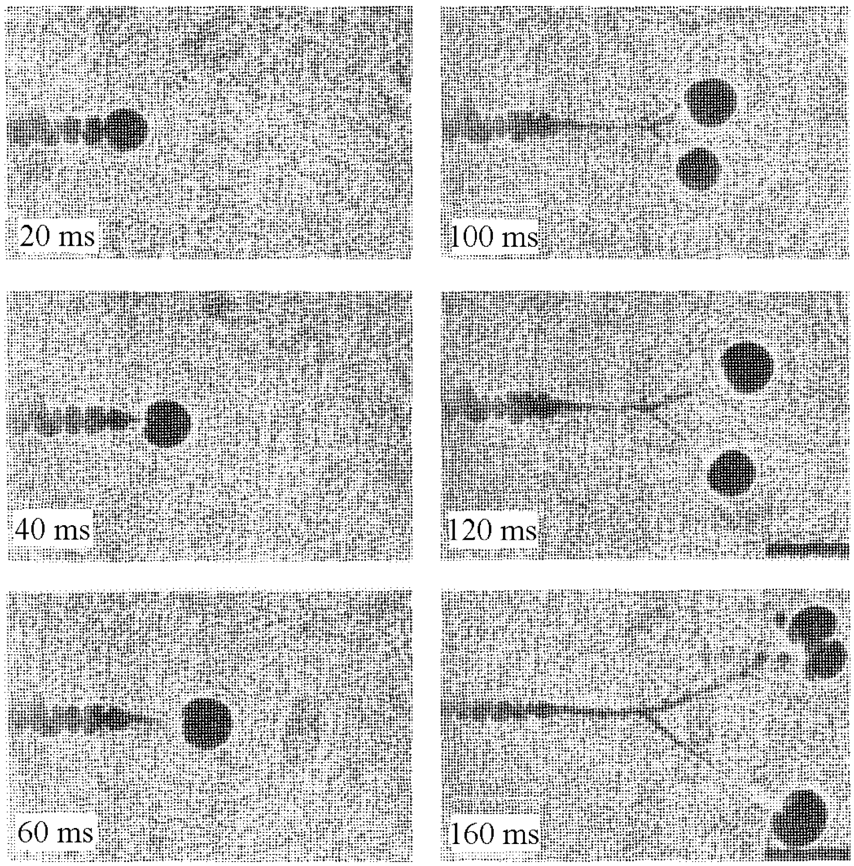

Fig. 3.3.

to the Jacobean coordinate transformation a value of zero:

$$\det\left[\delta_{\alpha,\beta} - 2z_0 f_{\alpha,\beta}\right] = 0, \quad \alpha, \beta = 1, 2, \tag{3.2}$$

where $\delta_{\alpha,\beta}$ is the Kroneker delta.

For the opening mode of a tensile crack we have:

$$f(r,\theta) = u_3(r,\theta) = -\frac{\nu h}{E\sqrt{2\pi r}} K_{\mathrm{I}} \cos\frac{\theta}{2}, \tag{3.3}$$

where K_{I} is the stress-intensity factor for mode I crack opening; E and ν are constants of elasticity (Young's modulus and Poisson's ratio); h is the thickness; and r, θ are the polar coordinates at the crack tip.

A substitution of (3.3) into the transformation (3.2) gives the equation of the caustic, shown on the screen, which turns out to be an epicycloid. The maximum diameter of the caustic is a function of the stress-intensity factor and can be described by the following formula:

$$K_{\mathrm{I}} = \frac{2\sqrt{2\pi}E}{3\lambda^{5/2}\upsilon h z_0} D^{5/2}, \tag{3.4}$$

where D is the caustic diameter; λ is a numerical coefficient, characterising the epicycloid form; and z_0 is the distance between the specimen and the screen.

Experimental realization of the method is simple enough. A monochromatic light beam, emitted by a laser, having passed through a system of lenses, falls on a specimen. Reflected (or transmitted) rays are captured on a screen. The specimen is loaded, and the maximal dimensions of the schlieren figure are measured. Then, substituting the parameter values in (3.4), one is able to calculate the stress intensity factor.

During dynamic tests schlieren figures are registered with the help of high-speed photography. The start is initiated by the crack itself.

Materials studied by the caustic method include: polymethylmethacrylate (PMMA), Homalite-100, epoxy, Araldite-B, plexiglas and polycarbonate.

3.5 On an asymptotic representation of the stress field near the crack tip

A real stress field appearing in a thin plate is always three-dimensional. Experiments on plates of plexiglas and martensitic steel carried out with the caustic method have shown (Krishnaswamy et al., 1988, Rosakis and Ravi-Chandar, 1986) that the radius of the space-stress-state zone near the tip of a macroscopic crack is not less than $0.5h$, where h is the plate thickness. Nevertheless, in practice there are many cases when a brittle-fracture analysis could be carried out with the help of a two-dimensional asymptotic description based on the stress intensity factor. As was already noted, this can be determined by measurement of the stresses in the crack-tip vicinity according to the well-known asymptotic formulas.

Thereby dimensions and shapes of the process zone of a stress state with a two-dimensional asymptotic description acquire a great significance. Let us examine this problem in terms of the opening mode of tensile crack behavior in static conditions (Petrov et al., 1991).

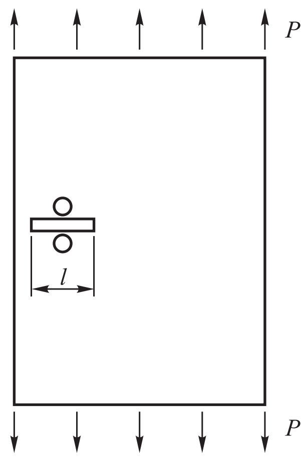

Fig. 3.4.

This problem has been solved by the photoelastic method using plane specimens made of organic glass. Specimen 1 was made of organic glass with the optical constant $C = -2.04 \times 10^{-2}\mathrm{Pa}^{-1}$, and specimen 2 of optically sensitive organic glass with the optical constant $C = 40.5 \times 10^{-2}\mathrm{Pa}^{-1}$.

Both specimens were shaped as plates with dimensions 220×68 mm. The thicknesses of the plates 1 and 2 were 3.25 and 4 mm respectively. The crack location and its dimensions are denoted in Fig. 3.4. For specimen 1 crack length l was 25.2 mm, and 26.8 mm for specimen 2. Special holes near the crack faces provided formation of an ideal crack end from the original notch when stretching forces p were applied.

The specimen was subjected to remote uniaxial stretching in the direction perpendicular to the notch plane by a loading device, UP-8. Each specimen was investigated for two remote tensile stresses p equal to 0.91 and to 2.23 *MPa*. The stretched specimen was placed in the field of a coordinate synchronous polarimeter, CSP-10. With its help, using the Saint-Armond method, the optical phase difference ψ and the parameter ϕ of optical isocline in monochromatic light with the wavelength λ=546.1 nm were measured (see, e.g., Alexandrov and Akhmetzyanov, 1973). The measurements were taken along the plane θ=*const* (θ is the polar angle). The values of tangential stresses τ_{xy} and the differences of normal stresses $\sigma_x - \sigma_y$ were calculated at these points according to the measured optical values by the photoelastic method:

$$\tau_{xy} = \frac{\delta}{2Ch} \sin\left(2\varphi_{xy}\right), \quad \sigma_x - \sigma_y = \frac{\delta}{Ch} \cos\left(2\varphi_{xy}\right), \tag{3.5}$$

where δ is the optical propagation difference, determined by the measured phase difference; C is the optical constant obtained from calibration of stretched specimens of the tudied material; and ϕ_{xy} is the angle determining the direction of the largest principal stress σ_1 relative to the *x-axis*. Moreover, $\phi_{xy} = \phi$ for material with $C > 0$, and $\phi_{xy} = \phi \pm 90°$ for material with $C < 0$; h being the thickness of the examined model.

It was supposed that the stress-field distribution near the crack tip is described by asymptotic (for $r \to 0$) Sneddon's formulas (see, e.g., Morozov, 1954):

$$\begin{aligned}
\sigma_x &= \frac{K_{\mathrm{I}}}{\sqrt{2\pi r}} \cos\frac{\theta}{2}\left(1 - \sin\frac{\theta}{2}\sin\frac{3\theta}{2}\right) - p + \mathrm{o}(1),\\
\sigma_y &= \frac{K_{\mathrm{I}}}{\sqrt{2\pi r}} \cos\frac{\theta}{2}\left(1 + \sin\frac{\theta}{2}\sin\frac{3\theta}{2}\right) + \mathrm{o}(1),\\
\sigma_{xy} &= \frac{K_{\mathrm{I}}}{\sqrt{2\pi r}} \cos\frac{\theta}{2}\sin\frac{\theta}{2}\cos\frac{3\theta}{2} + \mathrm{o}(1).
\end{aligned} \tag{3.6}$$

The relations (3.5) and (3.6) permit a link between measured optical values and the stress intensity factor K_{I}. The correctness of the asymptotic description (3.6) in the area around the crack tip can be confirmed by stability of K_{I} values, calculated according to optical values in such an area.

Coordinates of the point where optical values are measured were determined by the polarimeter CSP-10 with an accuracy of 0.02 *mm*. The accuracy of values ψ and ϕ did not exceed 0.5°. During the experiment the error of stress calculations for $\sigma_x - \sigma_y$ and τ_{xy} and consequently the error of the K_{I} value was established.

Measurements of the optical values were carried out along θ equal to ±135°, ±120°, ±90°, ±75°, ±45° and ±30°.

Fig. 3.5, a typical graph, shows the value modifications of K_{I} according to the coordinate r/h. It follows from the results obtained for each line θ=const that an interval can be selected where the value of K_{I} is nearly constant. The mid value of K_{I} in the given interval, when p=2.23 *MPa*, turned out to be equal to $0.58 MPa\sqrt{m}$. The deviations of mid values on different rays did not exceed 5% of the given value.

As an example of usage of the results of the specimen-1 study, let us denote the near and the far boundaries of the asymptotic representation acting at the zone of stress near the crack tip by r_1 and r_2 respectively. It is clear that for $0° \leq |\theta| \leq 90°$ the near boundary is situated at the distance of $r_1 \geq 0.7h$ from the crack. When $|\theta| \geq 90°$ the value r_1 increases to h, i.e. the distance from the crack tip to the near boundary is a bit larger.

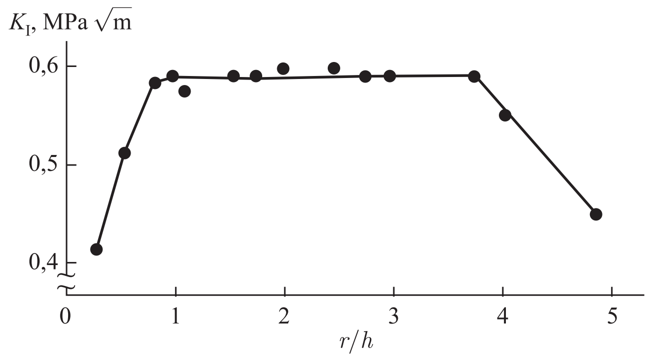

Fig. 3.5.

The far boundary of the indicated zone is $r_2 = 4h$ for $|\theta| \geq 90°$. When the angle θ changes from 90° to 30° the distance r_2 is reduced from $4h$ to $2.8h$. The values of $r_1$and $r_2$for θ=0° are obtained by extrapolation and are r_1=0.7h and r_2=2.6h respectively.

The final form of validity zone for two-dimensional stress state representation near the crack tip is shown in Fig. 3.6.

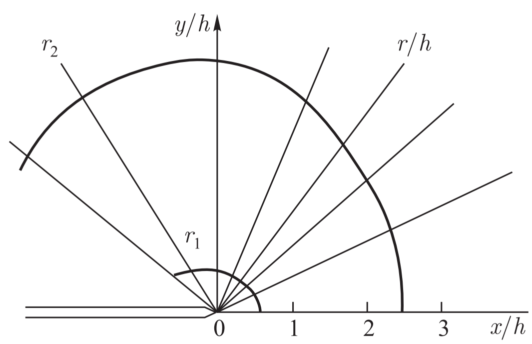

Fig. 3.6.

Elongation of this zone in the y direction to one and a half times its value in the x direction is very important and quite an unexpected result.

Thus, the studies carried out on two specimens of organic glass of different brands and thicknesses led us to the following results:

(1) the near boundary of the validity zone for two-dimensional asymptotic stress-state representation is greater than or equal to 0.7h from the crack tip. The far boundary of this zone in the examined problem

extends to a distance greater than or equal to 0.5 l from the crack tip;

(2) the validity zone for two-dimensional asymptotic stress representation has an unequal elongation in different directions from the tip and is more elongated in the direction perpendicular to the crack line.

The aforementioned results are very important in order to optimize the experimental determination of stress intensity factors in zones with cracks in static as well as in dynamics situation.

3.6 Theoretical contradictions of fracture dynamics

Let us study the problem of interaction between a longitudinal stress wave with a crack ($x \leq 0$, $y=0$) in an unbounded elastic plane xy. On the crack faces we have boundary conditions $\sigma_{xy}=0$, $\sigma_y=0$. Let the components of the displacement vector u and v in the incident wave be expressed by:

$$u = 0,$$
$$v = v_0\left[(c_1 t + y)\, H\,(c_1 t + y) - (c_1 t + y - c_1 T)\, H\,(c_1 t + y - c_1 T)\right].$$

Then the stress σ_y in the wave has a rectangular temporal profile:

$$\sigma_y = P\left[H\,(c_1 t + y) - H\,(c_1 t + y - c_1 T)\right],$$

where $P=(\lambda+2\mu)v_0$. P is the amplitude of the incident stress wave and T is the pulse duration.

Here and further $c_1 = \sqrt{(\lambda + 2\mu)/\rho}$ and $c_2 = \sqrt{\mu/\rho}$ are the speeds of the longitudinal and the transverse waves respectively, λ and μ are the Lame constants and $H(t)$ is the Heaviside step function.

At $t=0$ the interaction between the incident wave and the crack starts, whereupon near the crack tip ($r=0$) a singular stress field appears, characterised by asymptotic formulas:

$$\sigma_{ij} = \frac{K_{\mathrm{I}}(t)}{\sqrt{2\pi r}} g_{ij}(\theta) + \mathrm{O}(1), \quad r \to 0.$$

Here r, θ are polar coordinates at the crack tip.

Let T tend to zero, keeping the momentum of the external action $U=PT$ constant. Then, as proved by Cherepanov (Cherepanov, 1974),

$$K_{\mathrm{I}}(t) = \frac{U\Phi(c_1, c_2)}{2\sqrt{t}}. \tag{3.7}$$

According to this formula there always exists a time when the value of the stress intensity factor exceeds an arbitrarily large value. So, according to the classical approach, fracture may occure under arbitrary pulse U including those that are indefinitely small. Obviously this does not reflect the real situation.

Experiments show that dynamic fracture mechanics abounds in multitudinous effects that can not be incorporated into classical ideas. Many of them will be analysed in the next chapters. But we would like to point out here an important circumstance; a whole series of effects characteristic of dynamics can be explained, and even computed, with the help of a special generalisation of the principles of linear fracture mechanics based on the concept of the spatial-temporal structure of a fast-rupture process.

3.7 High rate fracture of brittle materials

One of the main problems in testing the properties of resistant materials in dynamics is the dependence of dynamic strength on the way how the exterior load is applied. This difficulty typically appears under conditions of high-rate loading. In this case the strength can be interpreted as a critical value of the stress intensity factor corresponding to microcracking near the crack tip. The strength can also be interpreted as a dynamic local stress leading to rupture. Both are intensity limits of a local stress field and the fracture occurs when these limits are reached. During fracture of 'intact' solids (i.e., not containing macroscopic defects) the critical local stress is not determined by material's properties but is a complex function of the loading history.

3.8 Fracture of initially 'intact' materials

Experiments on fracture of 'intact' specimens demonstrate the dependence of dynamic strength on the loading rate and duration even in materials characterised by nearly ideal elastic-brittle behavior. This situation is illustrated by the well-known diagram of the temporal dependence of strength that was investigated first for metals by Zlatin et al. (Zlatin et al., 1974, Zlatin et al., 1975).

Let us examine, in terms of mechanics, some of the principal results obtained in these experiments.

To create a controlled fracture as a result of intense load with duration of $10^{-6}\mu s$, the cleavage phenomenon was utilized.

The specimens examined were disk-shaped with thickness of 25 *mm*. Loading was created by a pneumatic gun accelerating projectile to speeds up to 1050 m/s. Stresses created at the cleavage region, were determined using interferometry measurements at the rear surface of the specimen. Time dependence of stresses in the cleavage region was calculated according to the formula:

$$\sigma(t) = \frac{1}{2}\rho c_1 (V - V_S),$$

where V is the free-surface velocity; V_S is the same function shifted in the argument on the interval, equal to doubled time during which the longitudinal wave runs through the plate thickness; ρ is the mass density; and c_1 is velocity of the longitudinal stress wave.

Method to estimate failure stress by drop in velocity of a free surface was used in many works (see, e.g., Kannel and Fortov, 1987, Meshcheryakov, 1988). Unfortunately it is suitable only for perfectly trapezoidal pulses having vertical forefront. This method cannot be mechanically transferred to, for example, triangular-shaped pulses. On the contrary the aforementioned approach allows tracing the full history of stress-state development at cleavage region and is more efficacious since it can also be applied to arbitrary pulse forms.

Using this approach in experiments with aluminum and copper specimens (see Zlatin et al., 1974, Zlatin et al., 1975), a dependence of time, while tensile stress was acting in the cleavage region on its amplitude, was found. These data were compared to corresponding temporal strength dependencies obtained in quasistatic experiments. The results obtained using these two methods are quite different.

According to the results of the dynamic tests, cleavage induced by high rate pulses of threshold duration occurs under stresses exceeding the static strength limit by many times. Similar tests with analogous results were carried out on a great number of specimens of different materials (see, e.g., Pugachev, 1985, Meshcheryakov, 1988, Meshcheryakov et al., 1988).

The results of these experiments show that it is not possible to treat the stress sample fractures at as an independ strength characteristic, as it is strongly affected by parameters of the exterior loading.

Another significant observation made in this and other experiments is that fracture can be delayed and can occur when the local stress is decreasing. The physical nature of this effect has been discussed in many theoretical works (see, e.g., Nikiforovskii and Shemyakin, 1979, Nikolaevskii, 1981, Shock, 1981, Zlatin et al., 1986).

We can conclude that the principal effects discovered in these cleavage experiments could not be explained by means of traditional fracture mechanics.

3.9 Critical stress intensity factor for dynamic fracture

Similar problems arise in attempts to characterise material's resistance to dynamic crack growth. Experimental studies carried out in American research centers in the 1970s and 80s (see, e.g., Freund, 1976, Irwin, 1957, Kalthoff, 1986, Kalthoff and Shockey, 1977, Kalthoff et al., 1980, Knauss, 1984, Krishnaswamy et al., 1988, Sih and Macdonald, 1974, Smith, 1975, Theocaris and Papadopoulos, 1987) acquire a vital significance for understanding of fracture under high-rate loading.

Ravi-Chandar and Knauss (Knauss and Ravi-Chandar, 1985, Ravi-Chandar and Knauss, 1984a,b,c) conducted many experiments on impact loading of cracked specimens.

Experiments were conducted using specimens of vitreous polymer Homalite-100.

The main result of these experiments is that the critical value of the stress-intensity factor K_{ID} increases with increasing loading rate and can significantly exceed the corresponding quasistatic value (Fig. 3.7). Moreover, it turned out that, if the time-to-fracture is $t_* \geq 50\mu s$ influence of the loading rate on the K_{ID} value can be neglected. With a loading rate in-

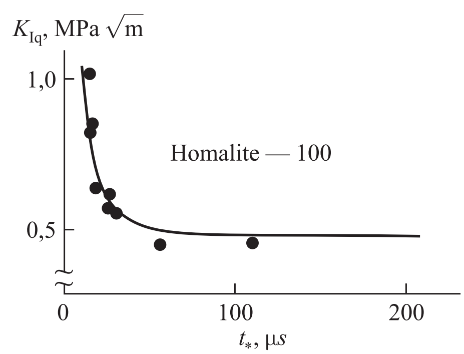

Fig. 3.7.

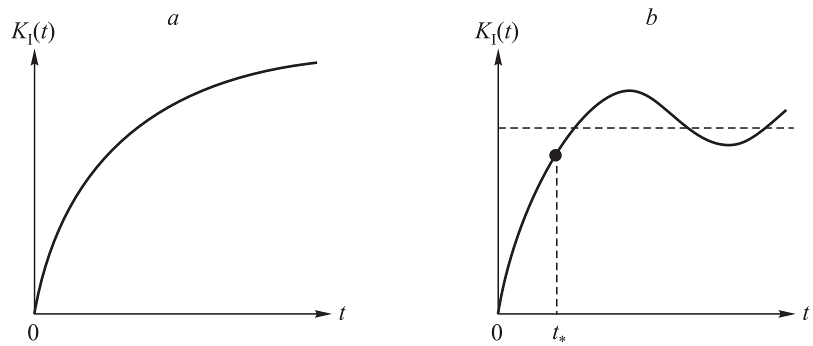

Fig. 3.8.

crease, the corresponding time-to-fracture decreases, and the critical value of the stress intensity factor increases significantly.

These experiments convincingly demonstrate that in dynamics the critical value of the stress intensity factor is not a material parameter, and, therefore, attempts to measure dynamic strength using ordinary static methods are quite erroneous. The authors of the experiments note the impossibility of using the traditional methods of continuum mechanics to simulate dynamic crack behavior.

3.10 Cracks loaded by impacts of threshold amplitude

Kalthoff and Shockey (Kalthoff and Shockey, 1977) were the first to study threshold amplitudes of short pulses causing fracture. Later similar experiments were continued by other researchers (Homma et al., 1983, Shockey et al., 1986).

Suppose a specimen having a crack of length L is subjected to an impact. Let this impact of duration T and amplitude P have a rectangular form.

In these conditions one can experimentally determine threshold (minimal) impact amplitude P leading to crack extension whilst impact duration T is fixed.

Kalthoff and Shockey (Kalthoff and Shockey, 1977) carried out an experimental investigation of this problem using polycarbonate specimens. A projectile accelerated by a pneumatic gun was hiting a plate. The pulse amplitude and its duration are simple functions of projectile velocity and plate thickness. They are easy to control, to compute or to measure directly.

The results of these studies are shown schematically in Fig. 3.8.

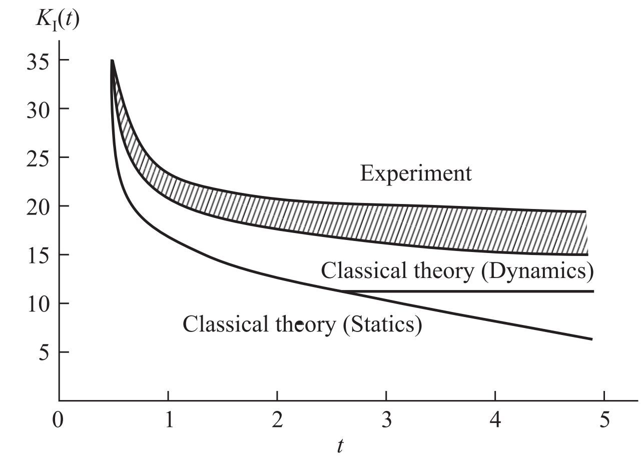

Fig. 3.9.

Homma et al. (Homma et al., 1983) have experimentally investigated the same problem on specimens of different geometries made of different materials. Short pulses of desired duration and amplitude were created by cylindrical shells and a special compressor device. Minimal amplitude, causing fracture of specimens, was determined. As a result of these tests dependency of critical amplitude on the initial crack length was constructed.

Tests on specimens made of different materials displayed decrease of critical values of amplitudes P as the crack length L is increased. These results were compared to the static dependence, given by the formula:

$$P = \frac{K_{\mathrm{IC}}}{\sqrt{L}} F\left(\frac{L}{W}\right),$$

where W is the specimen relative width. For short cracks (long pulses) the form of curves corresponding to dynamic and static loading is similar. For long cracks (short pulses) critical amplitudes, measured experimentally, tend to a finite value and the curve is located essentially higher than the static one (see Fig. 3.9), tending to zero.

Several undertaken attempts to compute threshold fracture characteristics appeared to be unsuccessful. According to classical approaches (Achenbach 1972, Sih, 1968), a crack, loaded by a critical pulse, advances under a condition that the dynamic stress-intensity factor reaches its maximum. The corresponding relation, whence threshold amplitudes can be determined, is written as:

$$\max_t K_{\mathrm{I}}(t) = K_{IC}. \tag{3.8}$$

Analysis has shown that for short pulses (long cracks) experimentally measured critical amplitude significantly exceed values calculated theoretically according to (3.8).

The analysis of the experimental data has shown (Homma et al., 1983, Shockey et al., 1986) that fracture can also happen when the stress-intensity factor is decreasing (effect of fracture delay), that is also unexplainable within the framework K of traditional fracture mechanics.

References

Achenbach, J. D., 1972, Dynamic effects in brittle fracture. Mechanics Today (S. Neamat-Nasser, Pergamon Press, Vol. 1, pp. 1–57).

Achenbach, J. D., 1974, Dynamic effects in brittle fracture. In: Nemat-Nasser S et al (eds) Mechanics today, 1. Pergamon, Elmsford, NY, pp. 1–57

Alexandrov, A. J. and Akhmetzyanov, M. H., 1973, Photoelastic Methods of Deformable Body Mechanics (Nauka, Moscow, 576 pp.). (In Russian.)

Atkinson, C., Eshelby, J. D., 1968, The flow of energy into the tip of a moving crack. Int J Fract 4:3–8

Bradley, W. B., Kobayashi, A. S., 1970, An investigation of propagating crack by dynamic photoelasticity. Exp Mech 10:106–113

Broberg, K. B., 1960, The propagation of a brittle crack. Archiv fur Fysik 18:159–192

Broberg, K. B., 1989, The near-tip field at high crack velocities. Int J Fract 39:1–13

Cherepanov, G. P., 1972, Elastic waves diffraction at linear cuts. Continuum Mechanics and Related Analysis Problems (Nauka, Moscow, pp. 615-622.). (In Russian.)

Cherepanov, G. P., 1974, Brittle Fracture Mechanics. (Nauka, Moscow, 640 pp.). (In Russian.)

Clark, A. B., and Sanford, R. J., 1956, Static and dynamic calibration of photoelastic model materials. Proc. Soc. Exp. Stress Anal. 14 (1), 195–204.

Dally, J. W., 1979, Dynamic photoelastic studies of fracture. Exp Mech 19:349–361

Dally, J. W., Barker, D. B., 1988, Dynamic measurements of initiation toughness at high loading rate. Exp Mech 28:298–303

Dally, J. W., Shukla, A., 1980, Energy loss in Homalite-100 during crack propagation and arrest. Eng Fract Mech 13:807–817

Freund, L. B., 1972a, Crack propagation in an elastic solid subjected to general loading. I: Constant rate of extension. J Mech Phys Solid 20:129–140

Freund, L. B., 1972b, Crack propagation in an elastic solid subjected to general loading. II: Nonuniform rate of extension. J Mech Phys Solid 20:141–152

Freund, L. B., 1972c, Energy flux into the tip of an extending crack in an elastic solid. J Elast 2:341–349

Freund, L. B., 1976, Dynamic crack propagation. Mechanics Fracture (F. Erdogan, ASME AMD, Vol. 19, pp. 105–134).

Freund, L. B., 1990, Dynamic fracture mechanics. Cambridge University Press, Cambridge

Golubev, V. K., Novikov, S. A., Sobolev, Y. S. and Yukina, N. A., 1987, On heating influence on cleavage fracture of some polymer composites. Appl. Mech. and Thec. Phys. 28 (6), 140–145. (In Russian.)

Homma, H., Shockey, D. A. and Murayama, Y., 1983, Response of cracks in structural materials to short pulse loads. J. Mech. Phys. Sol. 31 (3), 261–279.

Hopkinson, J., 1901, Original Papers. Cambridge University Press

Irwin, G., 1957, Analysis of stresses and strains near the end of a crack traversing a plate. J. Appl. Mech. 24 (3), 361–364.

Kalthoff, J. F. and Shockey, D. A., 1977, Instability of cracks under impulse loads. J. Appl. Phys. 48, 986–993.

Kalthoff, J. F., 1986, Fracture behavior under high rates of loading. Eng Fract Mech 23:289–298

Kalthoff, J. F., Beinert, J. and Winkler, S., 1977, Measurements of dynamic stress intensity factors for fast running and arresting cracks in double-cantilever-beam specimens. Fast Fracture and Crack Arrest. ASTM STP 627, 161–176.

Kalthoff, J. F., Beinert, J., Winkler, S. and Klemm, W., 1980, Experimental analysis of dynamic effects in different crack arrest test specimens. Crack Arrest Methodology and Applications. ASTM STP 711, 109–127.

Kannel, G. I. and Fortov, V. E., 1987, Condensed media mechanical properties under intensive pulse actions. Mechanics Successes 10 (3), 3–82. (In Russian.)

Knauss, W. G., 1984, Fundamental problems in dynamic fracture. Advances of Fracture Research. Proc. of the 6th Int. Conf. of Fracture, Delhi. (S. R. Vallury, Oxford, New York, Vol. 1, pp. 625–652).

Knauss, W. G., and Ravi-Chandar, K., 1985, Some basic problems in stress wave dominated fracture. Internat. J. Fracture 27, 127–143.

Kobayashi, A. S., Wade, B. G., Bradley, W. B., Chiu, S. T., 1974, Crack branching in Homalite-100 plates. Eng Fract Mech 6:81–92

Kobayashi, T. and Dally, J. W., 1977, Relation between crack velocity and stress intensity factor in birefringent polymers. Fast Fracture and Crack Arrest. ASTM STP 627, 257–273. (Translated in Russian: In Mechanics of Fracture. Fast Fracture and Crack Arrest. Book of Papers. Publishing House “Mir”, Moscow, P. 101–119. 1981).

Kobayashi, T., Wade, B. G. and Bradley, W. G., 1973, Fracture dynamics of Homalite-100. In: Deformation and Fracture High Polymers, by H. H. Kaush, J. A. Haseele and R. I. Jaffee. (Plenum Press, New York, pp. 487–500.)

Kostrov, B. V., 1966, Unsteady propagation of longitudinal shear cracks. Appl Math Mech 30:1241–1248

Kostrov, B. V., Nikitin, L. V., 1970, Some general problems of mechanics of brittle fracture. Archiwum Mechaniki Stosowanej 22:749–775

Krishnaswamy, S., Rosakis, A. J. and Ravichandran, G., 1988, On the domain of dominance of asymptotic crack tip fields in the dynamic fracture of metals: an investigation based on bifocal caustics and three-dimensional dynamic numerical simulations. SM Report 88–18, Pasadena, 27 pp.

Manogg, P. 1964, Schattenoptische Messung der spezifischen Bruchenergie wahrend des Bruchvorgangs bei Plexiglas. Proc. of the Internat. Conf. on Physics of Non-Crystalline Solids, Delft, pp. 481–490.

Meshcheryakov, Y. I., 1988, Statistic model of cleavage surface formation and fracture criterion. Surface Physics, Chemistry, Mechanics. No 3. P. 101–111. (In Russian.)

Meshcheryakov, Y. I., Divakov, A. K. and Kudryashov, V. G., 1988, On dynamic strength under cleavage and disruption. Physics Burning and Explosion 24 (2), 126–134 (In Russian.)

Morozov, N. F., 1954, Mathematical Problems of Crack Theory (Nauka, Moscow, 255 pp.). (In Russian.)

Nikiforovskii, V. S. and Shemyakin, E. I., 1979, Dynamic Fracture of Solids. (Novosibirsk University Press, Novosibirsc, 271 pp.). (In Russian.)

Nikolaevskii, V. N., 1981, Dynamic strength and fracture velocity. Impact, Explosion and Fracture (Nauka, Moscow, pp. 166–203). (In Russian.)

Parton, V. Z. and Morozov, E. M., 1985, Elastic-Plastic Fracture Mechanics (Nauka, Moscow, 504 pp.). (In Russian.)

Petrov, Y. V., Smirnova, S. I., Utkin, A. A. and Fedorovsky, G. D., 1991, On stress state asymptotics near crack tip in thin plate. Vestnik Leningrad University, Series 1, Issue 3, 123–125 (In Russian.)

Pugachev, G. S., 1985, Fracture of Solids under Pulse Loading: Self-Abstract of Mathematical Doctoral Thesis, Leningrad, 37 pp. (In Russian.)

Ravi-Chandar, K. and Knauss, W. G., 1984a, An experimental investigation into dynamic fracture: 1. Crack initiation and arrest. Internat. J. Fracture 25, 247–262.

Ravi-Chandar, K. and Knauss, W. G., 1984b, An experimental investigation into dynamic fracture: 2. Microstructural aspects. Internat. J. Fracture 26, 65–80.

Ravi-Chandar, K. and Knauss, W. G., 1984c, An experimental investigation into dynamic fracture: 3. On steady state crack propagation and crack branching. Internat. J. Fracture 26, 141–154.

Ravi-Chandar, K. and Knauss, WG, 1984d, An experimental investigation into dynamic fracture: IV. On the interaction of stress waves with propagating cracks. Int J Fract 26:189–200

Rosakis, A. J. and Ravi-Chandar, K., 1986, On crack tip stress state: an experimental evaluation of three dimensional effects. Internat. J. Solids and Structures 22, 121–128.

Rosakis, A. J., Zehnder, A. T. and Narasimhan, R., 1988, Caustics by reflection and their application to elastic-plastic and dynamic fracture mechanics. Opt. Engrg. 27 (8), 596–610.

Rosakis, A. J., Zehnder, A. T., 1985, On dynamic fracture of structural metals. Int J Fract 27:169–186

Schardin, H., Struth, W., 1938, Hochfrequezkinematographische untersuchung der bruchvorgänge in glas. Glastechnische Berichte 16:219

Shock, R., 1981, Formation behavior under strong stresses. Mechanics Impact, Explosion, Fracture. No 26. P. 166–203. (In Russian.)

Shockey, D. A., Erlich, D. C., Kalthoff, J. F. and Homma, H., 1986, Short-pulse fracture mechanics. Engrg. Fracture Mech. 23, 311–319.

Sih, G. C. and Macdonald, B., 1974, Fracture mechanics applied to engineering problems. Strain energy density fracture criterion. Engrg. Fracture Mech. 6 (2), 361–386.

Sih, G. C., 1968, Some elastodynamics problems of cracks. Internat. J. Fracture Mech. 4, 51–68.

Slepjan, L. I., 1981, Crack Mechanics (Leningrad University Press, Leningrad, 295 pp.). (In Russian.)

Smith, G. C., 1975, An Experimental Investigation of the Dynamic Fracture of a Brittle Material. Ph. D. Thesis, Pasadena, 93 pp.

Theocaris, P. S. and Gdoutos, E., 1972, An optical method for determining opening-mode and edge-sliding-mode stress intensity factors. J. Appl. Mech. 39, 91–97.

Theocaris, P. S. and Papadopoulos, G. A., 1987, The dynamic behavior of sharp V-notches under impact loading. Internat. J. Solids and Structures 23 (12), 1581–1600.

Wallner, H., 1938, Linienstrukturen an bruchflächen. Z. Physik 114:368–370

Wells, A. A., Post, D, 1958, The dynamic stress distribution surrounding a running crack—A photoelastic analysis. Proc Soc Exp Stress Anal 16:69–93

Willis, J. R. 1975, Equations of motion for propagating crack. Mech Phys Frac, The Metals Soc, London 1:57–67

Yoffe, E. H., 1951, The moving Griffith crack. Phil Mag 42:739–750

Zlatin, N. A., Peschanskaya, N. N. and Pugachev, G. S., 1986, On brittle solid delay fracture. Journal Tech. Phys. 56 (2), 403–406. (In Russian.)

Zlatin, N. A., Pugachev, G. S., Mochalov, S. M. and Bragov, A. M., 1974, Fracture process temporal regularities under intensive loading. Physics Solids 16 (6), 1752–1755. (In Russian.)

Zlatin, N. A., Pugachev, G. S., Mochalov, S. M. and Bragov, A. M., 1975, Temporal dependencies of metal strength at microsecond range durability. Physics Solids 17 (9), 2599–2602. (In Russian.)

Chapter 4

Incubation time approach: background and basic concept

Incubation time approach in brittle fracture. Historical prerequisites. Spatial-temporal nature of dynamic fracture. Fracture "quantum". Fracture incubation period. Fracture scale levels

4.1 Introduction

Nowadays two main approaches to prediction of dynamic crack initiation exist. The first one originating from the works of Freund (Freund, 1972) and later developed by Rosakes is based on an assumption, that fracture criterion in a tip of a crack can be received as a function of stress intensity factor rate: $K^d(t) < K_C^d(\dot{K}(t))$, with K^d being the dynamic stress intensity factor, changing in time, K_C^d being its critical value and dot denoting time derivative.

This approach showed its applicability to describe some of the experimentally observed phenomena of dynamic fracture, mainly in the case of well-developed plasticity (though still within the framework of small scale of yielding). The weak point of this approach is that, as shown in multiple works (ex. Owen et al., 1998), K_C^d used in proposed criterion is not only depending on the loading rate and fractured material properties, but is also a function of experiment geometry and loading conditions. This means that experimentally measured K_C^d cannot be treated as a material property that is given *a priori* and cannot be directly used to model experiments with other geometries and loading conditions.

The mentioned approach is also not trivial to use while predicting crack propagation. The reason for this is that using time derivative of a stress intensity factor in a tip of a fast moving crack we can hardly assess the history of stress field development in vicinity of a present crack tip location, as in times close to the present time, the crack tip was at a point that can be very distant from the current one.

4.2 Some non-classical approaches in fracture

Most of approaches in dynamic fracture are associated with introduction of non-elastic rheology and macroscopic crack development. In many cases this association is an inevitable physical necessity. However, for practical aims it is very important to provide a direct mechanical approach, providing reduction of the dynamic fracture analysis to a simple 'industrial' procedure. That is why rejection from the engineering mode of energy and power balance traditional schemes of fracture mechanics would be unjustified. Even within the framework of linear elasticity and brittle fracture these schemes are not complete. Their development, as will be shown below, can give sufficiently simple explanations of many peculiarities of high rate fracture (Morozov, Petrov, 1990, Morozov, Petrov, 1992, Morozov, Petrov, 1993, Morozov, Petrov, Utkin, 1990, Morozov, Petrov, Utkin, 1991, Petrov, 1991, Petrov, 1996, Petrov, Morozov, 1994)

Let us examine some nonclassical models of brittle fracture, especially efficient in situations where classical approaches and the Griffith—Irwin criterion do not ensure success.

4.3 Novozhilov—Neuber approach

Let us turn to static problems. We will consider an elastic plate with an angular notch. According to Griffith's classical scheme we write down an energy balance equation.

We have $\Delta\Pi \sim \varepsilon$. An estimation for $\Delta(A-U)$ is also known (Mazja, Nazarov, Plamenevskii, 1981):

$$\Delta(A-U) \sim \varepsilon^{2\pi/\alpha}.$$

It is evident that we would not be able to find critical load from the equality:

$$\Delta(A-U) = \Delta\Pi.$$

Let us study two elastic plates weakened by a rectilinear crack and a lune of small apex angle α. In the first case we have an asymptotic expression near the crack tip:

$$\sigma_{ij} = \frac{C^{\mathrm{I}}_{(1)}}{r^{\lambda^{\mathrm{I}}_1}} f^{\mathrm{I}}_{ij(1)}(\theta) + \frac{C^{\mathrm{I}}_{(2)}}{r^{\lambda^{\mathrm{I}}_2}} f^{\mathrm{I}}_{ij(2)}(\theta) + ...,$$

where $\lambda^{\mathrm{I}}_1 = \lambda^{\mathrm{I}}_2$; C_1, C_2 are coefficients characterising the stress-state intensity; and r, θ are polar coordinates with the origin at the crack tip.

In the second case the roots are separated:

$$\sigma_{ij} = \frac{C^{\mathrm{II}}_{(1)}}{r^{\lambda^{\mathrm{II}}_1}} f^{\mathrm{II}}_{ij(1)}(\theta) + \frac{C^{\mathrm{II}}_{(2)}}{r^{\lambda^{\mathrm{II}}_2}} f^{\mathrm{II}}_{ij(2)}(\theta) + ...,$$

where $\lambda^{\mathrm{II}}_1 < \lambda^{\mathrm{II}}_2$.

According to Irwin's criterion, in the second case only the dominating term should be taken into account; this leads to a significant difference between the situations I and II that is difficult to interpret. Neuber (Neuber, 1947) and Novozhilov (Novozhilov, 1969 Novozhilov, 1969) have suggested the following fracture criterion at different times and on the basis of different approaches:

$$\frac{1}{d}\int_0^d \sigma dr \leq \sigma_c. \qquad (4.1)$$

Here σ is the main tension stress near the crack tip (r=0); σ_c is the ultimate stress for 'intact' material.

The main peculiarity of (4.1) is introduction of some structural dimension d in an explicit form. One can note that a structural characteristic size dimension is already implicitly present in classical fracture mechanics, appearing in the form of dimensional combinations of the classical strength criterion parameters:

$$d \sim \frac{\Gamma E}{\sigma_c^2}, \quad d \sim \frac{K_{\mathrm{I}c}^2}{\sigma_c^2},$$

with E being the Young's modulus and Γ being the specific surface energy.

Scholars express various suppositions about physical nature of the parameter d (interatomic spacing for a medium with regular atomic structure, grain size for polycrystalline medium, scale correspondence parameter of strength characteristics etc.). We propose to consider this parameter as a linear dimension, characterising the fracture of an elementary cell on a chosen scale level (see, e.g., (Goldstein, Osipenko, 1978, Goldstein, Osipenko, 1993)). Without giving any details we choose d from the following condition:

$$d = \frac{2K_{\mathrm{I}c}^2}{\pi\sigma_c^2}, \tag{4.2}$$

providing coincidence of (4.1) with the Griffith—Irwin criterion in 'quasistatic' cases and simple geometries.

Criterion (4.1) in combination with (4.2) gives a possibility for effective prediction of fracture forecasting in many nonstandard situations, including the aforementioned cases of plate with angular and lune notches (Morozov, 1954).

4.4 Shockey—Kalthoff minimal time criterion

Testing threshold characteristics of a dynamic load pulse, considered in the preceding chapter, has permitted authors of those experiments to draw a conclusion on necessity to revise traditional fracture mechanics.

Kalthoff and Shockey (Kalthoff, Shockey, 1977) suggested new fracture criterion, which they call minimum-time criterion. The main novelty of the new approach is in introduction of a structural parameter t_{inc}, having time dimension and accounting incubation processes preceding macrofracture. Incubation time t_{inc} is declared to be constant, linked to material properties. According to this concept, fracture occurs under condition that the stress-intensity factor $K_I(t)$ is exceeding dynamic fracture toughness $K_{\mathrm{I}D}$ during this minimal time needed for macrocrack development.

t_{inc} was determined for different materials (Homma, Shockey, Murayama, 1983, Shockey, Erlich, Kalthoff, Homma, 1986). In particular, for steels 4340 (7 μs), 1018 (11 μs) and aluminum alloy 6061-T651 (9 μs).

Notwithstanding some eclecticism and absence of a neat analytical setting, the minimal time criterion is a notable step forward, as it introduces the following principal directives in fracture analysis.

Firstly, the existence of a certain structural parameter, having the time dimension and controlling the fracture process is considered. Let us remark that in quasistatics fracture is associated with a certain parameter having a length dimension. Thus, passing from static loading to dynamic situation a new structural characteristic appears.

Secondly, it is affirmed that the fracture is not stipulated by instantanious state of local stress field surrounding the crack tip, but is an integral process developing in time and distributed at structural-temporal interval.

Minimal-time criterion admits a possibility of such situation. In fact, from the point of view of classical mechanics, if fracture does not happen when the stress-intensity factor attains its maximal values, then it can not happen for smaller values of the stress-intensity factor. The minimal-time criterion, on the contrary, permits such a situation. As already noted, experiments on threshold loading proved existence of this effect, that could be called an 'effect of fracture delay', by analogy to a similar effect for cleavage.

4.5 Nikiphorovski—Shemyakin criterion

An other important principle of fracture dynamics was proposed by Nikiphorovski and Shemyakin (Nikiforovskii, Shemyakin, 1979). It consists in direct accounting of the local stress history. The criterion reads:

$$\int_0^{t_*} \sigma_d t \leq J_c. \tag{4.3}$$

This criterion was specially suggested for fracture analysis caused by short-term exterior pulses.

It is interesting that (4.3) itself could be interpreted from the phenomenological theory of defect accumulation (Kachanov, 1974). Suppose the following phenomenological law of defect development is valid:

$$\frac{d\Psi}{dt} = f(\sigma, \Psi) = \begin{cases} A\left(\frac{\sigma}{1-\Psi}\right)^n, & \sigma \geq 0 \\ 0, & \sigma > 0 \end{cases} . \tag{4.4}$$

Integrating (4.5), under condition that $\Psi \leq 1$, we get:

$$A \int_0^{t_*} \sigma^n dt \leq 1,$$

giving (4.3) for n=1.

Despite possible interpretations, (4.3) is a postulate, determining macroscopic rupture of an 'intact' solid medium. Its main deficiency is impossibility of transition to quasistatics. Thus, according to (4.3) any stress, even insignificant, of the form of $\sigma = \sigma_0 H(t)$, where H is the Heaviside step function, leads to fracture. Even for infinitely small σ_0. Obviously this is contradicting the common sence.

Introduction of criterion (4.3) was an important step forward, as it provided a possibility of direct consideration of loading history. Such an approach, within the framework of elastic–brittle model, gave an explanation to several principal effects of fast dynamic rupture of solids (Nikiforovskii, Shemyakin, 1979).

4.6 Incubation time criterion for brittle fracture

Analysis of experimental results shows that the main contradictions to results, obtained using traditional models, become apparent in the case when fracture happens in rather short time intervals after exterior pulse application, which corresponds to high loading rates. The fracture itself is accompanied by high local deformation velocities, both during cleavage and initiation of cracks. Indicated contradictions may appear because fracture models, used for analysis, remain essentially based on quasistatic principles. This can indicate that while modeling fracture mechanism one does not take into consideration that during high-rate rupture, together with elastic resistance of the material, it is also necessary to overcome medium inertia. While using energy balance equation in dynamic situation the term representing kinetic energy is traditionally neglected as being small comparing to other terms (Parton, Boriskovsky, 1985, Parton, Boriskovsky, 1988, Freund, 1972, Freund, 1974, Freund).

Evidently, this approach is incorrect for a high-rate deformation.

Physical imperfection of this criterion is that according to it material should be fractured at a rather high instantaneous local force, acting at the crack tip.

In dynamics one should consider inertia, since medium particles, adjacent to rupture place, can move extremely fast. At the same time, in analogy to structural dimension, known in statics, it is natural to consider structural time in dynamics. In the simplest case, for structural size d and maximal wave speed c, the ratio d/c give a characteristic time of energy transmission between adjacent elements of fractured structure.

Suppose we have a characteristic time interval τ, corresponding to an incubation (latent) period of macrofracture development. Parameters d and τ should be evaluated independently.

Hereby we introduce an elementary spatial-temporal fracture cell

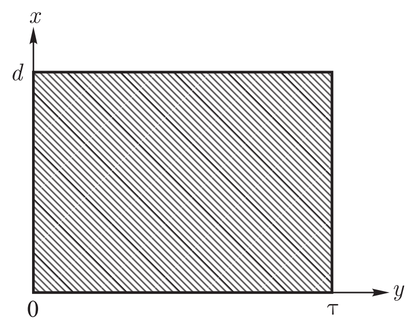

Fig. 4.1.

[0,d]x[t$-\tau$,t] (Fig. 4.1). In other words, we suppose that a certain structure, characterizing peculiarities of the fracture process on the prescribed scale level, is set on the spatial–temporal scale.

Assume that fracture happens, if we have an equality in the following condition:

$$\frac{1}{\tau}\int\limits_{t-\tau}^{t}\frac{1}{d}\int\limits_{x-d}^{x}\sigma(x^*,t^*)dx^*dt^* \geq \sigma_c, \tag{4.5}$$

where τ is the fracture structural time; σ_c is the static strength of material (ultimate stress); σ (x,t) is the tension stress near the crack tip (r=0); and d is a length scale parameter in correspondence to strength characteristics, determined according to static tests on specimens with macrocracks.

In accordance to (4.5), maximal tension stress near the crack tip, averaged over the spatial–temporal interval [0,d]x[t-τ,t], must be equal to static material strength in order to initiate fracture. Introducing new notations (4.5) can be rewritten:

$$\begin{aligned}
&J(t) \leq J_c,\\
&J(t) = \int\limits_{t-\tau}^{t}\int\limits_{x}^{x-d}\sigma(t^*,x^*)dt^*dx^*,\\
&J_c = \sigma_c\tau d.
\end{aligned}$$

The main problem of dynamic fracture is to determine critical fracture conditions. It is natural to consider fracture time t^f as a moment when the pulse attains its critical value: $J(t^f) = J_c$.

According to this approach σ_c, K_{IC} and τ form a system of parameters (in the simplest case — of constants), reflecting strength properties of the material.

4.7 On the discrete nature of dynamic fracture. Fracture 'quantum'

Let the material rupture in one-dimensional cleavage problem (Nikiforovskii, Shemyakin, 1979) be caused by a triangular-profile stress pulse with duration T. Let us determine the threshold, i.e. the smallest possible momentum $U = U_c(T)$ for the given T, leading to rapture. Using the classical critical stress criterion $\sigma \leq \sigma_c$, we obtain

$$U_c = \frac{1}{2}\sigma_c T.$$

The corresponding threshold is presented in Fig. 4.2 (hatched line). Hence, even infinitesimal momenta are capable, according to the accepted criterion, of causing fracture.

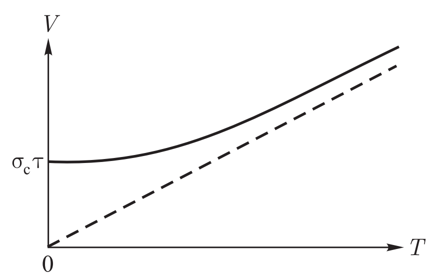

Fig. 4.2.

Now consider a problem for semi-infinite crack. Load is given by stress applied on the crack faces $x \leq 0$, $y = \pm 0$:

$$\sigma_y = P\left[H(t) - H(t-T)\right], \quad \sigma_{xy} = 0,$$

where P and T are load amplitude and duration. Then on the crack continuation we get:

$$\sigma_y = \frac{K_{\mathrm{I}}(t)}{\sqrt{2\pi r}} + O(1),$$

where $K_{\mathrm{I}}(t)$ is given by (4.1). Using the classical criterion of critical stress intensity factor $K_{\mathrm{I}} \leq K_{\mathrm{I}C}$ we have:

$$U_c = \frac{K_{\mathrm{I}C}\sqrt{T}}{\Phi(c_1, c_2)}.$$

Therefore, for $T \rightarrow 0$ threshold fracture momenta become infinitesimal.

This conclusion contradicts the common sense. We will show that a simple account of physical discreteness of dynamic rupture leads to structural–temporal criterion of fracture.

It has already been mentioned that the main parameter of crack mechanics is a linear size d, characterising an elementary fracture cell. Such a cell has no unambiguous physical interpretation suitable for all practical cases and is, in fact, a universal fracture characteristic. It can be interpreted in different ways depending on the class of the problems studied.

Here we introduce an elementary portion ('quantum') of momentum, required to fracture one structure cell: $U_1 = \sigma_c \tau$, w here τ is the incubation time, determined by the material properties and class of problems.

Suppose that in cleavage conditions a threshold pulse of a given shape, e.g. triangular or rectangular, with duration T is created in the medium. Suppose a certain number of structural elements was fractured. Fracture of m structural cells requires following momenta:

$$U_m = \sigma_c \tau m, m = 1, 2, 3 \ldots$$

Let us introduce a distribution:

$$P_m = C\ \exp\left(-\frac{U_m}{\alpha T}\right), \tag{4.6}$$

where P_m is the probability that m structural cells will fail; α is a parameter, depending on the shape of the temporal stress profile and C is a normalising multiplier, determined by relation

$$\sum_m P_m = 1. \tag{4.7}$$

The average threshold momentum can be found as

$$U = \sum_m P_m U_m. \tag{4.8}$$

From (4.6)–(4.8) for a triangular load we have:

$$U = \frac{\sigma_c \tau}{1 - \exp\left(-2^{\tau}/_{T}\right)}.$$

The corresponding threshold is shown in Fig. 4.2 as a continuous line. Under sustained loading ($\tau \ll T$) the threshold characteristics can be computed according to the classical critical stress criterion:

$$U = \frac{1}{2}\sigma_c T.$$

Let us determine macrorupture as fracture of at least one structural element (Novozhilov, 1969). Then the corresponding fracture criterion can be written in the following form:

$$\int\limits_{t-\tau}^{t} \sigma(t^*)dt^* \equiv \sigma_c\tau. \tag{4.9}$$

Here τ is the smallest possible time, neded for load of threshold amplitude to create fracture.

For media with cracks, the mean values of rupture stress on the structural interval are examined. Instead of (4.9) we have:

$$\int\limits_{t-\tau}^{t}\int\limits_{x-d}^{d} \sigma(t^*, x^*)dt^*dx^* \leq \sigma_c\tau d, \tag{4.10}$$

coinciding with (4.5). In particular case of quasistatic loading (4.10) coincides with the force criterion of Neuber—Novozhilov. The received condition coincides with introduced structural—temporal criterion. In this case in the absence of cracks (4.9) can be considered as a particular case of (4.5).

Now, according to (4.9) and (4.10) dynamic strength of a brittle media can be evaluated as a calculated characteristic. Moreover, it is natural to expect that both the critical rupture stress of 'intact' continuum and the fracture toughness of cracked domains will show a dependence on parameters of the exterior load, including the loading rate. It was established that such a behavior is the principal peculiarity of dynamic fracture, stipulated by 'quantum' nature of this process.

Essentially, the analysed problem of dynamic strength under high-rate loading is an analogue to the problem of low-temperature heat capacity of solids in classical molecular physics (Kikoin, 1976). This problem was solved using quantum mechanics. Postulates on the discreteness of structure (a solid is a combination of elementary oscillators), on the discrete nature of energy (energy is released and absorbed by elementary portions-quanta) and correspondence principle (within the limits of low loading rate quantum theory should not contradict the classical one) were taken as a basis. This approach gives a possibility to explain dependence of specific heat capacity of solids on temperature. It was shown that for the low temperatures (close to absolute zero) the energy is finite and is determined by the elementary energy quantum, and the corresponding temperature dependence of heat capacity can be calculated fairly easily.

The dependence of internal solid energy $\langle E \rangle$ on temperature θ, being calculated according to quantum (continuous line) and classical (dashed line) theories is shown in Fig. 4.3.

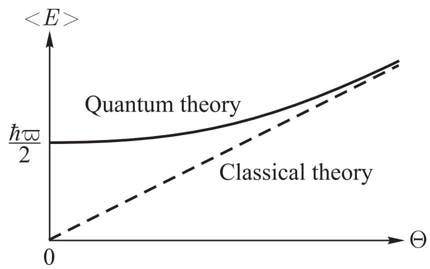

Fig. 4.3.

Analogy between quantum mechanics and basic principles of Novozhilov's theory is evident:

(1) "all solids consist of spatial–structural elements of a finite size";
(2) "an elementary act of fracture is a fracture of one structural element";
(3) "criterion parameters, including a structural element size, should be chosen in such a manner that for low load rates theory predictions should coinside with predictions given by classical theories".

This analogy becomes even more apparent if we compare dependence $\langle E \rangle - \theta$, presented in Fig. 4.3, to dependence of a threshold (minimal fracturing) momentum on its duration in cleavage (see Fig. 4.2).

The idea of fracture discreteness was discussed in several scientific works. Thus, ideas of substitution of a solid medium by discrete geometrical structures has important conclusions (see Novozhilov, 1969, Novozhilov, 1969, Thomson, Hsieh, Rana, 1971, Slepjan, 1974, Morozov, 1954, Nazarov, Paukshto, 1984, Morozov, Paukshto, 1991).

4.8 On the relaxation nature of the incubation time

We will show that the discussed structural-temporal criterion is closely connected to the relaxation processes accompanying rupture development in continuum.

We suppose that a given point of the material is characterised by intensity of a stress field $\sigma(t)$. Stresses result in deformation and development of

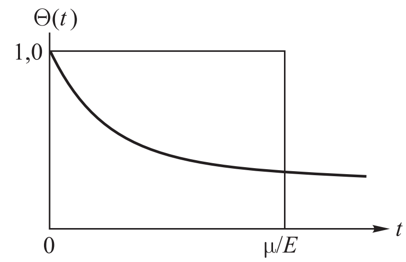

Fig. 4.4.

microdamage. Suppose the following deformation-based fracture criterion is valid under these conditions:

$$K\chi(t) \leq \Sigma_c, \tag{4.11}$$

where K and Σ_c are material constants, and $\chi(\mathrm{t})$ is a relative volume change, caused by deformation and microdamage in the given point.

If the material is linear-elastic, then $\Sigma(t)=K\chi(t)$ and from (4.11) we obtain an analogous critical stress criterion:

$$\Sigma(t) \leq \Sigma_c.$$

Suppose the material is following a rheological law:

$$\Sigma(t) = K\chi(t) + \mu\frac{d\chi}{dt}, \tag{4.12}$$

where μ stands for viscosity. Solving (4.12) with respect to $\chi(\mathrm{t})$ we get:

$$\chi(t) = \frac{1}{\mu}\int\limits_{-\infty}^{t} \exp\left[-\frac{K}{\mu}(t-s)\right]\Sigma(s)ds. \tag{4.13}$$

The kernel of the integrand (4.13) is the function $\exp\left[-\frac{K}{\mu}t\right]$. We replace it by a step function $\theta(t)$ (Fig. 4.4) in such a manner that:

$$\int\limits_{0}^{\infty} Q(s)ds = \int\limits_{0}^{\infty} \exp\left(-\frac{K}{\mu}s\right)ds = \frac{\mu}{K}.$$

Then (4.13) is transformed into the following relation:

$$K\chi(t) = \frac{1}{\mu/K} \int\limits_{t-\mu/K}^{t} \Sigma(s)ds,$$

whence, considering (4.11) and using notation $\tau = \mu/K$, it follows that:

$$\int\limits_{t-\tau}^{t} \Sigma(s)ds \le \Sigma_c \tau. \tag{4.14}$$

Condition (4.14) coincides with structural-temporal criterion (4.9) for 'intact' materials.

Small values of 'viscous' term in (4.12) correspond to small viscosity and long deformation:

$$\frac{\mu}{K}\frac{d\chi}{dt} \ll 1.$$

In this case the critical stress criterion is valid. The 'viscous' term should be taken into account for high-rate dynamic loading, and (4.14) must be used as fracture criterion.

The obtained characteristic $\tau = \mu/K$ has a physical meaning of relaxation time. However, it should be kept in mind that the real relaxation is caused not only by viscous deformation, but is result of microfracture, preceding a macrorupture of the material. Seaman et al. (Seaman, Curran, Aidun, Cooper, 1987, Seaman, Curran, Murri, 1985) have shown that dynamic macrofracture and change of volume, accompanying it, could be described by an equation similar to (4.12), and relaxation times for brittle steels and alloys appeared to be larger by several orders of magnitude as comparing to analogous characteristics of viscous deformation for these materials.

4.9 On choice of parameters of the incubation time criterion

The choice of appropriate parameters for fracture criterion has a basic influence on the possibility to obtain quantitative results in real problems. Only comparison to experimental results can reveral if this choice was correct.

Structural–temporal criterion for fracture is based on a system of three strength parameters: (σ_c, K_{IC}, τ), two of which, static strength and static fracture toughness are well-known. The third parameter, giving structural (incubation) time of fracture, could be interpreted in several different ways.

Insprite of this one should have a method to choose it in any situation.

Let us consider two main possibilities of such a choice:

(1) structural time τ is determined by the fracture structural size:

$$\tau = \frac{d}{c} = \frac{d\sqrt{\rho}}{k}. \tag{4.15}$$

Here c is the speed of the fastest wave; ρ is the mass density; k is a constant, depending on the material properties. According to this, τ has the physical meaning of average time of energy transmission between adjacent fracture cells.

Further, it will be shown that the structural-temporal criterion with parameter τ, obtained according to (4.15) gives a possibility of efficient calculations of dynamic strength characteristics for 'intact' materials. This results acquired using uncubation time approach with τ received on the basis of (4.15) are in a very good coincidence with known cleavage experiments (Zlatin, Pugachev, Mochalov, Bragov, 1974). Zlatin, Pugachev, Mochalov, Bragov, 1975, Meshcheryakov, 1988, Meshcheryakov, Divakov, Kudryashov, 1988);

(2) incubation time τ does not directly depend on fracture structural size and should be obtained experimentally. Processes of birth, growth and confluence of numerous microdefects in a certain (sufficiently large) area surrounding the crack tip, preceding macrorupture of a material, determine the characteristic scale level of macrorupture. The incubation time could be considered as some integral temporal characteristic of these processes. Further it will be established that the fracture structural time τ can be interpreted as the incubation time $\tau = t_{inc}$ from minimal-time criterion, as suggested in (Homma, Shockey, Murayama, 1983, Kalthoff, Shockey, 1977, Shockey, Erlich, Kalthoff, Homma, 1986).

References

Freund, L. B., 1972, The analysis of elastodynamic crack tip stress fields. Mechanics Today, S.-Neamat-Nasser, Pergamon Press, Vol. 3, pp. 55–91.

Freund, L. B., 1976, Dynamic crack propagation, Mechanics Fracture F. Erdogan, ASME AMD, Vol. 19, pp. 105–134).

Freund, L. B.,1974, The stress intensity factor due to normal impact loading of the faces of a crack, Internat. J.Engrg. Sol., 12 (2), 179–189.

Goldstein, R. V., Osipenko, N. M., 1978,Fracture and Structure Formation, Reports Science Acad. USSR, 240,(4), 829–832. (In Russian.)

Goldstein, R. V., Osipenko, N. M., 1993, Structures and processes of formation fracture. Modeling of Seismic Process Development and Earthquakes Prognosis, Nauka, Moscow, pp. 21–37. (In Russian.)

Homma, H., Shockey, D. A., Murayama, Y., 1983, Response of cracks in structural materials to short pulse loads, J. Mech. Phys. Sol., 31 (3), 261–279.

Kachanov, L. M., 1974, Fundamentals of Fracture Mechanics, Nauka, Moscow, 312pp. (In Russian.)

Kalthoff, J. F., Shockey, D. A., 1977, Instability of cracks under impulse loads, J. Appl. Phys., 48, 986–993.

Kikoin, A. K., Kikoin, I. K., 1976, Molecular Physics, Nauka, Moscow, 1976, 500 pp. (In Russian.)

Mazja, V. G., Nazarov, C. A., Plamenevskii B. A., 1981, Elliptic Boundary Problems Solution Asymptotics Under Singular Domain Perturbations, Tbilissi University Press, Tbilissi. 206 pp. (In Russian.)

Meshcheryakov, Y. I., 1988, Statistic model of cleavage surface formation and fracture criterion, Surface Physics, Chemistry, Mechanics, N 3, P. 101–111. (In

Meshcheryakov, Y. I., Divakov, A. K., Kudryashov, V. G., 1988, On dynamic strength under cleavage and disruption, Physics Burning and Explosion, 24, (2), 126–134. (In Russian.)

Morozov, N. F., 1954, Mathematical Problems of Crack Theory, Nauka, Moscow, 255 pp. (In Russian.)

Morozov, N. F., Paukshto, M. V., 1991, On the crack simulation and solution in the lattice, ASME J. Appl. Mech., 58, 290–292.

Morozov, N. F., Petrov, Y. V., 1990, Dynamic fracture viscosity in crack growth initiation problems, News Science Acad. USSR, Solid Mechanics, 6, P. 108–111.(In Russian.)

Morozov, N. F., Petrov, Y. V., 1992, On structural time concept in dynamic fracture theory of brittle materials, Reports Russian Science Acad., 324 (5), 964–967. (In Russian.)

Morozov, N. F., Petrov, Y. V., 1993, On structure-temporal description of high-speed dependence of dynamic brittle material fracture viscosity, News Russian Science Acad. Solid Mechanics, N 6. P. 100–104. (In Russian.)

Morozov, N. F., Petrov, Y. V., Utkin, A. A., 1990, On cleavage analysis under approaches of fracture structural mechanics, Reports Science Acad. USSR, 313 (2), 276–279. (In Russian.)

Morozov, N. F., Petrov, Y. V., Utkin, A. A., 1991, On Structure–temporal approach to dynamic brittle formation fracture analysis, Proceedings Leningrad Mining Institute, 125 (Rock Fracture), 76–86. (In Russian.)

Moscow–Leningrad, 204 pp. (In Russian.)

Nazarov, S. A., Paukshto, M. V., 1984, Discrete models and Averaging in Problems of Elasticity Theory, Leningrad University Press, Leningrad, 93 pp. (In Russian.)

Neuber, H., 1947, Concentration of Stresses, Nauka,

Nikiforovskii, V. S., Shemyakin, E. I., 1979, Dynamic Fracture of Solids, Novosibirsk University Press, Novosibirsk, 271 pp. (In Russian.)

Novozhilov, V. V., 1969, On fundamentals of equilibrium cracks theory in elastic bodies, Appl. Math. And Mech., 33 (5), 797–802. (In Russian.)

Novozhilov, V. V., 1969, On necessary and sufficient criterion of brittle strength, Appl. Math. and Mech., 33 (2), 212–222. (In Russian.)

Panin, V. E., Gridnev, Y. V., Danilov, V. I., et al., 1990, Structural Levels of Deforming and Fracture, Nauka, Novosibirsk.

Parton, V. Z., Boriskovsky, V. G., 1985, Dynamic Fracture Mechanics, Nauka, Moscow, 264 pp. (In Russian.)

Parton, V. Z., Boriskovsky, V. G., 1988, Brittle Fracture Dynamics, Nauka, Moscow, 239 pp. (In Russian.)

Petrov, Y. V., 1991, On 'quantum' nature of brittle media dynamic fracture, Reports Science Acad. USSR, 321 (1), 66–68. (In Russian.)

Petrov, Y. V., 1996, Quantum analogy in solids fracture mechanics, Physics Solids, 38 (11), 3386–3393. (In Russian.)

Petrov, Y. V., Morozov, N. F., 1994, On the modelling of fracture of brittle solids, ASME J. Appl. Mech., 61, 710–712. (In Russian.)

Seaman, L., Curran, D. R., Aidun, J. B., Cooper, T., 1987, A microstatistical model for ductile fracture with rate effects, Nuclear Engrg. Design, 105, 35–42.

Seaman, L., Curran, D. R., Murri, W. J., 1985, A continuum model for dynamic tensile microfracture and fragmentation, J. Appl. Mech., 52, 593–600.

Shockey, D. A., Erlich, D. C., Kalthoff, J. F., Homma, H., 1986, Short-pulse fracture mechanics, Engrg. Fracture Mech., 23, 311–319.

Slepjan, L. I., 1974, Approximate model of crack dynamics. Continuum Dynamics, N 19–20, P. 101–110. (In Russian.)

Thomson, R., Hsieh, C., Rana, V., 1971, Lattice trapping of fracture cracks, J. Appl. Phys., 42 (8), 3154–3160.

Zlatin, N. A., Pugachev, G. S., Mochalov, S. M., Bragov, A. M., 1974, Fracture process temporal regularities under intensive loading, Physics Solids, 16, (6), 1752–1755. (In Russian.)

Zlatin, N. A., Pugachev, G. S., Mochalov, S. M., Bragov, A. M., 1975, Temporal dependencies of metal strength at microsecond range durability, Physics Solids, 17, (9), 2599–2602. (In Russian.)

Chapter 5

Incubation time approach (continuation)

Reflection of an elastic wave from a boundary. Cleavage. Experimental study of cleavage. Dynamic branch of temporal strength dependence. Fracture delay. Incubation time based analysis of cleavage. Principal instability of strength rate dependencies. Dynamic fracture near the crack tip. Dynamic crack initiation

5.1 Fracture of initially intact media

We will consider materials without artificially made defects and concentrators, like cracks or sharp notches, to be 'intact' materials. Let us examine the specific features of these materials' fracture and possible methods of its modeling. In this chapter the works (Morozov et al., 1990, Morozov et al., 1991, Petrov, 1991, Petrov, 1996, Morozov and Petrov, 1996a, b, Petrov, 1993, Smith, 1975) are used.

5.2 Cleavage in solids: Dynamic strength of materials

Historically the first attempts to analyse cleavage were associated with the application of the critical stress criterion:

$$\sigma \leq \sigma_c. \tag{5.1}$$

As experiments have shown, this criterion could not describe many significant peculiarities of cleavage. It can be noticed that in the case of fracture, caused by a short-term pulse of large amplitude, the critical stress criterion contradicts the momentum variation law. Thus, accepting the fact that fracture is initiated by rectangular profile wave with duration t_0 and a for a threshold amplitude, we obtain $U_* = \sigma_c t_0$. Obviously, even infinitesimal force momenta, not able to change material particles' momentum significantly, can cause fracture.

A number of phenomena observed in this experiments, e.g. the phenomenon of dynamic branch and separated cavity zones and the necessity of their treatment, have led to a temporal criterion (Nikiforovsky, 1976, Nikiforovskii and Shemyakin, 1979):

$$\int_0^{t_*} \sigma(t)dt \leq J_c. \tag{5.2}$$

Integral fracture characteristic (5.2) allows theoretical justification of many important cleavage effects. However, experiments and fracture analysis indicate a considerable role of structure in this process. It is clear that accounting fracture structural peculiarities gives a possibility to obtain some new information about temporal dependence of material strength. Many modern studies, undertaken in the field of dynamic deformation and fracture of materials, are oriented on this. At the same time complicated physical fracture theories, accounting structure processes, are not always effective in analysis of practical engineering problems. That is why elaboration of approaches, explaining and predicting dynamic fracture peculiarities on the basis of simple mechanical principles is expedient.

Let us examine the aforementioned structural-temporal criterion. For analysis of 'intact' media fracture the criterion takes the following form:

$$\int_{t-\tau}^{t} \sigma(t')dt' \leq \sigma_c \tau. \tag{5.3}$$

For definiteness we assume $\tau = \frac{d}{c}$ and consider classical one-dimensional cleavage problem (see, e.g., Nikiforovskii and Shemyakin, 1979). The condition (5.3) differs from temporal criterion (5.2) by an existence of structural fracture characteristic τ. In order to determine what new effects this approach can predict, we will examine reflection of a triangular compressive pulse from the free end of a semi-infinite bar. Axis Ox is directed along the bar, which is located at $x > 0$. The incident pulse is given by:

$$\sigma_- = -P\left(1 - \frac{ct + x}{ct_0}\right)\left[H(ct + x) - H(ct + x - ct_0)\right].$$

Here P is the pulse amplitude, t_0 is its period and $H(t)$ is the Heaviside step function. The profile of the stress reflected from the free surface, will have the following form:

$$\sigma_+ = P\left(1 - \frac{ct - x}{ct_0}\right)\left[H(ct - x) - H(ct - x - ct_0)\right].$$

The real stress is expressed as $\sigma = \sigma_- + \sigma_+$. Maximum tensile stress is firstly reached at the point with coordinate $x_0 = \frac{ct_0}{2}$. By introducing dimensionless values $T = \frac{ct}{d}$, $T_0 = \frac{ct_0}{d}$, one can obtain:

$$\begin{aligned}
&\sigma\big|_{x=x_0} = F + G,\\
&F = P\left(\frac{1}{2} - \frac{T}{T_0}\right)\left[H\left(T + \frac{T_0}{2}\right) - H\left(T - \frac{T_0}{2}\right)\right],\\
&G = P\left(\frac{3}{2} - \frac{T}{T_0}\right)\left[H\left(T + \frac{T_0}{2}\right) - H\left(T - \frac{3T_0}{2}\right)\right].
\end{aligned} \tag{5.4}$$

Rupturing amplitude P_*, minimal for the given period t_0, can be found from the following condition:

$$\max_t I = \sigma_c, \quad I = \int_{T-1}^{T} \sigma(T')dT'. \tag{5.5}$$

It follows from (5.4) that the maximum of $I(T)$ is reached in the integration interval ($T_0/2$,$T_0/2$+1). Moreover, $\max\limits_t I(T) = PT_0/2$, if $T_0 < 1$ and $\max\limits_t I(T) = P(T_0 - \frac{1}{2})/T_0$, if $T_0 \geq 1$. Due to (5.5), it follows that:

$$T_* = \begin{cases} 1\Big/\left[4\left(1 - \sigma_c/P_*\right)\right] + 1, & 1 \leq P_*/\sigma_c \leq 2 \\ 1 + \sigma_c/P_*, & P_*/\sigma_c \geq 2 \end{cases}. \tag{5.6}$$

where $T_* = ct_*\Big/t$ is the normalised time-to-fracture, defined as the moment of time when the integral form attains its critical value (5.3). The appropriate curve is shown in Fig. 5.1.

5.3 Temporal dependence of strength

Obtained relation between fracture time t_* and corresponding threshold amplitude P_* is called the temporal dependence of strength. It shows that dynamic strength is not a material constant but depends on time-to-fracture

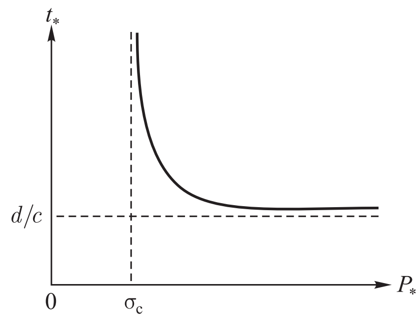

Fig. 5.1.

(specimen 'life time'). In terms of this dependence the critical stress criterion (5.1) and temporal approach of Nikiphorovski—Shemyakin (5.2) are on 'different poles'. Critical stress criterion qualitatively describes quasistatic fracture for long times. Experiments have shown that in the case of short-term loading we can observe a weak dependence of fracture time on threshold amplitude with a certain asymptote. This effect is called the dynamic branch of temporal strength dependence.

We notice that (5.2) gives a similar dependence for short term loading, but it does not cover the case of quasistatic loading. Dynamic branch location and its connection to a quasistatic one remain unsolved. Thus, the critical stress criterion and the temporal criterion (5.2) describe only limiting cases of the temporal strength dependence. As stated above an introduction of a structural element gives a possibility to construct a unified curve of temporal strength dependence (Fig. 5.1). Static and dynamic branches are smoothely connected. The physical meaning of the horizontal asymptote is following: under accepted assumption ($\tau = {}^{d}/_{c}$) it corresponds to transmission time of energy between structure elements. So, for aluminum alloy B95: (σ_c=460 MPa; K_{IC}=37 $MPa\sqrt{m}$; c=6500 m/s): $d/c=2K_{IC}^2/(\pi c\, \sigma_c^2)$ that gives approximately $0.6\mu s$. It follows from the obtained formulas that the threshold amplitude of dynamic loading (cleavage strength) increases from 600 to 1400 MPa while load duration is changed within the range between 2 to 0.5 μs. This fact agrees perfectly with experimental data from (Zlatin et al., 1975, Meshcheryakov 1988). The undertaken calculations have shown a satisfactory correspondence to experiments carried out on other materials.

As follows from (5.3)–(5.5), fracture in cleavage region happens with a delay, after passage of the peak of the local rupture stress (Fig. 5.2).

It is interesting to construct a fracture threshold, i.e. the dependence

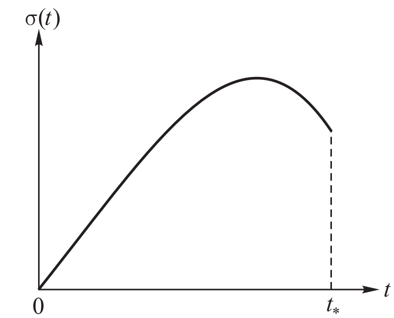

Fig. 5.2.

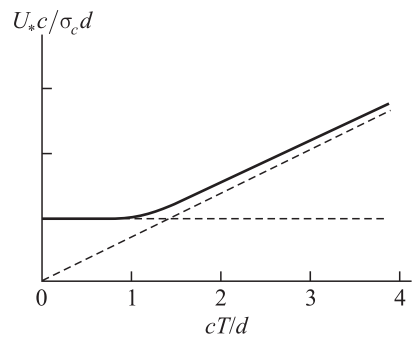

Fig. 5.3.

of minimal rupture momentum $U{=}PT_0/(2\sigma_0)$ on its duration. Such a threshold, obtained according to the critical stress criterion, is shown in Fig. 5.3 as a sloping dashed line. This line passes through the origin of the coordinate system; hence, in this case the fracture area in the plane (T_0,U) adjoins the origin. It denotes that even infinitesimal force momenta are able to cause fracture. This is contradicting the common sence. The temporal criterion of Nikiphorovski—Shemyakin corrects this situation — the fracture threshold on the plane (T_0,U) is denoted by a horizontal line. It gives a finite threshold value for small durations; however, it does not mateh quasistatic situation for long times.

Structural-temporal criterion (5.3) gives a unified threshold curve (full line in Fig. 5.3), suitable within the whole range of loading times. In our case the threshold curve is given by the following analytic formula:

$$U = \begin{cases} 1, \quad T_0 \le 1 \\ T_0^2/(2T_0 - 1)\,, \quad T_0 \ge 1 \end{cases} . \tag{5.7}$$

In the limit of very long and very short pulses it corresponds respectively to the quasistatic and temporal criteria.

5.4 Fracture zone behavior in cleavage

Fracture zone behavior in cleavage is an extremely interesting subject to study. Classical approaches can not provide an adequate prediction. Thus, according to the critical stress criterion, the fracture zone can have a form of sequentially alternating cleavage sections. According to the temporal criterion fracture occurs continuously in the domain. This domain can have a finite extent, and is called by V. S. Nikiphorovski and E. I. Shemyakin a zone of continuous fractionation. The real fracture is characterised by both cases. In K. B. Broberg's work (Broberg, 1960) the fracture domain has a form of fractionated parts, alternating with unfractured zones (Fig. 5.4a). De facto, the zone of continuous fracture is not continuous. It is also related to fractured domains in some other experiments (Fig. 5.4b) (see, e.g., Shockey, et al. 1983). Moreover, as shown in experiments, the qualitative view of fracture domains depends on exterior load parameters, such as loading rate, amplitude and duration.

Traditional approaches in fracture do not give a possibility to describe the whole variety of fracture zone geometries observed in experiments. Thus, usage of critical stress criterion (5.1) makes it possible to get a sequence of cleavage sections (cracks). The temporal criterion of Nikiphorovski-Shemyakin makes it possible to predict a zone of continuous fractionation (see, e.g., Nikiforovskii and Shemyakin, 1979).

It is interesting that the structural-temporal criterion (4.5) gives a possibility to model fracture zone dynamics in a more precise way. Let us examine a scheme of calculation of fractured domain parameters in cleavage conditions. We note that in one-dimensional situation rupture stresses are constant in the 'plane' of fracture, i.e. perpendicular to wave propagation. We suppose that the domain is linear, homogeneous and consists of successive identical structural strata with the thickness b. For definiteness, as a particular case, we take $b = d$. An element (stratum) will be fractured if the structural-temporal criterion in its center meets the following condition:

$$\int_{t-\tau}^{t} \sigma(t')dt' \geq \sigma_c \tau.$$

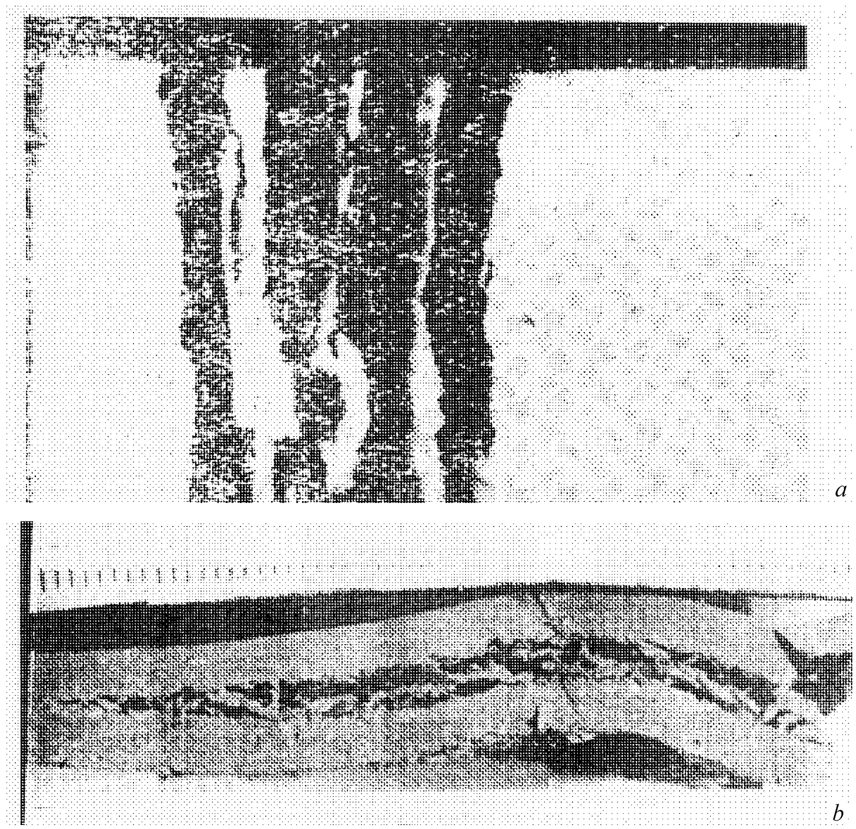

Fig. 5.4.

Let t_* be the time when this condition is first fulfilled. Then, for $t < t_*$ the properties and the geometry are unchanged. At time $t = t_*$ the fracture of the whole structural stratum occurs. In this connection the whole part of the specimen, located between the face and the fractured stratum, forms a cleavage plane. The fractured stratum is an obstacle to waves transmitted

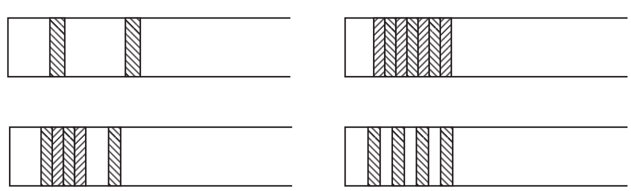

Fig. 5.5.

by the sample. Further waves, moving to the face and going from it are reflected by a new free surface.

Calculations, undertaken according to the aforementioned scheme, have shown that variations of fracture zones, shown in Fig. 5.5, can be created by a single trapezoidal pulse. The shape of these zones could be significantly changed by variation of rate, amplitude and duration of load. This completely agrees with the existing results of the experimental studies.

5.5 On relationship between quasistatic and dynamic mechanisms of solid fracture

The undertaken analysis gives a possibility to make a conclusion about interconnection between quasistatic and dynamic fracture mechanisms in cleavage. The main peculiarity of cleavage strength can be traced by means of the obtained diagram of temporal strength dependence. According to this diagram, the dynamic branch values, which are determined by structural characteristic d/c, correspond to dynamic fracture mechanism. Moreover, the dynamic branch location does not correlate with the static strength of the material σ_c, which is confirmed by experiments. Transition zone, extending for times of the order of several structural intervals, reflects the joint manifestation of dynamic and quasistatic fracture mechanisms. In the examined situation both the dynamic fracture parameter and the critical power characteristic influence fracture threshold essentially. Significantly large fracture times, e.g. one order of magnitude larger than the time it takes for a wave to travel through the structure, can be examined as times corresponding to the action range of the quasistatic fracture mechanism. Such a fracture can be analysed with the help of the critical static stress criterion. Estimation and comparison to experimental fracture times for some materials (see, e.g. Zlatin et al., 1975, Meshcheryakov, 1988) lead to a conclusion that the range of essential influence of structural-temporal fracture singularities is within the range of several microseconds.

As an example, we will cite some calculated results of dynamic strength for rail steels RS700 and RS1100. The input data for rail steels are well-known (Honeycombe, 1980): RS700: σ_c =780 MPa, $K_{\mathrm{I}C}$=70 $MPa\sqrt{m}$; RS1100: σ_c =1160 MPa, $K_{\mathrm{I}C}$=48 $MPa\sqrt{m}$.

RS1100 was subjected to thermoprocessing (oil tempering from 920° and release at 540°). The computed results of temporal strength dependence, for rail steels, are shown in Fig. 5.6. It is clear that RS1100, in spite

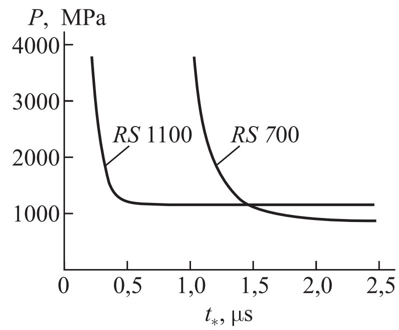

Fig. 5.6.

of higher quasistatic rupture strength, has lower strength under high-rate shock loading, which is stipulated by its lower crack resistance.

The obtained conclusion is not trivial and demonstrates the necessity of a qualitative approach to constructional material selection with regard to corresponding velocity operating conditions. The structural-temporal approach allows optimisation of this selection.

Fracture structural-temporal and force characteristics modification leads to a displacement of diagram of temporal strength dependence. Thus, the decrease of stress-wave propagation velocity changes the location of the dynamic branch in such a way that the material cleavage strength increases. Therefore, heating of polymer material up to the temperature of high-elastic state can lead to increase of its cleavage strength. This conclusion agrees with experimental studies of cleavage-strength dependence of polymer composites on temperature (Golubev et al., 1987). The threshold diagram in Fig. 5.3 gives a possibility to conclude that fracture intensity depends on initial static rupture strength and on stress wave velocities. The latter is determined by the elastic modulus and the material density. With regard to this, we can conclude that more rigid and less massive materials cannot qualitatively resist high-rate dynamic loading.

The dependence of the threshold pulse on its duration (Fig. 5.3) obtained using structural-temporal criterion shows that, if we know the threshold values of extremely short loading pulses, we can determine incubation time of fracture, corresponding to the given material. The latter allows the association of dynamic fracture and surface erosion phenomena in gas flows, containing hard particles. On the basis of fractographical analysis we can conclude (ed. Preece, 1979) that the factor controlling erosion fracture is formation of brittle annular cracks, produced by contact dynamic interaction of flying particles with the surface. Small particles with radius of several dozens or hundreds of microns, used in the experiments on erosion fracture, produce extremely short rupture pulses during contact interaction with the surface. If we know their characteristics and the velocity value of threshold impact during which erosion fracture of a surface occurs, we can determine an elementary fracture 'quantum' and the corresponding incubation time.

Now we will show how the given scheme can be realised in the simplest approximation. Let a spherical hard particle with radius R and velocity v fall on the surface of an elastic semi-space. Following the classical Hertz scheme (see, e.g., Kolesnikov and Morozov, 1989) we suppose the equation of particle (indenter) movement may be written as:

$$m\frac{d^2h}{dt^2} = -P, \tag{5.8}$$

where h is the impact speed, P is the contact force, and m is the particle mass. In the classical approximation it is supposed that the relation between contact force and impact speed remains the same as in statics. This relation can be presented in the following form:

$$P(t) = kh^{3/2}, \tag{5.9}$$

where

$$k = \frac{4}{3}\sqrt{R}\frac{E}{(1-v^2)}. \tag{5.10}$$

At the initial moment $\frac{dh}{dt} = v$; then, integrating (5.8), we have:

$$\frac{dh}{dt} = \sqrt{v^2 - \frac{2h^{\frac{5}{2}}}{5m}}. \tag{5.11}$$

The maximum approaching h_0 is attained for $\frac{dh}{dt} = 0$; hence:

$$h_0 = \left[\frac{5mv^2}{4k}\right]^{\frac{2}{5}}. \tag{5.12}$$

To compute the impact duration we integrate (5.11) from the beginning of the interaction to the moment of maximum penetration:

$$\int\limits_0^{h_0} \frac{dh}{\sqrt{v^2 - \frac{4kh^{\frac{5}{2}}}{5m}}} = \frac{t_0}{2},$$

where t_0 is the complete impact duration. Whence we have:

$$t_0 = \frac{2h_0}{v}\int_0^1 \frac{d\gamma}{1-\gamma^{\frac{5}{2}}} = 2.94\frac{h_0}{v}. \tag{5.13}$$

Numerical integration permits construction of the dependence of penetration as a function of time, i.e. via $h(t)$. This dependence is approximated with high precision by the expression (Kolesnikov and Morozov, 1989):

$$h(t) = h_0 \sin(2\pi/t_0). \tag{5.14}$$

The dependence of the maximum rupture stress on time at the surface, adjoining the contact platform, is computed according to the formula (Lawn and Wilshaw, 1975):

$$\sigma(v,R,t) = \frac{1-2v}{2}\frac{P(t)}{\pi a^2(t)}, \tag{5.15}$$

where the radius of the contact spot $a(t)$ is determined as:

$$a(t) = \left[3P(t)(1-v^2)\frac{R}{4E}\right]^{\frac{1}{3}} \tag{5.16}$$

and the contact force $P(t)$ is found using (5.9)–(5.14).

Let v be the threshold particle velocity, at which the material rupture happens. We introduce a function:

$$f(v,R,\tau) = \max_t \int_{t-\tau}^{t} \sigma(v,R,s)ds - \sigma_c\tau.$$

In accordance to the structural-temporal criterion we determine an incubation time τ as a positive root of the equation:

$$f(v,R,\tau) = 0, \tag{5.17}$$

for given values v and R.

The obtained formulas can be used for calculation of the incubation time on the basis of experimental data on threshold velocity of surface erosion fracture.

Let aluminum alloy B95 with mechanical characteristics E=73 GPa, ν=0.3, σ_c=456 MPa be subjected to erosion fracture with erodent characteristics R=150 μm, ρ=2400 kg (m=3πgρ r R^3/4).

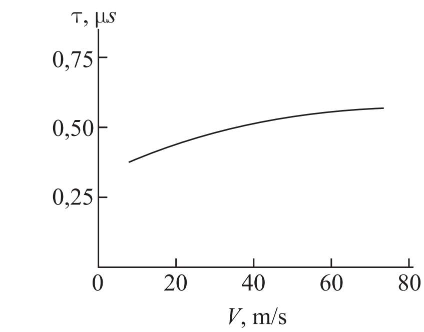

Fig. 5.7.

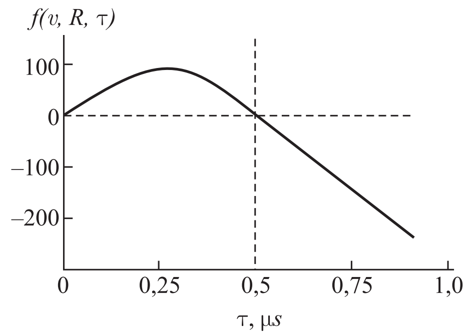

Fig. 5.8.

The dependence of incubation time τ on the threshold velocity of erosion fracture, calculated for the given parameters, is shown in Fig. 5.7. It is obvious that for a very extent range of velocities, observed for aluminum alloys (Urbanovich et al., 1990, Morozov et al., 1994), these methods produce adequate results.

The effective threshold particle velocity, at which the process of erosion surface fracture of the given material begins, must be determined experimentally and turns out to be equal to v=33 m/s (Morozov et al., 1994). Calculations according to the aforementioned formulas give the following values of characteristics of impact interaction between the particles and the surface: t_0=0.29 μs, h_0=3.46 μm. The study shows that function $f(v,R,\tau)$ has only one positive root (Fig. 5.8). The material incubation time, computed for the obtained data, turns out to be equal to τ=0.5 μs.

The obtained value of incubation time gives a possibility to construct a diagram of temporal dependence of strength for the indicated alloy. The

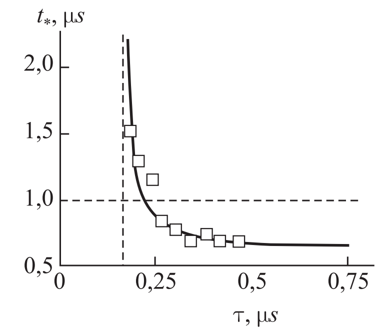

Fig. 5.9.

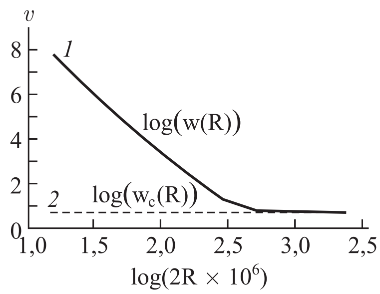

Fig. 5.10.

corresponding computed curve, including not only static, but also dynamic branches is presented in Fig. 5.9. Experimental points, taken from the experiments on cleavage fracture for the given material (Zlatin et al., 1974, Zlatin et al., 1975), included in the same figure, show the efficiency of the indicated methods of structural time evaluation on the basis of erosion data. It is noteworthy that approximately the same value for the structural time can be obtained using the simplified formula (4.15); σ_c=460 MPa; K_{IC}=37 $MPa\sqrt{m}$; c=6500 m/s): $d/c = 2\backslash K_{IC}^2/(pc\backslash\sigma_c^2)$ or approximately 0.6 μs.

On the other hand, if we know the material incubation time, e.g. from experiments on cleavage fracture, we can determine the principal characteristics of the erosion process. The dependence of the erosion fracture threshold velocity of B95 alloy on the radius of erodent particles, calculated for τ=0.5 μs, is represented in Fig. 5.10 (curve 1).

As these results show, the dependence is characterised by static and dynamic branches. The static part is characterised by a weak dependence of threshold velocity on the diameter of erodent particles. As opposed to that, the dynamic branch shows a rapid increase of threshold velocities with decreasing particle dimensions. Moreover, there is some characteristic length scale, in our case of the order of few hundreds of microns, corresponding to the quick transition from the quasistatic regime to the dynamic one. The constructed theoretical curve qualitatively coinsides with well-known experimental observations (Polezhaev, 1986). Notice that calculations according to this scheme with the use of the traditional critical stress criterion (Fig. 5.10, curve 2), cannot explain the observed behavior of threshold velocities of erosion fracture.

5.6 Dynamic fracture at the crack tip

It is well-known that when formulating the macrorupture criterion, complementing the solid-medium mechanics equations, one has to take into account the most important peculiarity of dynamic fracture — the existence of not only spatial but also temporal structure of the process. This circumstance must be reflected while choosing criterion-determining parameters and test methods of dynamic strength properties of a material. Structural-temporal criteria, considered previously, permit taking this dynamic fracture peculiarity into account and modeling the process of crack-growth initiation under the action of impact pulses.

In this chapter we examine some principal peculiarities, and present calculation methods and an interpretation of the well-known high-rate fracture effects of elastic bodies with cracks (Morozov and Petrov, 1990, Morozov and Petrov, 1991, Morozov and Petrov, 1992a, Morozov and Petrov, 1993, Morozov and Petrov, 1996, Morozov et al., 1988a, Morozov et al., 1988b, Morozov et al., 1991, Petrov and Utkin, 1989, Petrov and Morozov, 1994).

5.7 Threshold pulses of impact loading

An essential contribution to solution of the problem of taking the temporal structure of the dynamic fracture process into account comes with introduction of the already mentioned incubation time concept, which was suggested and developed (by Kalthoff and Shockey, 1977, Homma et al., 1983 and Shockey et al., 1986). Experiments, described in these works, testify that in the case of macrocrack initiated by intensive short pulses, threshold amplitude values, obtained experimentally, turn out to be significantly greater than those stipulated by a traditional critical stress intensity factor criterion. That is why Kalthoff and Shockey (Kalthoff and Shockey, 1977) suggested that one should refuse from this criterion and accept the fact that fracture occurs when the current value of the dynamic stress-intensity factor $K_{\mathrm{I}}(t)$ exceeds the value of the dynamic fracture toughness $K_{\mathrm{I}d}$ during some minimum time t_{inc}. The incubation time t_{inc} is considered to be a material constant, connected to structural processes.

Experimental determination of the incubation time is accompanied by a very cumbersome procedure, requiring multiple tests for different values of impact duration and complicated numerical calculations (Homma et al., 1983, Shockey et al., 1986). A priori knowledge of the functional dependence of the dynamic fracture toughness on the history of loading is also essential for the minimum-time criterion.

In chapter 4 we have examined another approach to fracture analysis, based on the structural-temporal criterion:

$$\frac{1}{\tau}\int\limits_{t-\tau}^{t} ds \frac{1}{d}\int\limits_{0}^{d} \sigma(s,r)dr \le \sigma_c, \tag{5.18}$$

where τ and d are the structural time of fracture and its structural size; σ_c is the material static strength (ultimate stress); and $\sigma(t,r)$ is the maximum tensile stress near the crack tip (r=0).

Structural size d is determined according to data of quasistatic tests on cracked specimens. In the case of a generalised plane-strain conditions it can be expressed using the static fracture toughness and strength by a simple formula (Morozov, 1954):

$$d = \frac{2}{\pi}\frac{K_{\mathrm{I}C}^2}{\sigma_c^2}.$$

According to this approach, σ_c, $K_{\mathrm{I}c}$and τ form a system of determining parameters, describing material strength properties. The structural fracture time τ is responsible for dynamic peculiarities of brittle fracture and must be found experimentally for each material.

We will show that in experiments, carried out in (Kalthoff and Shockey, 1977, Homma et al., 1983 and Shockey et al., 1986), the structural time τ may be interpreted as t_{inc}.

Let an infinite plate have a crack $x \le 0$, y=0, and an incident rectangular profile stress wave is:

$$\sigma_y = P\left[H\left(t+\frac{y}{c}\right) - H\left(t+\frac{y}{c}-T\right)\right], \quad \sigma_{xy}=0, \quad t<0, \tag{5.19}$$

where $H(t)$ is the Heaviside step function. We will find, for the given duration T, the minimal amplitude of an external load that will initiate the crack growth. The asymptotic expression of the maximal tensile stress corresponding to the load given by (5.19), on the crack extension for $t > 0$ has the following form:

$$\begin{aligned} &\sigma_y = \frac{K_{\mathrm{I}}(t)}{\sqrt{2\pi r}} + o(1), \quad r \to 0, \\ &K_{\mathrm{I}}(t) = P\varphi(c_1,c_2)f(t), \quad \varphi(c_1,c_2) = \frac{4c_2\sqrt{c_1^2-c_2^2}}{c_1\sqrt{\pi c_1}}, \\ &f(t) = \sqrt{t}H(t) - \sqrt{t-T}H(t-T), \end{aligned} \tag{5.20}$$

where c_1, c_2 are the speeds of the longitudinal and the transverse waves. According to (5.18) and (5.20) the expression of the minimal amplitude, that leads to fracture, obtains the following form:

$$P_1 = \frac{\tau K_{\mathrm{I}c}}{\varphi(c_1,c_2)\max\limits_t \int\limits_{t-\tau}^{t} f(s)ds}. \tag{5.21}$$

At the same time, from the traditional critical stress-intensity factor criterion, it follows that the minimum stress amplitude is given by:

$$P_2 = \frac{K_{\mathrm{I}c}}{\varphi(c_1,c_2)\max\limits_t f(t)}. \tag{5.22}$$

Now we note that

$$\max_t \frac{1}{\tau}\int\limits_{t-\tau}^{t} f(s)ds < \max_t f(t),$$

whence it follows that $P_1 > P_2$, which is reflected in the abovementioned experiments (Kalthoff and Shockey, 1977, Homma et al., 1983 and Shockey et al., 1986). They stated that for long cracks (short pulses) the values of the minimal fracture amplitude turn out to be greater than those obtained according to the traditional stress-intensity factor criterion.

The temporal dependence of the stress-intensity factor criterion is presented in Fig. 5.11.

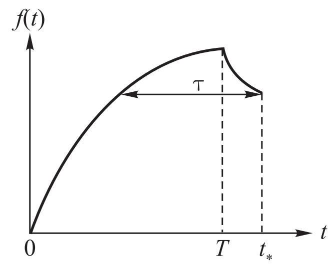

Fig. 5.11.

As calculations using (5.18) show, the initiation of crack growth happens with a delay, i.e. during the decrease stage of local stress-field intensity at the tip. At the moment of fracture t_* the integral $\int\limits_{t-\tau}^{t} f(s)ds$ obtains its maximum value, hence $f(t_*-\tau) = f(t_*)$. According to the monotonicity of the function $f(t)$, we obtain, that in the analysed case τ is the time during which the stress-intensity factor exceeds the value $K_{\mathrm{I}d} = K_{\mathrm{I}}(t_*)$.

We also note that the computed values of dynamic fracture toughness under the examined conditions turn out to be inferior to the corresponding quasistatic value:

$$K_{\mathrm{I}d} = P_1\varphi(c_1, c_2)f(t_*) = \frac{\tau K_{\mathrm{I}c} f(t_*)}{\int\limits_{t_*-\tau}^{t_*} f(s)ds} < K_{\mathrm{I}c} \tag{5.23}$$

as observed in experiments (Homma et al., 1983, Kalthoff and Shockey, 1977, Shockey et al., 1986).

This reasoning remains valid for a reasonable arbitrary temporal profile of a single impact, providing a monotonic increase followed by a decrease of stress intensities.

So, the analysis of fracture caused by threshold pulses allows the observation that structural parameter τ has all the formal properties of an incubation time from the minimum-time criterion, and in the problem of initiation of macrocrack growth it can be taken that:

$$\tau = t_{inc}. \tag{5.24}$$

Criterion (5.18) and (5.24) gives a possibility of efficient calculation of the values of external loading parameters.

Let us take an average incubation time, found in experiments on fracture of metal plates with a macrocrack: $t_{inc}{\approx}10\ \mu s$. Calculating the threshold

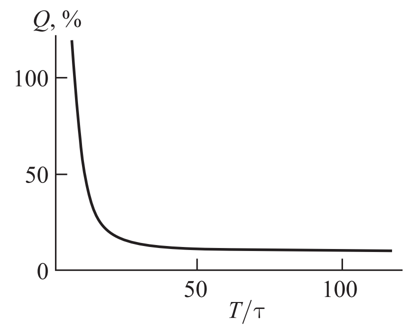

Fig. 5.12.

amplitude values in accordance to (5.21)–(5.24) we obtain values for the relative difference $Q=[(P_1-P_2)/P_2]\times 100\%$ thoroughly in line with the data of experimental observations (Homma et al., 1983, Shockey et al., 1986). The corresponding dependence is presented in Fig. 5.12.

Formulas (5.21) and (5.24) give a possibility to determine the incubation time of a material fracture at the known threshold value of external load amplitude. Thus, for steel 4340 (Homma et al., 1983) we have experimentally obtained a threshold amplitude value within the range of 140–150 MPa, for $T \approx 20\ \mu s$. According to (5.21) (K_{IC}=47 $MPa\ m^{1/2}$, c_1=6 $mm/\mu s$) we get $\tau \approx 7\ \mu s$, coinciding with the incubation-time evaluation for this material (Homma et al., 1983, Shockey et al., 1986).

For steel 4340, used in the experiments of Homma et al. (Homma et al., 1983), we have c_1=6 $mm/\ \mu s$, υ=0,3, K_{IC}=47 $MPa\ m^{1/2}$,σ_c=1490 MPa, t_{inc}=7 μs. For T=18 μs we get the critical value of amplitude P_1=155 MPa from (5.21) and (5.24).

This value is in line with the experimental data of Homma et al. (Homma et al., 1983), when a similar critical value of external load amplitude, causing a crack 'jump' at the distance was calculated:

$$d = \frac{2K_{IC}^2}{\pi\sigma_c^2} \approx 0.6\ mm.$$

5.8 On loading-rate dependence of dynamic fracture toughness

Now we suppose that there is a two-sided plane trapezoidal stress wave, approaching the crack:

$$\sigma_y = \frac{V}{2}\left[\left(t+\frac{y}{c}\right)H\left(t+\frac{y}{c}\right)-\left(t-t_0+\frac{y}{c}\right)H\left(t-t_0+\frac{y}{c}\right)-\right.$$
$$\left.\left(t-\frac{y}{c}\right)H\left(t-\frac{y}{c}\right)+\left(t-t_0-\frac{y}{c}\right)H\left(t-t_0-\frac{y}{c}\right)\right], \quad \sigma_{xy}=0,$$

where $V = P/t_0$; t_0 is the given time of the applied stress increase to its maximum value P. The corresponding asymptotic representation of the maximum normal stress for the crack extension is determined by (5.20), where:

$$f(t) = \frac{2\left[t^{\frac{3}{2}}H(t)-(t-t_0)^{\frac{3}{2}}H(t-t_0)\right]}{3t_0}. \tag{5.25}$$

Let t_* be the time-to-fracture, and t_0 be fixed. Using (5.18), (5.20) and (5.25) one can find the rapturing amplitude P_*, appropriate for t_*. Then calculating the critical stress-intensity factor value:

$$K_{\mathrm{I}q} = K_{\mathrm{I}}(t_*) = P_*\varphi(c_1,c_2)f(t_*),$$

we get:

$$\frac{K_{\mathrm{I}q}}{K_{\mathrm{I}c}} = \frac{5}{2}\frac{\tilde{t}_*^{\frac{3}{2}}-(\tilde{t}_*-\tilde{t}_0)^{\frac{3}{2}}}{\tilde{t}_*^{\frac{5}{2}}-(\tilde{t}_*-1)^{\frac{5}{2}}-(\tilde{t}_*-\tilde{t}_0)^{\frac{5}{2}}+(\tilde{t}_*-\tilde{t}_0-1)^{\frac{5}{2}}}, \tag{5.26}$$

where $\tilde{t}_* = \frac{t_*}{\tau}; \tilde{t}_0 = \frac{t_0}{\tau}$, and all power functions for negative values of their arguments, are considered to be equal to zero. The corresponding graphical dependence is shown in Fig. 5.13. The same dependence was observed in many experiments (see, e.g., the survey of Knauss, 1984).

From (5.26) it follows that the link between the critical stress intensity factor value and the fracture time depends on the time t_0 of the external loading increase. For bounded and semi-bounded domains this link depends also on geometric parameters of the problem. So, for example, if L is the crack length and $K_{\mathrm{I}}(t) = PG(t,L)$, then, according to (5.18), we get:

$$\frac{K_{\mathrm{I}q}}{K_{\mathrm{I}c}} = \frac{\tau G(t_*,L)}{\int\limits_{t_*-\tau}^{t_*} G(s,L)ds}.$$

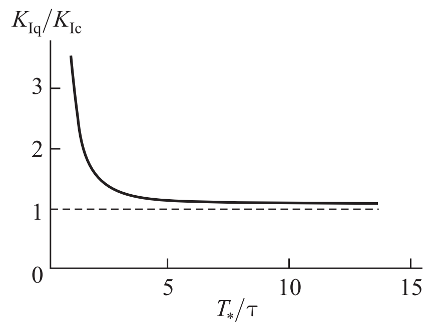

Fig. 5.13.

Let us note that in (5.20), (5.25) and (5.26) time of tension increase can tend to zero, then:

$$\frac{K_{\mathrm{I}q}}{K_{\mathrm{Ic}}} = \frac{3}{2}\frac{\tilde{t}_*^{\frac{1}{2}}}{\tilde{t}_*^{\frac{3}{2}} - (\tilde{t}_* - 1)^{\frac{3}{2}}},$$

which formally corresponds to an instantaneous application of a constant stress. Thus, the qualitative link between K_{Iq} and t_* persists even under an 'infinite' loading rate.

We will show that the dynamic fracture toughness can depend not only on the loading rate and the geometric parameters of the problem. Let us assume fracture initiation caused by means of trapezoidal impact applied directly on the crack faces:

$$\sigma_y = -V\left[tH(t) - (t - t_0)\, H\,(t - t_0)\right], \quad \sigma_{xy} = 0\ .$$

Then, in the infinitesimal order, on the crack plane we have:

$$\sigma_y = \frac{K_{\mathrm{I}}(t)}{\sqrt{2\pi r}} - V\left[tH(t) - (t - t_0)\, H\,(t - t_0)\right] + o(1), \quad r \to 0.$$

By the same reasoning as in the previous case, we get:

$$\frac{K_{\mathrm{I}Q}}{K_{\mathrm{Ic}}} = \frac{5}{2}\frac{\tilde{t}_*^{3/2} - \left(\tilde{t}_* - \tilde{t}_0\right)^{3/2}}{\tilde{t}_*^{5/2} - \left(\tilde{t}_* - 1\right)^{5/2} - \left(\tilde{t}_* - \tilde{t}_0\right)^{5/2} + \left(\tilde{t}_* - 1 - \tilde{t}_0\right)^{5/2}}$$
$$\left\{1 + \frac{\tau v_*}{2\sigma_c}\left[\tilde{t}_*^2 - \left(\tilde{t}_* - 1\right)^2 - \left(\tilde{t}_* - \tilde{t}_0\right)^2 + \left(\tilde{t}_* - \tilde{t}_0 - 1\right)^2\right]\right\} \tag{5.27}$$

For relatively big fracture times the critical stress-intensity factor value

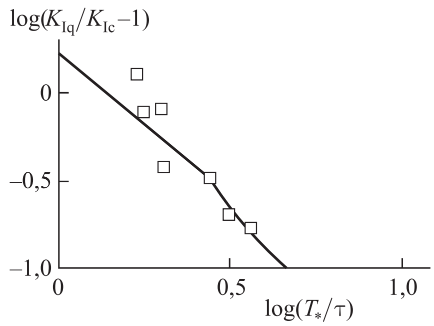

Fig. 5.14.

tends to the quasistatic value, and also:

$$K_{IQ} = K_{Ic} + \frac{\lambda\tau}{t_*}, \quad \frac{t_*}{\tau} \to \infty, \quad \lambda = \text{const}$$

Experiments, under conditions similar to the examined ones (Ravi-Chandar. and Knauss, 1984), have been carried out on specimens made of Homalite-100. A structural fracture time estimation for the named material can be made on the basis of comparison of data, found according to the theoretical formula (5.27), to the experimental ones.

The estimated curve $t_0 = 25\mu s$, $K_{Ic} = 0.48$ MPa$\sqrt{m}$, $\tau = 8\mu s$ and the related experimental points, in logarithmic coordinates, are presented in Fig. 5.14.

Ravi-Chandar and Knauss have suggested an empirical formula:

$$K_{IQ} = K_{Ic} + \frac{C}{t_*^2} \tag{5.28}$$

permitting an analytical description of experimental data. As follows from the results given above (see Fig. 5.14), (5.28) can be considered as an approximation of the exact formula (5.27). In this case:

$$C = \alpha\tau^2 K_{Ic}$$

Formula (5.27), just as (5.26), demonstrates an increasing effect of the stress intensity factor critical value with decreasing time-to-fracture, i.e. with the increase of the loading rate. However, in comparison to the previous case, there are smaller stresses near the crack tip.

It should be noted that the current value of the stress intensity factor in both cases is the same, and the difference in the way of loading manifests itself in the value of the second term of the asymptotic representation of

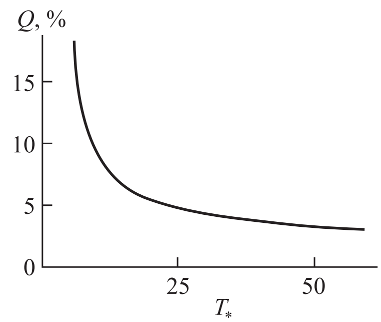

Fig. 5.15.

the solution. This is, ultimately, visualised via the experimentally obtained critical value of the stress intensity factor of crack growth initiation.

As follows from (5.27) and (5.26), the dynamic fracture toughness under wave loading turns out to be smaller than under the corresponding application of load directly on the crack faces.

Value differences for $Q = \left[\left(K_{\mathrm{I}q}^{\mathrm{II}} - K_{\mathrm{I}q}^{\mathrm{I}}\right) / K_{\mathrm{I}q}^{\mathrm{I}}\right] \times 100\%$ for Homalite-100, where superscripts I and II correspond to the first and to the second cases respectively, are presented in Fig. 5.15. As computing results testify, the difference in the way of loading for longer times is hardly observable via the critical value of the stress-intensity factor.

At increasing loading rate the fracture is faster but the dependence of dynamic fracture toughness on the way of loading becomes more conspicuous. Evidently, the physical mechanism, causing such an effect, is an additional contribution of transmitted wave energy to the fracture, which is the more powerful the less the time before fracture is. It leads to a decrease of the stress-intensity factor critical value necessary for creation of material rupture. This circumstance might be one of the reasons causing the apparent dispersion of results at experimental dynamic fracture toughness determination. So, from the experiments on loading Homalite-100 with the help of high-intensive waves Dally and Barker (Dally and Barker, 1988) have obtained smaller critical values of the stress-intensity factor than Ravi-Chandar and Knauss (Ravi-Chandar and Knauss, 1984). This fact caused a discussion on the exactness of the experimental methods employed. The result, presented in Fig.5.15, reflects the difference in dynamic fracture toughness values, measured in the experiments mentioned.

5.9 Minimum and maximum pulses. Limit characteristics of material dynamic fracture

Results of the analysis process, carried out with regard to structural-temporal characteristics, reveals that dynamic effects depend on geometrical parameters, method and history of loading, and that their interpretation can not be reduced only to a velocity dependence of dynamic fracture toughness. It can be one of the explanations of great dispersion and inconsistency of experimental data on dynamic fracture toughness of brittle materials.

Threshold loads, studied in the beginning of the chapter determine minimal (according to energy charges) loading conditions when crack initiation occurs. In this case the appearance of a fracture delay effect is essential: the criterion fullfillment takes place not at the initial stage of crack growth, but at the decrease of the current value of the stress intensity. This effect contradicts classical mechanics of brittle fracture but is observed experimentally both in tests on cleavage (see, e.g., Zlatin et al., 1975, Zlatin et al., 1986, Nikiforovskii and Shemyakin, 1979), and in tests on fracture of cracked specimens (see, e.g., Homma et al., 1983, Kalthoff and Shockey, 1977, Shockey et al., 1986). Here, the calculated critical values of the stress-intensity factor (dynamic fracture toughness) turn out to be inferior to the corresponding quasistatic value K_{Ic} for the given material. The latter is also a very important distinctive feature of the experiments mentioned.

Together with the examined threshold loads, another situation was investigated, i.e. when the applied stress on the crack faces is maintained up to the moment of fracture. This guarantees a monotonic increase of the stress-intensity factor values during the whole structural-temporal interval τ. Consequently, fulfilment of the inequality $K_{\mathrm{I}q} > K_{\mathrm{Ic}}$ is also observed in corresponding tests (Kalthoff, 1986, Knauss, 1984, Ravi-Chandar. and Knauss, 1984).

Thus, the use of the structural-temporal criterion (5.18) for analysis of fast rupture in the crack-tip neighbourhood gives a possibility to calculate dynamic fracture toughness of brittle materials. The results of application of (5.18) to the problem of rectangulary shaped load on the crack faces are presented in Fig. 5.16.

Curve 1 in Fig. 5.16 determines the stress-intensity factor values at the moment of fracture under threshold loads of duration T. In this case the material rupture occurs with a delay, i.e. at the stage of stress-intensity factor decrease and $t_* > T$, where t_* is the fracture time.

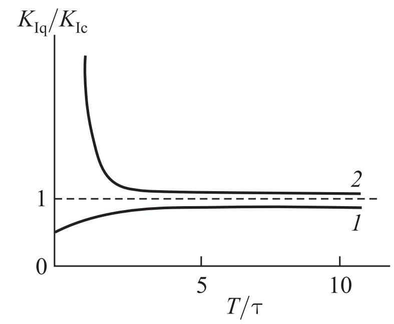

Fig. 5.16.

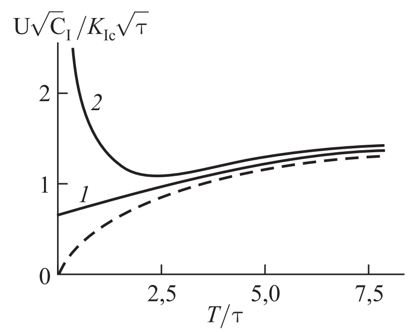

Fig. 5.17.

Curve 2 in Fig. 5.16 matches the case when a suddenly applied constant stress operates up to the fracture moment, so that $t_* = T$.

Such a dispersion of dynamic fracture toughness values, observed in the experiments, has become a reason for discussion on correctness and exactness of the experimental methods used (see, e.g., Kalthoff, 1986, Kobayashi et al., 1973).

The analysis suggests that the behavior of the critical stress-intensity factor is the principal peculiarity of dynamic fracture, stipulated by the discrete, structural-temporal nature of this process.

Let us analyse the behavior of fracturing loads while their duration is changed. Let the fracture at the crack tip be created by a rectangular-profile stress pulse (5.19). $U(T)=PT$ denotes the total momentum of the external load. The computed dependence of the minimum fracture pulse $U = U_*(T)$ on its duration is presented in Fig. 5.17 (curve 1).

Note that if the applied pulse is inferior to U_*, but is of the same duration (through the amplitude decrease), fracture will not occur. Hence, all the points of the domain UT, situated below curve 1 (see Fig. 5.17), do not correspond to fracture. An important result is that the threshold load tends to a finite value for $T \to 0$. If we use the classical criterion of the critical stress-intensity factor (Fig. 5.17, dashed line), we can see, that fracture could be caused even by infinitesimal pulses, they only have to be sufficiently short, which is obviously erroneous. However, the comparison of the computed threshold curves gives grounds to state that for sufficiently large values of the duration $T(\geq 10\ \tau)$ it is possible to use the classical criterion in order to evaluate fracture. Hence, the threshold load calculation reveals a fracture delay, the existence of its lower boundary in the coordinate plane UT and the finiteness of fracturing momentum values U_* for short times of loading.

Now we fix the loading time T, and let U be the applied and U_* the minimum rupturing momenta. It is obvious that for $U > U_*$ fracture occurs, with the result that the fracture time exceeds the loading duration: $t_* > T$.

A question arises, how large the value of U could be for fixed T. Computed data show that if the pulse exceeds the threshold value to some degree, a fracture occurs with a smaller delay. The absence of delay corresponds to a coincidence of the fracture time with the load duration: $t_* = T$. Such a situation can be treated as a load applied up to the moment of fracture. In rapture case this occurs just when the stress intensity factor reaches its maximum. An attempt of further pulse increasing with the help of an amplitude increase leads to a decrease of the duration of the applied loading time, i.e. the fracture condition is fulfilled at time smaller than T.

Taking into consideration the aforesaid, we will call load, acting up to the moment of fracture, maximum rupture loads and denote them U*. Dependence of the maximum rupture pulse on the loading time $U = U^*(T)$ is presented in Fig. 5.17 (curve 2).

Let us consider some peculiarities of fracture caused by maximum rupture loads. At the decrease of loading time one observes the increase of U^* in comparison to U_*, and that $U^* \to \infty$ for $T \to 0$. So, if it is necessary to speed up the fracture process the condition: 'more intense the applied load is, faster the fracture will occur', is correct. And, lastly, to cause an instantaneous fracture an infinitely intense load is required. Evidently, the latter is connected to overcoming of medium's inertia. For large T, i.e. when media 'manages' to start moving, values U_* and U^* practically coincide.

As already noticed, points of the plane UT, placed above curve 2, could not be reached: the fracture domain is under this curve, and at the same time, as stated during the study of the minimum rupturing pulse, above curve 1. Thus, points corresponding to fracture are located between curves 1 and 2 on the plane UT.

5.10 On the material testing principles. Dynamic strength properties

Let us classify some approaches in fracture, corresponding material strength properties and study main possibilities of their evaluation (Morozov and Petrov, 1992b) (Table 5.1).

#	Method	Material Parameters	Criterion
1	Classical approach of static fracture mechanics	σ_c, K_{IC}	$\sigma \leq \sigma_c$ $K_{\mathrm{I}} \leq K_{\mathrm{I}c}$
2	Classical approach of dynamic fracture mechanics	$\sigma_c^d(v), K_{\mathrm{I}c}^d(v)$	$\sigma(t) \leq \sigma_c^d$ $K_{\mathrm{I}}(t) \leq K_{\mathrm{I}c}^d$
3	Stanford, Kalthoff, Shockey	$\sigma_c^d(v), K_{\mathrm{I}c}^d(v), t_{inc}$	$\sigma(t) \leq \sigma_c^d$ Minimum time criterion
4	Incubation time approach	σ_c, K_{IC}, τ	Incubation time criterion

Table 5.1

In Table 5.1 the parameters σ_c and K_{IC} are material constants and $\sigma_c^d(v)$ and $K_{\mathrm{I}c}^d(v)$ are material dependent functions, representing the dependence of critical characteristics on the loading rate v (Morozov and Petrov, 1992b).

Classical approach in dynamic fracture, based on principles of quasistatics and linear fracture mechanics, connects the material dynamic strength properties to two characteristics: $\sigma_c^d(v)$ and $K_{\mathrm{I}c}^d(v)$, which are considered to be material functions. As allready noted, direct transition of static principles into dynamic problems turns out to be uneffective: aside from the great complexity of functions $\sigma_c^d(v)$ and $K_{\mathrm{I}c}^d(v)$ experimental determination an investigator has to face a number of effects, that principally cannot be explained utilizing the approach discussed. For example it occurs that $\sigma_c^d(v)$

and $K^d_{\mathrm{I}c}(v)$ depend not only on the loading rate, but also on other external load parameters. Experimentally obtained values of $\sigma^d_c(v)$ and $K^d_{\mathrm{I}c}(v)$ are normally characterised by significant dispersion, and, consequently, their behavior is poorly predictable.

The minimum-time criterion, elaborated by the Stanford International Research Center (California), includes a new material parameter t_{inc}, the incubation time. In comparison to the classical approach it brings a number of new possibilities, in particular it gives a possibility to explain fracture delay effect and the behavior of threshold loads. An evident deficiency of this approach is its 'inheritance' of all the problems of the classical approach: the analysis in compliance with the minimum-time criterion still requires a priori knowledge of rate dependencies of material strength and fracture toughness.

From the point of view of the structural-temporal approach fracture analysis combines the evident advantages of the static fracture classical method and the efficiency of Stanford's approach. Determining fracture parameters are represented by three material constants: $\sigma_c, K_{\mathrm{I}C}$ and τ. Limiting values for intensity of the dynamics stress fields i.e. dynamic strength and fracture toughness, can be considered as computed characteristics. According to calculations their behavior is stipulated by strong dependence on history and way of loading, which coincides with experimental results. However, to determine exterior loading limiting values we do not need an a priori knowledge of these dependencies. The established link between the fracture structural time τ and the incubation time t_{inc} gives a possibility to use well-known experimental methods (Homma et al., 1983, Kalthoff and Shockey, 1977, Shockey et al., 1986) in order to obtain τ in the case of macrocracks. An important peculiarity of the structural-temporal approach is that it allows evaluation of fracture at the macrocrack tip and fracture of 'intact' materials within the framework of the same approach. Structural time for 'intact' media can be determined on the basis of cleavage fracture experiments (Zlatin et al., 1974, Zlatin et al., 1975, Meshcheryakov et al., 1988, Nikiforovskii and Shemyakin, 1979). Lastly, we emphase that the structural-temporal criterion can be used in order to evaluate critical load characteristics, unique for statics and dynamics, as functions of three material constants ($\sigma_c, K_{\mathrm{I}C}$ and τ).

References

Broberg, K. B., 1960, Some aspects of the mechanism of scabbing. Stress Wave Propagation in Materials (Interscience, New York, London, pp. 229–246).

Dally, J. W., Barker, D. B., 1988, Dynamic measurements of initiation toughness at high loading rate. Exp Mech 28:298–303

Ed. C. M. Preece., 1979, Treatise on Material Science and Technology, Vol. 16. Erosion. Book of papers. (Ed. by C. M. Preece. New York, San Francisco, London, Ltd., 464 pp.).

Golubev, V. K., Novikov, S. A., Sobolev, Y. S. and Yukina, N. A., 1987, On heating influence on cleavage fracture of some polymer composites. Appl. Mech. and Thec. Phys. 28 (6), 140–145. (In Russian.)

Homma, H., Shockey, D. A. and Murayama, Y., 1983, Response of cracks in structural materials to short pulse loads. J. Mech. Phys. Sol. 31 (3), 261–279.

Honeycombe, R. W. K., 1980, Steels, Microstructure and Properties (Edward Arnold, Cambridge, 270 pp.)

Kalthoff, J. F. and Shockey, D. A., 1977, Instability of cracks under impulse loads. J. Appl. Phys. 48, 986–993.

Kalthoff, J. F., 1986, Fracture behavior under high rates of loading. Eng Fract Mech 23:289–298

Knauss, W. G., 1984, Fundamental problems in dynamic fracture. Advances of Fracture Research. Proc. of the 6th Int. Conf. of Fracture, Delhi. (S. R. Vallury, Oxford, New York, Vol. 1, pp. 625–652).

Kobayashi, T., Wade, B. G. and Bradley, W. G., 1973, Fracture dynamics of Homalite-100. In: Deformation and Fracture High Polymers, by H. H. Kaush, J. A. Haseele and R. I. Jaffee. (Plenum Press, New York, pp. 487–500.)

Kolesnikov, Y. V. and Morozov, E. M., 1989, Contact Fracture Mechanics (Nauka, Moscow, 219 pp.). (In Russian.)

Lawn, B. R. and Wilshaw, T. R., 1975, Indentation fracture: principles and application. J. Mater. Sci. 10 (6), 1049–1081.

Meshcheryakov, Y. I., 1988, Statistic model of cleavage surface formation and fracture criterion. Surface Physics, Chemistry, Mechanics. N 3. P. 101–111. (In Russian.)

Meshcheryakov, Y. I., Divakov, A. K. and Kudryashov, V. G., 1988, On dynamic strength under cleavage and disruption. Physics Burning and Explosion 24 (2), 126–134 (In Russian.)

Morozov, N. F. and Petrov, Y. V., 1990, Dynamic fracture viscosity in crack growth initiation problems. News Science Acad. USSR. Solid Mechanics. N 6. P. 108–111. (In Russian.)

Morozov, N. F. and Petrov, Y. V., 1991, On fracture analysis near fast growing crack tip. Vestnik Leningrad State University Series 1, Issue 1, 121–122. (In Russian.)

Morozov, N. F. and Petrov, Y. V., 1992a, On structural time concept in dynamic fracture theory of brittle materials. Reports Russian Science Acad. 324 (5), 964–967. (In Russian.)

Morozov, N. F. and Petrov, Y. V., 1992b, New principles of testing of dynamic strength of materials. Macro- and Micromechanical Aspects of Fracture. Proc. EUROMECH-291, St. Petersburg, 22–27 June, p. 25.

Morozov, N. F. and Petrov, Y. V., 1993, On structure-temporal description of high-speed dependence of dynamic brittle material fracture viscosity. News Russian Science Acad. Solid Mechanics. N 6. P. 100–104. (In Russian.)

Morozov, N. F. and Petrov, Y. V., 1996a, On the macroscopic parameters of brittle fracture. Arch. Mech. Internat. J. 48 (5), 825–833.

Morozov, N. F. and Petrov, Y. V., 1996b, The problems of high rate loading: the new criterion of fracture, the erosion, the asymmetric impact loading. IUTAM Constitutive Relation in High/Very High Strain Rates (Springer-Verlag, Tokyo, pp. 225–232).

Morozov, N. F. and Petrov, Y. V., 1996c, On threshold velocities of solid surface erosive fracture. News Russian Science Acad. Solid Mechanics. N 3. P. 72–75. (In Russian.)

Morozov, N. F., 1954, Mathematical Problems of Crack Theory (Nauka, Moscow, 255 pp.). (In Russian.)

Morozov, N. F., Petrov, Y. V. and Utkin, A. A., 1988a, On fracture near crack tip under impact loading. Physical-Chemical Material Mechanics. N 4. P. 75–77. (In Russian.)

Morozov, N. F., Petrov, Y. V. and Utkin, A. A., 1988b, On limit intensity computation of dynamic pulse loadings. News Russian Science Acad. Solid Mechanics. N 5. P. 180–182. (In Russian.)

Morozov, N. F., Petrov, Y. V. and Utkin, A. A., 1990, On cleavage analysis under approaches of fracture structural mechanics. Reports Science Acad. USSR 313 (2), 276–279 (In Russian.)

Morozov, N. F., Petrov, Y. V. and Utkin, A. A., 1991, On Structure-temporal approach to dynamic brittle formation fracture analysis. Proceedings Leningrad Mining Institute 125 (Rock Fracture), 76–86. (In Russian.)

Morozov, N. F., Urbanovich, L. I., Kramchenkov, E. M. and Petrov, Y. V., 1994, Influence of mechanical and physical properties of both solid particles and target materials on the critical impact velocity. Proc. Internat. Conf. Arzamas-16, Nizhny Novgorod, p. 47.

Nikiforovskii, V. S. and Shemyakin, E. I., 1979, Dynamic Fracture of Solids. (Novosibirsk University Press, Novosibirsc, 271 pp.). (In Russian.)

Nikiforovsky, V. S., 1976, On solid brittle fracture kinetic character. Appl. Mech. and Tech. Phys. 18 (5), 150–157. (In Russian.)

Petrov, Y. V. and Morozov, N. F., 1994, On the modeling of fracture of brittle solids. ASME J. Appl. Mech. 61, 710–712.

Petrov, Y. V. and Utkin, A. A., 1989, On dynamic strength dependence on loading rate. Physio-Chemical Material Mechanics. N 2. P. 38–42. (In Russian.)

Petrov, Y. V., 1991, On 'quantum' nature of brittle media dynamic fracture. Reports Science Acad. USSR 321 (1), 66–68. (In Russian.)

Petrov, Y. V., 1993, Criterion of dynamic fracture of brittle solids. Proc. 8th Internat. Conf. Fracture, Kiev, 8–14 June, p. 97.

Petrov, Y. V., 1996, Quantum analogy in solids fracture mechanics. Physics Solids 38 (11), 3386–3393. (In Russian.)

Polezhaev, Y. V., 1986, Thermogasdynamic Aircraft Treating (Nauka, Moscow, 69 pp.). (In Russian.)

Ravi-Chandar, K. and Knauss, W. G., 1984, An experimental investigation into dynamic fracture: 1. Crack initiation and arrest. Internat. J. Fracture 25, 247–262.

Shockey, D. A., Erlich, D. C., Kalthoff, J. F. and Homma, H., 1986, Short-pulse fracture mechanics. Engrg. Fracture Mech. 23, 311–319.

Shockey, D. A., Seaman, L. and Curran, D. R., 1983, Application of microstatistical fracture mechanics to dynamic fracture problems. In: Material. Behavior under High Stress and Ultrahigh Loading Rates, by J. Mescal and V. Welse (Plenum Publishing Inc., New York, pp. 273–293).

Smith, G. C., 1975, An Experimental Investigation of the Dynamic Fracture of a Brittle Material. Ph. D. Thesis, Pasadena, 93 pp.

Urbanovich, L. I., Kramchenkov, E. M. and Chunosov, Y. N., 1990, Experimental study technics of low-temperature erosion, appearing under hard particles impact action. Friction and Deterioration 11 (5), 889-894. (In Russian.)

Zlatin, N. A., Peschanskaya, N. N. and Pugachev, G. S., 1986, On brittle solid delay fracture. Journal Tech. Phys. 56 (2), 403–406. (In Russian.)

Zlatin, N. A., Pugachev, G. S., Mochalov, S. M. and Bragov, A. M., 1974, Fracture process temporal regularities under intensive loading. Physics Solids 16 (6), 1752–1755. (In Russian.)

Zlatin, N. A., Pugachev, G. S., Mochalov, S. M. and Bragov, A. M., 1975, Temporal dependencies of metal strength at microsecond range durability. Physics Solids 17 (9), 2599–2602. (In Russian.)

Chapter 6

Near tip fields in crack dynamics

Exact solution of the problem for impact loaded elastic plane with a semi-infinite crack utilizing contour integrals. Asymptotic representations of elastic fields in a vicinity of the crack tip. Transient effects of near tip fields in crack dynamics

6.1 Introduction

Transient effects connected to dynamic behavior of impact loaded cracks have been studied and observed analytically, numerically and experimentally for the last 50 years. Remarkable analytical solutions in crack dynamics belong to Yoffe (Yoffe, 1951), Ang (Ang, 1987, 1988), Freund (Freund, 1990), Achenbach (Achenbach, 1970a-b, 1974), Eshelby (Eshelby, 1969), Broberg (Broberg, 1960, 1999) and Kostrov (Kostrov, 1966, Kostrov, Nikitin, 1970, Kostrov, 1975). As a particular case, Kostrov's solution gives an exact representation of stress-strain fields in the vicinity of an impact loaded stationary semi-infinite crack. Similar solution will be extensively used in this chapter as a reference result, which will be compared to stress-strain fields prescribed by leading terms of the Williams asymptotic expansion (Williams, 1957). Though utilizing Kostrov's approach one can achieve solutions for a wide range of problems and loads (it gives a possibility to construct a solution for arbitrary moving cracks subjected to arbitrary loads) the result is normally very complicated and hard or even impossible to analyze. This is one of the reasons why the stress intensity factor is traditionally used to describe stressed conditions surrounding a crack tip.

Another reason for this is that the first approaches in fracture dynamics were connected with attempts to migrate Irwin's approach (Irwin, 1957), successful for majority of materials, geometries and loads in static conditions, directly into dynamical situation.

Williams expansion (Williams, 1957) of crack tip stress field for mode I loaded crack reads:

$$\sigma_{ij}(t,r,\theta) = \frac{K_{\mathrm{I}}(t)}{\sqrt{2\pi r}} \cdot \phi_{ij}(1,\theta) + \sum_{n=2}^{\infty} R_n(t) r^{\frac{n}{2}-1} \cdot \phi_{ij}(n,\theta), \tag{6.1}$$

where σ stands for stress depending on time t, distance to the crack tip r and angle θ, indices i and j assume the values 1 and 2, K_{I} is the mode I stress intensity factor, changing with time. Angular functions $\phi_{ij}(n,\theta)$ are given by:

$$\begin{aligned}
\phi_{11}(n,\theta) &= \left(2 + \frac{n}{2} + (-1)^n\right) \cos\left[\left(\frac{n}{2} - 1\right)\theta\right] - \left(\frac{n}{2} - 1\right) \cos\left[\left(\frac{n}{2} - 3\right)\theta\right], \\
\phi_{22}(n,\theta) &= \left(2 - \frac{n}{2} - (-1)^n\right) \cos\left[\left(\frac{n}{2} - 1\right)\theta\right] - \left(\frac{n}{2} - 1\right) \cos\left[\left(\frac{n}{2} - 3\right)\theta\right], \\
\phi_{12}(n,\theta) &= \phi_{12}(n,\theta) = \\
&= \left(\frac{n}{2} - 1\right) \sin\left[\left(\frac{n}{2} - 3\right)\theta\right] - \left(\frac{n}{2} + (-1)^n\right) \sin\left[\left(\frac{n}{2} - 1\right)\theta\right].
\end{aligned}$$

In static conditions $K_{\mathrm{I}}(t)$ and $R_n(t)$ are constants. While solving quasistatic problems, the first singular term of Williams expansion normally gives a good representation of stress field adjacent to a crack tip. In this case analysis of critical fracture conditions can be done utilizing only stress intensity factor (SIF) — Irwin's critical SIF criterion is applicable. In dynamic case $K_{\mathrm{I}}(t)$ and $R_n(t)$ change with time. Each of these functions will depend not only on time but on loads applied as well. Therefore accuracy of singular K_{I} field will depend not only on a point location (i.e. r and θ) as in statics but even on time.

Numerous researchers observed that K_{I} field is not always correctly reflecting results they receive while numerically solving dynamic problems of linear fracture mechanics (e.g. utilizing finite element method (FEM), boundary element method (BEM) or meshless methods)(Ma, Freund, 1986). They observe that for some class of problems, dynamic field surrounding the vicinity of a crack tip is not K_{I} dominated.

Though Kostrov's solution is known for more than 50 years and is applicable to a big variety of problems, there is no general unanimity among researchers working in fracture dynamics field about conditions and reasons leading to appearance of these transient effects. Some authors correctly associate this with impossibility to apply K_{I} singular field while describing some of extremely dynamic problems.

In this chapter we determine the range of problems for which singular field created in a crack tip region is not K_{I} dominated. For such problems possibility to represent stress-strain fields with a finite number of terms of Williams expansion is also studied. It will also be shown that for some problems Williams expansion is not converging to real stress field. In this case only the exact solution can give the correct description of a dynamic process.

6.2 Problem formulation and analytical solution 1: anti-plane case

Infinite elastic plane with a semi-infinite cut $\{(x_1, x_2)\} : x_2 = \pm 0,\ x_1 \le 0$ is considered. Displacement field is given by $W = W(t, x)$, where t stands for time and x and is coupled with stresses by:

$$\sigma_{x_1 x_3} = \mu \frac{\partial W}{\partial x_1}, \quad \sigma_{x_2 x_3} = \mu \frac{\partial W}{\partial x_2}, \tag{6.2}$$

where μ is the shear modulus and W is satisfying wave equation:

$$\frac{\partial^2 W}{\partial x_1^2} + \frac{\partial^2 W}{\partial x_2^2} = \frac{1}{c_2^2}\frac{\partial^2 W}{\partial t^2}, \tag{6.3}$$

with c_2 being the speed of the transversal wave. For negative times media is stress free:

$$W|_{t<0} = 0. \tag{6.4}$$

On the cut $\{(x_1, x_2)\} : \ \ x_2 = \pm 0, \ \ x_1 \le 0$ we suppose:

$$\sigma_{x_2 x_3}|_{\substack{x_2 = \pm 0 \\ x_1 < 0}} = 0. \tag{6.5}$$

To receive a unique solution of (6.2)–(6.5) absence of energy sources in the vicinity of a crack tip is required:

$$W = O(r^\lambda), \ \ r = \sqrt{x_1^2 + x_2^2} \to 0, \ \ \lambda > 0, \ \ \forall t \ge \delta > 0 \ . \tag{6.6}$$

Solution of (6.2)–(6.6) is well-known (e.g. Filippov, 1956). For the case of $f(t) = -PH(t)$, where $H(t)$ is the Heaviside step function, solution for stresses on crack continuation gives:

$$\sigma_{x_2 x_3} = \begin{cases} 0, & c_2 t < x_1 \\ \frac{2\mathrm{P}}{\pi}\left(\sqrt{\frac{c_2 t}{x_1} - 1} - \arctan\sqrt{\frac{c_2 t}{x_1} - 1}\right), & c_2 t \ge x_1 \end{cases} . \tag{6.7}$$

Expanding (6.7) into series one can get:

$$\sigma_{x_2x_3} = P\left(\frac{2\sqrt{c_2t}}{\pi\sqrt{x_1}} - 1 + \frac{\sqrt{x_1}}{\pi\sqrt{c_2t}}\right) + O\left[\left(\frac{x_1}{c_2t}\right)^{\frac{3}{2}}\right], \quad x_1 \to 0, \quad x_1 \le c_2t \ . \tag{6.8}$$

Corresponding value of the stress intensity factor in this case will be:

$$K_{\mathrm{I}}(t) = \frac{2\sqrt{2}P}{\sqrt{\pi}\sqrt{c_2t}}. \tag{6.9}$$

Suppose that the impact is not applied on the crack faces, but is delivered to the crack region by a wave generated by load applied at infinity:

$$\sigma_{x_2x_3}\left(t, x_1, x_2\right)\big|_{t<0} = f\left(t + \frac{x_2}{c_2}\right). \tag{6.10}$$

In this case (6.5) is substituted by:

$$\sigma_{x_2x_3}\big|_{\substack{x_2=\pm 0\\ x_1<0}} = 0. \tag{6.11}$$

If $f(t) = P \cdot H(t)$, then the solution of (6.2), (6.3), (6.6), (6.11), (6.12) gives:

$$\sigma_{x_2x_3} = \begin{cases} P, & c_2t < x_1 \\ \frac{2P}{\pi}\left(\sqrt{\frac{c_2t}{x_1} - 1} - \arctan\sqrt{\frac{c_2t}{x_1} - 1}\right) + P, & c_2t \ge x_1 \end{cases}, \tag{6.12}$$

for stresses on continuation of the crack. Stress intensity factor time dependence will be the same as (6.9) and series expansion of $\sigma_{x_2x_3}$ will differ from (6.8) by eliminated constant pressure term — P:

$$\sigma_{x_2x_3} = P\left(\frac{2\sqrt{c_2t}}{\pi\sqrt{x_1}} + \frac{\sqrt{x_1}}{\pi\sqrt{c_2t}}\right) + O\left[\left(\frac{x_1}{c_2t}\right)^{\frac{3}{2}}\right], \quad x_1 \to 0, \quad x_1 \le c_2t \ . \tag{6.13}$$

Using (6.7) and (6.12) it is easy to construct a solution for arbitrary $f(t)$. Corresponding result is achieved using time convolution of (6.7) or (6.12) with $f(t)$. Arbitrary load can be presented as a convolution with the Heaviside step function:

$$f(t) = \int_{-\infty}^{\infty} H(s) f'(t-s) ds. \tag{6.14}$$

Then $\sigma^f_{x_2x_3}(t, x_1, x_2) = \int_{-\infty}^{\infty} \sigma_{x_2x_3}(s, x_1, x_2) f'(t-s) ds$, where $\sigma_{x_2x_3}(s, x_1, x_2)$ is taken from (6.7) for the case of load applied on the crack faces or (6.12) for the case of load delivered by a wave, will give a solution for stresses.

Later the solution for load that is linearly growing with time will be used. In this case $f(t) = VtH(t) = V \int\limits_{-\infty}^{\infty} H(s)H(t-s)ds$. For the case of load applied at crack faces solution for stresses on crack continuation reads:

$$\sigma_{x_2x_3} = \\ = \begin{cases} 0, & c_2t < x_1 \\ \frac{2V}{\pi c_2}\left(\frac{2}{3}\frac{(c_2t-x_1)^{3/2}}{\sqrt{x_1}} + \sqrt{x_1(c_2t-x_1)} - c_2t \arctan\sqrt{\frac{c_2t}{x_1}-1}\right), & c_2t \geq x_1 \end{cases}. \tag{6.15}$$

Series expansion of (6.15) gives:

$$\sigma_{x_2x_3} = Vt\left(\frac{4\sqrt{c_2t}}{3\pi\sqrt{x_1}} - 1 + \frac{2\sqrt{x_1}}{\pi\sqrt{c_2t}}\right) + O\left[\left(\frac{x_1}{c_2t}\right)^{\frac{3}{2}}\right], \quad x_1 \to 0, \quad x_1 \leq c_2t\ . \tag{6.16}$$

Corresponding stress intensity factor will be:

$$K_{\mathrm{I}}(t) = \frac{4\sqrt{2}V}{3\sqrt{\pi}} t\sqrt{c_2t}. \tag{6.17}$$

6.3 Problem formulation and analytical solution 2: plane case

Plane dynamic problem of elasticity is considered. Homogeneous isotropic infinite plane has a semi-infinite cut $\{(x_1, x_2)\} : \ x_2 = \pm 0, \ \ x_1 \leq 0$. Stress field is given by potentials φ and ψ, satisfying the following conditions:

$$\begin{aligned} \frac{\partial^2\varphi}{\partial x_1^2} + \frac{\partial^2\varphi}{\partial x_2^2} &= \frac{1}{c_1^2}\frac{\partial^2\varphi}{\partial t^2}, \\ \frac{\partial^2\psi}{\partial x_1^2} + \frac{\partial^2\psi}{\partial x_2^2} &= \frac{1}{c_2^2}\frac{\partial^2\psi}{\partial t^2}. \end{aligned} \tag{6.18}$$

Here φ and ψ are longitudinal and transversal wave potentials, c_1 is the speed of longitudinal wave. Components of displacement u and v are coupled with φ and ψ by:

$$\begin{aligned} u &= \frac{\partial\varphi}{\partial x_1} + \frac{\partial\psi}{\partial x_2}, \\ v &= \frac{\partial\varphi}{\partial x_2} - \frac{\partial\psi}{\partial x_1}. \end{aligned} \tag{6.19}$$

Crack faces are free from tractions:

$$\begin{aligned} &\sigma_{x_2x_2}|_{\substack{x_2=\pm 0\\ x_1\leq 0}} = 0, \\ &\sigma_{x_1x_2}|_{\substack{x_2=\pm 0\\ x_1\leq 0}} = 0. \end{aligned} \tag{6.20}$$

Initial conditions are given by a wave approaching to the crack region from infinity:

$$\begin{aligned} &\psi\big|_{t<0} = 0, \\ &\varphi\big|_{t<0} = H\left(t + \frac{x_2}{c_1}\right). \end{aligned} \tag{6.21}$$

It is requested that displacements are bounded at area adjacent to the crack tip, which guarantees the uniqueness of the solution.

Stresses can be evaluated via potentials:

$$\begin{aligned} \sigma_{x_1x_1} &= \rho c_1^2\left[\frac{\partial^2\varphi}{\partial x_1^2} + \left(1-2\gamma^2\right)\frac{\partial^2\varphi}{\partial x_2^2} + 2\gamma^2\frac{\partial^2\psi}{\partial x_1\partial x_2}\right], \\ \sigma_{x_2x_2} &= \rho c_1^2\left[\frac{\partial^2\varphi}{\partial x_2^2} + \left(1-2\gamma^2\right)\frac{\partial^2\varphi}{\partial x_1^2} - 2\gamma^2\frac{\partial^2\psi}{\partial x_1\partial x_2}\right], \\ \sigma_{x_1x_2} &= \rho\gamma^2 c_1^2\left[2\frac{\partial^2\varphi}{\partial x_1\partial x_2} - \frac{\partial^2\psi}{\partial x_1^2} + \frac{\partial^2\psi}{\partial x_2^2}\right], \end{aligned} \tag{6.22}$$

where ρ is the mass density and $\gamma = c_1/c_2$.

The solution for (6.12)–(6.22) (Petrov, Utkin, 2001), received for wave potentials is:

$$\begin{aligned} \Psi'(\Omega) &= \frac{i\sqrt{2}\gamma_R G(\Omega)\sqrt{1+\Omega}}{\pi\gamma^3\sqrt{1-\gamma^2}\left(1+\gamma_R\Omega\right)}, \\ \Phi'(\Omega) &= \frac{i\gamma_R G(\Omega)\left(1-2\gamma^2\Omega^2\right)}{\pi\sqrt{2}\gamma\sqrt{1-\gamma^2}\Omega\left(1+\gamma_R\Omega\right)\sqrt{1-\Omega}}, \end{aligned} \tag{6.23}$$

where $\psi = Re(\Psi)$ and $\varphi = Re(\Phi)$, with Ψ and Φ being analytical everywhere. Ω is a coordinate on a complex plane. $\gamma_R = c_R/c_1$, where c_R is the

Rayleigh wave speed. $G(\Omega) = \exp\left(\frac{1}{\pi}\int\limits_{-1/\gamma}^{-1} \frac{\arg(R(s))}{\Omega - s} ds\right)$, with $R(z)$ being the Rayleigh function: $R(z) = \left(1 - 2\gamma^2 z^2\right) + 4\gamma^3 z^2 \sqrt{1 - z^2}\sqrt{1 - \gamma^2 z^2}$ and $\arg(z)$ being the argument function $\arg(z) = -i \log \frac{z}{|z|}$.

Substituting (6.23) into (6.19) displacements can be found.

Presented formulas give the solution for load created by an elementary longitudinal wave. Solution for load created by an elementary transversal wave can be achieved analogously. Solutions for more complex loads can be achieved as a time convolution of presented solution or/and solution for transversal wave.

Using the presented solution and (6.22) stresses on continuation of a semi-infinite crack for the problem when a load is delivered to the crack region by a falling wave can be found:

$$\begin{aligned}\sigma_{x_2 x_2} = \rho \frac{c_1^2}{r^2} Re \Bigg[\left(1 - 2\gamma^2 \left(\frac{c_1 t}{r}\right)^2\right) \Phi''\big|_{x_2=0} - 4\gamma^2 \frac{c_1 t}{r} \Phi'\big|_{x_2=0} + \\ + 2i\gamma \left(\frac{c_1 t}{r} \sqrt{\gamma^2 \left(\frac{c_1 t}{r}\right)^2 - 1}\, \Psi''\big|_{x_2=0} + \frac{2\gamma^2 \left(\frac{c_1 t}{r}\right)^2 - 1}{\sqrt{\gamma^2 \left(\frac{c_1 t}{r}\right)^2 - 1}} \Psi'\big|_{x_2=0} \right) \Bigg].\end{aligned} \tag{6.24}$$

Load corresponding to constant pressure suddenly applied on the crack faces can be presented as a wave:

$$\begin{aligned}\psi\big|_{t<0} &= 0, \\ \varphi\big|_{t<0} &= \frac{P}{2\rho}\left(t + \frac{x_2}{c_1}\right)^2 H\left(t + \frac{x_2}{c_1}\right).\end{aligned} \tag{6.25}$$

Convolution of (6.24) with loads given by (6.21) or (6.25) will give exact solutions for plane problem with load delivered to the crack region by a falling wave or a load applied directly on the crack faces.

Evaluating asymptotic expansion for stresses on continuation of a cut in this problem one will get:

$$\begin{aligned}\sigma_{x_2 x_2} = P \frac{2\sqrt{2}\sqrt{c_1}\gamma\sqrt{1 - \gamma^2}}{\pi} \left[\frac{\sqrt{t}}{\sqrt{x_1}} - \frac{(\gamma_R + 2\gamma_R R_1 - 2)}{2 c_1 \gamma_R} \frac{\sqrt{x_1}}{\sqrt{t}} \right] - \\ - P + O\left[\left(\frac{x_1}{c_1 t}\right)^{3/2} \right],\end{aligned} \tag{6.26}$$

for the case of impact applied on the crack faces and

$$\sigma_{x_2x_2} = P\frac{2\sqrt{2}\sqrt{c_1}\gamma\sqrt{1-\gamma^2}}{\pi}\left[\frac{\sqrt{t}}{\sqrt{x_1}} - \frac{(\gamma_R + 2\gamma_R R_1 - 2)}{2c_1\gamma_R}\frac{\sqrt{x_1}}{\sqrt{t}}\right] + \\ + O\left[\left(\frac{x_1}{c_1 t}\right)^{3/2}\right], \quad (6.27)$$

when the load is delivered to the crack by a wave approaching from infinity.

6.4 Accuracy of asymptotic representation of stress state surrounding dynamically loaded crack tip

At this section accuracy of presented asymptotic solutions will be analyzed. To compare stresses evaluated accounting several first terms of Williams expansion to exact analytical solution the following expression is introduced:

$$Q = \left[\frac{\sigma - S_i}{\sigma}\right] \cdot 100\% \quad (6.28)$$

Here $\sigma = \sigma_{x_2x_3}$ for anti-plane case and $\sigma = \sigma_{x_2x_2}$ for plane problem. S_i is the sum of the first i terms of Williams expansion (6.1). Thus, (6.28) gives a relative error of asymptotic approximation.

To start with, behavior of Q at anti-plane problem with load suddenly applied on the crack faces is discussed. To evaluate Q in this situation one should use stress σ given by (6.7) and S_i given by (6.8) taking first 1, 2 or 3 terms. Results are presented in Fig. 6.1a and 6.1b.

The horizontal axis in figures (figures 6.1a, 6.1b and all the following figures) stands for the dimensionless value ct/x_1. This value shows the distance from the studied point x to the position on the crack continuation where the wave front is currently situated. After the front had passed point x, ct/x_1 >1 is fulfilled. According to computational results given in figure 6.1a, if the front of the wave is less than 100*x_1 away from the point with coordinate x_1 on the crack continuation, representation using only singular term of the Williams expansion — stress intensity factor (upper curve in figure 6.1a) is appreciably incorrect (by more than 20%). For ct/x_1 >200 the misfit is considerably reduced (less than 10%). When the second term of Williams expansion is taken into consideration (lower curve in figure 6.1a or upper curve in figure 6.1b), the situation is improved significantly. In this case already for ct/x_1 >10 error is less than 10%. Taking the third term of the expansion into account (lower curve in figure 6.1b) improves

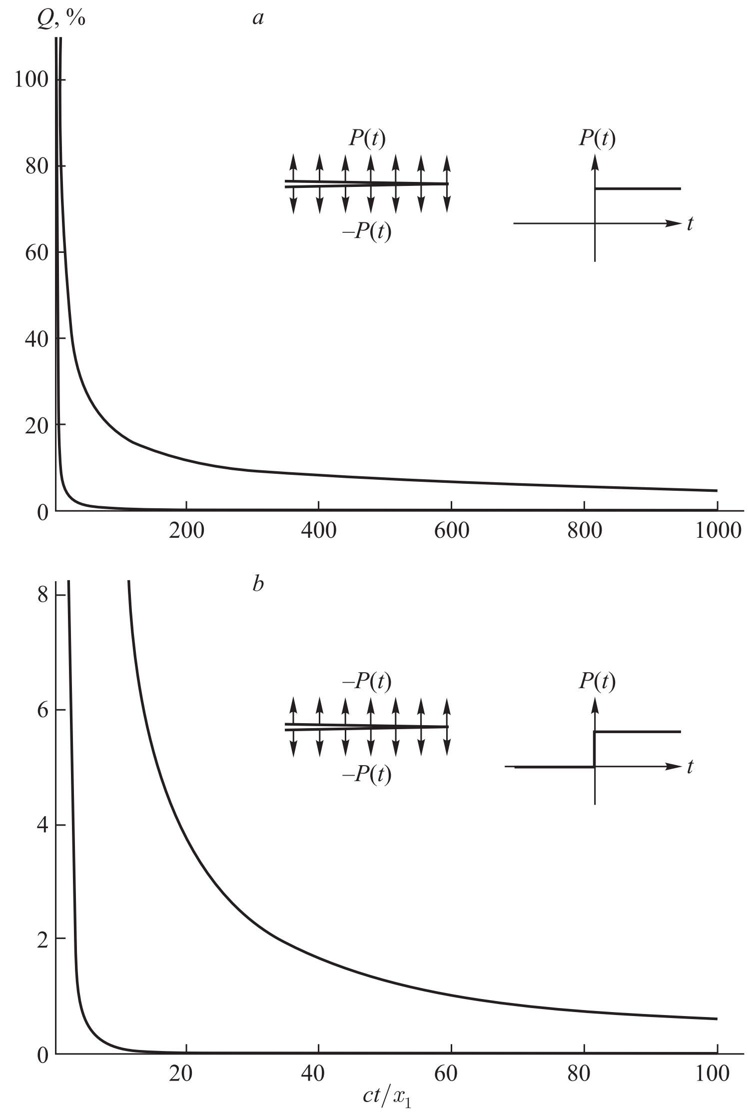

Fig. 6.1. Relative error of asymptotic series solution of anti-plane problem with constant load suddenly applied on the crack faces:
a: upper curve — first term (SIF), lower curve — two first terms.
b: upper curve — two terms, lower curve — three terms.

the result even more. Already for $ct/x_1 > 2$ the error is below 10%. For $ct/x_1 > 5$ the misfit between the result received using the first three terms of Williams expansion and the exact solution is less than 1%.

To continue with, a problem for crack faces loaded by uniformly distributed pressure growing in time with a constant rate V is studied. To receive the desired error estimation in this case one should substitute corresponding exact solution (6.15) and approximation (6.16) into (6.28). The respective curves are presented in figures 6.2a and 6.2b. As we can see from these figures, behavior of the misfit between the exact solution and the first terms of the asymptotic expansion remains qualitatively unchanged. The accuracy is slightly reduced.

The next problem to be analyzed is the problem with stress free crack faces and a load given by a wave with constant amplitude P, moving from infinity with front parallel to the crack. The exact expression for stresses in this problem is given by (6.12) and an approximate asymptotic solution differs from (6.8) by absence of $-P$ term. Substituting these solutions into (6.28) and performing computations one can receive data presented in figure 6.3. As one can see in this problem the accuracy of approximation using only stress intensity factor is essentially better. It is even more exact than representation using two first terms of Williams expansion in the previous problems (figures 6.1a and 6.2a). This is connected to the fact that in this case the term following stress intensity factor $K(t)$ in (6.1) is missing ($R_0(t)=0$).

The analogous analysis is performed for solution of the problem in the plane case. The first of the examined load options is a uniformly distributed pressure suddenly applied on the crack faces ($\sigma_{x_2x_2} = -PH(t), \quad \sigma_{x_1x_2} = 0$). Solution for $\sigma_{x_2x_2}$ on the crack continuation is given by convolution of stress given by (6.24) with load (6.25). The corresponding asymptotic solution is given by (6.27). In this case both the exact and the asymptotic solution are depending on the ratio between longitudinal and transversal wave speeds $\gamma = c_2/c_1$. The misfit between the solution achieved using only singular term of the asymptotic expansion (K) and exact solution is presented in figure 4 for different values of γ. Accuracy of the approximation in a limiting case of Poisson's ratio ν equal to 0 ($\gamma = \frac{1}{\sqrt{2}}$) is worse as comparing to the corresponding anti-plane problem results. The decrease of γ (increase of ν) results in reduction of accuracy of approximation using the stress intensity factor. This is explained by the fact that the multiplier at square root singular term in anti-plane problem ($1/\pi \approx 0.64$) is bigger than the multiplier at the plane case ($2\sqrt{2}\gamma\sqrt{1-\gamma^2}\pi$,

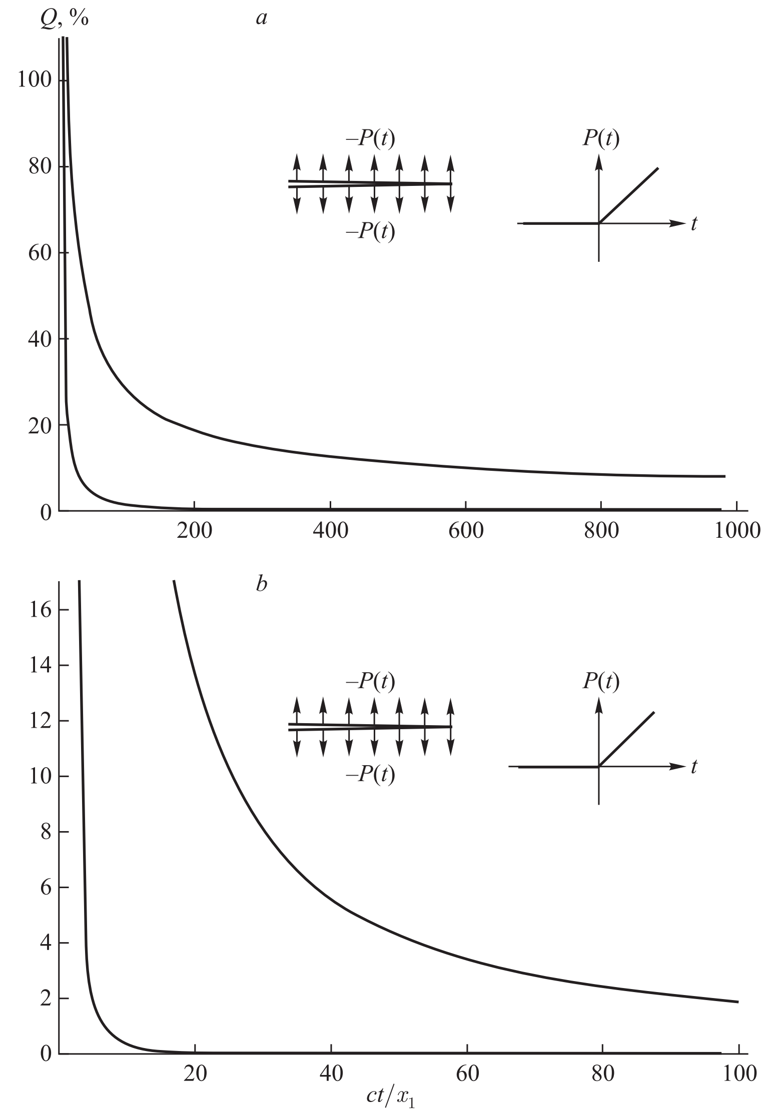

Fig. 6.2. Relative error of asymptotic series solution of anti-plane problem with load growing at a constant rate suddenly applied on the crack faces:
a: upper curve — first term (SIF), lower curve — two first terms
b: upper curve — two terms, lower curve — three terms.

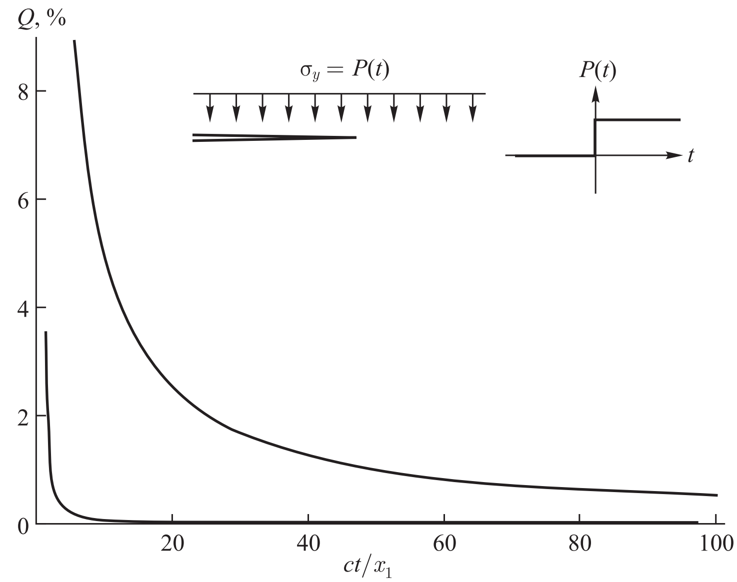

Fig. 6.3. Relative error of asymptotic series solution of anti-plane problem with load given by a wave with constant amplitude, moving from infinity with a front parallel to the crack. Upper curve — first term (SIF), lower curve — two first terms.

with $\gamma{=}\frac{1}{\sqrt{2}}-0.45$). Figures 6.5a and 6.5b give a comparison of accuracy of the asymptotic approximation using one (stress intensity factor), two and three first terms (while $\gamma{=}\frac{1}{\sqrt{3}}$ and ν =0.25). Character of the curves is close to the character those presented in figure 6.1a. As already discussed above, accuracy of asymptotic approximations is somewhat lower in the plane case.

For example, at a point on the crack continuation, 10 mm distant from the tip of the crack and a material with longitudinal wave speed c_1=5000 m/s, error achieved using the stress intensity factor approximation will exceed 20% for times t <400 microseconds. Only for times exceeding 1200 microseconds the error is below 10%.

Figure 6.6 presents the misfit between approximation using stress intensity factor or two first terms of asymptotic expansion (6.26) and the exact solution of the plane problem for a crack loaded by a wave, approaching from infinity with a front parallel to the crack (convolution of (6.24) with (6.21)). Stress distribution inside the wave is given by the Heaviside step function. The situation is similar to the anti-plane problem (figure 6.3).

As demonstrated above in the case of load applied on the crack faces

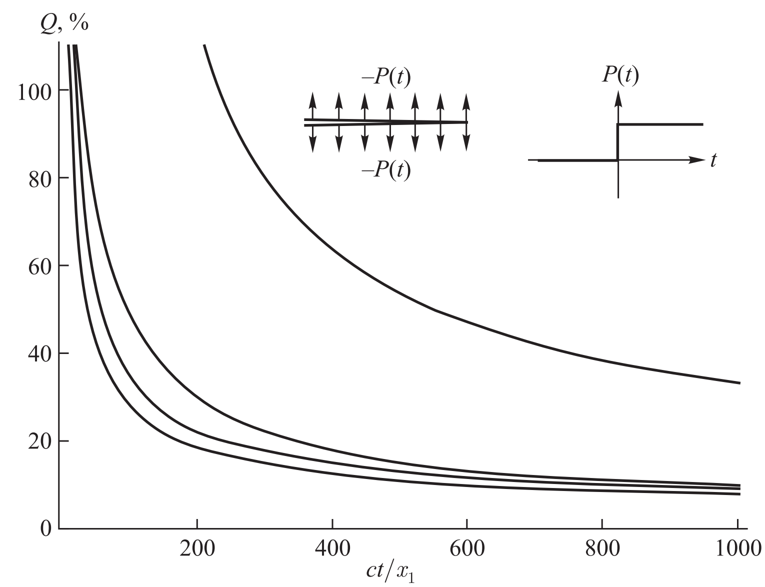

Fig. 6.4. Relative error of SIF solution of plane problem with constant load suddenly applied on the crack faces. Upper curve — γ=0.14 (ν =0.49), middle curve — γ=0.48 (ν =0.35), lower curve — $\gamma=\frac{1}{\sqrt{2}}$ (ν =0).

(figures 6.1a,b and 6.5a,b), the accuracy of approximation using the first term of the Williams expansion is less as comparing to the analogous problem where the load is created by a passing wave (figures 6.3 and 6.6). This is due to the absence of regular terms (terms non-depending on coordinate) in the asymptotic expansion of solutions in the case of load created by a falling wave.

It can be demonstrated that in the case of the load applied on the crack faces the same effect can be achieved as a result of a special choice of a time shape for the load function. In order to do this rectangularly shaped load pulse with amplitude P and duration T *(f(t)=P [H(t)-H(t-T)])* is applied on the crack faces. Anti-plane conditions are supposed. In this situation for times $t > T$ term independent on coordinate (regular term) is vanishing. Figure 6.7 plots the misfit between approximation given by the stress intensity factor and the exact solution for the problem. One can see that for $t > T$ the accuracy of solution given by stress intensity factor is noticeably increased.

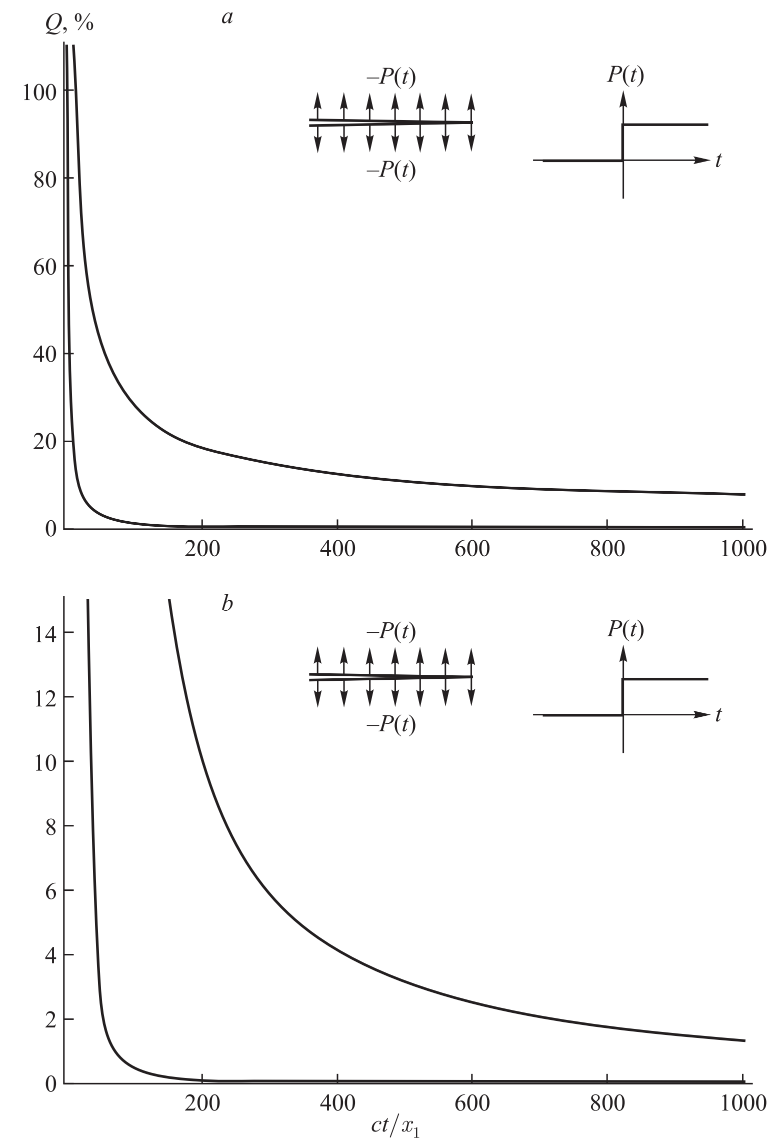

Fig. 6.5. Relative error of asymptotic series solution of plane problem with constant load suddenly applied on the crack faces:
a: upper curve — first term (SIF), lower curve — two first terms.
b: upper curve — two terms, lower curve — three terms.

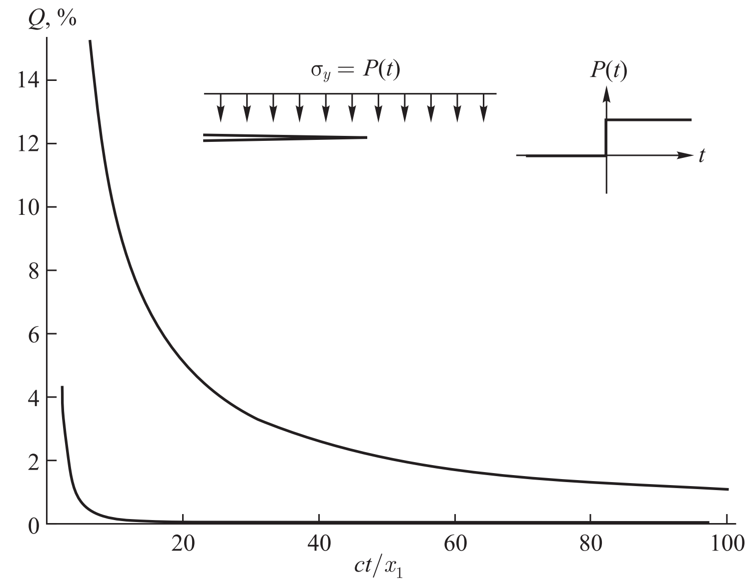

Fig. 6.6. Relative error of asymptotic series solution of plane problem with load given by a wave with constant amplitude, moving from infinity with a front parallel to the crack. Upper curve — first term (SIF), lower curve — two first terms.

6.5 Discussion

As clearly demonstrated by previous examples, behavior of asymptotic representations of stress-strain fields in a vicinity of a crack tip in dynamic problems is characterized by substantial non-uniformity. Obviously the accuracy of representation using just stress intensity factor in dynamic problems cannot be sufficiently increased by introduction of special "dynamic correction", even time dependent. To achieve a correct solution in dynamic conditions one should account terms of the Williams asymptotic expansion following the SIF term.

Interesting observations can be made examining dependency of accuracy SIF stress field approximation can perform in dynamic problems on Poisson's ratio of the studied material (figure 6.4). One can note that for incompressible materials (υ=1/2) infinite number of terms in Williams asymptotic expansion should be taken in order to obtain reasonable coincidence between approximation and reality. It is demonstrated (figure 6.4) that the lager is the Poisson's ratio of material, the worse is the approximation using the SIF. For material with υ=0.48 the misfit between real stress

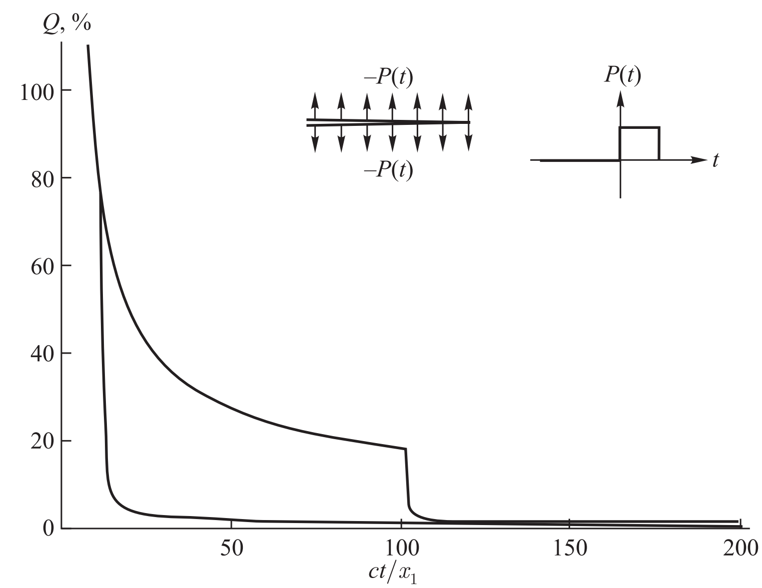

Fig. 6.7. Relative error of SIF solution of anti-plane problem with constant load of duration T suddenly applied on the crack faces. Upper curve — T=100x_1/c, lower curve — T=10x_1/c.

and stress prescribed by SIF square root singularity is exceeding 20% even for times c_1t/x_1 =1000.

Presented results demonstrate the framework for problems where the SIF can be used to describe stress-strain fields surrounding the tip of a dynamically loaded crack. It is shown how a load (both the way a load is applied and it's time shape), material properties (Poisson's ratio) and experimental conditions (plane or anti-plane problem) can affect accuracy of asymptotic approximations for stress-strain field in vicinity of a crack tip. It is demonstrated that in many cases, when the SIF square root singular field cannot provide correct approximation of dynamic stress filed surrounding the crack tip, accounting one or two additional terms following the SIF in power expansion can greatly improve the situation. At the same time there are situations when infinite number of terms is needed in order to approximate solution in an accurate way.

Although presented solutions refer to stationary dynamically loaded cracks, we also want to discuss applicability of SIF approximation of a singular stress field surrounding the crack tip in problems with propagating cracks. As discussed by Morozov and Petrov (Morozov, Petrov, 2000), the closer the crack tip speed is approaching the Rayleigh wave speed C_R, the worse is the approximation given by the SIF for stress field in vicinity of the tip of the crack. Therefore, for moving cracks speed is another important factor that is affecting the SIF approximation accuracy. Having this in mind one may wish to revise Freund's solution for the limiting speed of crack propagation (ex. Freund, 1990) for mode I cracks and solutions for permitted speeds for shear cracks (Freund, 1979, 1990, Broberg, 1989, 1994, 1995). Though we maybe do not question the fact that C_R is the limiting speed for mode I cracks in problems without local scale and microstructure since there are other physical and empirical reasons for why mode I cracks cannot propagate with greater speeds, but obviously a revision of solutions for shear crack propagation can give a better understanding of recent experiments on ultrasonic dynamic cracking (Rosakis et al., 1999, etc.).

References

Achenbach, J. D., 1970a, Extension of a crack by a shear wave, Zeitschrigt fur angewandte Mathematic und Physik, 21:887–900.

Achenbach, J. D., 1970b, Crack propagation generated by a horizontally polarized shear wave. Journal of the Mechanics and Physics of Solids 18:245–259.

Achenbach, J. D., 1974, Dynamic effects in brittle fracture. In S. Nemat-Nasser (ed) Mechanics Today. Pergamon, Elmsford, New York, pp. 1–57

Ang, W. T., 1987, Transient response of a crack in an anisotropic strip. Acta Mech. 70:97–109

Ang, W. T., 1988, A crack in an anisotropic layered material under the action of impact loading. J. Appl. Mech. 55: 120–125

Broberg, K. B., 1960, The propagation of a brittle crack. Archiv fur Fysik, 18:159–192

Broberg, K. B., 1989, The near-tip field at high crack velocities. International Journal of Fracture 39:1–13

Broberg, K. B., 1994, Intersonic bilateral slip. Geophys. J. Int. 119:706–714

Broberg, K. B., 1995, Intersonic mode II crack expansion. Arch. Mech. 47:859–871

Broberg, K. B., 1999, Cracks and Fracture. Academic Press, London

Eshelby, J. D., 1969, The elastic 3eld of a crack extending nonuniformly under general anti-plane loading. J. Mech. Phys. Solids 17:177–199

Filippov, A. V., 1965, Applied Mathematics and Mechanics, 20:688–703 (in Russian)

Freund, L. B., 1979, The mechanics of dynamic shear crack propagation. J. Geophys. Res. 84:2199–2209

Freund, L. B., 1990, Dynamic Fracture Mechanics. Cambridge University Press, Cambridge

Irwin, G. R., 1957, Analysis of stresses and strains near the end of a crack traversing a plate. J. Appl. Mech. 24(3):361–364

Kostrov, B. V., 1966, Unsteady propagation of longitudinal shear cracks. Appl. Math. Mech. 30:1241–1248

Kostrov, B. V., Nikitin, L. V., 1970, Some general problems of mechanics of brittle fracture. Archiwum Mchaniki Stosowanej, 22:749–775

Kostrov, B. V., 1975, On the crack propagation with variable velocity. Int. J. Fracture. 11:47–56

Ma C. C., Freund L. B., 1986, The extent of the stress intensity factor during crack growth under dynamic loading conditions. ASME J. Appl. Mech. 303–310.

Morozov, N., Petrov Y., 2000, Dynamics of fracture. Springer-Verlag, Berlin

Petrov, Y. V., Utkin, A. A., 2001, Asymptotic representation of stresses surrounding the crack tip in dynamic problems of elasticity, IPME RAS, St.-Petersburg

Rosakis, A. J., Samudrala, O., Coker, D., 1999, Cracks Faster than the Shear Wave Speed. Science, 284(5418):1337–1340

Williams, M. L., 1957, On the Stress Distribution at the Base of a Stationary Crack. Journal of Applied Mechanics, 24:109–114

Yoffe, E. H., 1951, The moving Griffith crack. Philosophical Magazine. 42:739–750, 1951

Chapter 7

Numerical simulations of dynamic fracture evolution

Application of incubation time approach in numerical simulations of dynamic crack propagation. Problems with moving fracture zone boundaries. Impact fracture of elastic media. Crater formation

7.1 Introduction

Along with prediction of initiation of dynamically loaded cracks incubation time criterion is able to predict dynamic crack propagation, arrest, reinitiation and even fracture of initially intact media. The criterion (7.3), albeit able to predict dynamic crack initiation, cannot be used to predict crack or fracture development in dynamic conditions. The main reason for this is that time dependency of a stress intensity factor in the tip of a crack moving at high speeds does not directly reflect the history of stress-strain fields in vicinity of a current crack tip location since at preceding times crack tip was located at distant (and usually significantly distant) points of a body. This was also discussed by Ma and Freund, 1986, and Ravi-Chandar and Knauss, 1987.

In this chapter examples on how the incubation time approach, being incorporated into finite element computational codes, can be used to predict fracture initiation, propagation and arrest in real experimental conditions are given.

7.2 Application of incubation time approach in numerical simulations of dynamic fracture

As shown in chapters 5 and 8 the incubation time criterion (originally formulated in Petrov, Morozov, 1994, Morozov, Petrov, 2000), is able to describe crack initiation in dynamic conditions. General form of the criterion for rupture at a point x at time t reads:

$$\frac{1}{\tau}\int\limits_{t-\tau}^{t}\frac{1}{d}\int\limits_{x-d}^{x}\sigma(x^*,t^*)dx^*dt^*\leq\sigma_c,\tag{7.1}$$

where τ is the microstructural time of a fracture process (or fracture incubation time) — a parameter characterizing the response of the material on applied dynamical loads (i.e. τ is constant for a given material and does not depend on problem geometry, the way a load is applied, the shape of a load pulse and its amplitude). d is the characteristic size of a fracture process zone and is constant for the given material and chosen scale. σ is stress at a point, changing with time and σ_c is its critical value (ultimate stress or critical tensile stress found in quasistatic conditions). x^* and t^* are local coordinate and time.

Assuming

$$d=\frac{2}{\pi}\frac{K_{\mathrm{I}C}^2}{\sigma_c^2},\tag{7.2}$$

where $K_{\mathrm{I}C}$ is a critical stress intensity factor for mode I loading (mode I fracture toughness), measured in quasistatic experimental conditions, it can be shown that within the framework of linear fracture mechanics, for case of fracture initiation in the tip of an existing crack, loaded by mode I, (7.1) is equivalent to:

$$\frac{1}{\tau}\int\limits_{t-\tau}^{t}K_{\mathrm{I}}(t^*)dt^*\leq K_{\mathrm{I}C}.\tag{7.3}$$

Condition (7.2) arises from the requirement that (7.1) is equivalent to Irwin's criterion ($K_{\mathrm{I}}\geq K_{\mathrm{I}C}$), in case of $t\to\infty$.

As it was shown in chapter 8 as well as in many previous publications, criterion (7.3) can be successfully used to predict fracture initiation for brittle solids (e.g. Petrov et al., 2003, Petrov and Sitnikova, 2005). For slow loading rates and, hence, times to fracture that are much bigger than τ, condition (7.3) for crack initiation gives the same predictions as Irwin's criterion of a critical stress intensity factor. For high loading rates and times to fracture comparable to τ all the variety of effects experimentally observed in dynamic experiments (ex. Ravi-Chandar and Knauss, 1984a, Kalthoff, 1986, Dally and Barker, 1988) can be obtained using (7.3) both qualitatively and quantitatively (Petrov, 2004).

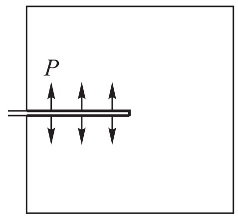

Fig. 7.1. Experimental scheme used by Ravi-Chandar and Knauss (1984a).

Application of condition (7.3) to the description of real experiments or usage of (7.3) as the critical fracture condition in finite element numerical analysis gives a possibility of better understanding of the nature of fracture dynamicse (e.g. Bratov et al., 2004) and even predicts new effects typical of dynamic processes (e.g. Bratov and Petrov, 2006).

Though criterion using stress intensity factor (7.3) is easier to use when simply describing crack initiation, general form of the incubation time criterion (7.1) was used even to assess early stages of fracture development.

7.3 Classical experiments of Ravi-Chandar and Knauss

Incubation time criterion was used to predict dynamic crack development in the classical fracture dynamics experiments reported by Ravi-Chandar and Knauss in 1984 (Ravi-Chandar, Knauss, 1984a). In these experiments a rectangular sample with a cut simulating a crack is loaded by application of an intense load pulse to the crack faces. Fig. 7.1 presents the experimental scheme and Fig. 7.2 gives an approximation of the load applied on the crack faces.

Behavior of the loaded sample is described by the Lame equations:

$$\rho u_{i,tt} = (\lambda + \mu) u_{j,ji} + \mu u_{i,jj}, \tag{7.4}$$

where "," refers to the partial derivative with respect to time and spatial coordinates. ρ is the mass density, and the indices i and j assume the values 1 and 2. Displacements are given by u_ι in the directions x_ι respectively. t stands for time, λ and μ are Lame constants. Stresses are coupled with strains by the Hooke's law:

$$\sigma_{ij} = \lambda \delta_{ij} u_{k,k} + \mu(u_{i,j} + u_{j,i}). \tag{7.5}$$

where σ_{ij} represents components of the stress tensor, δ_{ij} is the Kronecker

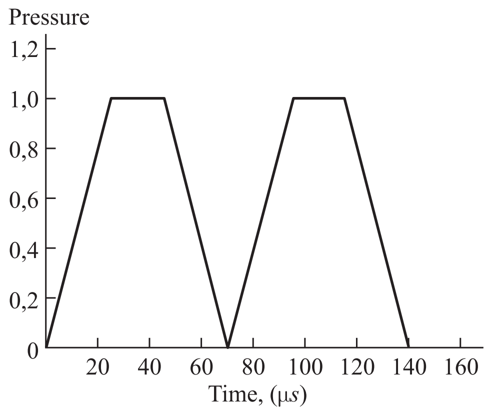

Fig. 7.2. Temporal shape of pressure pulse released at experiments by Ravi-Chandar and Knauss (1984a).

delta assuming value of 1 for $i = j$and 0 otherwise. At $t = 0$ the sample is stress free and velocity field is zero everywhere in the body:

$$\sigma_{ij}|_{t=0} = u_{,t}|_{t=0} = 0. \tag{7.6}$$

Crack faces are free from tractions:

$$\sigma_{21}|_{x_1<0,x_2=0} = 0. \tag{7.7}$$

The load applied to the crack faces is given by:

$$\sigma_{22}|_{x_1<0,x_2=0} = Af(t), \tag{7.8}$$

where $f(t)$ is given graphically in Fig. 7.2 and A is the amplitude of the load. The load was created by electromagnetic experimental equipment. The authors create an intense electric discharge that is passed through a flat conductor inserted into the crack. The electric discharge results in a repulsing force between the conductors. This creates a pressure pulse, constant over the cut surface and with a shape and amplitude controlled by the electric flow in the conductor, which can be easily measured.

Fig. 7.3a and Fig. 7.3b present some of the results achieved by Ravi-Chandar and Knauss. Figure 7.3a gives the stress intensity factor history for four of the experiments conducted. Figure 7.3b gives the crack propagation histories for the same experiments. Even though all of the experiments presented were conducted under nominally identical conditions, the results shown do differ. This might be explained by a slightly different charge accumulated in condensers prior to discharge through a conductor, resulting

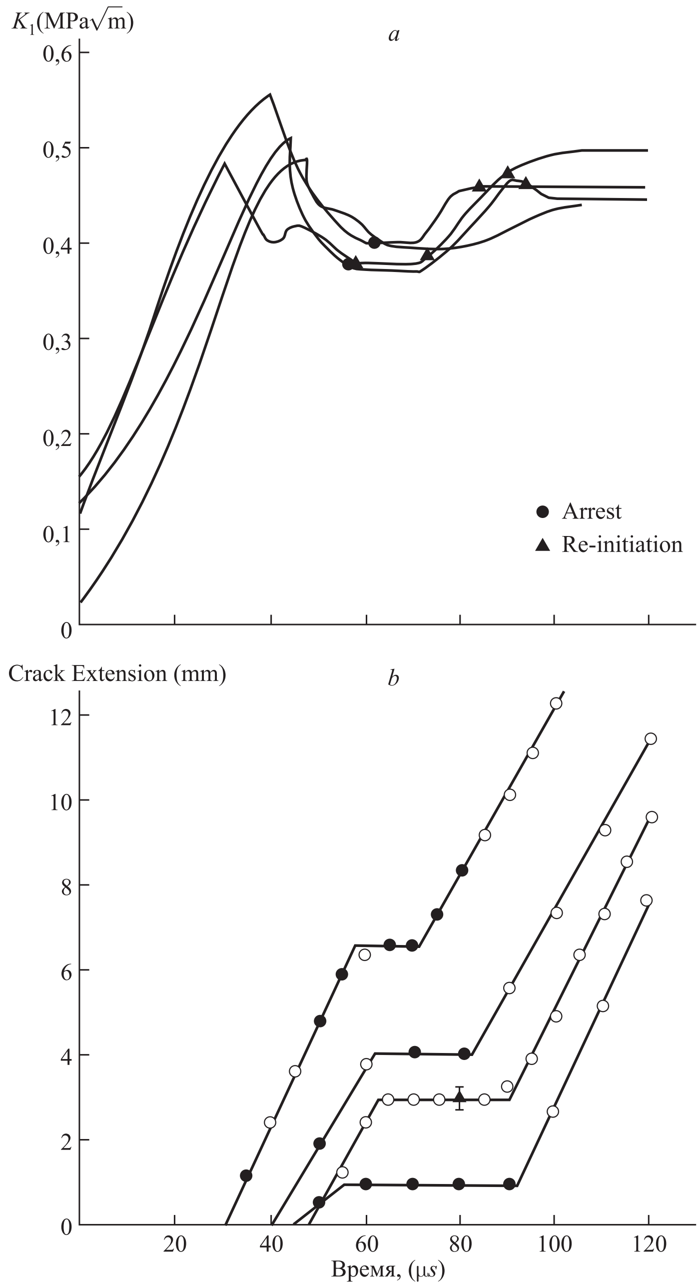

Fig. 7.3. *a* — Stress intensity factor histories for crack arrest experiments (Ravi-Chandar and Knauss, 1984a), *b* — Crack extension histories for crack arrest experiments (Ravi-Chandar and Knauss, 1984a).

in slightly different amplitude of electric flow and, hence, a different amplitude of pressure created on the crack surfaces. Another possible reason for this difference that the authors mention is a slight disparity in sample geometry from one experiment to another.

Unfortunately, in the article by Ravi-Chandar and Knauss information about the amplitude of pressure created in the presented experiments (Ravi-Chandar, Knauss, 1984a) is missing. Moveover, as it can be seen from Fig. 7.3b, at $t = 0$ the initial crack is already prestressed ($K_{\mathrm{I}}(0) \neq 0$).

To check applicability of (7.1) to predict dynamic crack propagation experimental conditions of (Ravi-Chandar, Knauss, 1984a) were modeled utilizing the finite element method.

7.4 Finite element formulation

In order to obtain a closed mathematical description of the dynamic fracture problem (7.4)–(7.8) is supplemented with fracture criterion (7.1). Due to symmetry, we suppose that the crack can propagate only along the x_1 axis. When condition (7.1) is fulfilled somewhere along the crack path, we suppose creation of a new surface in that point. Time integration in (7.1) is performed numerically using the trapezoidal rule.

The problem defined by (7.1) and (7.4)–(7.8) is solved numerically utilizing the finite element method. ANSYS finite element package was used to implement (7.4)–(7.8), and the fulfillment of condition (7.1) was checked by an external program after each time step (ANSYS User's Guide, 2006).

Rectangular 4-node elements were used to mesh a body. The size of elements along the crack path was taken to be exactly $d = \frac{2}{\pi}\frac{K_{IC}^2}{\sigma_c^2}$. The reason for such a choice of element size is that d is a size that characterizes fracture on a chosen scale. From this point of view all the defects and spatial discontinuities with sizes essentially less than d cannot be called fractures within the framework of the scale used. Since critical stress intensity factors and ultimate stresses evaluated in laboratory conditions are used, then, by this, a scale to be used is set up. If, searching for K_{IC} and σ_c, one will use experiments performed on, for example, geological or microscopic scales, one will get values for the studied fracture parameters, different from those acquired while testing specimens on a laboratory scale, and, hence one will get a different value for d, giving a characteristic size for the scale one is currently using.

Following this idea, the size of an element used in the FE model along

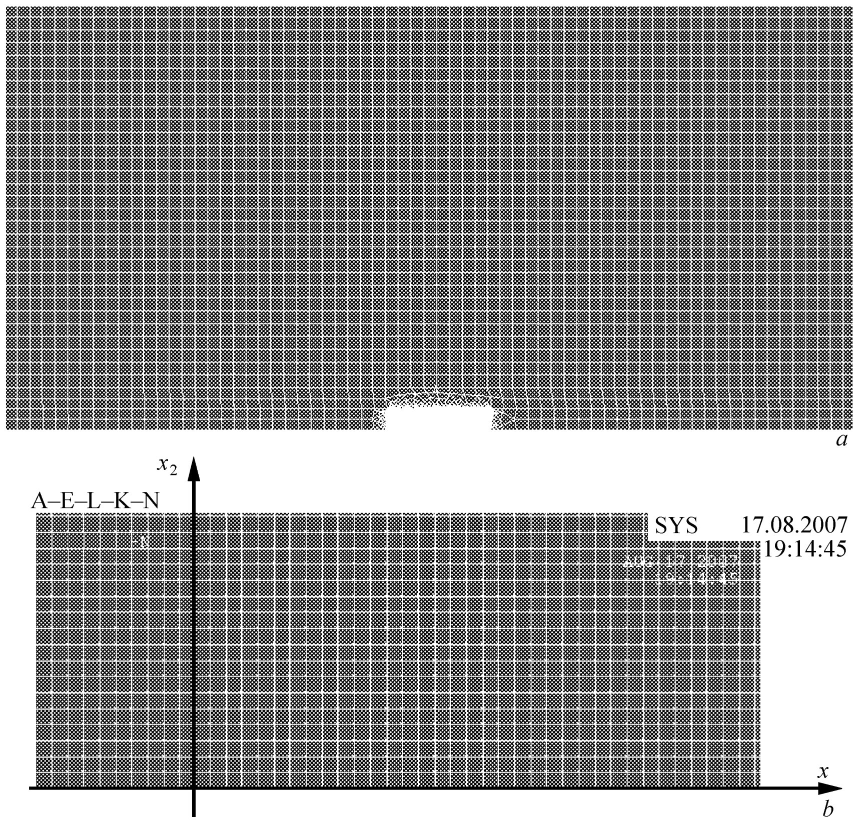

Fig. 7.4. a — Mesh used in the FE model, b — Mesh surrounding the crack tip.

the crack path is the minimal size of a crack that we can call a "fracture". Analogously, d is the minimal increment of a crack length that we can call "crack propagation" on a chosen scale. In the FE model used, release of a node along the crack path increases existing crack length by d — basic crack propagation takes place. Such a choice of the element size simplifies spatial integration in (7.1) as well.

Due to the symmetry of the problem across the x_1 axis the problem was solved only for the upper half of the sample. Dimensions of the modeled sample were the same as in the experiments of Ravi-Chandar and Knauss (Ravi-Chandar and Knauss, 1984a). Fig. 7.4a presents a mesh used in the solution. Fig. 7.4b gives details on the mesh surrounding the crack tip. The crack can propagate along the x_1 axis within the zone with the fine mesh adjacent to the crack tip. The length of this zone is 17 mm.

A total of 18,621 nodes and 18,404 elements was used to form the mesh. Small elements with sizes equal to d were placed adjacent to the crack path to provide the needed accuracy of computation. Distant elements are larger in order to minimize the computational time and expense.

Due to the symmetry of the problem the crack path should follow the x_1-axis. Nodes along the path were subjected to symmetrical boundary conditions up to the moment when the condition (7.1) is satisfied at a particular node (node movements in the vertical direction are restricted). At this moment the restriction on movement of the particular node is removed and a new surface is created. The technique used is similar to the node release technique.

The shape of the pressure pulse applied on the crack faces is given by Fig. 7.2, and its amplitude A is alternated in simulations. Material parameters typical of Homalite-100, used in the experiments of Ravi-Chandar and Knauss, were used in the calculations. These parameters are presented in Table 7.1.

Density, $\rho, \frac{kg}{m^3}$	1230
Young's modulus, E, MPa	3900
Poisson's ratio, ν	0.35
Critical stress intensity factor, $K_{IC}, MPa\sqrt{m}$	0.48
Ultimate tensile stress, σ_c, MPa	48
Incubation time of fracture, τ, μs	9

Table 7.1

The microstructural time of the fracture process, τ, for Homalite-100 was found by Petrov et al. (Petrov et al., 2003) from the analysis of experiments of Ravi-Chandar and Knauss (Ravi-Chandar and Knauss, 1984a). The values of the critical stress intensity factor and the ultimate tensile stress gives a value for d. It appears to be 0.1 mm for Homalite-100 on a laboratory size scale.

The constructed model was checked for convergence. Usage of smaller time steps and smaller elements does not significantly affect the computational results. The ability of the FEM model to solve the stated dynamic problem was also checked by comparison of computational results to the analytical solution for the stress intensity factor in the tip of a crack prior to crack initiation. The analytical solution for K_{I} temporal dependence in

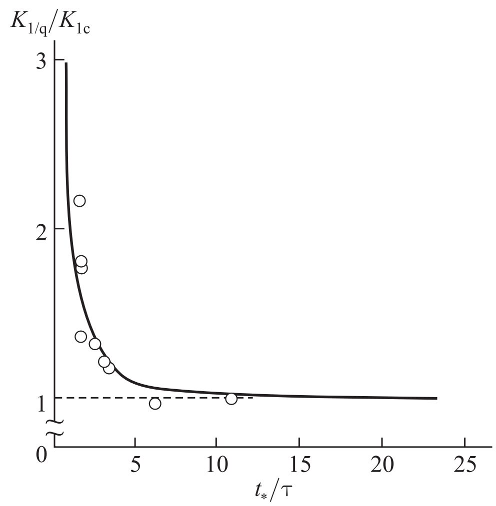

Fig. 7.5. Dependence of normalized stress intensity factor at crack initiation on normalized time-to-fracture. Comparison of experimental data to analytical result received using crack initiation criterion (3).

the studied problem is given, for example, in Petrov and Morozov (Petrov, Morozov, 1994). The FEM computed K_{I} temporal dependence matches the analytical result with a maximum disparity of not more then 5%. The good matching between the computational and analytical result shows the applicability of the constructed model to the investigation of the problem stated by (7.4)–(7.8). Fig. 7.5 gives a comparison between the experimental data of Ravi-Chandar and Knauss for the stress intensity factor at crack initiation for different times-to-fracture (i.e. different amplitudes of applied load pulse) and the analytical solution using criterion (7.3) (Ravi-Chandar and Knauss, 1984a). The figure is reprinted from Petrov and Morozov (Petrov, Morozov, 1994). This result shows that criterion (7.1), being a more general form of (7.3), has an ability to describe the crack initiation problem.

7.5 Solution results

After the stated problem is solved by the ANSYS FEM package, together with an external program controlling crack propagation, information about K_{I} time dependency and the crack extension history is provided for further analysis. $K_{\mathrm{I}}(t)$ is computed using the asymptotic behavior of the stress

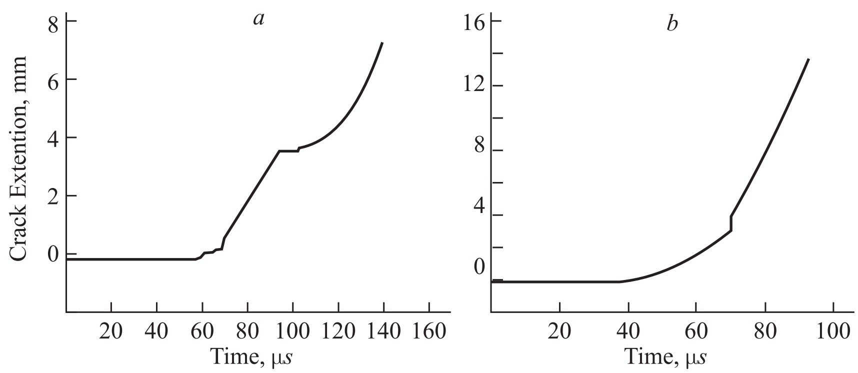

Fig. 7.6. *a* — Crack extension history. A = 5 MPa, *b* — Crack extension history. A = 12 MPa.

field surrounding the crack tip.

It was observed that, depending on the amplitude of the applied pressure pulse A, three different modes of crack propagation are possible. The first one is trivial — amplitude that is too low results in no crack extension. The second one is the mode observed by Ravi-Chandar and Knauss (Fig. 7.3b). The crack starts propagating at a constant speed. Then it arrests, due to the energy flow into the crack tip which is no longer sufficient for its propagation. When the energy from the second trapezoid of the loading pulse approaches the crack tip region, the crack reinitiates and starts propagating at approximately the same speed as in the first stage of its extension (Fig. 7.6a).

Further increase of load amplitude A results in a propagation mode change. Now the crack is initiated, propagates at some constant speed, and when the energy from the second part of the loading pulse is delivered to the crack tip region the crack is accelerated and continues propagation at a higher speed (Fig. 7.6b).

By adjusting the pressure amplitude A, it was found that amplitudes around 5 MPa result in crack extension histories very close to those observed by Ravi-Chandar and Knauss (Ravi-Chandar and Knauss, 1984a). In Fig. 7.7, the computational result for A=5.1 MPa is compared to one of the experiments presented in Fig. 7.3b.

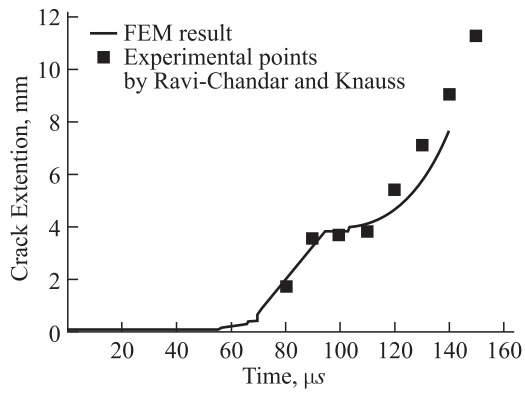

Fig. 7.7. Crack extension history. Comparison of FEM calculation with experimental data points of Ravi-Chandar and Knauss (1984a).

7.6 Conclusions on dynamic crack simulations

It has been shown that, solving the dynamic problem of linear elasticity by FEM and criterion (7.1) being used to assess critical conditions for crack advancement, the propagation of dynamically loaded cracks can be predicted. It has also been shown that criterion (7.1) with d, chosen from the condition of coincidence of (7.1) with Irwin's criterion in static conditions can be used to describe dynamic crack initiation, propagation and arrest.

Criterion (7.1), unlike (7.3), which is applicable only to crack initiation problems, can also be used as the condition for crack propagation and arrest. In the presented model (7.3) is used as a condition for node release. This criterion does not even require the presence of a crack. Thus, the condition for crack propagation and arrest appears automatically. The crack propagates whilst (7.1) is fulfilled for nodes ahead of the moving crack tip; otherwise the crack arrests.

Using a similar method one can model cracks that change their direction of propagation and even branch. In this case (7.1) should be applied not only to stresses acting perpendicular to the x_1 direction, as is done in the presented research, but in all the possible directions surrounding the x^* point.

According to the incubation-time based approach (see Petrov, 1991, or Petrov, Morozov, 1994) in combination with a variety of widely known experimental observations the critical stress intensity factor at the crack initiation moment under high rate loads may, depending on the experimental geometry, loading conditions and history, either be noticeably smaller or greater than K_{IC}. This instability of dynamic fracture toughness is particularly evident while comparing two different load application histories (Petrov et al., 2003). In the first case, a suddenly applied dynamic load is maintained at a constant level up to the moment of crack initiation (e.g. Smith, 1975, Ravi-Chandar and Knauss, 1984a, Rizal and Homma, 2000, Homma et al., 1992). In this case K_{I}^d usually significantly exceeds the static K_{IC}. In the second case, when the fracture is excited by short load pulses with time shapes close to the delta function, threshold amplitude, K_{I}^d is usually significantly less than K_{IC} (e.g. Atroshenko et al., 2002, Shokey et. al, 1986).

This reasoning shows that the dynamic fracture toughness, K_{I}^d, is not an intrinsic characteristic of a material and that usage of critical stress intensity factor criterion ($K_{\mathrm{I}}(t) \geq K_{\mathrm{I}}^d$) to describe dynamic fracture initiation cannot be universally correct. For the same reasons it is impossible to describe dynamic fracture initiation using rate dependent K_{I}^d. Application of the incubation-time based approach allows one to describe all the variety of experimentally observed effects in fracture dynamics. An important consequence of this approach is that it provides an effective way of testing dynamic strength by direct measurement of τ, a parameter intrinsic to the material and not dependent on experimental geometry or the way the load is applied (Petrov, 2004). This provides a tool that can be directly incorporated into practical engineering.

The results presented in above show that a similar approach can be successfully used to describe dynamic crack propagation and arrest.

7.7 Simulation of SMART1 satellite impacting the Moon surface

As shown above, incubation time fracture criterion (7.1) can be applied to study the evolution of the fracture process. This includes not only a simulation of crack propagation in bodies with initial cracks but also fracture of initially intact media. In this section an example of how the incubation time approach can be incorporated into the finite element code in order to simulate fracture of initially intact media is presented. The example presented is the simulation of conditions of satellite SMART1 lunar impact conducted by European Space Agency year 2006 (ESA, 2006a, ESA, 2006b). Aim of the simulation is to compare dimensions of crater created due to SMART1 contact to the Moon surface to the results received using finite element method utilizing incubation time criterion as the critical rupture condition.

An approach similar to the one used to predict crack propagation in the experiments of Ravi-Chandar and Knauss (Ravi-Chandar and Knauss, 1984a), can be used to simulate fracture of initially intact media. The difference is that in this case finite element code should trace fracture condition fulfilment in all the nodes of the modelled sample and be able to create a new surface in respective points once rupture criterion is implemented somewhere in the body.

The traditional way to create a new surface in finite element formulation is associated with splitting of the existing nodes. Using this approach is reasonable in most cases, though this normally requires remeshing and remapping, that are rather time consuming procedures. For the studied problem the situation is different. To guarantee correct integration in (7.1) one should use small (as comparing to τ) time steps. Thus the solution is resulting in long series of tiny substeps. Solution (convergence) on every substep is achieved comparably fast — finite element solver is almost not iterating. It was found, that in this case it is more effective to use multiple nodes in the same location from the beginning, rather than to split the node in question. Each element the full model is constructed of, is not sharing nodes with other elements.

2-D problem with rotational symmetry is solved. Quadratic 4-node elements are used. Dimensions of every element is exactly d times d (where d is given by (7.2)). Obviously, 4 nodes have the same location for inner points of a body and 2 nodes have the same location for the points belonging to the boundary. These nodes originally have their dimensions of freedom (DOF's) coupled. This results in exactly the same FE solution before the fracture condition is implemented in a respective point as if elements had shared nodes. When the fracture condition is fulfilled, restriction on nodes DOF's is removed — a new surface is created. This is done automatically by finite element code after every substep.

Figure 7.8 gives a schematic representation of the internal points of a body. Originally all the 4 nodes sharing the same location have all of their DOF's coupled. Condition (7.1) for this point can be written as:

$$\frac{1}{\tau}\int\limits_{t-\tau}^{t} \sigma_{ii}(t^*)dt^* \geq \sigma_c, \tag{7.9}$$

where i assumes values 1 and 2. Repeating indices does not dictate sum-

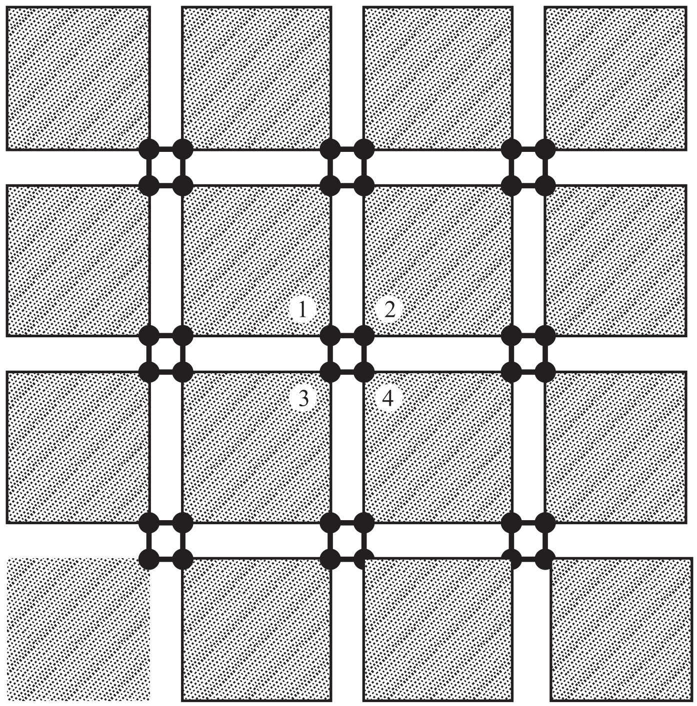

Fig. 7.8. Model consisting of elements without shared nodes.

mation in this case. Spatial integration is removed, because the stress in the respective direction calculated by finite element program is already a mean value over size d (as d is the element size being used). If (7.9) is fulfilled for σ_{11} or σ_{22} then displacements of nodes 1,2,3 and 4 on figure 7.8 get uncoupled. If (7.9) is fulfilled for σ_{11}, two new couple sets consisting of nodes 1, 2 and 3,4 are created. If (7.9) is fulfilled for σ_{22}, new couple sets are created for nodes 1, 3 and 2,4. For later times condition (7.9) in applicable direction is traced for newly created couple sets separately.

The problem is solved for a half-space $x_2 < 0$. (7.4)–(7.6) give state equations and initial conditions for the half-space. Half-space representing the Moon had following material properties: σ_c=10.5 MPa, $K_{IC} = 2.94MPa\sqrt{m}$,$\tau = 80\mu s$,E=60 GPa, ρ=2850 kg/m^3, ν=0.25 typical for earth basalt. This results in $d = 5\ cm$. Half-space is impacted by a cylinder with diameter of 1 meter and height of 1 meter. Density for the cylinder is chosen so that its mass coincides with the one of SMART1 satellite. We suppose that the material of the cylinder is linear elastic and has no possi-

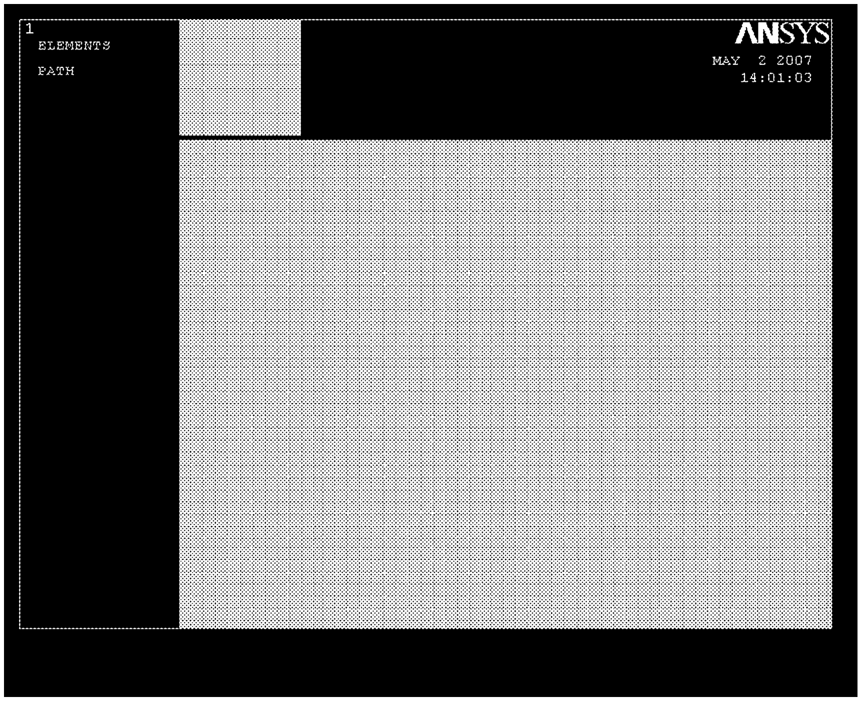

Fig. 7.9. FE model overview.

bility to fracture. SMART1 satellite had a form close to cubic with side of 1 meter and had a mass of 366 kg. SMART1 impacted the Moon surface at a speed of approximately 2000 m/s. In finite element formulation the cylinder was given an initial speed of 2000 m/s prior its contact to the half-space boundary. Figure 7.9 gives an overview of the finite element model. The size of the sample, representing the half-space is chosen from a condition that the waves reflected from the sample boundaries are not returning to the region where the crater is formed in the process of simulation.

ANSYS finite element package (ANSYS, 2006) was used to solve the stated problem. Control of the fracture condition (7.9) fulfillment in all of the sample points and new surface creation when rupture criterion is implemented was carried out by a separate ANSYS ADPL subroutine.

Figure 7.10 shows the sample state after the simulation is finished. Damage localized at down part of the sample is due to finite dimensions of the sample and represents cleavage fracture that occurred after compressive waves were reflected from the lower boundary. In figure 7.11 locations of

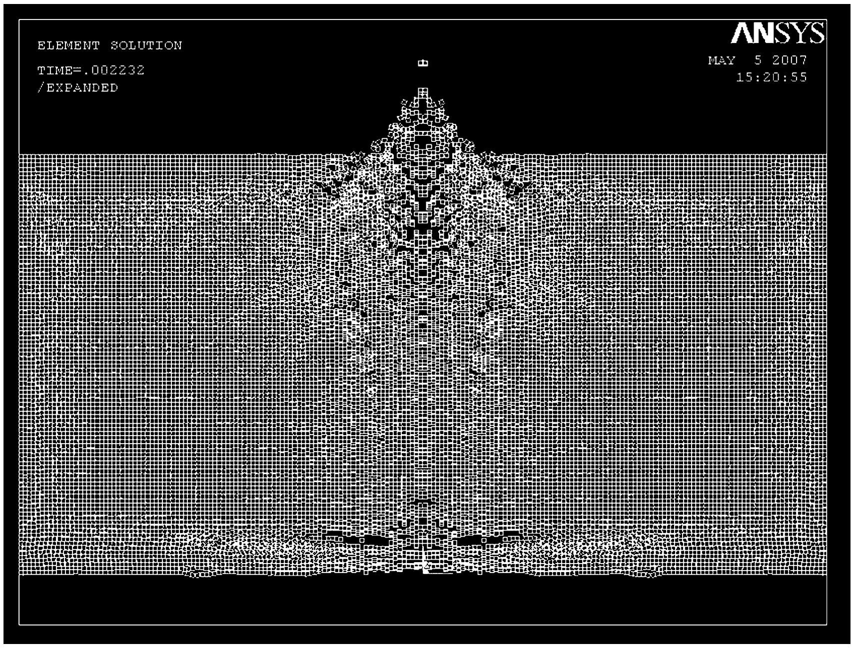

Fig. 7.10. Sample after impact.

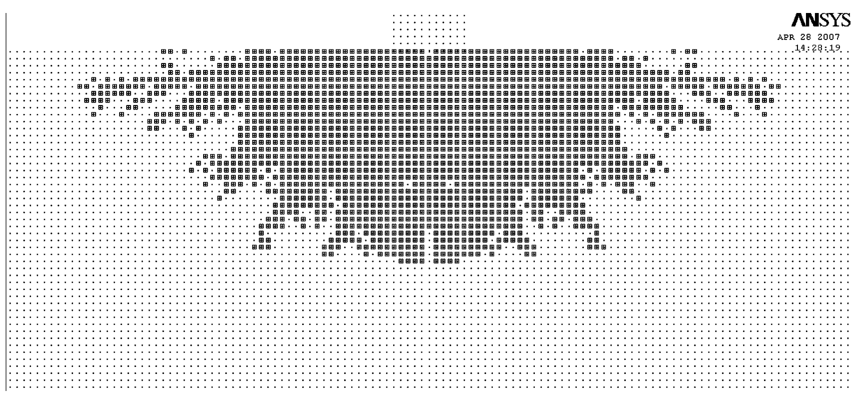

Fig. 7.11. Locations of ruptured nodes.

nodes where the fracture occurred are marked. This gives a possibility to assess dimensions of the crater formed after the SMART1 impact. The damaged zone is found to be about 10 meters in diameter and about 3 meters deep. The zone where the material was fully fragmented (the crater formed) can be assessed having 7–10 meters in diameter and 3 meters deep. This result coincides with ESA estimations of dimensions of the crater formed due to the SMART1 impact (ESA, 2006a, ESA, 2006b).

7.8 Conclusions

Incubation time fracture criterion has a wide area of applicability. As real dynamic fracture problems rarely can be solved analytically, the majority of applications require numerical simulations. In this connection incubation time approach has a significant advantage — it can be applied in order to receive a correct description of both quasistatic and dynamic fracture, so one does not have to use separate criteria for different load rates. It is shown that using incubation time criterion incorporated into finite element code a correct description of dynamic fracture initiation, dynamic crack propagation and fracture of initially fractured media is possible. It is remarkable that staying within the framework of linear elastic fracture mechanics, it is possible to predict all the variety of effects inherent in dynamic fracture. And all this is possible while utilizing a rather simple fracture model, not incorporating complicated cohesive laws. The same approach can be used to model dynamic crack arrest, dynamic cleavage etc.

References

Achenbach, J. D., 1974, Dynamic effects in brittle fracture. In: Nemat-Nasser, S., et al. (eds) Mechanics Today, 1, Pergamon, Elmsford, NY, pp. 1–57

ANSYS, 2006, User's Guide, Release 11.0. ANSYS Inc., Pennsylvania, USA

Atkinson, C., Eshelby, J. D., 1968, The flow of energy into the tip of a moving crack. International Journal of Fracture 4:3–8

Atroshenko, S. A., Krivosheev, S. I., Petrov, Y. V., 2002, Crack propagation upon dynamic failure of polymethylmethacrylate, Technical Physics, 47, 194–199

Barenblatt, G. I., 1962, The mathematical theory of equilibrium cracks in brittle fracture, Advances in Applied Mechanics, 7, 55–129

Bradley, W. B., Kobayashi, A. S., 1970 An investigation of propagating crack by dynamic photoelasticity. Experimental Mechanics 10:106–113

Bratov, V., Gruzdkov, A., Krivosheev, S., Petrov, Y., 2004, Energy Balance in the Crack Growth Initiation under Pulsed-Load Conditions. Doklady Physics 49:338–341

Bratov, V., Petrov, Y., 2007, Optimizing energy input for fracture by analysis of the energy required to initiate dynamic mode I crack growth. International Journal of Solids and Structures, 44, 2371–2380

Broberg, K. B., 1960, The propagation of a brittle crack. Archiv fur Fysik 18:159–192

Broberg, K. B., 1989, The near-tip field at high crack velocities. International Journal of Fracture 39:1–13

Camacho, G. T., Ortiz, M., 1996, Computational modelling of impact damage in brittle materials, International Journal of Solids and Structures, 33, 2899–2938

Dally, J. W., 1979, Dynamic photoelastic studies of fracture. Experimental Mechanics 19:349–361

Dally, J. W., Shukla, A., 1980, Energy loss in Homalite-100 during crack propagation and arrest. Engineering Fracture Mechanics 13:807–817

Dally, J. W., Barker, D. B., 1988, Dynamic measurements of initiation toughness at high loading rate. Experimental Mechanics 28:298–303

ESA, 2006a, ESA Press Release 31-2006. Impact landing ends SMART-1 mission to the Moon. http://www.esa.int/esaCP/SEM7A76LARE_index_0.html

ESA, 2006b, Intense final hours for SMART-1, http://www.esa.int/esaCP/SEMV386LARE_index_0.html

Freund, L. B., 1972a, Crack propagation in an elastic solid subjected to general loading. I: Constant rate of extension. Journal of the Mechanics and Physics of Solids 20:129–140

Freund, L. B., 1972b, Crack propagation in an elastic solid subjected to general loading. II: Nonuniform rate of extension. Journal of the Mechanics and Physics of Solids 20:141–152

Freund, L. B., 1972c, Energy flux into the tip of an extending crack in an elastic solid. Journal of Elasticity 2:341–349

Freund, L. B., 1990, Dynamic Fracture Mechanics, 1st Cambridge Press, Cambridge

Homma, H., Kanto, Y., Tanka, K., 1992, Rapid load fracture testing, In: Chona, R., Corwin, W. R., editors, Cleavage fracture under short stress pulse loading at low temperatures, ASTM STP 1130, Philadelphia: American society for testing and materials, 37–49

Hopkinson, J., 1901, Original Papers, Cambridge University Press.

Kalthoff, J. F., 1986, Fracture behavior under high rates of loading. Engineering fracture Mechanics 23:289–298

Kobayashi, A. S., Wade, B. G., Bradley, W. B., Chiu, S. T., 1974, Crack branching in Homalite-100 plates. Engineering Fracture Mechanics 6:81–92

Kostrov, B. V., 1966, Unsteady propagation of longitudinal shear cracks. Applied Mathematics and Mechanics 30:1241–1248

Kostrov, B. V., Nikitin, L. V., 1970, Some general problems of mechanics of brittle fracture. Archiwum Mechaniki Stosowanej 22:749–775

Ma, C. C., Freund, L. B., 1986, The Extent Of The Stress Intensity Factor Field During Crack Growth Under Dynamic Loading Conditions. ASME Journal of Applied Mechanics 53:303–310

Morozov, N., Petrov, Y., 2000, Dynamics of Fracture. Springer-Verlag, Berlin-Hidelberg-New York

Owen, D. M., Zhuang, S., Rosakis, A. J., Ravichandran, G., 1998, Experimental Determination of Dynamic Crack Initiation and Propagation Fracture

Toughness in Aluminum Sheets. International Journal of Fracture 90:153–174

Petrov, Y. V., 1991, On “Quantum” Nature of Dynamic Fracture of Brittle Solids. Doklady Akademii Nauk USSR 321:66–68

Petrov, Y. V., Morozov, N. F., 1994, On the modeling of fracture of brittle solids. Journal of Applied Mechanics 61:710–712

Petrov, Y. V., Morozov, N. F., Smirnov, V. I., 2003, Structural micromechanics approach in dynamics of fracture. Fatigue and fracture of Engineering Materials and Structures 26:363–372

Petrov, Y. V., 2004, Incubation time criterion and the pulsed strength of continua: fracture, cavitation, and electrical breakdown. Doklady Physics 49:246–249

Petrov, Y., Sitnikova, E., 2005, Temperature dependence of spall strength and the effect of anomalous melting temperatures in shock-wave loading. Technical Physics 50:1034–1037

Ravi-Chandar, K., Knauss, W. G., 1984a, An experimental investigation into dynamic fracture: I. Crack initiation and arrest. International Journal of Fracture 25:247–262

Ravi-Chandar, K., Knauss, W. G., 1984b, An experimental investigation into dynamic fracture: II. Microstructural aspects. International Journal of Fracture 26:65–80

Ravi-Chandar, K., Knauss, W. G., 1984c, An experimental investigation into dynamic fracture: III. On steady state crack propagation and crack brunching. International Journal of Fracture 26:141–154

Ravi-Chandar, K., Knauss, W. G., 1984d, An experimental investigation into dynamic fracture: IV. On the interaction of stress waves with propagating cracks. International Journal of Fracture 26:189–200

Ravi-Chandar, K., Knauss, W. G., 1987, On the characterization of the transient stress field near the tip of a crack. Journal of Applied Mechanics 54:72:78

Remmers, J. J. C., Borst, R. de, Needleman, A., 2004, A cohesive segments approach for dynamic crack growth, In S Ahzi, M Cherkaoui, MA Khaleel, HM Zbib, MA Zikry, & B Lamatina (Eds.), Multiscale modeling and characterization of eleastic-inelastic behavior of engineering materials, dordrecht: Kluwer, 299–306

Rizal, S., Homma, H., 2000, Dimple fracture under short pulse loading, International Journal of Impact Engineering, 90, 83–102

Rosakes, A. J., Zehnder, A. T., 1985, On dynamic fracture of structural metals. International Journal of Fracture 27:169–186

Schardin, H., Struth, W., 1938, Hochfrequezkinematographische untersuchung der bruchvorgänge in glas, Glastechnische Berichte 16:219

Shokey, D. A., et al., 1986, Short pulse fracture mechanics, Journal of Engineering Fracture Mechanics, 23, 311–319

Smith, G. C., 1975, An experimental investigation of the fracture of a brittle material, Ph. D. Thesis, California Institute of Technology

Wallner, H., 1938, Linienstrukturen an bruchflächen. Z. Physik 114:368–370

Wells, A. A., Post, D., 1958, The dynamic stress distribution surrounding a running crack — A photoelastic analysis. Proceedings of the Society for Experimental Stress Analysis 16:69–93

Willis, J. R., 1975, Equations of motion for propagating crack. The Mechanics and Physics of Fracture, The Metals Society 1:57–67

Xu, X., Needleman, A., 1995, Numerical simulations of dynamic crack growth along an interface, International Journal of Fracture, 74, 289–324

Yoffe, E. H., 1951, The moving Griffith crack. Philosophical Magazine 42:739–750

Chapter 8

Energy input optimization problems

Possibility to optimize energy input for fracture and structural transformations on the basis of analysis using the incubation time theory. Evaluation of optimal energy saving parameters in rock fracture, cavitation of liquids and detonation of gaseous media

8.1 Introduction

Possibility to optimize (minimize) energy needed to create structural transformations is of importance that is hard to overestimate in connection to a variety of industrial processes. Here we can mention mining and further rock processing, drilling, detonation initiation (for example, in connection to pulsed detonation engines). In cavitation problems one is usually interested in maximization of energy that can be radiated into liquid media without uncontrolled growth of voids (cavitation).

Criteria for structural transformations discussed in the previous chapters (fracture, detonation initiation, cavitation, electric breakdown) based on the idea of the incubation time provides a tool that can, with relative simplicity, be used to predict optimal parameters for pulsed energy input in different industrial processes.

In this chapter available experimental data on high rate fracture of different rock materials is presented and analyzed in order to evaluate incubation time of fracture for these materials to use in incubation time based fracture criteria. On the basis of the incubation time theory and evaluated parameters possibility to optimize (minimize) energy input for fracture is studied in connection to industrial rock fracture processes. Possibility to optimise energy input for detonation initiation and cavitation in liquids is also demonstrated.

8.2 Rock fracture dynamics

Understanding mechanisms underlying dynamic fracture of rock is one of the central challenges in the modern rock mechanics. Dynamic range loads working for fracture or fragmentation of rock represent the essence of many industrial processes in mining and further handling of rock. Though for several decades it is known and generally recognized that the static fracture criteria (critical stress criterion for fracture of intact media and Irwin's critical stress intensity factor criterion for fracture of cracked bodies) are not applicable to study fracture caused by loads of dynamic range, no conventional approach to the problem is formed to the moment.

In chapter 5 a criterion able to describe all the variety of experimentally observed effects typical of dynamic fracture was discussed. It was shown that staying within the framework of linear elastic fracture mechanics it is possible to describe all the features typical of fracture caused by high rate loads. And even more attractive is the fact, that the same critical fracture condition can be used for all load rates — from quasistatic situations, when incubation time criterion repeats classical fracture criteria, to extreme dynamic conditions, when incubation time criterion is in a very good qualitative and quantitative agreement with experimentally observed processes.

8.3 Prediction of dynamic fracture toughness for rock materials

An important conclusion from the previous chapters is that in order to use incubation time fracture criterion for practical predictions of critical rupture conditions one should supplement static material specific strength parameters (ultimate stress σ_c and critical stress intensity factor K_{IC}), that are known for majority or rock materials, with incubation time of the fracture process for the material in question (τ). In this section the theoretical background for one class of experiments aimed for evaluation of τ is given and corresponding experimental results for rock materials are presented.

An infinite plane with a semi infinite crack ($\{x_1,x_2\}$:x_2=0, x_1 <0) is considered. Plane strain conditions are supposed. The load is given as a pressure pulse applied on the crack faces. Displacements of the plane are described by:

$$\rho u_{i,tt} = (\lambda + \mu) u_{j,ji} + \mu u_{i,jj}, \tag{8.1}$$

where "," refers to the partial derivative with respect to time and spatial coordinates. ρ is the mass density, and the indices i and j assume the values 1 and 2. Displacements are given by u_ι in the directions x_ι respectively. t stands for time, λ and μ are Lame constants. Stresses and strains are coupled by Hooke's law:

$$\sigma_{ij} = \lambda \delta_{ij} u_{k,k} + \mu (u_{i,j} + u_{j,i}), \tag{8.2}$$

where σ_{ij} represents stresses in direction ij, δ_{ij} is the Kronecker delta assuming value of 1 for $i = j$and 0 otherwise. For negative times the plane is stress free and velocity field is zero everywhere in the body:

$$\sigma_{ij}|_{t<0} = u_{,t}|_{t<0} = 0. \tag{8.3}$$

Crack faces are free from tractions:

$$\sigma_{21}|_{x_1<0, x_2=0} = 0. \tag{8.4}$$

Load on the crack faces is given by:

$$\sigma_{22}|_{x_1<0, x_2=0} = -p(t). \tag{8.5}$$

It is assumed that the leading term of Williams asymptotic expansion of crack tip stresses is controlling the stress field on the crack continuation:

$$\sigma_{22}\Big|_{x_1>0, x_2=0} = \frac{K_{\mathrm{I}}(t)}{\sqrt{2\pi x_1}} + O(1), x_1 \to 0. \tag{8.6}$$

Rectangular shaped load pulse is applied on the crack faces:

$$p(t) = P\left[H(t) - H(t - t_0)\right], \tag{8.7}$$

where P and t_0 prescribe amplitude and duration for the load pulse and $H(t)$ denotes the Heaviside step function. Solving (8.1)–(8.7) one can find stress intensity factor history:

$$K_I(t) = P\varphi(c_1, c_2)\left[\sqrt{t}H(t) - \sqrt{t - t_0}H(t - t_0)\right] \tag{8.8}$$

where

$$\varphi(c_1, c_2) = \frac{4c_2\sqrt{c_1^2 - c_2^2}}{c_1\sqrt{\pi c_1}},$$

with c_1 and c_2 being the speeds of longitudinal and transversal wave in the studied material.

Supposing the amplitude of the load pulse is the threshold one (i.e. the minimal possible amplitude resulting in crack extension), time when incubation time fracture condition (7.3) is fulfilled can be found from:

$$I(t) = K_{\mathrm{IC}}\tau,\ I(t) = \int\limits_{t-\tau}^{t} K_{\mathrm{I}}(s)ds. \tag{8.9}$$

Substituting K_{I} from (8.8) into (8.9) one can get:

$$\begin{gathered} I(t) = \frac{2}{3}P\varphi(c_1,c_2)\left[t^{\frac{2}{3}}H(t) - (t-\tau)^{\frac{2}{3}}H(t-\tau)\right] - \\ -\frac{2}{3}P\varphi(c_1,c_2)\left[(t-t_0)^{\frac{2}{3}}H(t-t_0) + (t-\tau-t_0)^{\frac{2}{3}}H(t-\tau-t_0)\right] \end{gathered} \tag{8.10}$$

Obviously $I(t)$ reaches its maximum overtime value at $t = t'$:

$$t' = \frac{1}{3}\left[\tau + t_0 + 2\sqrt{\tau^2 - \tau t_0 + t_0^2}\right] \tag{8.11}$$

Thus, conducting series of experiments on cracked plates with such sizes, that the waves from the specimen boundaries are not reaching crack tip prior to crack initiation, tending to find the threshold load amplitude for pulses with given duration $t_{0,}$ one can obtain value of the incubation time τ for material tested. Table 8.1 gives the values for critical stress intensity factor, ultimate stress and incubation time for several rock materials. Data presented in table 8.1 was experimentally evaluated in Research Center of

	Material	σ_c, MPa	K_{IC}, $MPa\sqrt{m}$	d, mm	τ, μs
1.	Limestone	12.40	1.31	7.11	15
2.	Gabbro-Diabase	44.04	2.36	1.83	40
3.	Marble	6.19	1.34	30.00	44
4.	Sandstone	31.18	1.19	0.93	54
5.	Granite	19.50	2.40	1.95	72
6.	Clay	1.63	0.12	3.45	75

Table 8.1: Fracture properties of some rock materials

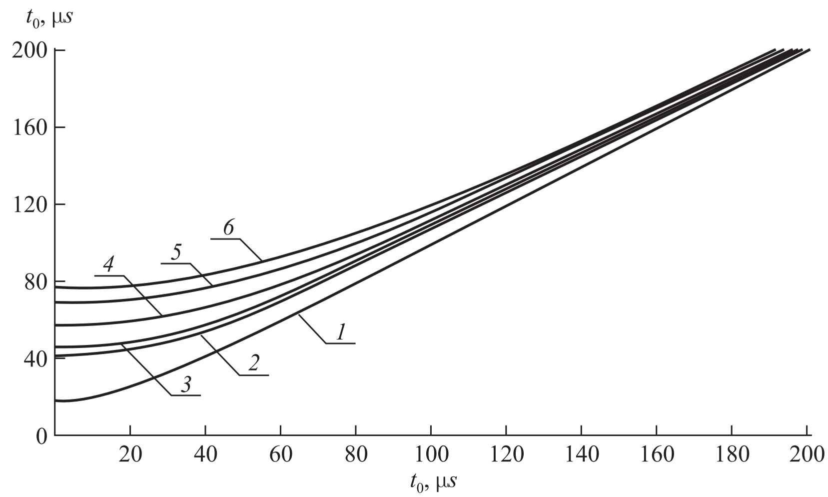

Fig. 8.1. Time-to-fracture — load duration curves for rock materials. 1 — limestone, 2 — gabbro-diabase, 3 — marble, 4 — sandstone, 5 — granite, 6 — clay.

Dynamics (St.Petersburg State University) by Petrov et al. (Petrov et al., 2005). Value for d is calculated utilizing (7.2).

Figure 8.1 reflects experimentally observed dependencies of time-to-fracture t' on a threshold pulse duration t_0 for such materials. Presented curves computed by incubation time criterion using parameters from table 8.1 are in a very good coincidence with experimentally observed behavior.

8.4 Optimization of energy input in industrial processes connected with fracture of rock materials

A possibility to optimize the amount of energy, required to fracture materials is of a large interest in connection to numerous applications. Energy inputs for fracture induced by short pulsed loadings are of the major importance in such areas as percussive, explosive, hydraulic, electro-pulse and other means of mining, drilling, pounding etc. In these cases energy input usually accounts for the largest part of the process cost (see, for example, Royal Dutch Petroleum Company Annual Report, 2003). Taking into consideration the fact that the efficiency of the mentioned processes rarely exceeds few percent the importance of energy input optimization gets evident.

The purpose of the presented investigation is to find and explore the

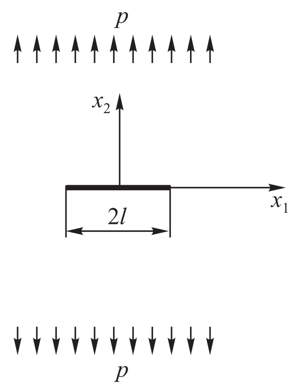

Fig. 8.2. Experiment scheme. Central crack in an infinite plane is loaded by a wave approaching from infinity. Wave front is parallel to the crack plane.

amount of energy sufficient to initiate the propagation of a mode I loaded central crack in a plate subjected to plane strain deformation. Two ways to apply the dynamic load to the body are studied. In the first case the load is applied at infinity. The study involves the analysis of interaction of the wave package approaching from infinity with an existing central crack in a plane. The existing crack is oriented parallel to the front of the wave package. In the second case the load is applied on the crack faces. Tractions are normal to the crack faces.

Following the superposition principle these two loading cases should produce identical stress-strain field in the vicinity of the crack tip. It will be shown later that the amount of total energy applied to the body needed to initiate crack growth is depending on the load application manner in different way for the two cases under investigation.

8.5 Load applied at infinity

Consider an infinite plane with a central crack (Fig. 8.2). The load is given by the wave falling on the crack. Displacements of the plane are described by (8.1). Stresses and strains are coupled by Hooke's law (8.2). Boundary conditions are:

$$\sigma_{22}|_{|x_1|<l, x_2=0} = \sigma_{21}|_{|x_1|<l, x_2=0} = 0. \tag{8.12}$$

The impact is delivered to the crack by the falling wave:

$$\sigma_{22}|_{t<0} = P\left(H\left(t+\frac{x_2}{c_1}\right)+H\left(t-\frac{x_2}{c_1}\right)-\right.$$
$$\left.-H\left(t+\frac{x_2}{c_1}-T\right)-H\left(t-\frac{x_2}{c_1}-T\right)\right), \quad (8.13)$$

where c_1 is the longitudinal wave speed, H is the Heaviside step function and T is the impact duration. P represents the pressure pulse amplitude and has a dimension of Pa. The described problem is solved using finite element method.

8.6 Modelling interaction of the wave coming from infinity with the crack

The process is analyzed utilizing the finite element method. ABAQUS (see ABAQUS USER MANUAL) finite element package was used to solve the problem. The task was formulated for a quarter sample using the symmetry of the problem about x- and y-axes. Plane strain conditions were supposed. Area adjacent to the crack tip was meshed by triangular isoparametric quarter-point elements available in ABAQUS package. Thus, mesh in the vicinity of the crack tip may assume a square root singularity in stress/strain fields. The total of about $30E5$ elements was used to model the cracked sample. Crack surface was represented by 50 nodes along the crack's half-length. Explicit time integration was utilized to solve the dynamic problem in question.

Computations were performed for granite (E = 96.5 *GPa*, ρ = 2810 *kg/m3*, υ = 0.29, where E is the elasticity modulus, ρ is the mass density and υ the Poisson's ratio). The results of investigation will qualitatively hold for a big variety of quasi-brittle materials. In conditions of the plane strain interaction of the wave approaching from infinity with a central crack was investigated.

Firstly, infinite pulse durations were supposed, i.e. T = 1. Time dependence of the stress intensity factor K_{I} was studied. K_{I} used in a further analysis was calculated from J-integral that is available as a direct output from ABAQUS solution. Computations were performed for different amplitudes of the loading pulse applied. Typical dependence of K_{I} on time is presented in Fig. 8.3.

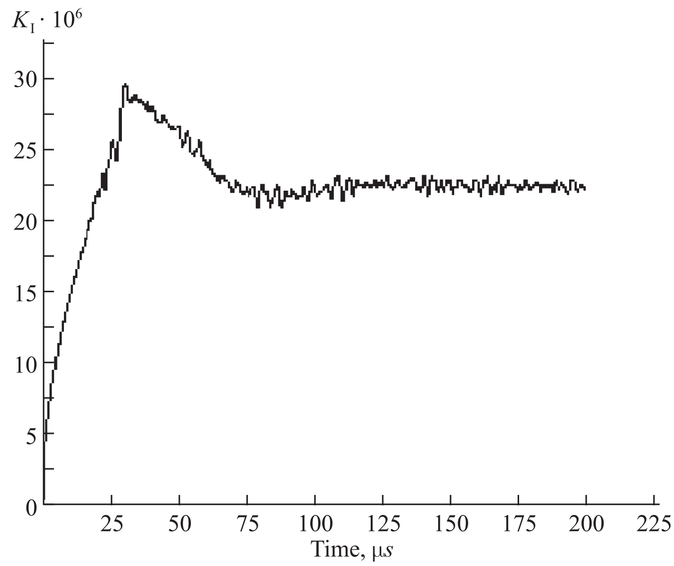

Fig. 8.3. Typical stress intensity factor ($Pa\sqrt{m}$) time (μs) dependence in FE solution.

Apparently, K_{I} is rapidly approaching the static level. Thus, the time to approach the steady-state situation in a vicinity of a crack tip can be estimated as 5–10 times more than the time required by the wave to travel along a crack's half-length.

Fracture criterion fulfilment was checked for different load amplitudes and durations. Dependence of time-to-fracture T^* on the amplitude of the load applied was investigated. Time-to-fracture is the time from the beginning of interaction between the wave package and the crack to the crack start. Incubation time criterion of fracture (Chapter 5, Morozov and Petrov, 2000) was chosen to be used. Similar approach to be used in case of short cracks is given by Petrov and Taraban (Petrov and Taraban, 1997).

Using the incubation time criterion the dependence of time-to-fracture on the amplitude of the load pulse applied was studied. Values of $K_{IC} = 2 - 4Mpa\sqrt{m}$ and $\tau = 72\mu$s typical for granite (Table 8.1) were used. Integration of the temporary dependence of stress intensity factor was done numerically. In Fig. 8.4 x-axis represents the time from the beginning of interaction of the wave coming from infinity with the crack to the fracture initiation. y-axis represents the corresponding amplitude of the load applied at infinity. Point in Fig. 8.4 marked with a cross corresponds to the maximum possible time-to-fracture for the given problem. As follows, for

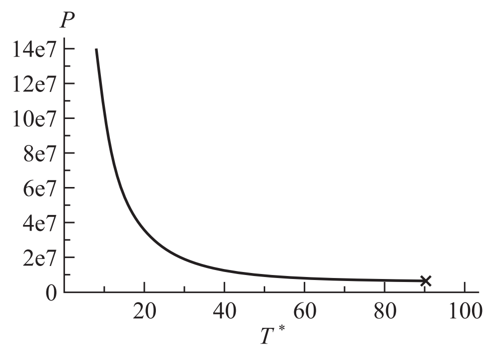

Fig. 8.4. Curve limiting the pulses leading to crack propagation. Time-to-fracture (ls) vs. applied pressure amplitude (Pa).

investigated granite and studied experimental conditions fracture is only possible for times less than 92 μs.

At the same time the critical (threshold) amplitude of the applied load was found. This amplitude corresponds to the maximum time-to-fracture possible. Loads with amplitudes less than the critical one do not increment the crack's length.

8.7 Dependence of the energy inputs for fracture on the load amplitude and duration

At this point we examine the specific momentum transferred to the plane under investigation by a loading device. In our case

$$P(t) = P\left(H\left(t\right) - H\left(t - T\right)\right), \tag{8.14}$$

so the specific (per unit of length) momentum of the impact will be:

$$R = PT. \tag{8.15}$$

Area filled in Fig. 8.5 corresponds to a set of momentum values causing fracture. For the values not belonging this area crack propagation does not occur. The minimum value for the momentum incrementing the crack length (44.7 *kg m/s*) is reached at load with duration of 72 μs while the amplitude of the load exceeds the minimal one by more than 10%.

Now we come to examination of the energy transmitted to the sample by a virtual loading device in the process of impact. The shape of the load applied is given by (8.15). A specific (per unit of length) energy transmitted

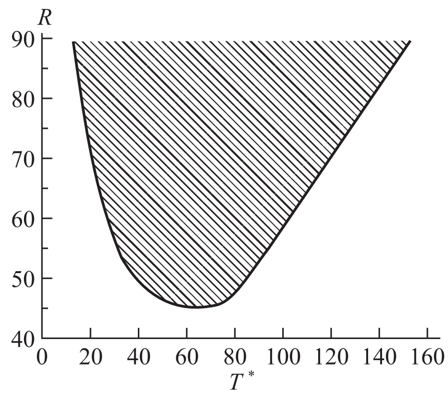

Fig. 8.5. Filled area corresponds to a set of possible pulses leading to crack initiation. At T = 72 μs momentum R (kg m/s) needed to advance the crack is minimized.

to the stripe can be calculated using solution for the uniformly distributed load acting on a half plane.

This problem can be easily solved utilizing D'Lambet method. Solution for a specific energy transmitted to the half plane appears to be:

$$\varepsilon_{\text{spec}} = \frac{1}{\rho c} \int_0^T P^2(t)dt. \tag{8.16}$$

c here is the same as c_1 and gives the longitudinal wave speed. This result can be used for the problem under investigation as interaction of the loading device and the sample is finished before the waves reflected from the crack come back. Substitution of (8.14) into (8.18) gives $\varepsilon_{\text{spec}} = \frac{P^2 T}{c\rho}$.

Analogously to Fig. 8.5, we plot a limiting curve for a set of energies that, being transmitted to the sample, cause the crack propagation (Fig. 8.6).

Minimum energy able to increment the crack length ($172E6$ J) is reached at load pulses with duration of 78 μs. As it is evident from Fig. 8.6, minimal energy, required to propagate the crack by impacts with durations differing much from the optimal one, significantly exceeds the minimal possible value. Thus, minimum energy, incrementing the crack for the load with duration of 92 μs (at this impact duration crack propagation is possible from the impact of threshold amplitude), will exceed minimal energy possible by 10%, and at duration of 40 μs it will be more than two times bigger.

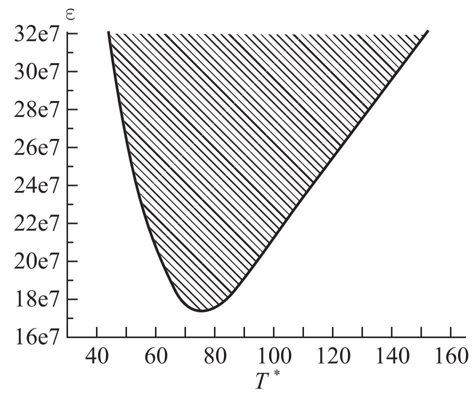

Fig. 8.6. Filled area corresponds to a set of possible pulses leading to crack initiation. At T = 78 ls energy e (J) needed to advance the crack is minimized.

8.8 Case of a load applied on the crack faces

Now we consider a problem similar to the previous one, but with the load applied not at infinity but on the crack faces. The problem is solved numerically and in the same manner as the one for the load applied at infinity. Obviously, according to the superposition principle, the solution will coincide with the one for the stripe stretched by a load applied at infinity. Thus, all the consequences of the previous solution are applicable, except for estimations of energy. Specific momentum transmitted to the sample will be the same as the one in the previous problem.

It is not possible to estimate energy transmitted to the sample analytically for the situation, when the load is applied at the crack faces. However, the finite element solution can be used in this case to estimate this energy. Fig. 8.7 represents time dependence of full, kinetic and potential energies of deformation contained in a loaded sample for a particular pressure amplitude.

Firstly, the kinetic energy is growing linearly along with the potential one, in the same manner as it happens in the case with the loaded half-plane. However, at the moment of time equal to the time sufficient for a wave to travel along the crack length, kinetic energy is starting to transform into potential energy of deformation. Some part of the energy is returned to the loading device.

Limiting curve for the set of energies incrementing the crack length is presented in Fig. 8a. As it can be noticed in the case of the load applied at the crack faces, the energy input to increment the crack length has no

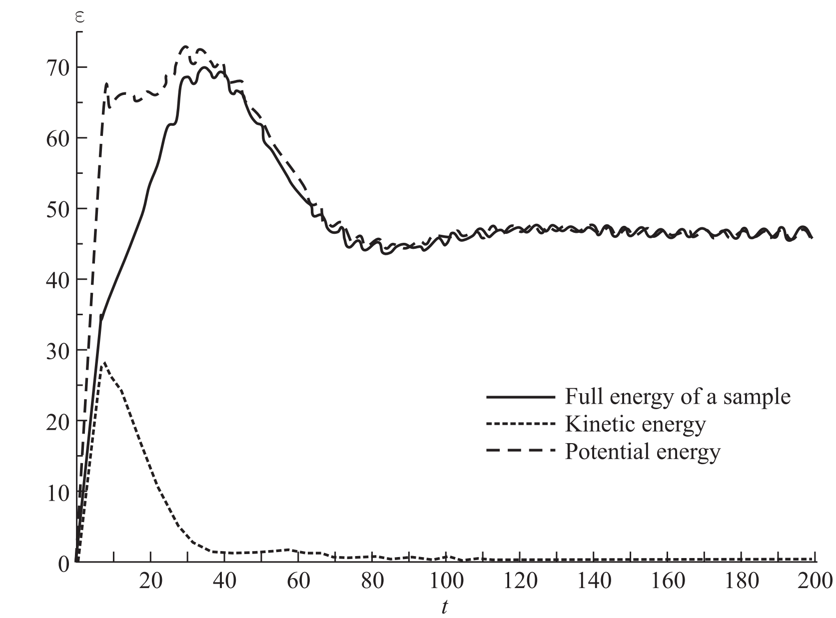

Fig. 8.7. Transmitted energy (J) time (μs) dependence.

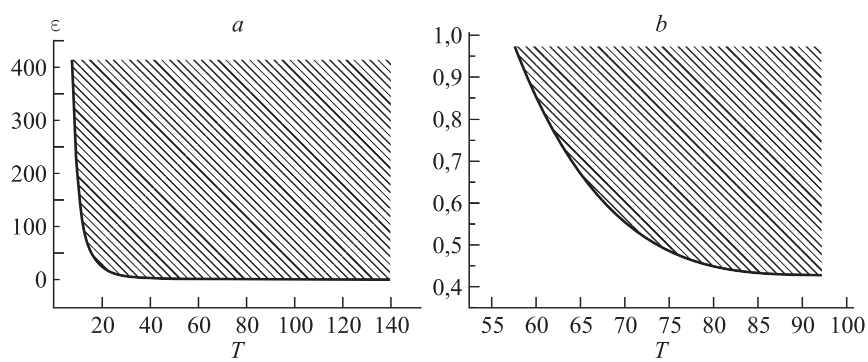

Fig. 8.8. Energy minimization. Possible energy (J) quantities transmitted to a sample by a loading device depending on load duration (μs). (b) Enlarges part of (a).

marked minimum. Minimum energy needed to produce fracture in this case is decreasing with the growth of load duration. When the duration is equal to maximal time-to-fracture possible, energy reaches the minimal value.

Fig. 8b enlarges the area adjacent to the point where the minimal energy is firstly reached in Fig. 8a. As follows from Fig. 8b for the pulse durations close to the maximal possible time-to-fracture (92 μs), minimal energy input needed to increment the crack is not much different from the minimum value firstly achieved at 92 μs.

8.9 Optimization of the load parameters to minimize energy cost for the crack growth

With the majority of non-explosive methods used to fracture materials (drilling, grinding, etc.) it is possible to control amplitude and frequency of impacts from the side of a rupture machine. The performed modelling shows that at a certain load duration (at impact fracture of big volumes of material pulse duration is connected to the frequency of the machine impacts) energy inputs for crack propagation have a marked minimum.

Analogously to Fig. 8.6 it is possible to plot the limiting curve for the set of energy values leading to propagation of a crack in the sample at different load amplitudes. This is done in Fig. 8.9. Thus, it is possible to establish ranges of amplitudes and frequencies of load at which energy costs for fracture of the material are minimized. These ranges are dependent on parameters of the fractured material, predominant length of existing cracks and the way the load is applied.

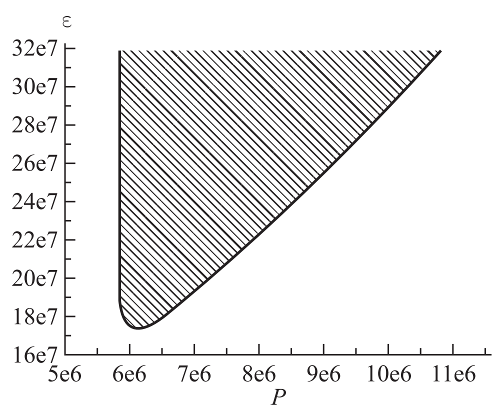

Fig. 8.9. Finding optimal pulse amplitude. Possible energy ε (J) values for different pressure amplitudes P (Pa).

8.10 Dependence of the load parameters minimizing the energy for fracture on the length of the existing crack

Dependence of the optimal load parameters on the crack length was also studied. The results received are represented in Fig. 8.10a and b. As follows from Fig. 8.10a duration of the load, that minimizes energy and momentum inputs is linearly or quasi-linearly dependent on the existing crack length. With the disappearing crack length the duration of the load minimizing momentum needed to increment the crack approaches zero. At the same time the duration optimal for the energy input most probably tends to the microstructural time of the fracture process τ. The maximum possible time-to-fracture also tends to the microstructural time of fracture.

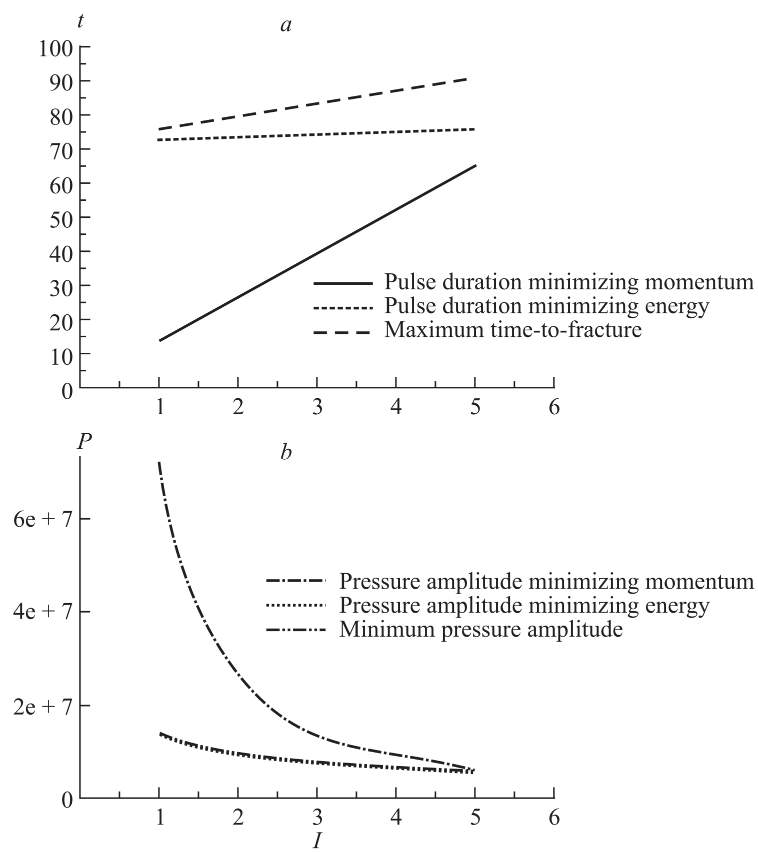

Fig. 8.10. (a) Dependence of optimal load duration (μs) on the crack length (mm), (b) Dependence of optimal load amplitude (Pa) on the crack length (mm).

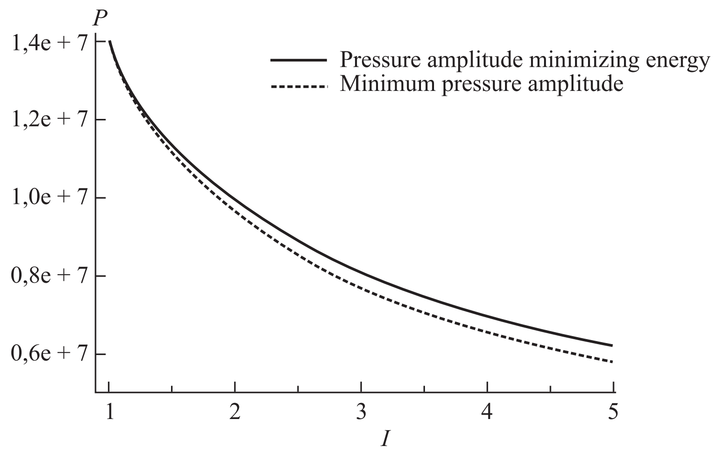

Fig. 8.11. Dependence of optimal load amplitude (Pa) on the crack length (mm).

Thus, considering intact media as the extreme case of media with cracks when the crack length goes to zero, we find that the maximum possible time-to-fracture is the same as the microstructural time of the fracture process. Durations of the loads being optimal for the energy inputs for the fracture of intact media are also equal to the microstructural time of the fracture process. Amplitudes of loads, that minimize energy and momentum sufficient to increment the crack length, are presented in Fig. 8.10b.

As expected, the amplitude of the threshold pulse is inversely dependent on $\sqrt{l}$, where l is the crack length. Dependence of amplitude, minimizing energy inputs, from the crack length is close to $\frac{1}{\sqrt{l}}$. The amplitude, minimizing momentum, is back proportional to the crack length. When the crack length is close to zero, the amplitude of the load, that minimizes the energy cost of the crack propagation, is close to the threshold amplitude. However, the amplitude, minimizing the energy input, deviates from the threshold amplitude more and more with the growing crack length (Fig. 8.11).

8.11 Conclusions on energy input optimisation in dynamic fracture

The results received stand for a possibility to optimize energy consumption of different fracture connected industrial processes (e.g. drilling, grinding, pounding, etc.). It is shown that the energy cost of crack propagation strongly depends on the amplitude and frequency of the load applied. For example, in the studied problem when the frequency of the load differs from the optimal one by 10%, energy cost of the crack initiation is exceeding the minimal value by more than 10%.

The obtained dependencies of the optimal characteristics of a load pulse on the existing crack length can help predicting optimae energy saving parameters for fracture processes by means of investigating the predominant crack size in a fractured material.

8.12 Energy input minimisation in detonation initiation

Possibility to minimise energy needed to initiate detonation in different (gaseous, spray, solid) explosive media is of extreme importance in connection to a big number of applications. Among these we can mention pulse detonation engines. For pulse detonation engines initiation of detonation is one of the central design problems and in many cases energy requited to detonate the fuel is exceeding practically attainable limits.

In chapter 12 incubation time criterion for detonation is presented and analysed. It is shown how one can find optimal energy saving parameters for electric discharges initiating detonation in gaseous media utilising the incubation time approach in detonation. Having parameters of the detonating media (incubation time of the detonation and critical energy input rate) that can be evaluated experimentally, the problem of finding the optimal (minimising energy input) shape for pulse producing detonation is reduced to simple calculations.

References

ABAQUS USER MANUAL, Version 6.4, Hibbit, Karlson & Sorensen, Inc.

Dally, J. W., Barker, D. B., 1988. Dynamic measurements of initiation toughness at high loading rates. Experimental Mechanics 28, 298–303.

Irwin, G., 1957. Analysis of stresses and strains near the end of a crack traversing a plate. Journal of Applied Mechanics 24, 361–364.

Morozov, N., Petrov, Y., 2000. Dynamics of Fracture. Springer, Berlin.

Petrov, Yu. V., Utkin, A. A., 1989. On the rate dependences of dynamic fracture toughness. Soviet Material Science 25 (2), 153–156.

Petrov, Y. V., Morozov, N. F., 1994. On the modeling of fracture of brittle solids. ASME Journal of Applied Mechanics 61, 710–712.

Petrov, Y., Taraban, V., 1997. On double-criterion models of the fracture of brittle materials. St.-Petersburg University Mechanics Bulletin 2, 78–81.

Petrov, Y. V., Morozov, N. F., Smirnov, V. I., 2003. Structural macromechanics approach in dynamics of fracture. Fatigue and Fracture of Engineering Materials and Structures 26, 363–372.

Petrov, Y. V., Smirnov, V. I., Krivosheev, S. I., Atroshenko, S. A., Fedorovsky, G. D., Utkin, A. A. Pulse loading of rocks. In: Extreme strength of materials and structures. Detonation. Shock waves. Proc. of the International conference VII Khariton's topical scientific readings (March 14–18, 2005). Absracts. Sarov. 2005; p. 189–190.

Ravi-Chandar, K., Knauss, W. G., 1984. An experimental investigation into dynamic fracture. International Journal of Fracture 25, 247–262.

Royal Dutch Petroleum Company Annual Report, 2003.

Smith, G. C., 1975. An experimental investigation of the fracture of a brittle material. Ph. D. Thesis, California Institute of Technology.

Chapter 9

Kinetic approach in fracture*

Kinetic approach in fracture. Autowave fracture model. Crack as a wave of damage

9.1 Introduction

Classical quasistatic fracture criteria are usually represented in the terms of instant values of the local stresses (or the stress intensity factor for the crack problems) at the supposed fracture point. In contrast, dynamic fracture modeling is principally based on a characteristic time of microfracture and corresponding micro-relaxation (micro-redistribution) processes preceding the macro-fracture event. In order to account the integral contribution of such processes to the dynamic fracture phenomenon an incubation time approach was proposed in Morozov et al. (1990) and developed in Petrov (1991, 1996). Introducing a characteristic time of micro-relaxation processes (the incubation time) as a structural material parameter together with the static fracture toughness it is possible to state the criterion of macroscopic fracture (e.g. see Petrov et al., 2003, and Pugno, 2006). But a continual description of fracture evolution at the microscopic scale has not been provided.

To describe the microfracture evolution (including processes of nucleation, interaction and following coalescence of microfracture — microcracks, microdamage, vacancies and so on) we have defined the function describing an instant local microfracture state (the damage function). Then we have derived the law of damage function behavior based on the transfer equation, the principles of damage mechanics and the incuba-

*Authors acknowledge Dr. A. Kashtanov for his significant contribution to this chapter.

tion time approach. A detailed analysis has been conducted for the one-dimensional problem. Finally the process of dynamic crack nucleation has been simulated starting from experimental results.

In this chapter paper by A. Kashtanov, Y. Petrov et al. (Kashtanov et al., 2008) is extensively used.

9.2 Diffusion description of dynamic fracture

Firstly let us derive the kinetic equation describing the microfracture process as a particular case of the transfer equation. We fix an arbitrary stationary domain Ω inside the considered solid and introduce the damage function $\theta(\bar{r},t) \in [0,1]$ to characterize the relative volume of microfracture (microdamage) in solid's mass unit in the neighborhood of every point $\bar{r} \in \Omega$. Then $\theta = 0$ corresponds to the intact material whereas $\theta = 1$ to the local state of macroscopic fracture. $\theta_\Omega(t) = \int_\Omega \rho(\bar{r})\ \theta(\bar{r},t)\ d\bar{r}$ describes the evolution of local material density in Ω during the microfracture process, where ρ is the local density of the initial intact material. We can apply the transfer principle for θ_Ω: the change of θ_Ω inside of Ω is caused by a flux of microfracture J_{θ_Ω} through the boundary $\partial\Omega$ and by an internal sources of microfracture Σ_{θ_Ω}. That is

$$\frac{d}{dt}\theta_\Omega(t) = -J_{\theta_\Omega} + \Sigma_{\theta_\Omega}. \tag{9.1}$$

Let $\bar{j}_\theta d\bar{s}$ denote the elementary flux of θ through the area $d\bar{s}$ having the outer normal $\bar{n}$; similarly $\sigma_\theta d\bar{r}$ defines the rate of internal sources of θ in the neighborhood of point $d\bar{r}$ inside Ω. Then, according to the divergence theorem, we obtain:

$$J_{\theta_\Omega} = \int\limits_{\partial\Omega} \bar{j}_\theta d\bar{s} = \int\limits_{\Omega} \nabla\cdot\bar{j}_\theta d\bar{r} \tag{9.2}$$

and

$$\Sigma_{\theta_\Omega} = \int\limits_{\Omega} \sigma_\theta d\bar{r}. \tag{9.3}$$

Owing to the fact that the domain Ω is fixed in space we have:

$$\frac{d}{dt}\theta_\Omega = \frac{d}{dt}\int\limits_{\Omega} \rho\theta d\bar{r} = \int\limits_{\Omega} \frac{\partial}{\partial t}(\rho\theta)\, d\bar{r}, \tag{9.4}$$

and due to arbitrary choice of Ω, (9.1) can be rewritten as:

$$\frac{\partial}{\partial t}(\rho\theta) + \nabla \cdot \bar{j}_\theta = \sigma_\theta. \tag{9.5}$$

Supposing the flux of microfracture over the boundary $\partial\Omega$ to be totally determined by diffusion-type processes of microfracture redistribution we can use the Fick's law $\bar{j}_\theta = -D(t)\ \nabla(\rho\theta)$. The function $D(t)$ might be termed relaxation factor. It has the physical meaning of the rate of relaxation processes at the microscale.

Further we will not go beyond the one-dimensional case. Hence, if neglecting the variation of density of an undamaged part of solid (9.5) is reduced to:

$$\frac{\partial\theta}{\partial t} = D(t)\ \frac{\partial^2\theta}{\partial x^2} + f(\theta, x, t), \tag{9.6}$$

where $f(\theta, x, t) = \sigma_\theta/\rho$. (9.6) describes the microfracture evolution in the form of diffusion equation. This equation involves two functions, namely the relaxation factor D and the microfracture source function f, expressions of which with reference to the fracture process have to be clarified. Following this aim, we examine the one-dimensional process of microfracture accumulation from the viewpoint of damage mechanics.

In the general form of damage equation

$$\frac{\partial\theta}{\partial t} = g(\theta, x, t) + f(\theta, x, t) \tag{9.7}$$

the functional $f(\theta, x, t)$ describes the macroscopically uniform process of microfracture accumulation whereas $g(\theta, x, t)$ describes a local stochastic (fluctuating) processes around the point x, namely the local processes of relaxation (redistribution) of microfracture. Let $P(x, t)\ dx$ be the probability of defect "migration" from the point x within a distance dx at the time t. Then we can write

$$g(\theta, x, t) = \psi\left(\int_{-\infty}^{+\infty} \theta(\zeta, t)\, P(\zeta - x, t)\ d\zeta - \theta(x, t)\right), \tag{9.8}$$

where ψ is a constant characterizing the intensity of microfracture redistribution. Since $\int_{-\infty}^{+\infty} P(\zeta, t)\, d\zeta = 1$ then $\int_{-\infty}^{+\infty} \zeta\, P(\zeta, t)\, d\zeta = 0$ as an integral of an odd function. Denoting $R(t) = \sqrt{\int_{-\infty}^{+\infty} \zeta^2 P(\zeta, t)\, d\zeta}$ and expanding the function θ into Taylor series up to the second order terms

$$\theta(\zeta, t) = \theta(x, t) + \frac{\partial \theta(x, t)}{\partial x}(\zeta - x) + \frac{1}{2}\frac{\partial^2 \theta(x, t)}{\partial x^2}(\zeta - x)^2 + o(\zeta - x)^2 \quad (9.9)$$

we can rewrite (9.8) as $g(\theta, x, t) = \frac{\psi}{2} R^2(t) \ \frac{\partial^2 \theta(x,t)}{\partial x^2}$. Then, (9.7) can be reduced to:

$$\frac{\partial \theta}{\partial t} = \frac{\psi R^2(t)}{2} \frac{\partial^2 \theta}{\partial x^2} + f(\theta, x, t). \quad (9.10)$$

This equation has the same form (9.6). Comparing them we can express the relaxation factor as:

$$D(t) = \frac{\psi R^2(t)}{2} \quad (9.11)$$

and conclude that the source function $f(\theta, x, t)$ in (9.6) is the term describing the uniform process of microfracture accumulation at the macroscale. We will obtain its exact expression based on the principle of mass conservation.

9.3 Uniform process of microfracture accumulation

Let us choose a sufficiently small domain inside the considered solid to be sure that its density is changing homogeneously with time. Its mass is denoted as m, its volume before deformation is V_0 whereas the total volume of microfracture (microdefects) accumulated inside the chosen portion is V_*. Thus, during the damage process its volume changes as $V = V_0 + V_*$. Change of volume is obviously accompanied by a variation of local density ρ, described by the mass conservation:

$$\frac{1}{\rho}\frac{d\rho}{dt} = -div\, \bar{v}, \quad (9.12)$$

where $\bar{v}$ is a local velocity of material particles.

From the other side we can express the local density as $\rho = \frac{dm}{dV} = \frac{dm}{dV_0}\frac{dV_0}{dV} = \frac{dm}{dV_0}\left(1 - \frac{dV_*}{dV}\right)$. Introducing the damage parameter $\theta = \frac{dV_*}{dV}$ and setting $\rho_0 = \frac{dm}{dV_0}$ we obtain

$$\rho = \rho_0 (1 - \theta). \quad (9.13)$$

Substituting (9.13) into (9.12) yields

$$\frac{d\theta}{dt} = (1 - \theta)\ div\, \bar{v}. \tag{9.14}$$

(9.14) represents the mass conservation law in the form of a kinetic damage equation. To approximate the divergence of local velocity belonging to the right side of (9.14) let us expand it into a power series of θ:

$$div\, \bar{v} = C_0 + C\theta + \bar{o}\,(\theta) + \ldots\ . \tag{9.15}$$

Omitting higher terms in (9.15) and noting absence of volume expansion for the intact material ($div\, \bar{v}|_{\theta=0} = 0$), (9.14) becomes:

$$\frac{d\theta}{dt} = C\theta\,(1 - \theta)\ . \tag{9.16}$$

Here $C = C\,(x,t)$ is an unknown function. In the particular case of C = const, (9.16) represents the well-known simpliest logistic equation, which is often used in damage mechanics to describe the process of damage accumulation.

Recollecting the arguments mentioned above it is suggested:

$$f\,(\theta, x, t) = C\,(x,t)\,\theta\,(1 - \theta)\,. \tag{9.17}$$

The last to define is the exact form of microfracture source intensity $C\,(x,t)$. When $C\,(x,t) = 0$, only microfracture redistribution takes place and a new microfracture is not provided. Besides that, it is natural to suppose that fracture is intensified under the strain and, hence, the intensity of microfracture source has to be determined by the velocity of change of the stress field (or the stress intensity factor in the case of macrocrack existence). Taking into account the incubation time phenomenon, according to Kashtanov and Petrov (Kashtanov and Petrov, 2007), we can define the intensity of microfracture source as

$$C\,(x,t) = \frac{1}{F_c \tau}\,(F\,(t) - F\,(t-\tau))\,. \tag{9.18}$$

Here $F\,(t)$ is the local intensity of stress field and F_c represents its critical value. In the crack problems $F\,(t)$ coincides with the stress intensity factor $F\,(t) = K_{\mathrm{I}}\,(t)$ and F_c is the static fracture toughness. The structural material parameter τ in (9.18) is the structural (incubation) time, which has the meaning of a characteristic time of micro-relaxation processes and could be measured experimentally (e.g. see Morozov and Petrov, 2000).

9.4 Model validation

Let us consider a particular case of (9.6) assuming $D = \text{const}$ and introducing the new dimensionless variables $X = x\Big/\sqrt{\tau D}$ and $T = t/\tau$. Then, (9.6) takes a dimensionless form:

$$\frac{\partial \theta}{\partial T} = \frac{\partial^2 \theta}{\partial X^2} + \Phi\left(\theta, X, T\right), \quad \Phi\left(\theta, X, T\right) = \frac{F\left(T\right) - F\left(T-1\right)}{F_c}\theta\,\left(1-\theta\right). \tag{9.19}$$

In general this equation cannot be solved analytically. Nevertheless, in the particular case when $F\left(T\right)$ increases at constant rate (9.19) becomes the classical Kolmogorov-Petrovsky-Piskunov equation, see Kolmogorov et al. (Kolmogorov et al., 1937)

$$\frac{\partial \theta}{\partial T} = \frac{\partial^2 \theta}{\partial X^2} + \Phi\left(\theta\right), \quad \Phi\left(\theta\right) = \alpha\,\theta\left(1-\theta\right), \tag{9.20}$$

where $\alpha = \frac{F(T)-F(T-1)}{F_c} = \text{const} > 0$. It is well-know that this equation admits the solutions in the form of a kink-type autowave. Indeed, (9.20) is invariant with respect to translation by X and T. Therefore, imposing the appropriate boundary conditions, we can obtain the solutions of this equation which are not depending on the initial condition. It means that after some period of time the solution "forgets" the initial condition and goes in steady-state when the wave front remains the same with time and the front profiles are self-similar (see also Carpinteri, 1994). Supposing that the wave front moves with constant velocity λ from right to left and in the autowave solution $\theta = \theta\left(X - \lambda T\right)$, we can reduce (9.20) to an ordinary differential equation:

$$\varphi\left(\lambda + \frac{d\varphi}{d\theta}\right) = -\alpha\,\theta\left(1-\theta\right), \tag{9.21}$$

where $\varphi\left(\theta\right) = \frac{d\theta}{d(X-\lambda T)}$. The problem (9.21) is known from the theory of laminar flame (e.g. see Zeldovich et al., 1985). In particular, it was proved that under the boundary conditions $\varphi\left(0\right) = 0$ and $\varphi\left(1\right) = 0$ it has an infinite set of solutions with the corresponding spectrum of wave velocities $\lambda \geq 2\sqrt{\alpha}$. Moreover, $\theta = 0$ and $\theta = 1$ are the lower and the upper asymptotes of its solutions. Accordingly, we have verified that, at least in the case when $F\left(T\right)$ increases at a constant rate our equation can be used to describe the propagation of fracture surface as a nonlinear microfracture wave.

It is easy to see that $\theta = 0$ and $\theta = 1$ also bound the solutions of (9.19). Indeed, when $\theta(X_0, T_0) = 0$ or $\theta(X_0, T_0) = 1$ then $\Phi(\theta, X_0, T_0) = 0$ and (9.19) becomes purely diffusive $\theta_T(X_0, T_0) = \theta_{XX}(X_0, T_0)$.

For further investigation of (9.19) the finite-difference scheme of forth order of approximation is designed (see Appendix 1). Having the numerical solution of (9.19), we can define the dimensionless front velocity $V(T)$ of the microfracture wave. Then returning to the dimension variables we obtain:

$$v(t) = \frac{dx}{dt} = V(T)\sqrt{\frac{D}{\tau}}, \tag{9.22}$$

where $v(t)$ is the experimentally measured velocity of macrocrack. Accordingly, the value of the relaxation factor is

$$D = \tau \left(\frac{v(t)}{V(T)}\right)^2. \tag{9.23}$$

(9.23) completes the model for the particular case of the constant rate of microfracture relaxation during fracture process.

Let us note that (9.22) gives an important qualitative result: the dynamic crack speed decreases by increase of the square root of incubation time as $v \sim \tau^{-1/2}$. This result could be useful to design the materials which are able to resist effectively against dynamic fracture.

9.5 Numerical example

We will simulate the process of nucleation rather than propagation of a crack because in this case the microfracture source function $\Phi(\theta, X, T)$ is having a very simple form. The problem of macrocrack propagation can be investigated using the same procedure but with another, more complicated source function.

Let us consider the problem of an elastic plane with initial semi-infinite rectilinear crack $x \in (-\infty, 0]$. The crack faces are subjected to symmetric shock loading $p(t) = PtH(t)$, where $P = \text{const}$ is the loading rate and $H(\varsigma) = \begin{cases} 0, & \varsigma < 0 \\ 1, & \varsigma \geq 0 \end{cases}$ is the Heaviside step function. In this problem the stress intensity factor is defined as $K_{\mathrm{I}}(t) = 2/3\ P\varphi\ (c_1,\ c_2)\ t^{3/2}H(t)$ (Petrov and Sitnikova, 2004), where c_1 and c_2 are the velocities of the longitudinal and transverse waves and $\varphi(c_1,\ c_2) = 4\frac{c_2}{c_1}\sqrt{\frac{c_1^2 - c_2^2}{\pi\ c_1}}$. Then, in compliance to (9.19) we can write the microfracture source function as:

$$\Phi(\theta, X, T) = \\ = \frac{2}{3}\frac{P}{K_{\mathrm{I}c}}\varphi\,(c_1,\ c_2)\ \tau^{3/2}\theta\,(1-\theta)\,\Big(T^{3/2}H\,(T) - (T-1)^{3/2}\,H\,(T-1)\Big)\,. \tag{9.24}$$

In compliance to the analysis conducted in Kashtanov and Petrov (Kashtanov and Petrov, 2007), we can define time t_* as the time from the moment of loading application to the moment of macrocrack initiation from

$$P = \frac{15\,\tau\,K_{1c}}{4\varphi}\ \left(t_*^{5/2} - (t_* - \tau)^{5/2}\right)^{-1}. \tag{9.25}$$

Therefore,

$$\Phi(\theta, X, T) = \frac{5}{2}\,\frac{T^{3/2}H\,(T) - (T-1)^{3/2}\,H\,(T-1)}{T_*^{5/2} - (T_* - 1)^{5/2}}\ \theta\,(1-\theta)\,, \tag{9.26}$$

where $T_* = t_*/\tau$ is the dimensionless time-to-crack initiation.

The right side of (9.26) does not depend on x. Much more important is that $\Phi(\theta, X, T)$, as well as the corresponding solution of (9.19), is fully determined by a single parameter — time-to-crack initiation. That is, for every value T_* we have the same dimensionless solutions $\theta\,(X, T)$, not depending on the material properties. It makes the problem of crack nucleation much simpler than the problem of the subsequent propagation. The difference in the material properties is accounted by the inverse transformation to dimensional variables through the values of τ and D.

We simulate the process of dynamic crack nucleation at the extension of initial crack, namely inside the interval $[0, X_N]$ sufficiently wide to neglect the effect of a right boundary. The initial and boundary conditions are stated in the form

$$\theta\,(X, 0) = 1 - H\,(X)\,, \quad \theta\,(0, T) = 1, \quad \theta\,(X_N, T) = 0. \tag{9.27}$$

Let us consider the experimental data from Ravi-Chandar and Knauss (Ravi-Chandar and Knauss, 1984a, 1984b) obtained on Homalite-100 ($K_{\mathrm{I}c} = 0.48$ MPa m$^{1/2}$ and $\tau = 8$ μs). In Fig. 9.1 the experimental results related to the time-to-crack initiation t_* (squares) as well as the initial velocity of macrocrack v (circles) are plotted versus four different “reduced” loading rates $P\varphi$.

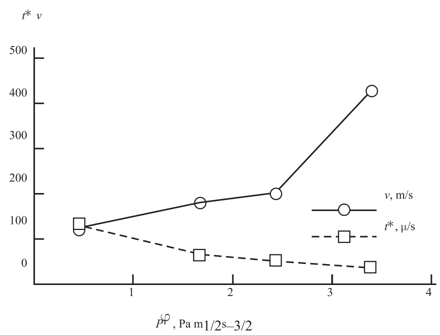

Fig. 9.1. The experimental values of the initial crack velocity v and the corresponding time to crack start t_* for different "reduced" loading rates $P\varphi$.

Fig. 9.2 displays the microfracture accumulation in the process of the crack nucleation for the experimental value $T_* = 4.616$ ($t_* = 37\,\mu$s) in different points close to the tip of the initial crack. Apparently, the dynamic macrocrack is nucleated up to the time T_*.

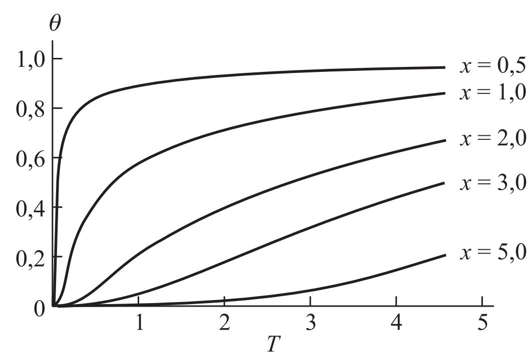

Fig. 9.2. The dependence of the damage function θ on time during the crack nucleation process in different points at the given distances from the initial crack.

The dynamic evolution of damage wave front for the experimental value $T_* = 4.616$ ($t_* = 37\,\mu$s) is presented in Fig. 9.3. The initial crack is continuously diffusing and the fracture process zone (pre-crack zone) corresponding to $0 < \theta < 1$ is being formed.

Fig. 9.4 shows the computed dimensionless velocities V of the microfracture wave front (circles) and the values of relaxation factor D (squares), defined in compliance with (9.23) for different experimental values of the time-to-crack initiation.

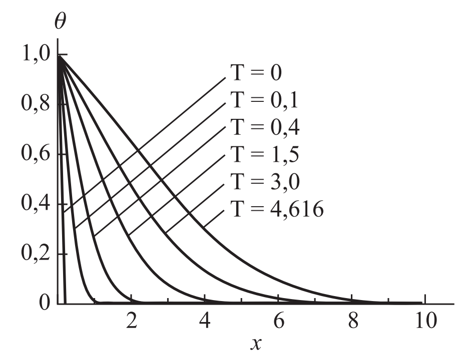

Fig. 9.3. The dependence of the damage function θ on the distances from the initial crack during the macrocrack nucleation process.

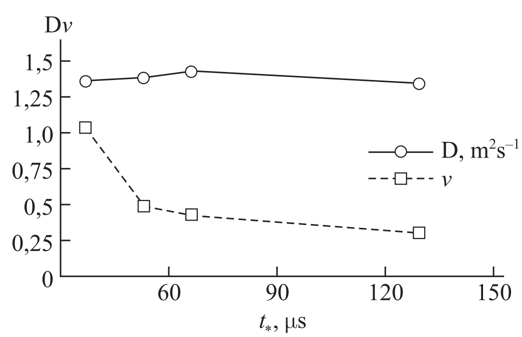

Fig. 9.4. The dependences of relaxation factor D and dimensionless crack velocity V on the time to crack start t_*.

In conclusion, let us make a reference to how one can take the dependence of relaxation factor on the stress state and, hence, on time into account. It is required to simulate dynamic fracture, for example, under a pulsating load. Supposing $D = D(t)$ and changing to dimensionless variables in (9.6) we will not succeed in excluding $D(t)$ from the final equation. Thus, we are obliged to construct a finite-difference scheme with a varied time step and to determine the dependence of relaxation factor on time before starting the simulation. For example, we can determine this dependence having an experimental data describing the morphology of fractured surface or the fracture process zone. Indeed, the relaxation factor determines the characteristic redistribution area of microfracture whereas the incubation time has the physical meaning of the characteristic time of microfracture redistribution processes. Then, the magnitude $\sqrt{D(t)\ \tau}$

determines the characteristic linear size of the fracture process zone accompanying the crack propagation.

9.6 Conclusion

The equation of dynamic fracture evolution as a process of nucleation and subsequent coalesce of microfracture has been derived. Relations between the model parameters and the macroscopic physical characteristics of fracture process (the static fracture toughness and the incubation time) have been defined from the principles of damage mechanics and incubation time approach. Obtained equation describes the propagation of macrocrack as a nonlinear microfracture wave. It was shown that in the case of uniformly increasing stress field (or stress intensity factor) the model can be reduced to the well-known Kolmogorov-Petrovsky-Piskunov equation.

The numerical finite-difference scheme of the forth order of approximation was developed. The stability and convergence of this scheme was proved. For the one-dimensional case, corresponding to the propagation of macrocrack under the assumption of "independent" microfracture relaxation, the equation has been numerically solved. A process of dynamic macrocrack nucleation was simulated using experimental data related to the time-to-crack initiation and the initial crack velocity. The model describes also the crack propagation following the nucleation stage.

Appendix. The finite-difference scheme

The equation to be solved is:

$$\frac{\partial \theta\left(X,T\right)}{\partial T} = \frac{\partial^2 \theta\left(X,T\right)}{\partial X^2} + \Phi\left(\theta, X, T\right) \tag{9.28}$$

with the initial and boundary conditions given by:

$$\begin{gathered} \theta\left(X,0\right) = \Psi\left(X\right), \quad A_0 \frac{\partial \theta\left(0,T\right)}{\partial X} + B_0 \theta\left(0,T\right) = C_0\left(T\right), \\ A_N \frac{\partial \theta\left(X_N,T\right)}{\partial X} + B_N \theta\left(X_N,T\right) = C_N\left(T\right). \end{gathered} \tag{9.29}$$

The approximate solution $\theta \in [0,\ \infty)$ is built inside the domain $(X,T) \in [0, X_N] \times [0, T_M]$, in the vertexes of rectangles of the dimension $h \times s$, that creates a grid sized $0..N \times 0..M$.

Let us rewrite (9.28) in the following form:

$$\Lambda\theta = \Phi\left(\theta, X, T\right), \tag{9.30}$$

where $\Lambda\theta = \theta_T - \theta_{XX}$, and fix the relation between the grid dimensions according to

$$k = s/h^2 = \text{const.} \tag{9.31}$$

We would like to construct the six-nodes implicit finite-difference scheme to approximate the solution of (9.30) with accuracy $O\left(s^2 + h^4\right) = O\left(h^4\right)$. That is, in every point of the grid we have to find the approximation polynomial having the form:

$$\Lambda_h \theta^{\,i,j} = a_1\theta^{\,i-1,j} + a_2\theta^{\,i,j} + a_3\theta^{\,i+1,j} + a_4\theta^{\,i-1,j+1} + a_5\theta^{\,i,j+1} + a_6\theta^{\,i+1,j+1}, \tag{9.32}$$

where a_1,...,a_6 are the constant coefficients identical throughout the grid and $\theta^{i,j} = \theta\left(ih, js\right)$ is the value of the required solution in the corresponding grid point (see Fig. 9.5).

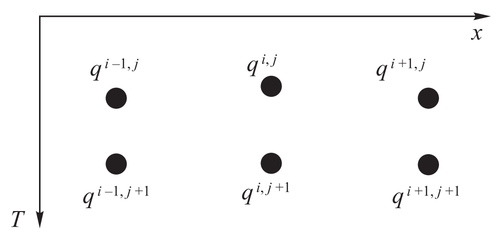

Fig. 9.5. The parabolic equation stencil.

Thus the finite-difference equation corresponding to (9.30) can be written as:

$$\Lambda_h \theta^{i,j} = \Phi\left(\theta^{i,j}, ih, js\right) + O\left(h^4\right), \quad i = 0, 1, ..., N, \quad j = 0, 1, ..., M. \tag{9.33}$$

To construct an approximated solution $\theta^{i,j}$ we have to match the coefficients a_1,...,a_6 to provide the desired accuracy. For simplicity let us impose the following conditions: $a_1 = a_3$ and $a_4 = a_6$. Then, using the expansion into Taylor series we can obtain the expression for$\Lambda_h \theta^{\,i,j}$ in any fixed grid point

(i, j):

$$\begin{aligned}\Lambda_h \theta^{\,i,j} = \ & (2a_1 + a_2 + 2a_4 + a_5)\, \theta^{\,i,j} + \\ & + h^2 (a_1 + a_4)\, \theta^{\,i,j}_{XX} + \frac{h^4}{12} (a_1 + a_4)\, \theta^{\,i,j}_{XXXX} + \\ & + kh^2 (2a_4 + a_5)\, \theta^{\,i,j}_{T} + \frac{k^2 h^4}{2} (2a_4 + a_5)\, \theta^{\,i,j}_{TT} + kh^4 a_4 \theta^{\,i,j}_{XXT} + \\ & + O\left(a_1 h^6, a_4 h^6, (a_4 + a_5)\, k^3 h^6, a_4 k^2 h^6, a_4 k h^6\right). \quad (9.34)\end{aligned}$$

Due to $\theta_T = \Lambda\theta + \theta_{XX}$ we have:

$$\theta_{XXT} = \theta_{TXX} = \Lambda\theta_{XX} + \theta_{XXXX}$$

and

$$\theta_{TT} = (\Lambda\theta + \theta_{XX})_T = \Lambda\theta_T + \Lambda\theta_{XX} + \theta_{XXXX}$$

and (9.34) becomes:

$$\begin{aligned}\Lambda_h \theta^{\,i,j} = \ & (2a_1 + a_2 + 2a_4 + a_5)\, \theta^{\,i,j} + h^2 (a_1 + a_4 + \\ & + k (2a_4 + a_5))\, \theta^{\,i,j}_{XX} + \frac{h^4}{2} \left(\frac{a_1 + a_4}{6} + 2ka_4 + k^2 (2a_4 + a_5) \right) \theta^{\,i,j}_{XXXX} + \\ & + kh^2 (2a_4 + a_5)\, \Lambda\theta^{\,i,j} + \frac{k^2 h^4}{2} (2a_4 + a_5)\, \Lambda\theta^{\,i,j}_{T} + \\ & + kh^4 \left(a_4 + \frac{k}{2} (2a_4 + a_5) + \right) \Lambda\theta^{\,i,j}_{XX} + \\ & + O\left(a_1 h^6, a_4 h^6, (a_4 + a_5)\, k^3 h^6, a_4 k^2 h^6, a_4 k h^6\right). \quad (9.35)\end{aligned}$$

Therefore, to obtain the required accuracy we have to demand (e.g. see Godunov and Ryaben'kii, 1987)

$$\begin{cases} 2a_1 + a_2 + 2a_4 + a_5 = 0 \\ a_1 + a_4 + k (2a_4 + a_5) = 0 \\ \frac{a_1 + a_4}{6} + 2ka_4 + k^2 (2a_4 + a_5) = 0 \end{cases} . \quad (9.36)$$

Using the option to specify the closure condition to combined equations (9.36) we impose:

$$kh^2 (2a_4 + a_5) = 1. \quad (9.37)$$

By solving the system of algebraic equations (9.36)–(9.37) we obtain:

$$a_1 = a_3 = -\frac{1}{2h^2}\left(1+\frac{1}{6k}\right), \quad a_2 = \frac{1}{h^2}\left(1+\frac{1}{6k}-\frac{1}{k}\right),$$
$$a_4 = a_6 = -\frac{1}{2h^2}\left(1-\frac{1}{6k}\right), \quad a_5 = \frac{1}{h^2}\left(1-\frac{1}{6k}+\frac{1}{k}\right). \tag{9.38}$$

Substituting (9.38) into (9.35) and using (9.30) yields:

$$\Lambda_h \theta^{\,i,j} = \Phi^{\,i,j} + \frac{kh^2}{2}\left(\Phi_T^{i,j} + \frac{1}{6k}\Phi_{XX}^{i,j}\right) + O\left(h^4\right), \quad \Phi^{\,i,j} = \Phi\left(\theta^{\,i,j}, ih, js\right). \tag{9.39}$$

Expanding the derivatives of $\Phi^{\,i,j}$ into Taylor series we finally obtain:

$$\Lambda_h \theta^{\,i,j} = \Phi_0^{i,j} + O\left(h^4\right), \tag{9.40}$$

where $\Phi_0^{i,j} = \frac{4}{3}\Phi^{\,i,j} + \frac{1}{12}\left(\Phi^{\,i+1,j} + \Phi^{\,i-1,j} - 6\Phi^{\,i,j-1}\right)$. Thus, (9.28) becomes:

$$a_4\theta^{\,i-1,j+1} + a_5\theta^{\,i,j+1} + a_6\theta^{\,i+1,j+1} = -a_1\theta^{\,i-1,j} - a_2\theta^{\,i,j} - a_3\theta^{\,i+1,j} + \Phi_0^{i,j}. \tag{9.41}$$

It is easy to see that the constructed scheme is a refined modification of the Crank-Nicholson scheme (e.g. see Godunov and Ryaben'kii, 1987):

$$\frac{\theta^{\,i,j+1} - \theta^{\,i,j}}{s} = \mu\frac{\theta^{\,i-1,j+1} - 2\theta^{\,i,j+1} + \theta^{\,i+1,j+1}}{h^2} + \\ + (1-\mu)\frac{\theta^{\,i-1,j} - 2\theta^{\,i,j} + \theta^{\,i+1,j}}{h^2},$$

where $\mu = \frac{1}{2}\left(1 - \frac{1}{6k}\right)$.

Finalizing the implicit difference formula the initial and boundary conditions (9.29) can be rewritten, using the expansion into Taylor series, as

$$\theta^{\,i,0} = \Psi\left(ih\right),$$
$$-\frac{A_0}{2h}\theta^{\,2,j} + \frac{4A_0}{2h}\theta^{\,1,j} + \left(B_0 - \frac{3A_0}{2h}\right)\theta^{\,0,j} = C_0\left(js\right),$$
$$\frac{A_N}{2h}\theta^{\,N-2,j} - \frac{4A_N}{2h}\theta^{\,N-1,j} + \left(B_N + \frac{3A_N}{2h}\right)\theta^{\,N,j} = C_N\left(js\right). \tag{9.42}$$

Finally, (9.41) and (9.42) (for every value of $j > 1$) can be combined in the following matrix form:

$$\mathrm{A}\Theta^{^{j+1}} = -\mathrm{B}\Theta^{^{j}} + Y^{^{j}}, \tag{9.43}$$

where

$$\mathrm{A} = \begin{pmatrix} B_0 - \frac{3A_0}{2h} & \frac{4A_0}{2h} & -\frac{A_0}{2h} & 0 & \dots & 0 \\ a_4 & a_5 & a_6 & 0 & \dots & 0 \\ 0 & a_4 & a_5 & a_6 & \dots & 0 \\ \vdots & \vdots & \vdots & \vdots & \vdots & \vdots \\ 0 & \dots & 0 & a_4 & a_5 & a_6 \\ 0 & \dots & 0 & \frac{A_N}{2h} & -\frac{4A_N}{2h} & B_N - \frac{3A_N}{2h} \end{pmatrix}_{(N+1)\times(N+1)}, \tag{9.44}$$

$$\mathrm{B} = \begin{pmatrix} 0 & 0 & 0 & 0 & \dots & 0 \\ a_1 & a_2 & a_3 & 0 & \dots & 0 \\ 0 & a_1 & a_2 & a_3 & \dots & 0 \\ \vdots & \vdots & \vdots & \vdots & \vdots & \vdots \\ 0 & \dots & 0 & a_1 & a_2 & a_3 \\ 0 & \dots & 0 & 0 & 0 & 0 \end{pmatrix}_{(N+1)\times(N+1)},$$

$$\Theta^{\,j} = \begin{pmatrix} \theta^{\,0,j} \\ \theta^{\,1,j} \\ \theta^{2,j} \\ \vdots \\ \theta^{\,N-1,j} \\ \theta^{\,N,j} \end{pmatrix}_{N+1}, \quad Y^{\,j} = \begin{pmatrix} C_0\left(js\right) \\ \Phi_0^{1,j} \\ \Phi_0^{2,j} \\ \vdots \\ \Phi_0^{N-1,j} \\ C_N\left(js\right) \end{pmatrix}_{N+1}. \tag{9.45}$$

The solution for $j=0$ is given by the initial condition (9.42) but for $j=1$ it has to be defined from different considerations. The reason of picking out the case of $j=1$ is obvious. The relation (9.40) shows that the value $\Phi_0^{i,0}$ depends on $\Phi^{\,i,-1}$, which is undetermined. Nevertheless we can define the value of $\theta^{\,i,1}$ directly from the initial condition (9.42), which can be written as $\theta_{XX}^{i,0} = \Psi_{XX}^{\,i}$. Using a Taylor expansion we have $\theta^{\,i,1} = \theta^{\,i,0} + s\theta_T^{i,0} + O\left(s^2\right)$, and from (9.30) $\theta_T^{i,0} = \Lambda\theta^{\,i,0} + \theta_{XX}^{i,0}$ and $\Lambda\theta^{\,i,0} = \Phi^{\,i,0}$. Therefore, the approximate solution for $j=1$ can be expressed as

$$\theta^{\,i,1} = \Psi^{\,i} + kh^2\left(\Phi^{\,i,0} + \Psi_{XX}^{\,i}\right) + O\left(h^4\right), \quad i = 0, 1, ..., N \tag{9.46}$$

Thus we have constructed the implicit numerical scheme of the forth order of approximation to solve nonlinear parabolic equation (9.28–9.29). Further considerations are concerned to a particular case of our interest corresponding to the process of fracture, characterized by $\theta\left(x,t\right) \in [0,\,1]$.

Now let us prove the stability of the constructed approximation scheme and the convergence of numerical solution to the exact one. We will carry out the proof for the case $1/6 \le k \le 5/6$. This is sufficient for our applications and in this case the proof is extremely simple. Firstly let the problem described by (9.28) and (9.29) be rewriten in the following form

$$\begin{aligned} \Lambda_h \theta^{\,i,j} &= \Phi_0^{i,j} \\ \theta^{\,i,0} &= \Psi^{\,i} \end{aligned}, \tag{9.47}$$

where $\Lambda_h \theta^{\,i,j}$ are defined by (9.32) and (9.38), $\Phi_0^{i,j}$ is determined by (9.40) and $\Psi^{\,i} = \Psi\,(ih)$. It is easy to show that if the inequality

$$\max_j \sup_i \left|\theta^{\,i,j}\right| \le C\,\left(\sup_{i,j}\left|\Phi_0^{i,j}\right| + \sup_i \left|\Psi^{\,i}\right|\right) \tag{9.48}$$

is valid then the numerical scheme is stable (e.g. see Godunov and Ryaben'kii, 1987). Here C is a positive constant. For the considered case $1/6 \le k \le 5/6$ the coefficients are limited by

$$\begin{aligned} a_1, a_3 &\in \left[-\frac{1}{h^2}, -\frac{3}{5h^2}\right], \quad a_2 \in \left[-\frac{4}{h^2}, 0\right], \\ a_4, a_6 &\in \left[-\frac{2}{5h^2}, 0\right], \quad a_5 \in \left[\frac{2}{h^2}, \frac{6}{h^2}\right]. \end{aligned} \tag{9.49}$$

The codomain of the approximated solution is the interval $[0,1]$, and using (9.32) we obtain the estimation $\left|\Lambda_h \theta^{\,i,j}\right| \ge \left|a_2 \theta^{\,i,j} + a_5 \theta^{\,i,j+1}\right| = -\left|a_2\right| \left|\theta^{\,i,j}\right| + \left|a_5\right| \left|\theta^{\,i,j+1}\right|$. According to (9.47) and after simple manipulations we have

$$\sup_i \left|\theta^{\,i,j+1}\right| \le 2 \sup_i \left|\theta^{\,i,j}\right| + C_1 \sup_{i,j} \left|\Phi_0^{i,j}\right|, \quad C_1 = h_0^2 \left(1 - \frac{1}{6k} + \frac{1}{k}\right)^{-1}. \tag{9.50}$$

In the same manner we can write the inequalities

$$\begin{aligned} &\sup_i \left|\theta^{\,i,j}\right| \le 2 \sup_i \left|\theta^{\,i,j-1}\right| + C_1 \sup_{i,j} \left|\Phi_0^{i,j}\right|, \\ &\cdots \\ &\sup_i \left|\theta^{\,i,1}\right| \le 2 \sup_i \left|\theta^{\,i,0}\right| + C_1 \sup_{i,j} \left|\Phi_0^{i,j}\right|. \end{aligned}$$

After composition of all the inequalities, including the initial condition and the fact that $j \leq M$, we finally estimates:

$$\sup_i \left|\theta^{\,i,j+1}\right| \leq 2^M \left(1 + C_1\right) \left(\sup_{i,j} \left|\Phi_0^{\,i,j}\right| + \sup_i \left|\Psi^{\,i}\right|\right), \quad i = 0, 1, ..., N. \tag{9.51}$$

This means that inequality (9.48) is valid for every $C \geq 2^M \left(1 + C_1\right)$ and, hence, the numerical scheme (9.47) is absolutely stable in the considered particular case $1/6 \leq k \leq 5/6$. Thus, according to Philippov's theorem (e.g. see Godunov and Ryaben'kii, 1987) the numerical solution converges to the exact solution of problem the (9.28) and the order of its convergence coincides with the order of scheme approximation.

References

Carpinteri, A., 1994, *Scaling* laws and renormalization groups for strength and toughness of disordered materials. *International Journal of Solids and Structures* 31, 291–302.

Godunov, S. K., Ryaben'kii, V. S., 1987, *Difference schemes: an introduction to underlying theory*. North-Holland, New York-Amsterdam.

Kashtanov, A. V., Petov, Yu. V., 2007, Kinetic description of incubation processes under dynamic fracture. *Doklady Physics* 52, 270–273.

Kashtanov, A. V., Petrov, Yu. V., Pugno, N., Carpinteri A., 2008, Dynamic fracture as a process of nonlinear damage wave propagation, International Journal of Fracture, 150, 2:227–240.

Kolmogorov, A. N., Petrovsky, I. G., Piskunov, N. S., 1937, Etude de l'équation de la diffusion avec croissance de la quantité de matière et son application à un problème biologique. *Bull. Univ. d'Etat Moscou*, *Série internationale* A 1, 1–26.

Morozov, N. F., Petrov, Y. V., 2000, *Dynamics of Fracture*. Springer-Verlag, Berlin-Heidelberg.

Morozov, N. F., Petrov, Y. V., Utkin, A. A., 1990, On the analysis of spalling on the basis of structural fracture mechanics. *Doklady Akademii Nauk USSR* 313, 276–279 (in Russian).

Petrov, Y. V., 1991, On "quantum" nature of dynamic fracture of brittle solids. *Doklady Akademii Nauk USSR* 321, 66–68 (in Russian).

Petrov, Y. V., 1996, Quantum analogy in the mechanics of fracture of solids. *Physics of Solid State* 38, 1846–1850.

Petrov, Y. V., Morozov, N. F., Smirnov, V. I., 2003, Structural macromechanics approach in dynamics of fracture. *Fatigue and Fracture of Engineering Materials and Structures* 26, 363–372.

Petrov, Yu. V., Sitnikova, E. V., 2004, Dynamic cracking resistance of structural materials predicted from impact fracture of an aircraft alloy. *Technical Physics* 1, 57–60.

Pugno, N., 2006, Dynamic quantized fracture mechanics. *International Journal of Fracture* 140, 158–168.

Ravi-Chandar, K., Knauss W. G., 1984a, An experimental investigation into dynamic fracture: I. Crack initiation and arrest. *International Journal of Fracture* 25, 247-262.

Ravi-Chandar, K., Knauss W. G., 1984b, An experimental investigation into dynamic fracture: II. Microstructural aspects. *International Journal of Fracture* 26. 65-80.

Zeldovich, Ya. B., Barenblatt, G. I., Librovich, V. B., and Makhviladze, G. M., 1985, *Mathematical theory of combustion and explosions.* Consultants Bureau, New York.

Chapter 10

Incubation time criterion for dynamic yielding*

Dynamic yielding of metals. Application of the incubation time approach to predict rate dependency of yielding. Ductile-to-brittle transition at dynamic fracture. Anomalous yielding under high rate loading

10.1 The Incubation Time and Criteria of Fracture and Yielding

An efficient criterion for the analysis of brittle fracture for defect-free material was formulated in Chapter 4:

$$\int_{t-\tau}^{t} \sigma(s)ds < \sigma_S \tau, \tag{10.1}$$

where τ is the incubation time, σ_S is ultimate stress for quasi-static loading and $\sigma(t)$ is the local stress. The moment of fracture t_* corresponds to equality in (10.1) or, in the general case, non-compliance with this condition. Criterion (10.1) has shown a good correspondence with experimental results for many materials in wide range of loading rates.

A similar approach can be used to predict dynamic yielding. Various applications (e.g. practical engineering problems, analysis of experimental data obtained by different techniques) require a simple and usable yield criterion applicable for arbitrary loading history. For mild steel such a criterion was proposed by J. D. Campbell (Campbell, 1953). According to the dislocation theory of Cotrell—Bilby (Cotrell, Bilby, 1949), time necessary to nucleate a dislocation is proportional to

$$\exp\left(\frac{U(\sigma/\sigma_0)}{kT}\right), \tag{10.2}$$

*Authors acknowledge Dr. A. Gruzdkov and Ms. Sitnikova for their significant contribution to this chapter.

where T is the absolute temperature, σ_0 is the yield limit at T=0K (obtained by extrapolation), k is the Boltzman constant, U is the activation energy and σ is the local stress. Assuming that yielding occurs when the dislocation density reaches a critical value, J. D. Campbell received yielding criterion in the following form:

$$\int_0^{t_*} \exp\left(-\frac{U(\sigma(t)/\sigma_0)}{kT}\right) dt = Const.$$

T. Yokobory proposed (Yokobory, 1952) the following approximation for the activation energy:

$$U(\sigma/\sigma_0) = -\frac{1}{n}\ln\frac{\sigma}{\sigma_0},$$

where n is a constant. Thus, Campbell's criterion can be rewritten:

$$\int_0^{t_*} (\sigma(t))^\alpha dt = Const, \tag{10.3}$$

where $\alpha = (nkT)^{-1}$. It is evident that this criterion contradicts the quasi-static approach:

$$\sigma(t) \le \sigma_Y, \tag{10.4}$$

where σ_Y is the static yield limit. Here we can conclude that Campbell's criterion is valid for very short loading pulses. Although in his later works (e.g. Campbell, 1953) Campbell claims that the dislocation theory of Cotrell—Bilby can perform unsatisfactory for mild steel, (10.3) may be considered as a good phenomenological dynamic yield criterion for various materials.

Nevertheless in many problems (for example, studying brittle-to-ductile fracture transition or temperature dependencies that will be discussed below) it is very important to have a criterion applicable for arbitrary load duration and amplitude. Obviously, Campbell's criterion is not an issue. In (Gruzdkov, Petrov, 1991, Gruzdkov, Petrov, 1999) a new yield criterion was proposed:

$$\frac{1}{\tau_Y}\int_{t-\tau_Y}^{t} \left(\frac{\sigma(s)}{\sigma_Y}\right)^\alpha ds < 1, \tag{10.5}$$

where τ_Y is the incubation time of yielding process, σ_Y is the static yield limit, α is the dimensionless shape parameter (usually $\alpha > 1$). It is easy to show that if stresses change "slowly" (as comparing to τ_Y) then the criterion given by (10.5) is in a close agreement with the static criterion of critical stress (10.4). In case of loads with durations comparable or less than the incubation time τ_Y the criterion (10.5) is evidently similar to the criterion of Campbell (10.3).

Some advantages of criteria given by (10.1) and (10.5) should be mentioned. They are applicable for arbitrary stress-time dependencies. For example criterion for yielding given by (10.5) can explain both the growth of the yield limit in tests with constant strain rate (e.g. Campbell, Ferguson, 1970, Meyers, 1994) and "yield delay" in experiments with constant stress applied to a sample (e.g. Kraft, Sullivan, 1959). These criteria are valid for arbitrary load duration. It should be also mentioned that behavior of material is described using a limited set of constants that can be determined experimentally.

10.2 Determination of Dynamic Yield Limit and Dynamic Strength for Some Class of Experiments

Consider uniaxial tension or compression of a bar.

10.2.1 *Constant Strain-Rate*

In this case

$$\sigma(t) = E\dot{\varepsilon}\, tH(t), \tag{10.6}$$

where $H(t)$ is the Heaviside step function, E is the Young's modulus, $\dot{\varepsilon}$ is the strain rate (supposed to be a constant). Substituting (10.6) into (10.5) one receives:

$$\left(\frac{t_*^{(Y)}}{\tau_Y}\right)^{\alpha+1} - \left(\frac{t_*^{(Y)}}{\tau_Y} - 1\right)^{\alpha+1} H\left(\frac{t_*^{(Y)}}{\tau_Y} - 1\right) = \frac{(\alpha+1)\sigma_Y^{\alpha}}{(\tau_Y E\dot{\varepsilon})^{\alpha}}, \tag{10.7}$$

where t_* is time-to-yielding. The yield stress is given by:

$$\sigma_* = \sigma(t_*).$$

Auxiliary variables are introduced:

$$y = \frac{\sigma_*}{\sigma_Y} \quad \text{and} \quad x = \frac{E\,\tau\,\dot{\varepsilon}}{\sigma_Y}.$$

As follows from (10.7), for "rapid" (i.e. $y \le x$) loading

$$y = (x \cdot (1+\alpha))^{1/(\alpha+1)}\,, \quad \text{for} \quad x \ge (\cdot 1+\alpha)^{1/(\alpha+1)}\,.$$

For "slow" (i.e. $y > x$) loading y can be easily found by iterations using:

$$y^{\alpha+1} - (y-x)^{\alpha+1} = x \cdot (1+\alpha)\,, \quad \text{for} \quad x < (\cdot 1+\alpha)^{1/(\alpha+1)}\,.$$

For $\alpha = 1$ (see (10.1)) the solution can be obtained explicitly:

$$\sigma_* = \begin{cases} 2\sigma_S \cdot \sqrt{\dot{\varepsilon}/\dot{\varepsilon}_S}, & \dot{\varepsilon} \ge \dot{\varepsilon}_S \\ \sigma_S\,(1 + \dot{\varepsilon}/\dot{\varepsilon}_S) & \dot{\varepsilon} < \dot{\varepsilon}_S \end{cases}\,,$$

where $\dot{\varepsilon}_S = \frac{2\sigma_S}{E\tau}$. From (10.7) one can also determine time-to-yielding or time-to-fracture (t_*). For $\alpha = 1$ solution for $t_*(\dot{\varepsilon})$ can be received in an explicit form:

$$t_* = \begin{cases} \tau \cdot \sqrt{\dot{\varepsilon}_S/\dot{\varepsilon}}, & \dot{\varepsilon} \ge \dot{\varepsilon}_S \\ \frac{\tau}{2}\,(1 + \dot{\varepsilon}_S/\dot{\varepsilon}) & \dot{\varepsilon} < \dot{\varepsilon}_S \end{cases} \tag{10.8}$$

In case of $\alpha \ne 1$ (10.7) can be easily solved by iterations.

10.2.2 *Constant Stress*

In some experimental schemes (e.g. Kraft, Sullivan, 1959) the applied stress is maintained at a constant level throughout the experiment. Despite the fact that the value of the stress applied (σ_*) is significantly exceeding the static yield limit, yielding occurs not immediately but after some measurable period of time, ("yield delay"). In order to find this time using the incubation time approach one can substitute (10.5) with $\sigma(t) = \sigma_* \cdot H(t)$. For $\sigma_* < \sigma_Y$ according to (10.5) yielding is not possible. For $\sigma_* \ge \sigma_Y$ one can obtain:

$$t_* = \tau_Y \cdot \left(\frac{\sigma_*}{\sigma_Y}\right)^{\alpha} \tag{10.9}$$

(10.9) can be rewritten as

$$\log t_* - \alpha \log \sigma_* = C$$

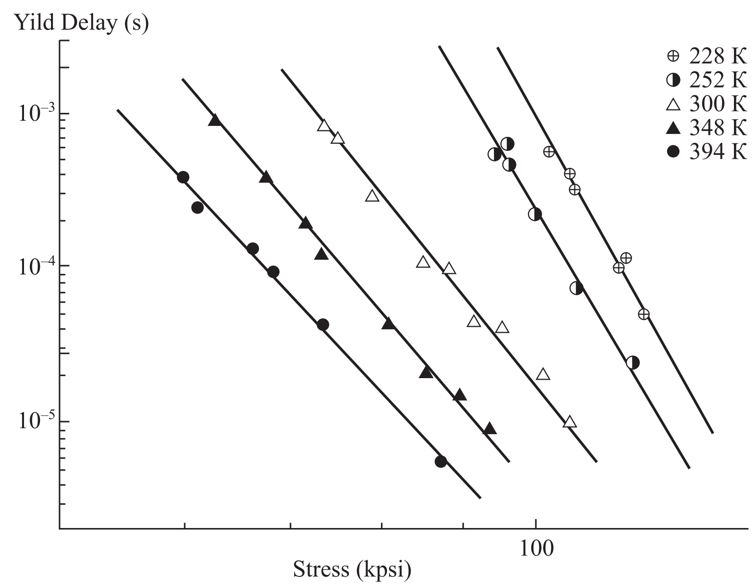

Fig. 10.1. Yield delay as a function of stress applied (mild steel, C0.22, Mn0.36). Experimental points are taken from Kraft and Sullivan (Kraft, Sullivan, 1959).

According to this the shape parameter α is the slope of the line in the logarithmic scale. Comparison of (10.9) to experimental data reported by Kraft and Sullivan (Kraft, Sullivan, 1959) and reprinted in Fig. 10.1 shows a good coincidence. It can also be noticed that α is decreasing with increasing temperature.

10.2.3 *Impact Loading*

In case of a pressure pulse with duration D and amplitude A the stress-time dependence can be approximated by:

$$\sigma(t) = \begin{cases} A \sin\left(\frac{\pi\, t}{D}\right), & 0 < t < D \\ 0, & otherwise \end{cases} \tag{10.10}$$

The problem is to determine the threshold value of amplitude A (i.e. the smallest possible value of the pulse amplitude that will lead to yielding (fracture), for given D. For the threshold pulse the following equality is satisfied:

$$\max_t \left\{ \frac{1}{\tau_Y} \cdot \int\limits_{t-\tau_Y}^{t} \left(\frac{\sigma(s)}{\sigma_Y} \right)^\alpha ds \right\} = 1 \tag{10.11}$$

For "short" pulses ($D \leq \tau_Y$) it is evident that $t_* = D$ and substituting (10.10) into (10.11) one can get:

$$\frac{A^\alpha}{\tau_Y \sigma_Y^\alpha} \cdot \int\limits_0^D \left(\sin\left(\frac{\pi \cdot s}{D} \right) \right)^\alpha ds = 1$$

Substituting $X = \frac{\pi\, s}{D}$ one obtains:

$$A^\alpha \frac{2D}{\pi \tau_Y} \cdot \int\limits_0^{\pi/2} (\sin X)^\alpha \, dX = \sigma_Y^\alpha$$

Parameters μ and I_α are defined by:

$$\mu = \frac{2D}{\pi \tau_Y} \quad \text{and} \quad I_\alpha = \int\limits_0^{\pi/2} (\sin X)^\alpha \, dX = \frac{\sqrt{\pi}}{2} \frac{\Gamma\left(\frac{\alpha+1}{2}\right)}{\Gamma\left(\frac{\alpha}{2}+1\right)},$$

where $\Gamma(x)$ is the Euler's gamma function. Then the amplitude is found to be:

$$A = \sigma_Y \cdot \left(\frac{\mu}{I_\alpha} \right)^{1/\alpha}.$$

For "long" pulses ($D > \tau_Y$) in (10.11) one should use $t_* = (D + \tau)/2$. Using a substitution $Z = \pi\,(1/2 - t/D)$ one can obtain:

$$A = \sigma_Y \cdot \left(\frac{1}{\mu} \int\limits_0^{\mu} (\cos Z)^\alpha dZ \right)^{-1/\alpha}.$$

One can find the fracturing amplitude from (10.1), supposing $\alpha = 1$:

$$A = \begin{cases} \sigma_S \cdot \mu, & \mu \geq \frac{\pi}{2} \\ \frac{\sigma_S \cdot \mu}{\sin \mu}, & \mu < \frac{\pi}{2} \end{cases}.$$

For very long pulses ($D \gg \tau$) $\mu \ll 1$ and hence $A \approx \sigma_S$. In this situation the criterion of critical stress (10.4) is valid.

10.3 Temperature Dependence

Loading rate is not the only parameter that influences yielding. Another important parameter is the temperature of the sample tested. The material parameters (σ_Y,τ_Y,α) are known to be strongly dependent on temperature. Analyzing available experimental data for different materials some approximations of these dependencies can be proposed.

The static limit of yielding decreases along with the temperature growth. The following approximation is used to predict temperature dependence of σ_Y:

$$\sigma_y = \sigma_0 \cdot \exp\left(-\frac{T}{T_P}\right), \tag{10.12}$$

where T_P is a constant. The dependency given by (10.12) is frequently used for analysis of low-temperature plasticity. Although it can be derived on the basis of (10.2), we treat it as phenomenological.

Incubation time exponentially grows with decreasing temperature. The dependency is the following:

$$\tau_Y = \tau_0 \exp\left(\frac{U}{kT}\right) , \tag{10.13}$$

where U and τ_0 are constants. (10.13) is directly following from (10.2), assuming that the incubation time is an average time required to nucleate a dislocation. At the same time another explanation is also possible. The value of τ_Y characterizes the rate of a certain process affecting the material structure. Since the transition to the plastic state is connected to the development of some dislocation structure, it is reasonable to assume that this value is related to the temporal characteristic of dislocation motion. Hence the incubation time is expected to be inversely proportional to the velocity of dislocations (v_D):

$$\tau_Y = \frac{\text{const}}{v_D}.$$

The relation proposed by Gilman (see Kraft, Sullivan, 1959):

$$v = v_0 \exp\left(-\frac{U}{kT}\right) ,$$

can act as a theoretical background for (10.13).

The dimensionless shape parameter α decreases with increasing temperature. The analysis of numerous experimental data had shown that the relation proposed by J. D. Campbell (equation (10.3)):

$$\alpha = \frac{\text{const}}{T}$$

is not valid for many materials. In some cases it can be used only for relatively high temperature, for some materials parameter α is slightly depending on temperature. Here a more general formula for shape parameter α is proposed:

$$\alpha = \alpha_0 \left(1 - \exp\left(-\frac{W}{kT}\right)\right), \tag{10.14}$$

where α_0 and W are constants.

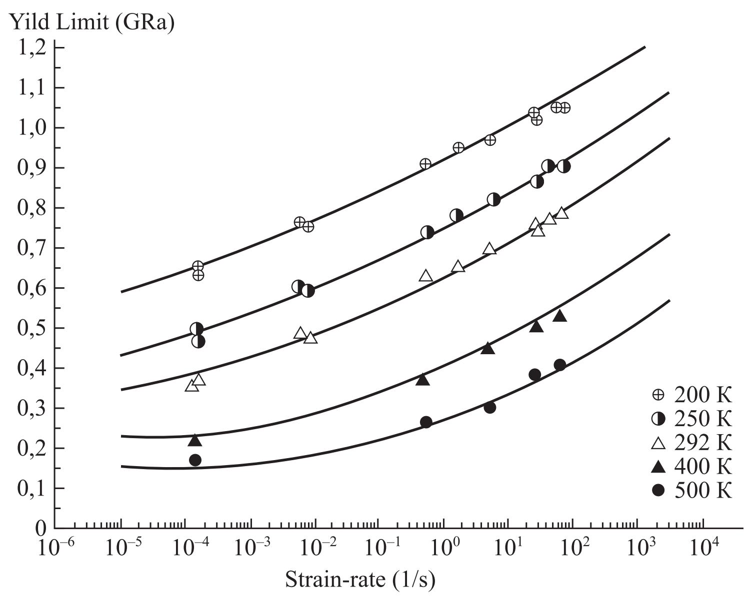

Fig. 10.2. Yield limit of molybdenum as a function of strain rate for various temperatures. Experimental points from Campbell (Campbell, 1973). Theoretical curves obtained using (10.5,10.12–10.14)) with parameters from Table 10.1.

Criterion given by (10.5) with additional relations given by (10.12–10.14) was applied to analyze available experimental data for various materials. The comparison of experimental (Campbell, 1973) and theoretical strain-rate dependencies of yield limit for molybdenum is presented in Fig. 10.2. Analogous comparison for niobium (Campbell, 1973) is presented in Fig. 10.3. Previously published results for mild steel (Gruzdkov,

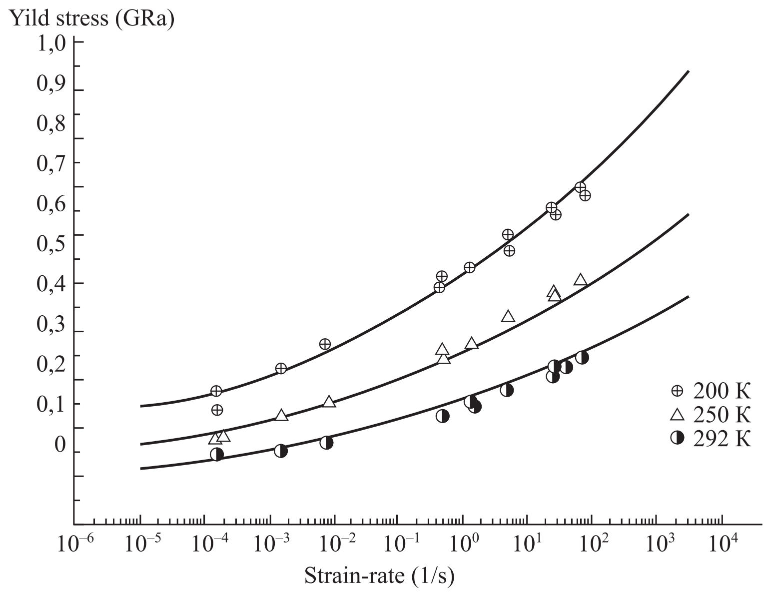

Fig. 10.3. Yield limit of niobium as a function of strain rate for various temperatures. Experimental points from from Campbell (Campbell, 1973). Theoretical curves obtained using (10.5, 10.12–10.14)) with parameters from Table 10.1.

Petrov, 1999) were revised. Fig. 10.4 compares experimental (Campbell, Ferguson, 1970) and theoretically predicted, using the incubation time approach, strain-rate dependencies of yield limits of mild steel. Here the parameters used in criterion (10.5) (α, τ, σ_Y) are not chosen separately for each temperature as in (Gruzdkov, Petrov, 1999) but according to (10.12–10.14). Experimental data for titanium alloy from (Krüger, Meyer, 2003) and theoretically predicted dependencies are compared in Fig. 10.5. Values of parameters appearing in (10.12–10.14) for all the materials discussed, are given in Table 10.1 (with E being the Young's modulus).

Proceeding to fracture properties there are numerous results confirming that σ_S is not so temperature sensitive (e.g. Kanel, Razorenov, 2001). Influence of temperature on the incubation time of fracture was discussed in (Morozov et al., 2002). In the same paper the following relation was proposed:

$$\tau = \tau_0 \frac{G}{kT} , \tag{10.15}$$

where $\tau_0 = 10^{-13}$ s is the period of thermal oscillations of atoms in solids, G

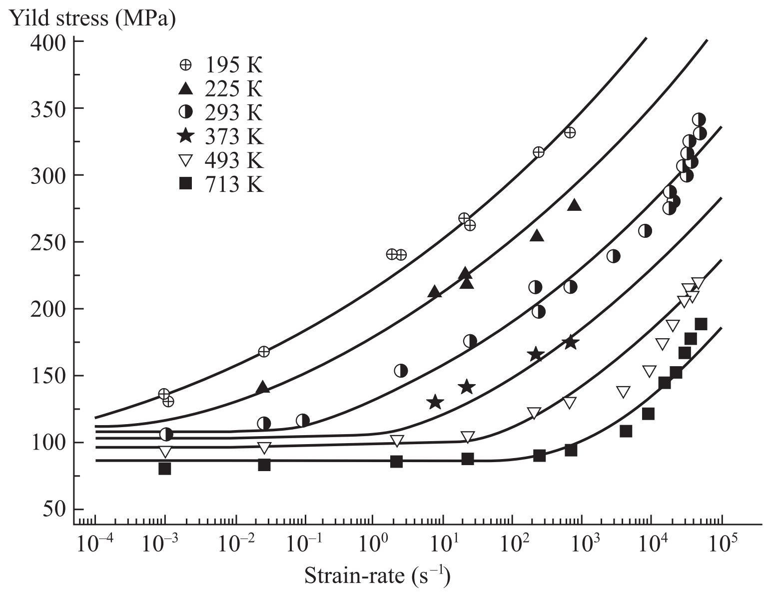

Fig. 10.4. Yield stress of mild steel as a function of strain rate for various temperatures. Experimental points from Campbell and Ferguson (Campbell, Ferguson, 1970). Theoretical curves obtained using (10.5, 10.12–10.14)) with parameters from Table 10.1.

is the portion of energy required to fracture an elementary structural cell of the modeled material. (10.15) gives a possibility to explain the temperature anomaly of strength and melting behavior of aluminum observed in (Kanel, Razorenov, 2001).

10.4 Application to prediction of Brittle-to-Ductile Transition

10.4.1 *The Phenomenological Aspect*

The idea to distinguish brittle and ductile fracture modes has a long history. Despite that, different approaches to fracture classification exist. Moreover, numerous experimental results demonstrate that the above-mentioned classification is rather conventional. Distinction between these two modes of fracture is usually implying the amount of mechanical energy dissipated before fracture occurs. Ductile fracture consumes much more energy as

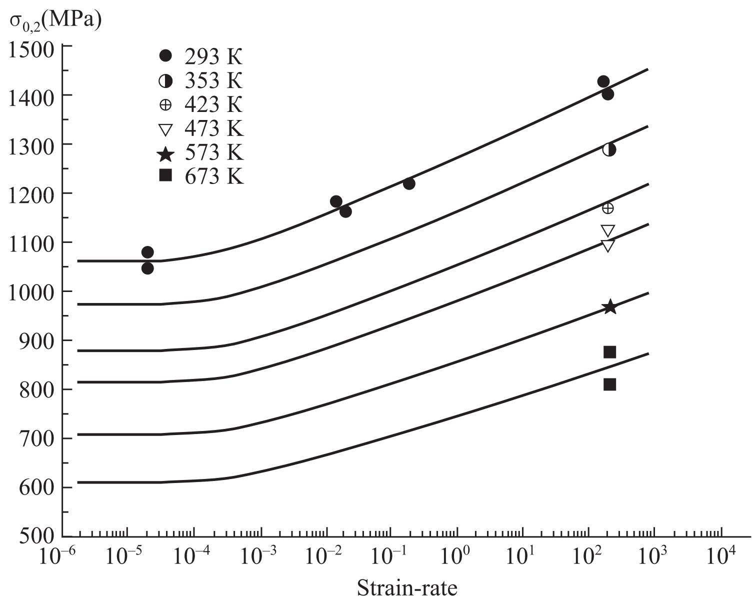

Fig. 10.5. Conventional yield limit of titanium alloy Ti-6-22-22S as a function of strain rate for various temperatures. Experimental points from Krüger and Meyer (Krüger, Meyer, 2003). Theoretical curves obtained using (10.5, 10.12–10.14)) with parameters from Table 10.1.

comparing to the brittle one. However sometimes there is no explicit distinction between these two cases and mixed failure mode is taking place.

In case of dynamic loading determination of the amount of energy dissipated during fracture process can be complicated. Thus, other characteristics of fracture are normally used to distinguish between different fracture modes. Some of them can be mentioned: the orientation of fracture surface, the size of a plastic zone, the value of a limit strain (i.e. strain at the moment of fracture), micro mechanisms of the fracture process etc.

It is well-known that realization of one or another fracture mode depends on both the loading conditions and the material properties. Two different materials may exhibit different fracture modes at similar loading conditions. At the same time the same material can pronouncedly change its behavior if temperature or strain-rate is changed. Therefore it is not correct to call a given material “brittle” or “ductile”.

Here brittle-to-ductile transition is defined as a phenomenon of sudden change in macroscopic fracture characteristics (ductility, strength, size of a plastic zone, fracture toughness, energy dissipated for fracture process

Material	Experimental Data	σ_0	T_P	$E\tau_0$	$\frac{U}{k}$	α_0	$\frac{W}{k}$
		GPa	K	Pa s	K		K
molybdenum	Campbell, 1973	1.04	2632	$6.254 \cdot 10^6$	3534	19150	0.262
niobium	Campbell, 1973	1.22	123.6	$4.79 \cdot 10^{11}$	26.6	12.51	6994
mild steel	Campbell, Ferguson, 1970	0.127	1862	110	4000	16.75	328.7
Ti-6-22-22S	Krüger et al., 2003	1.757	585	$2.762 \cdot 10^9$	1191	75.6	303

Table 10.1: Material properties for materials discussed

etc.) as a result of small changes in loading parameters. These changes in macroscopic fracture characteristics are usually accompanied by a noticeable change of the fracture surface. Brittle-to-ductile transition was observed experimentally for several metals (steels, molybdenum) and alloys (bimetals TiAl, NiAl).

Fracture is influenced by different parameters of the loading process and hence the transition between fracture modes (ductile to brittle and vice versa) may occur due to variation of several parameters: strain-rate, temperature, grain size, size of a specimen etc. Brittle fracture is normally taking place at low temperatures and high strain-rates while ductile fracture can be expected at high temperature and slow loading rates. Many experimental works were aimed on determination of the transition temperature or the critical strain-rate. These investigations are of a practical interest for engineering purposes because the transition temperatures for some sorts of steel are in the range of typical winter season temperatures in some regions of Earth (Siberia, Arctic areas etc.).

10.4.2 *Modeling the Brittle-to-Ductile Transition*

Brittle-to-ductile transition is usually interpreted as the result of competition between two mechanisms of deformation and fracture. The approach presented here is similar to the one developed by A. Yoffe (1929), J. Fridman (1974) and some others. The idea is to consider resistance to cleavage and plastic shear separately. Following this ideology one can obtain dependencies of critical stress on temperature (or on strain-rate) for both cases. The transition temperature (strain-rate) corresponds to the intersection point of these diagrams. What fracture mode will occur depends on what critical value of stress (cleavage or plasticity) is less for given conditions.

This approach can be modified. As the first approximation a model neglecting interaction between these two processes is considered. Using criteria of brittle fracture (10.1) and plastic yielding (10.5) the time necessary for each of the processes to initiate ("fracture delay" and "yield delay") can be estimated. Hence one is able to predict which of them (cleavage or plastic yielding) should happen earlier. If time to fracture (i.e. t_* determined from (10.1)) is less than time to yielding (value $t_*^{(Y)}$ from (10.5) then the brittle mode of fracture will occur and vice versa.

Consider a bar tensioned at a constant rate $\dot{\varepsilon}$. From (10.8) one can obtain $t_*(\dot{\varepsilon})$ for cleavage and solving (10.7) $t_*^{(Y)}(\dot{\varepsilon})$ for yielding can be found. The condition for brittle fracture is :

$$\frac{t_*(\dot{\varepsilon})}{t_*^{(Y)}(\dot{\varepsilon})} < 1 \ .$$

The point of intersection corresponds to the transition strain-rate, i.e.:

$$t_*(\dot{\varepsilon}_T) = t_*^{(Y)}(\dot{\varepsilon}_T)$$

The example presented in Fig. 10.6 is given for hypothetical doped steel with the following characteristics: $\sigma_S = 700\ MPa$, $\sigma_Y = 400\ MPA$, $\tau = 0.5\ \mu s$, $\tau_Y = 0.5\ s$, $\alpha = 11$.

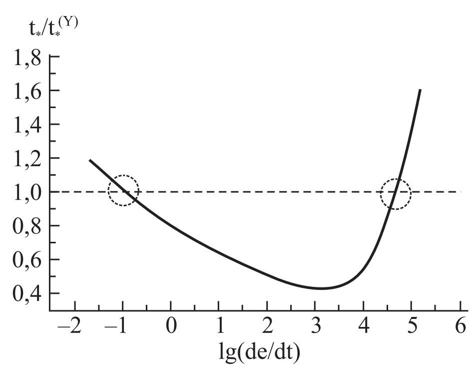

Fig. 10.6. Fracture mode as a function of strain-rate.

Fracture should follow ductile scenario if the strain-rate is less than $\dot{\varepsilon}_T$ and should be brittle otherwise. It is to be mentioned that for extremely high strain-rates there exists another point of intersection. It corresponds to the reverse transition from brittle to ductile mode of fracture if, of course, our model is still applicable for so high loading rates. It should be mentioned that some of the available experimental results indirectly confirm the existence of such a point. The ratio of "fracture delay" t_* to the "yield delay" $t_*^{(Y)}$ plotted in Fig. 10.6 is minimized at some point. Strain-rate corresponding to this point should be the most "dangerous" because the probability of brittle fracture in this case is the highest.

This approach was used (Morozov et al., 2002) to estimate critical size of a particle causing fracture in erosion problems. For particles with sizes less than the critical one the erosion is ductile, otherwise it is brittle.

Now it is possible to find a correspondence between how rate and temperature are affecting the fracture mode. Analysis based on criteria (10.1) and (10.5) should take into account equations (10.12–10.15). If the temperature of ductile-to-brittle transition is experimentally determined for a given loading rate then one can numerically obtain the critical loading rate for any other temperature. And vice versa: if the critical loading rate is known for given temperature then one can calculate the temperature of mode transition for any other loading rate.

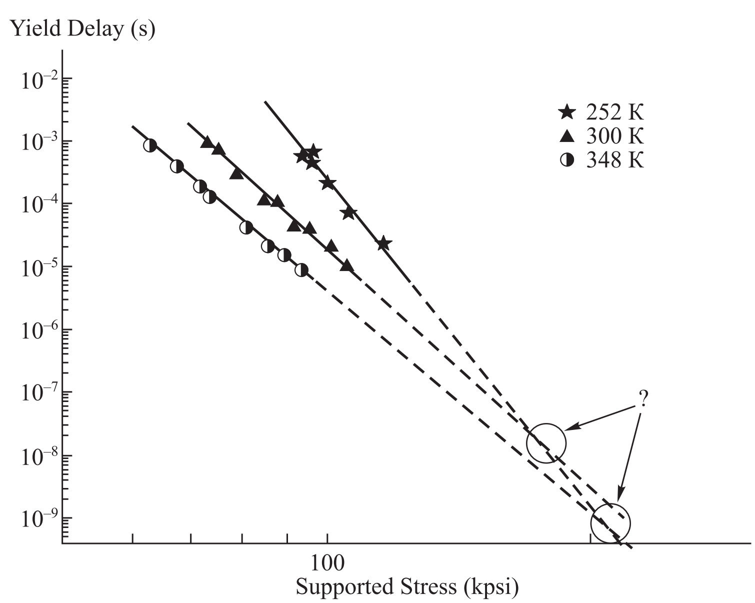

Fig. 10.7. Reversed temperature dependence of yield delay. Experimental points from and Sullivan (Kraft, Sullivan, 1959).

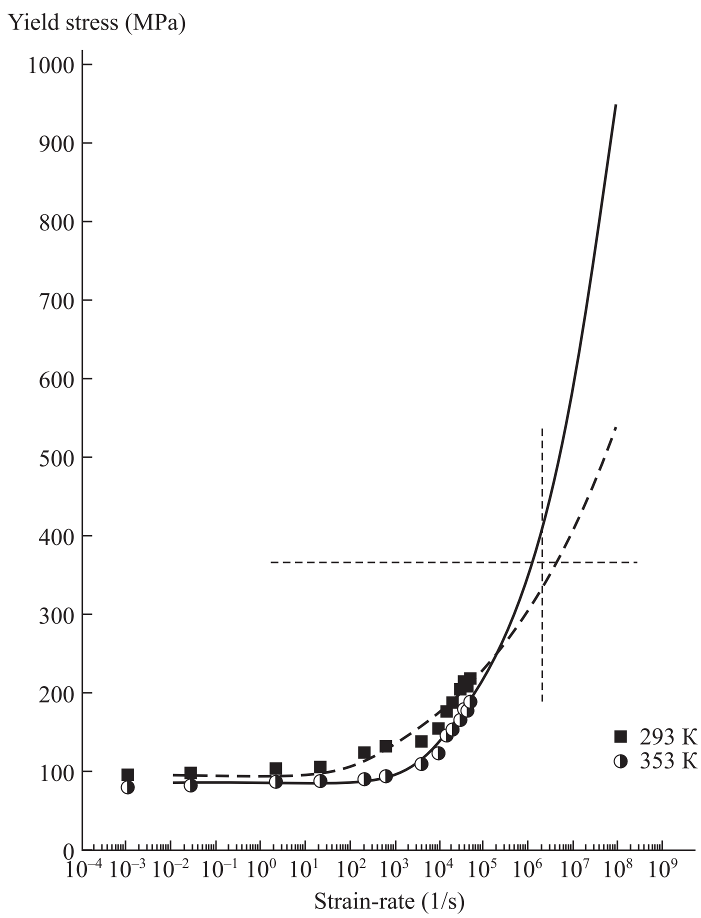

Fig. 10.8. Extrapolation of stress-strain-rate diagrams for mild steel to the range of extremely high strain-rates.

Analysis of (10.13) and (10.15) shows that the incubation time of yielding τ_Y is much more temperature sensitive as comparing to the incubation time of fracture τ. Therefore, for low temperatures the increase in "yield delay" is more significant than the increase in "fracture delay". Hence for a given loading rate decrease in temperature can result in occurrence of brittle fracture instead of the ductile one. Moveover these equations show that increase in the loading rate can remarkably increase the temperature of fracture mode transition. Discussed phenomenon was observed in numerous experimental works.

10.5 Anomalous Behaviour of Yield Limit and High Temperature Embrittlement

Consider yield delay dependencies presented in Fig. 10.1. In Fig. 10.7 one can see that the slope of curves corresponding to higher temperature is higher (α decreases as the temperature grows). Extrapolating these lines for higher stresses one will receive intersection points corresponding to a very small yield delay (or a very high stress applied). In connection with this several questions arise. Are these values reachable? Can this phenomenon be observed experimentally? If so, then for very short pulses increase in temperature should lead to increase of the yield limit. If the value for yield limit becomes higher than the strength (σ_S does not increase with temperature) then the material embrittles as a result of heating. Examination of data for mild steel (Figs. 10.4 and 10.8) leads to a similar conclusion. For strain-rates in a range of $10^5 - 10^6\ s^{-1}$, heating results in increase of the yield limit and possible transition to brittle mode of fracture.

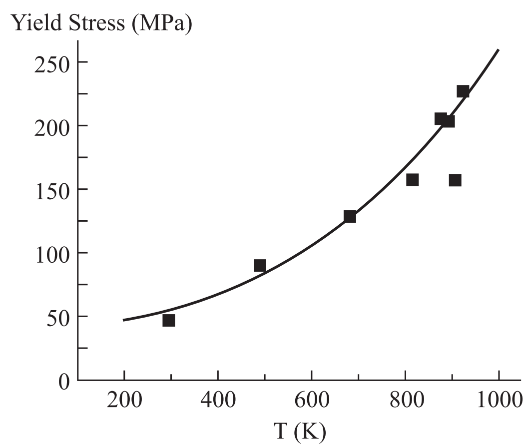

Fig. 10.9. Yield limit of single-crystal aluminum as a function of temperature. Experimental points from Razorenov et al. (Razorenov et al., 2004), theoretical curve from Petrov et al. (Petrov et al., 2007).

Experimental confirmation of these conclusions was recently received at experiments with pure titanium (Kanel et al., 2003) and single-crystalline aluminum (Razorenov et al., 2003). Using (10.5, 10.12–10.14) dependency of the yield limit on temperature can be received. In Fig. 10.9 theoretical prediction for yield limit as a function of temperature (Petrov et al., 2007) is compared to experimental data (Razorenov et al., 2003). Explanation and detailed investigation of this phenomenon on the basis of the incubation time approach was given by Petrov et al. (Petrov et al., 2007).

10.6 Conclusions

The incubation time based criteria for fracture and yielding showed to be in a close agreement with experimental data for various materials in a wide range of temperatures and strain-rates. Equations (10.5, 10.12–10.14) give an explanation to both: "typical" decreasing and "anomalous" increasing of the yield limit along with increasing temperature.

References

Campbell, J. D., 1953, Dynamic Yielding of Mild Steel, Acta Metallurgica, Vol. 1, N 6, p. 706.

Campbell, J. D., Ferguson, W. G., 1970, The Temperature and Strain-Rate Dependence of Shear Strength of Mild Steel, The Philosophical Magazine, Vol. 21, p. 63.

Campbell, J. D., 1973, Dynamic Plasticity: Macroscopic and Microscopic Aspect, Materials Science and Engineering, vol. 12, pp. 3–21.

Cotrell, A. H., Bilby B. A., 1949, Proc. Phys. Soc. (London), A62, p. 49.

Gruzdkov, A. A., Petrov, Y. V., 1991, On the general yield criterion of mild steel for both slow loading and high-strain-rate deformation, Proc. of 1-st USSR conf. on Technological Problems of the Strength of Structures, Zaporozh'e, Vol. 1, Part 2, pp. 378–383.

Gruzdkov, A., Petrov, Y., 1999, On Temperature-Time Correspondence in High-Rate Deformation of Metals, Doklady Physics, Vol. 44, p. 114.

Kanel, G, Razorenov, S., 2001, Anomalies of the temperature dependencies of volume and shear strength of single-crystals of aluminum in sub-microsecond range, Phizika Tverdogo Tela, Vol. 43, p. 839.

Kanel, G. I., Razorenov, S. V., Zaretsky, E. B., Herrmann, B., Meyer, L., 2003, Phizika Tverdogo Tela, Vol. 45, N 4, pp. 625–629,.

Kraft, J. M., Sullivan, A. M., 1959, Effect of Grain Size and Carbon Content on Yield Delay Time of Mild Steel // Trans. of Am. Soc. Metals, Vol. 51, p. 643.

Krüger, L., Meyer, L. W., Razorenov, S. V., Kanel, G. I., 2003, International Journal of Impact Engineering. Vol. 28, pp. 877–890.

Meyers, M., 1994, Dynamic Behavior of Materials, N.Y., ch. 13, p. 323.

Morozov, N. F., Petrov, Y. V., 2000, Dynamics of Fracture, Springer-Verlag, 132 p.

Morozov, N., Petrov, Y., Smirnov, V., 2002, Transition between Brittle and Ductile Erosional Fracture, Doklady Physics, Vol. 47, p. 525.

Petrov, Y. V., 1999, On "Quantum" Nature of Dynamic Fracture of Brittle Solids. Dokl. Akad. Nauk USSR, Vol. 321, No 1, pp. 66–68, (in Russian).

Petrov, Y. V., Morozov, N. F., 1994, On the modeling of fracture of brittle solids, Journal of Applied Mechanics, 61, 710–712.

Petrov, Y., Sitnikova, E., 2005, Temperature dependence of spallation strength and the effect of anomaly of melting temperature in case of impact loading, Doklady Akademii Nauk, Vol. 400, N 4, p. 1.

Petrov, Y., Gruzdkov, A., Sitnikova, E., 2007, Anomalous Behaviour of Yield Limit for Elevated Temperature in Case of High Strain-Rate Loading, Doklady Physics, Vol. 52, 12, 691–694.

Razorenov, S. V., Savinykh, A. S., Kanel, G. I., Skakun, S. N., 2004, Submicrosecond yield and tensile strength of metals and alloys at elevated temperatures, Shock Compression of Condensed Matter 2003, eds. M. D. Furnish, Y. M. Gupta, J. W. Forbes, pp. 491–494, AIP.

Yokobori, T., 1952, Phys. Rev., Vol. 88, p. 1423.

Chapter 11

Incubation time criterion for cavitation of liquids*

Cavitation fracture of liquids. Incubation time approach to predict cavitation in liquids. Influence of viscosity on cavitation criterion

11.1 Introduction

Cavitation, discontinuity arising in a liquid under the action of tensile stress, is a highly time-dependent process. If the load is applied for a sufficiently long time, cavitation occurs at some critical tensile stress (cavitation threshold, P_c). For a short-term load, however, achievement of a threshold is the necessary but not sufficient condition. In (Chebaevskii, Petrov, 1973) the effect of cavitation delay was found. In Venturi experiments with water-glycerol mixtures, it was shown that cavitation occurs only if the critical stress (pressure) persists for a certain time (about 80 μs). In other experiments, an increase of the threshold load with decreasing time of its application was noted. For example, in experiments on pulsed loading of distilled water (Besov, Kedrinskii, Morozov et al., 2001), the dependence of threshold (the lowest failure) pressure P_* on pulse duration T was obtained. For microsecond pulses, the pulsed threshold load exceeded the static value by several orders of magnitude. Similar dependences were observed for glycerol (Utkin, Sosikov, Bogach, 2003, Erlich, Wooten, Crewdson, 1975). Thus, one cannot adequately characterize cavitation initiation conditions under short-term loading in terms of cavitation threshold. Consequently, there arises a need for additional parameters describing the strength properties of liquids.

In this chapter papers by A. Gruzdkov, G. Volkov and Y. Petrov (Gruzdkov, Petrov, 2008, Volkov et al., 2007) are extensirely used.

*Authors acknowledge Dr. A. Gruzdkov and Mr. G. Volkov for their significant contribution to this chapter.

11.2 Incubation time based criterion for cavitation

Existence of static and dynamic strength is a common property of liquids and solids. Qualitative change in strength under short-term loading is associated with the fact that its duration in this case becomes comparable to the characteristic time of transitions in the material. As for cavitation, this process starts with appearance of cavitation nuclei, for which purpose nearby layers of the liquid must be set in motion. If the quasi-static cavitation criterion

$$P_* \geq P_c \tag{11.1}$$

were valid for the loading duration as short as desired, it would come in conflict with the momentum conservation law. Thus, not only the pressure but also the momentum must reach a critical value to initiate cavitation.

Such an argumentation leads us to the momentum criterion:

$$\int_0^t P(s)ds \geq W_c, \tag{11.2}$$

where $P(s)$ is the tensile pressure. A number of authors (see, e.g., (Galiev, 1981)) suggested that criterion (11.2) should be applied to predict cavitation under short-term loading. One can note that, in the case of slow loading, criteria (11.1) and (11.2) contradict each other. In fact according to (11.2), if the loading duration is large, cavitation may occur at as small applied pressure amplitude as desired. To remedy the situation it was proposed (Galiev, 1981) to carry out integration only over time instants the applied pressure exceeds P_c. However, such a proposition seems to be doubtful, since it assumes the irreversibility of load-induced variations, which is not the case for liquids. In addition, it is well known that a below-critical pressure also has a considerable effect on cavitation nuclei.

We suggest a cavitation criterion similar to that used in analysis of spall fracture in solids. To our opinion, the momentum should be taken into consideration not throughout the loading process but over some finite time interval, the characteristic time of bubble nucleation and growth. This time will be called the incubation time (the "preparation" time of cavitation) and designated by τ. Within a finite time interval the critical momentum criterion takes the following form:

$$\int_{t-\tau}^{t} P(s)ds \geq P_c\tau. \tag{11.3}$$

It is assumed that the zero time coincides with the instant of load application; that is, $P(t) = 0$ at $t < 0$. It is easy to check that criterion (11.3) is equivalent to (11.2) at short-term loading with characteristic time $T < \tau$ and to (11.1) at long-term loading ($T \gg \tau$). The latter assertion becomes clear if (11.3) is recast as a kinetic relationship.

Designating:

$$W(t) = \frac{1}{\tau}\int_{t-\tau}^{t} \frac{P(s)}{P_c}ds,$$

we obtain criterion (11.3) in the form:

$$W \geq 1.$$

For parameter W having the meaning of accumulated damage, we can write:

$$\frac{dW}{dt} = \frac{1}{P_c}\frac{P(t) - P(t-\tau)}{\tau}, \quad W(0) = 0.$$

In the formal limit $\tau \to 0$ corresponding to loading with a characteristic time far exceeding the incubation time, we have the relationship which is the differential form of the static criterion (11.1). In essence, the the of criterion (11.3) signifies discretization of the time scale.

Experimental data, however, indicate that it is appropriate to generalize criterion (11.3) by introducing an additional parameter. From experiments on very short loading (see, e.g. Besov, Kedrinskii, Morozov et al., 2001, Utkin, Sosikov, Bogach, 2003, Erlich, Wooten, Crewdson, 1975), it follows that respective data points are well fitted by a straight line in logarithmic coordinates (Fig. 11.1). Thus, for threshold pressure in the cases of long- and short-term loading, we have:

$$P_* = P_c = \text{const}$$

and

$$P_*^{\alpha} T = \text{const} \tag{11.4}$$

respectively (α is a dimensionless constant). Extending relationship (11.5) for an arbitrary pressure versus time dependence, we modify criterion (11.3) by introducing dimensionless formfactor α, which will describe the weight (relative influence) of force and time factors. Taking into account the variability of the sign of pressure, we get the formula:

$$\frac{1}{\tau}\int_{t-\tau}^{t} sign(P(s))\left(\frac{|P(s)|}{P_c}\right)^{\alpha} ds \geq 1. \tag{11.5}$$

The onset of cavitation corresponds to the least value of time t for which condition (11.5) is fulfilled.

11.3 Experimental data for water and glycerol

Cavitation in distilled water and glycerol subjected to microsecond loading pulses was studied in (Besov, Kedrinskii, Morozov et al., 2001) and (Utkin, Sosikov, Bogach, 2003, Erlich, Wooten, Crewdson, 1975) respectively.

In those experiments the zone of tensile stress appeared when a compression wave was reflected from the free surface of the liquid. The pressure versus time dependence in the incident (compression) wave was determined by measuring the velocity of the free surface. The compression pressure in the incident wave can be approximated by relationships (Besov, Kedrinskii, Morozov et al., 2001, Utkin, Sosikov, Bogach, 2003, Erlich, Wooten, Crewdson, 1975):

$$q(t) = -P_{\mathrm{amp}}\sin(\frac{\pi t}{T})e^{-\frac{t}{T_1}}$$

for water (the damping period T_1= 2.85 μs) and

$$q(t) = -P_{\mathrm{amp}}\left(1-\frac{t}{T}\right)[H(t)-H(t+T]$$

for glycerol ($H(t)$ is the Heaviside step function). The pressure in liquid is a superposition of forward (compression) and backward (stretching) waves,

$$P(x,t) = q\left(x-\frac{t}{c}\right) - q\left(x+\frac{t}{c}\right).$$

Here, c is the sound speed and x is the distance to the free surface. The compression wave arrives at the free surface at time instant $t = 0$; hence:

$$q(t) = -\frac{P_{amp}}{T}\left(T - t - \frac{x}{c}\right)\left[H\left(t + \frac{x}{c}\right) - H\left(t + \frac{x}{c} - T\right)\right]$$

In calculations, the threshold (minimal) value of pressure amplitude P_{amp} at which condition (11.5) was met at least for one value of coordinate x was determined for each pulse duration T and then the threshold pressure amplitude P_{q} was plotted against the load pulse duration. We used static thresholds of cavitation, P_c, found experimentally: $P_c = 0.1$ MPa for water and 6.3 MPa for glycerol. Parameters τ and α gere chosen so that the calculated plots fitted the experimental data (for details of calculation see (Besov, Kedrinskii, Morozov et al., 2001)).

Good agreement with the experiment (Figs. 11.2, 11.3) was achieved at $\alpha = 0.5$ and $\tau = 19\ \mu s$ for water and $\alpha = 1$ and $\tau = 2\ \mu s$ for glycerol. Fig. 11.2 plots the threshold value against the pulse duration; Fig. 11.3 respectively, against parameter $\dot{\varepsilon} = \frac{P_*}{\rho c^2 T}$ introduced in (Utkin, Sosikov, Bogach, 2003), and having the meaning of the strain rate.

While the difference between the dimensional parameters, static cavitation threshold and incubation time was quite predictable for the liquids studied, the considerable distinction between formfactors is unexpected.

11.4 Convection of the cavitation criterion with the rayleigh equation

11.4.1 *Statics and Dynamics of a Microbubble*

It is of great interest to try to relate the macroscopic parameters describing the strength properties of the material to other characteristics and attendant processes proceeding on the microlevel. The existence of the static threshold is a direct consequence of the balance condition for a bubble (Harkin, Nadim, Kaper, 1999, Pernik, 1966, Besov, Gruzdkov, Utkin, 2000). When the radius of a bubble exceeds critical value R_c, the bubble becomes unstable and expands in the absence of the stretching pressure. Since the static radius of bubble directly depends on the applied pressure, the criterion:

$$R(t) \geq R_c \tag{11.6}$$

turns out to be equivalent to the criterion (11.1). Parameter R_c depends primarily on initial radius R_0 of cavitation nuclei and surface tension σ.

Under dynamic loading radius of the bubble is related to the loading history rather than being dependent on the current value of the applied pressure. One equation of microbubble dynamics has the form (Harkin, Nadim, Kaper, 1999, Pernik, 1966, Besov, Gruzdkov, Utkin, 2000):

$$R\ddot{R} + \frac{3}{2}\dot{R}^2 = -\frac{2\sigma}{\rho R} - \frac{4\mu\ddot{R}}{\rho R} + \frac{p_0}{\rho} + \frac{p_\infty(t)}{\rho} + \frac{p_1}{\rho}\left(\frac{R_0}{R}\right)^{3\gamma}, \tag{11.7}$$

where ρ is the density, μ is the viscosity, $p_\infty(t)$ is the applied stretching pressure, p_0 is the saturated vapor pressure, p_1 is the gas pressure inside the bubble, and γ is the adiabatic index.

11.4.2 ***Inviscid Liquid***

In the case in question, the pressure amplitude significantly exceeds P_c (by several orders of magnitude compared to the conditions considered in (Besov, Kedrinskii, Morozov et al., 2001)). Since the surface tension force, saturated vapor pressure, and pressure inside the bubble are of the same order of magnitude as P_c, the quantities listed can be ignored and (11.7) simplifies to (Pernik, 1966):

$$R\ddot{R} + \frac{3}{2}\dot{R}^2 = \frac{p_\infty(t)}{\rho}. \tag{11.8}$$

In terms of dimensionless variables

$$r = \frac{R(t)}{R_0}, \quad \tilde{t} = \frac{t}{T}, \quad P(t) = \frac{p_\infty(t)}{P_{amp}}.$$

Equation (11.8) takes the form:

$$\frac{R_0^2\rho}{P_{amp}T^2}\left(rr'' + \frac{3}{2}(r')^2\right) = P(t).$$

It is seen that this equation remains unchanged provided that the quantity

$$M = \frac{R_0^2\rho}{P_{amp}T^2}, \tag{11.9}$$

which has the meaning of the reduced mass, is constant.

Parameters R_0 and ρ are the characteristics of the liquid; therefore, we are interested in the duration and the amplitude of the applied loading pulse. Let, as in statics, cavitation start when the bubble grows up to a critical size; that is, it is assumed that criterion (11.6) is valid. Then for any threshold amplitude of the pulse the relationship:

$$P_{amp}T^2 = \text{const} \quad \text{or} \quad T\sqrt{P_{amp}} = \text{const} \tag{11.10}$$

holds true.

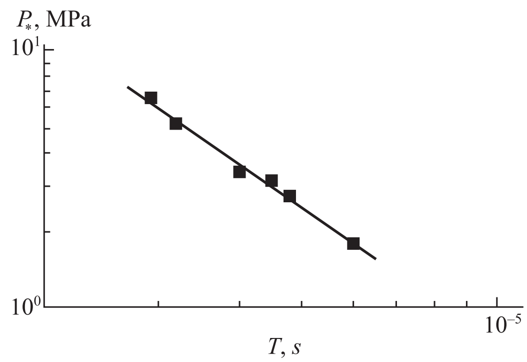

Fig. 11.1.

It follows from (11.10) that the formfactor should be set equal to $\alpha = 1/2$. Note that relationship (11.10) is depicted by the straight line in Fig. 11.1, which fits the experimental data.

11.4.3 *Viscous Liquid*

If the viscosity is high, one more term should be left in (11.7). Then, simplified equation (11.8) changes to:

$$R\ddot{R} + \frac{3}{2}\dot{R}^2 + \frac{4\mu\dot{R}}{\rho R} = \frac{p_\infty(t)}{\rho}. \tag{11.11}$$

Passing to the dimensionless variables yields:

$$M\left(rr'' + \frac{3}{2}(r')^2\right) = -4m\frac{r'}{r} + P(t), \tag{11.12}$$

where $m = \frac{\mu}{P_{\mathrm{amp}}T}$ is the dimensionless viscosity and M is given by (11.9). Let us estimate these dimensionless variables for glycerol, in which case σ =0.07 N/m, $P_c = 6.3$ MPa, $T \approx 0.1$ μs, $P_{amp} \approx 10$ MPa, $\mu = 1.48$ Pa s, and $\rho = 1260$ kg/m^3.

Since $P_c \approx \frac{2\sigma}{R_0}$, we find that $R_0 \approx 2 \cdot 10^{-8}$ m and thus $M \approx 5 \cdot 10^{-6}$ and $m \approx 1.5$.

Since the right-hand side of (11.12) is of the order of unity and the left-hand side is six orders of magnitude smaller, the latter can be neglected. Then, the equation of bubble growth becomes similar to the equation of pore growth (Shockey, Seaman, Curran, 1983) or microcrack propagation (Seaman, Curran, Murri, 1985) in solid:

$$\frac{r'}{r} = \frac{P(t)}{4m}, \quad r(0) = 1. \tag{11.13}$$

Accordingly:

$$\begin{gathered}\frac{dr}{r} = \frac{P(t)}{4m} d\tilde{t}, r(0) = 1, \\ \int\limits_{o}^{\tilde{t}} D(s)ds = 4m \ln r(\tilde{t}).\end{gathered} \tag{11.14}$$

From (11.14) it follows, in particular, that the critical radius criterion for a bubble given by (11.6) is equivalent to critical momentum criterion (11.2) in the given case.

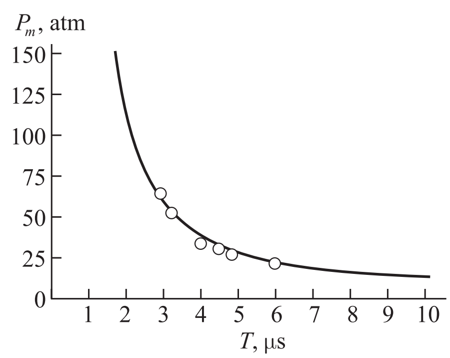

Fig. 11.2.

Equation (11.13) remains unchanged provided that dimensionless viscosity m is constant. Taking into account that viscosity m is the property of the liquid and is not related to loading conditions, we arrive at the conclusion that threshold loads must satisfy the relationship:

$$P_{amp}T = \text{const}; \tag{11.15}$$

consequently, formfactor α must be equal to unity, which is in agreement with the experimental data for glycerol (Fig. 11.3).

11.4.4 *Some Comments about Scaling Invariance*

The incubation time criterion is closely related to the scaling invariance of the loading parameters, which is defined, in general, by formula (11.4). Depending on the ratio between M and m, formula (11.4) may coincide with (11.10) or (11.15). Note, however, that both relationships are valid for short pulses, since the expressions for m and M include pulse duration and applied pressure amplitude. If loading is very slow ($T \to \infty$), both parameters are small; accordingly, terms of the order of P_c entering into (11.7) cannot be neglected and the terms involved in the balance equation for the bubble become leading terms.

It is easy to see from (11.7) that the energy transferred to the liquid via loading is converted to the surface energy of bubbles, work done against viscosity, and kinetic energy of adjacent layers of the liquid. Under quasi-static loading the major part of the energy is converted into the surface energy. If loading pulses are very short, the surface energy, conversely, is low and the cavitation process is governed by competition between inertia and viscosity. Of fundamental importance here is the ratio of the reduced mass to the dimensionless viscosity:

$$\frac{m}{M} = \frac{T\mu}{R_0^2 \rho}.$$

While this ratio formally becomes infinitesimal at $T \to 0$, such a situation is unrealistic, e.g., for glycerol. It is natural to suppose that the contributions of the viscous and inertial resistances are comparable to each other for many real liquids. It seems that in this case the cavitation initiation condition may be described by criterion (11.5) but with an intermediate value of the formfactor.

11.5 Conclusions

It is shown that the incubation time criterion can be applied to analysis of experimental data for cavitation in liquids subjected to short-term loading.

The parameters describing the dynamic strength of distilled water and glycerol are determined.

It is demonstrated that scaling (11.4) of the pressure pulse parameters (which is postulated by criteria (11.2), (11.3), and (11.5)) and the formfactor value used in calculations can be explained using the equation of bubble dynamics.

References

Besov, A. S., Gruzdkov, A. A., Utkin A. A., 2000, Proceedings of the 2nd Polyakhov Readings, St. Petersburg, pp. 135–143.

Besov, A. S., Kedrinskii, V. K., Morozov N. F., et al., 2001, Dokl. Phys. 46, 363.

Chebaevskii, N. F., Petrov, V. I., 1973, Cavitation Characteristics of High-Speed Endless Screw-Type of Centrifugal Pumps, Mashinostroenie, Moscow, (in Russian).

Erlich, D. C., Wooten, D. C., Crewdson, R. C., 1975, J. Appl. Phys. 46, 1594.

Galiev Sh. U., 1981, Dynamics of Hydroelastoplastic Systems, Naukova Dumka, Kiev, 1981) [in Russian].

Gruzdkov, A. A., Petrov, Y. V., 2008, Cavitation Breakup of Low- and High Viscosity Liquids, Doklady Physics, 53, 3, 291–295.

Volkov, G. A., Gruzdkov, A. A., Petrov, Y. V., 2007, The Incubation Time Criterion and the Acoustic Strength of Sea Water, Physical Acoustics, 53, 2, 119–122.

Harkin, A., Nadim, A., Kaper, T. J., 1999, Phys. Fluids 11, 274.

Morozov, N, Petrov, Y., 2000, Dynamics of Fracture, Springer, Berlin.

Pernik, A. D., 1966, Problems of Cavitation, Sudostroenie, Leningrad, [in Russian].

Petrov, Y. V., 2004, Dokl. Phys. 49, 323.

Utkin, A. V., Sosikov V. A., Bogach A. A., 2003, Prikl. Mekh. Tekh. Fiz. 44, 27.

Shockey, D. A., Seaman, L., Curran, D. R., 1983, Material Behavior under High Stress and Ultrahigh Loading Rates, Plenum, New York.

Seaman, L., Curran, D. R., Murri, W. J., 1985, J. Appl. Mech. 107, 593.

Chapter 12

Incubation time criterion for detonation*

Detonation caused by pulsed energy input. New criterion to predict conditions for detonation initiation. Application of the new criterion to predict parameters of the external impact producing detonation of gaseous media

12.1 Introduction

Construction of a critical condition for detonation initiation is one of the main issues while theoretically modelling processes incorporating media detonation and deflagration-to-detonation transition (DDT).

An example illustrating an absolute necessity of the correct criterion, providing a possibility to predict critical detonation initiation conditions is the development of pulse detonation engines (PDE) carried out in different scientific centres around the world. One of the central challenges while constructing this type of engines is to develop an optimal way to initiate detonation inside a combustion chamber. It was shown by multiple authors (e.g. Frolov et al., 2005), that utilising traditional mixture lighting schemes amount of energy that is hard or even impossible to achieve in practice should be radiated inside the mixture in order to initiate detonation inside PDE combustion chamber. Thus, a problem of optimization of mixture lighting conditions appears. This problem is complicated by absence of a simple criterion able to predict with effectivity and reliability the critical conditions leading to media detonation under every possible way of supplying energy into the detonated media.

Currently the majority of utilized approaches in detonation initiation (e.g. Levin et al., 2002, Levin et al., 2004, Vasil'ev, 2005) are connected to the concept of critical detonation energy, introduced by Knystautas and

*Authors acknowledge Mr. L. Isakov for his significant contribution to this chapter.

Lee (Knystautas and Lee, 1976). At the same time a number of experimental studies of detonation initiated in gaseous media by electrical discharge is known (e.g. Knystautas and Lee, 1976, Levin et al., 2004). In experiments (Knystautas and Lee, 1976) authors were studying direct detonation initiation in a gaseous mixture subjected to electric discharge. It was found empirically (Fig. 12.2) that for their experimental conditions (Knystautas and Lee, 1976) there exists a critical (minimal) energy E_{cr} that needs to be radiated inside the mixture in order to initiate its detonation and time t_{mix} such, that for electric discharges with times t_f from load onset to moment when peak averaged power $(E(t)/t)_{\max}$) is reached less than t_{mix}, critical energy E_{cr} does not depend on the discharge duration and is equal to a constant E^0 — minimal energy needed to initiate detonation of media in question. For $t_f > t_{\text{mix}}$ critical energy is increasing with increasing discharge duration. In (Knystautas and Lee, 1976) authors, using results of their previous experiments assume that time t_f, defined as time from the moment of electric discharge onset to the moment when overtime average power $(E(t)/t)$ is maximized, is the main characteristic of electric discharge concerning detonation initiated by this discharge. Authors claim that energy transmitted to media after t_f cannot affect the fact of detonation.

Similar results were received in analogous experiments by Levin et al. (Levin et al., 2004). In the same work an empirically derived formula to estimate minimal energy of detonation initiation for electric discharges with $t_f > t_{\text{mix}}$ was proposed:

$$E_{cr} = \frac{E^0}{\sin^2(\pi \cdot t_{\text{mix}}/2t_f)}.$$

Though in the particular experimental conditions carried out in (Levin et al., 2004) this formula is able to describe the dependency of critical energy on the electric pulse history, it is evident that for a different time shape of the electric pulse this formula will be inapplicable. When the time shape of an electric pulse creating discharge is changed one will need a new empiric formula derivation. Evidently, this approach is hardy applicable for practical use.

Thus, none of currently known theoretical approaches in detonation is able to reliably predict a critical detonation conditions in arbitrary situation (for example, to predict minimal amount of energy that should be radiated by electric pulse of arbitrary shape, frequency and duration into gaseous media in order to generate detonation of this media).

Also the physical meaning of the time t_{mix}, being, obviously, one of the most important detonation process characteristics, is not evident yet.

Different criteria based on the concept of incubation time of a transient process are discussed in the other chapters. A general form for criteria based on the concept of the incubation time is given by:

$$\frac{1}{\tau}\int\limits_{t-\tau}^{t}\left(\frac{N(s)}{N_c}\right)^{\alpha}ds \leq 1, \tag{12.1}$$

where τ is the incubation time of the studied dynamic transition process, being a parameter of the media subjected to transition and independent of the way a load (or energy) is applied, $N(t)$ — time dependent value characterising the intensity of force impact (or energy input), N_c — its critical value in conditions of "slow" energy input, α — dimensionless parameter characterising sensitivity of a media to the rate of external force impact (or energy input), t and s — are global and local time.

12.2 New criterion to predict detonation conditions

A new criterion to predict detonation in gaseous mixture was introduced by Bratov, Isakov and Petrov (Bratov et al., 2008). As a critical condition for detonation initiation in gaseous media the criterion using a new concept of incubation time of a transient detonation process was proposed:

$$\frac{1}{\tau}\int\limits_{t-\tau}^{t}U(s)ds \leq U_c, \tag{12.2}$$

where $U(t)$ is time dependent power (time derivative of energy transmitted to the media — speed of the energy input) transmitted to detonating media. τ is the incubation time of the detonation process (physical nature of τ and possible ways of it's experimental evaluation will be discussed below), being an experimentally measured parameter characterising detonating media. U_c is the critical (minimal) value of energy input rate that is able to initiate detonation of the media in question. It should be outlined that by definition the incubation time τ and critical energy input rate U_c are not depending on the way the energy is transmitted to the media, shape and rate of energy pulse. These parameters depend only on the properties of the detonating media (i.e. chemical composition, temperature, pressure etc.). Moment t_* when equality in (12.2) is fulfilled corresponds to the moment when critical situation that will definitely result in detonation initiation (steady-state detonation wave will be formed) is reached.

Critical energy input rate U_c is the minimal rate at which one should transmit energy to the media in order to initiate direct detonation. Suppose that one has an ability to transmit energy to the media at arbitrary constant rate U_A: $U = U_A H(t)$, where$H(t)$is the Heaviside step function. Obviously direct detonation will never be initiated at "low" rates $U_A < U_c$ — formed detonation wave will never reach steady-state regime. Increasing the rate, its critical value U_c leading to formation of steady-state detonation wave can be found. Thus, input of energy at rates lower than U_c do not lead to detonation, while energy transmitted to media at higher $U_A \geq U_c$ rate will lead to detonation.

The incubation time of a detonation process is directly related to the processes preceding formation of steady-state regime of the detonation wave (this also includes chemical processes). τ is defined as a time from onset of energy input to formation of critical media state that will definitely lead to a steady-state detonation wave formation in an "ideal" experiment, when energy is transmitted (starting from t=0) to the detonating media at the constant rate equal to U_c: $U = U_c H(t)$.

From (12.2) it is evident that if energy is transmitted to the media within time period t_* that is shorter than the incubation time τ, all this energy can be used to form a steady-state detonation wave. This explains why in experiments (e.g. Knystautas and Lee, 1976, Levin et al., 2004) critical (minimal) energy E_{cr} needed to initiate detonation is constant whilst mixture is detonated by "short" (shorter than τ) electric discharges. At this point it can be concluded that time t_{mix} experimentally measured in (Knystautas and Lee, 1976) and (Levin et al., 2004) and above defined incubation time τ are congruent.

12.3 Application of incubation time criterion of detonation to predict experimental observation on detonation initiation in gaseous media

Utilising formulated incubation time criterion for detonation, results of known experiments on detonation initiation in gaseous media (Knystautas and Lee, 1976) are modelled. In these experiments detonation was initiated by electric discharges of controllable frequency and amplitude. Critical situation leading to formation of steady-state detonation wave was studied.

Energy of an electric discharge transmitted to detonating mixture within time t is given in these experiments by:

$$E(t) = \int_0^t i^2(t)Rdt, \tag{12.3}$$

where R is the resistance of the discharge gap, i is the current in electric circuit, t is the absolute time. Current time-history at the electric discharge initiating the detonation in (Knystautas and Lee, 1976) is approximated by:

$$i(t)=Ae^{-at}\sin(\omega t) \tag{12.4}$$

with A being the amplitude, a being the damping factor and ω being the oscillation frequency of the current in the electric circuit.

In the conditions of the modelled experiments (Knystautas and Lee, 1976) incubation time criterion for detonation initiation (12.2) will take the form:

$$\frac{1}{\tau}\int_{t-\tau}^{t} A^2R\cdot e^{-2as}\sin^2(\omega s)ds \le U_c. \tag{12.5}$$

For a given discharge frequency ω minimal amplitude sufficient to initiate direct detonation can be found from:

$$\varepsilon(t) = U_c, \quad \text{where} \quad \varepsilon(t) = \frac{1}{\tau}\int_{t-\tau}^{t} A^2R\cdot e^{-2as}\sin^2(\omega\cdot s)ds. \tag{12.6}$$

$\varepsilon(t)$ here gives the average discharge power (energy time derivative) over time period $(t-\tau;\ t)$.

Obviously integration interval in (12.6) can be found from the following condition:

$$-\frac{1}{2}e^{-2at}\left(-1+e^{2a\tau}+\cos(2t\omega)-e^{2a\tau}\cos(2(t-\tau)\omega)\right)=0. \tag{12.7}$$

$\varepsilon(t)$ value for time t, calculated from (12.7), should be compared to $\varepsilon(\tau)$. The required integration interval (t_*-τ; t_*), where t_* is the time when critical media state, that will result in formation of the detonation wave is reached, will correspond to the largest of these values. Substituting the received t_* into (12.6) one can find the critical value for pulse amplitude A.

Now the energy transmitted to the detonating media by an electric discharge can be calculated. Using amplitude A, given by (12.6)–(12.7), the value for the critical energy, leading to detonation initiation, can be received as a function of frequency of the electric discharge ω:

$$E_{cr}(T) = \int_0^t A^2 R \cdot e^{-2as} \sin^2(\omega s) ds. \tag{12.8}$$

Using the experimental data (Knystautas and Lee, 1976) presented by dots on Fig. 12.2, it is easy to find the value for minimal energy E^0 required to initiate detonation in mixture used in the experiments (this is exactly the critical detonation energy for "short" discharges) and the value for incubation time of detonation process τ, characterising processes preceding steady-state detonation wave formation in the mixture used by Knystautas and Lee (Knystautas and Lee, 1976) (as discussed above incubation time and time t_{mix} are congruent). These values are found to be: $E^0 = E_{cr}(t_* < \tau) = 0.11$ J/cm and $\tau = t_{\text{mix}} = 0.6$ μs. Dividing the found critical energy by the incubation time one can find the critical energy input rate U_c:

$$U_c = E^0/\tau = 0.183 \cdot 10^6 \ J/cm \cdot s.$$

Substituting obtained values for τ and U_c into (12.6)–(12.8), one will find the required critical energy of detonation initiation as a function of time t_* when critical detonation state is reached. (12.6)–(12.8) are solved numerically. Fig. 12.1 presents the received dependency.

As was correctly noticed by Knystautas and Lee (Knystautas and Lee, 1976), in their experimental conditions time t_*, when the critical state that will lead to formation of stationary detonation wave is reached, is close to the time t_f when average power transmitted to media is maximized. Although this is approximately correct for the shape of energy pulse used in (Knystautas and Lee, 1976), according to (12.2) it can be wrong for differently shaped pulses. According to (12.2) critical media state that will result in direct detonation can be formed at a moment of time different from the moment of peak average power. This should be particularly visible for short (shorter then τ) discharges of threshold amplitude.

Thus, albeit experimental conditions (Knystautas and Lee, 1976), results presented in Fig. 12.1 are very close to the experimental points reported in (Knystautas and Lee, 1976) (this due to previously discussed coincidence of $t_*$and t_f), we make another calculation of energy transmitted to gaseous media by threshold shaped discharge of duration t_f using incubation time criterion (12.2) in order to make an absolutely correct comparison to data presented at (Knystautas and Lee, 1976). To do this,

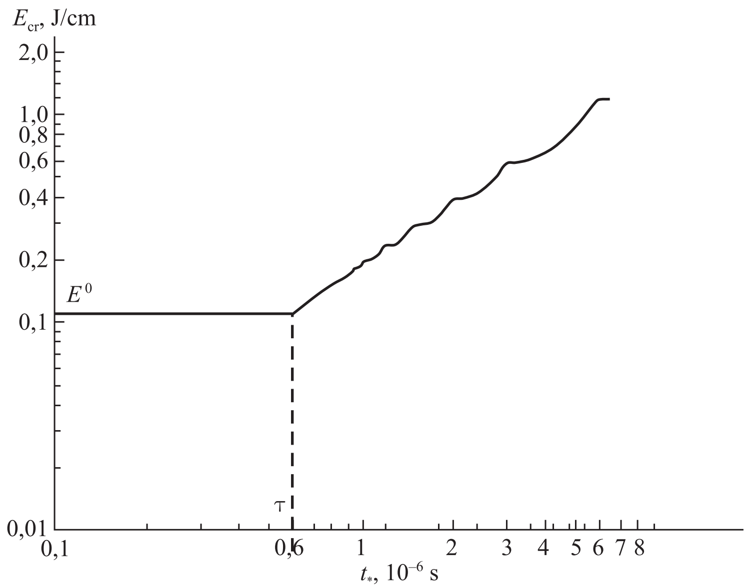

Fig. 12.1. Critical detonation initiation energy as a function of time t_* when critical detonation state is reached.

threshold amplitude leading to formation of steady-state detonation wave is found utilising (12.2) for every frequency of electric discharge (corresponding to definite discharge duration t_f). Having the critical amplitude, energy transmitted to detonating media by critical discharge with duration t_f, can be easily evaluated using (12.3) and (12.4). In Fig. 12.2 the experimental results of Knystautas and Lee (Knystautas and Lee, 1976) are compared to the results received using the new incubation time based criterion for detonation initiation.

As seen from Fig. 12.2 incubation time model for direct detonation initiation based on the new criterion (12.2) is in a very good coincidence with experimentally observed effects of detonation of gaseous mixtures.

12.4 Discussion

As already mentioned above, U_c and τ are parameters defining detonation-connected properties of a media. Experimental evaluation of these constants is possible utilising almost any possible experimental scheme. Here it should be outlined that for the same media at similar conditions (tem-

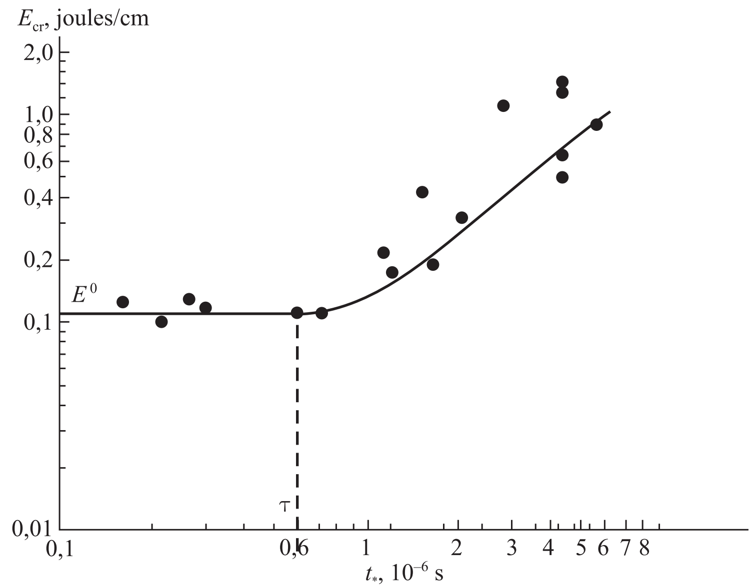

Fig. 12.2. Critical detonation initiation energy as a function of time to average input power maximization. Results received using new model (firm line) are compared to experimental points reported by Knystautas and Lee (Knystautas and Lee, 1976).

perature, pressure etc.) measured values for incubation time of detonation process and critical energy input rate should not depend on the experimental scheme used (i.e. how the energy is transmitted into the media).

One of the possible methods to measure U_c and τg is to conduct series of experiments with detonation initiated by energy transmitted to detonating media at different rates. In this case the threshold situation, when detonation is induced by a pulse having minimal energy input rate sufficient to initiate steady-state detonation wave, is of a special interest. If this condition is fulfilled, then the incubation time of detonation process will be equal to the time interval between energy input onset and the moment when critical state leading to formation of the detonation wave is reached. Critical energy input rate U_c in this case will be equal to the actual experimental energy input rate.

12.5 Conclusions

It is shown that using the incubation time approach it is possible to predict experimentally observed effects of detonation of gaseous media by electrical discharge. Presumably the same or similar approach can be used to predict critical detonation initiation conditions in liquid and solid explosives.

Having media parameters (incubation time and critical energy input rate), that without considerable difficulties can be evaluated experimentally, one is able to predict detonation of the media under arbitrary energy pulse. Thus, for example, the problem of mixture lighting optimization (having in mind energy input minimisation) is reduced to evaluation of incubation time of the detonation process τ and the critical energy input rate U_c for media in question (and possibly temperature-pressure dependency of these parameters). When this is done, optimal energy saving shape and amplitude for a pulse initiating detonation can be found using (12.2).

The concept of the incubation time of a detonation process is clearly demonstrating the influence of recent energy input history on detonation connected processes caused inside the media. Following this concept it is important that a definite minimal energy should be transmitted to the media within the incubation time τ in order to initiate its detonation. It can be expected that the same (or a similar) approach can be used to predict conditions influencing DDT in various explosive media.

References

Bratov, V. A., Isakov, L. M., Petrov, Yu. V., 2008, A Criterion for Detonation Initiation in Gas Mixtures, Doklady Physics, 422, 507–510

Frolov, S. M., Basevich, Y. Ya., Aksenov, V. S., Polikhov, S. A., 2005, Shock Waves 14 (3) 175–186.

Levin, V. A.; Markov, V. V.; Osinkin, S. F.; Zhuravskaya, T. A., 2002, Combustion, Explosion and Shock Waves 38 (6) 693–699

Levin, V. A., Zhuravskaya, T. A., Markov, V. V., Osinkin, S. F., 2004, Russian Journal of Physical Chemistry B 23 (9) 52

Vasil'ev A. A., 2005, Proceedings of the European Combustion Meeting 2005

Knystautas, R., Lee, J. H., 1976, Combust. Flame 27:221–228